Preparation of Low-Cost Kaolin Based Tubular Ceramic and Chabazite Zeolite-Ceramic Composite Membranes: Application in Microalgae Recovery and Wastewater Treatment

Thesis submitted in partial fulfilment of the requirements for the degree of

DOCTOR OF PHILOSOPHY

by

MADU PURNIMA

(176107104)

Department of Chemical Engineering

Indian Institute of Technology Guwahati

Assam -781039, India

January 2023

Preparation of Low-Cost Kaolin Based Tubular Ceramic and Chabazite Zeolite-Ceramic Composite Membranes: Application in Microalgae Recovery and Wastewater Treatment

Thesis submitted in partial fulfilment of the requirements for the degree of

DOCTOR OF PHILOSOPHY

by

MADU PURNIMA

(176107104)

Department of Chemical Engineering

Indian Institute of Technology Guwahati

Assam -781039, India

January 2023

Preparation of Low-Cost Kaolin Based Tubular Ceramic and Chabazite Zeolite-Ceramic Composite Membranes: Application in Microalgae Recovery and Wastewater Treatment

-Madu Purnima

Department of Chemical Engineering

Indian Institute of Technology Guwahati

Assam -781039, India

CERTIFICATE

This is to certify that the thesis entitled "**Preparation of Low-Cost Kaolin Based Tubular Ceramic and Chabazite Zeolite-Ceramic Composite Membranes: Application in Microalgae Recovery and Wastewater Treatment**" being submitted by Ms. MADU PURNIMA for the award of degree of Doctor of Philosophy, is an authentic record of the research carried out by her in the Department of Chemical Engineering, Indian Institute of Technology Guwahati, India, under my supervision. The work documented in this thesis has not been submitted to any other university or institute for the award of any degree.

(Signature of Thesis Supervisor)
Dr. G. Pugazhenthi
Professor
Department of chemical Engineering,
Indian Institute of Technology,
India.

DEDICATION

This Thesis is Dedicated to the Almighty GOD and to My Parents: Shri Madu Satyanarayana ❤ Smt. Satyavathi

Acknowledgements

First and foremost, my sincere heartfelt gratitude towards my supervisor **Prof. G. Pugazhenthi** for his tremendous support, guidance and patience towards me during my tenure in IIT Guwahati as a PhD scholar. His aim to help his students to gain maximum knowledge in each discussion helped me to do my research and writing thesis. His vision towards any project to reach society gave me lot of motivation to work and utilize the facilities available in the institute in best possible manner; he was there with me at every single step throughout the course. I am so blessed to work under him, as his critical analysis on different topics and scientific approach, which every student desires as their mentor.

I am also indebted to my Doctoral Committee members **Prof. R. Prasanna Venkatesh**, **Prof. N.R. Peela** and **Prof. S. Senthilkumar** for reviewing my work and providing their valuable suggestions, which definitely had helped me in improvising my work. I would like to convey my sincere thanks and gratitude to all the faculty members and staffs of Department of Chemical Engineering, IIT Guwahati for providing me all the required facilities to complete my degree in time. I am also thankful to Central Instruments Facility, IIT Guwahati for providing me necessary help and support in carrying out my experimental works. I thank Ministry of Human Resource Development (MHRD) for supporting financially to continue this project.

I would also like to acknowledge my seniors Dr. Arul Manikandan, Dr. Arun Sakthivel, Dr. Tanushree Paul, Dr. Manoj kumar, Mr. Deepak, Dr. Surjit Ramaswamy, Dr. Rajashree Borgohain, Ms. Thangsei Nengneilhing Baite, and Dr. Pradip Das for their help and support in smooth completion of my degree.

I wish to convey my heartfelt special thanks to my dearest friend Ms. Satti Venu Gopala Kumari for constantly motivating me to complete this project in the best possible manner. Her corrections motivated and improved me during this journey.

I would also like to thank my lab mates Ms. Preeti singh, Dr. Kakali Priyam Goswami, Ms. Poorva Mishra, Mr. Sashi Bhushan Singh, Mr. Arif Ahmed, Mr. Manoj kumar for their friendly support.

I would like to thank all my friends where I used to go to church. I thank everyone for their prayers to complete my Ph.D.

My beloved parents, Shri. Madu Satyanarayana and Smt. Madu Satyavathi, my sisters Mrs. Sirisha, Mrs. Neelima, Mrs. Vijayalakshmi and my husband Mr. Arun Sakthivel for sticking by my side throughout this journey. A thank you will definitely not be sufficient for the love, care and encouragement you showed for me. Above all, I would like to bow down in front of the Lord Jesus for giving me this life. His blessings kept me motivated to stay stronger and work harder.

Sincerely,

Madu Purnima

Abstract

The fascinating advantages of ceramic membranes due to their superior properties of chemical/thermal resistance, mechanical strength, and ease of cleaning increase their use in different valuable product recovery and wastewater treatment applications. On the other hand, the high raw material cost and high sintering temperatures pull back their potential industrial application. In view of this, researchers have been working on the development of low-cost ceramic membranes by utilizing inexpensive precursors such as kaolin, Moroccan clay, Tunisian clay, perlite, fly ash and phosphate, etc. Among these inexpensive precursors, kaolin has delighted many researchers for the production of ceramic membranes owing to its low cost and unique properties such as high strength, good hydrophilicity, and lower sintering temperature than alumina. Also, the particle size and chemical composition of kaolin aid for manufacturing excellent porous ceramic membranes, which is key to its success in ceramic membrane application compared to other raw materials. In this study, raw materials, such as kaolin (50 wt%), quartz (25 wt%) and calcium carbonate (25 wt%), along with organic binders, were used to fabricate ceramic membranes. In order to evaluate the effect of different binders on membrane properties, three different aqueous binder solutions (3 wt% Sodium salt of carboxy methyl cellulose (CMC), 3 wt% Guar gum (GG) and 3 wt% Hydroxypropyl methylcellulose (HPMC)) were used. Tubular ceramic membranes with dimensions of 11.5 mm outer diameter, 5.5 mm inner diameter and 100 mm length were prepared by extrusion technique. Several characterization techniques were employed to evaluate the properties of the fabricated membranes, including X-ray diffraction analysis, X-ray fluorescence analysis, Energy dispersive analysis, Field emission scanning electron microscope. The average pore size, pure water permeability, porosity, mechanical strength and chemical stability of the fabricated membranes were also evaluated. In addition to excellent corrosion resistance in acidic and basic medium, the prepared membranes have porosity in the range of 36 - 48%,

water permeability of 0.93×10^{-7} - 1.86×10^{-7} m^3/m^2 s kPa, an average pore diameter of 0.137 - 0.182 µm and mechanical strength of 21-38 MPa. The characterization results revealed that the membrane prepared with 3 wt% HPMC binder solution (Kaolin-HPMC) was found to be best. It possessed an average pore size of 0.178 µm and porosity of 40% along with outstanding chemical and mechanical strength. Also, the estimated membrane cost was found to be 253 USD/m^2 based on raw materials, energy consumption, manpower and equipment cost.

The produced kaolin based tubular ceramic membranes with different organic binder solutions (Kaolin-CMC, Kaolin-GG, Kaolin-HPMC) were tested for their potential application in the recovery of microalgae from its broth solution. All three ceramic membranes were tested for the microfiltration of microalgae, *Chlorella Sorokiniana*, with an initial concentration of 500 mg/L at various applied pressures (69-345 kPa) and a constant crossflow rate (6.42×10^{-3} m/s). The results revealed that the permeate flux increased significantly when the pressure increased from 69 to 276 kPa, and a sharp flux decline was noticed at higher operating pressures (276-345 kPa). The separation results elucidated that all the membranes yielded a maximum permeate flux of 1.39 – 1.98×10^{-5} m^3/m^2 s with algae recovery of almost 100% at an applied pressure of 276 kPa. Kaolin-HPMC membrane was found to be the best as it offers the greatest combination of recovery (100%) and permeate flux (1.78×10^{-5} m^3/m^2 s). Furthermore, in order to explain the fouling mechanism in microfiltration, the experimental results were fitted with four pore blocking models. The cake filtration model was best fitted with the experimental data of all the membranes compared to the other three models. This Kaolin-HPMC membrane was taken for further wastewater treatment applications such as recovery of TiO_2 nanoparticles from its suspension and onshore oilfield produced water treatment.

Cross-flow microfiltration experiment was conducted to recover TiO_2 nanoparticles from its suspension by varying the applied pressure (138 - 414 kPa), cross flow velocity (2.41×10^{-3} - 5.63×10^{-3} m/s), pH (4 - 11) and feed concentration (0.05 - 1 wt%). A maximum permeate flux

of 4.24×10^{-5} m^3/m^2s was noticed at 414 kPa, whereas a reduction in permeate flux was observed with increasing feed concentration of TiO_2. The membrane displayed 100% separation efficiency at all the investigated pressures. Further, the onshore oilfield produced water was targeted for the treatment. Here various strategies were employed: microfiltration, biological treatment, microfiltration followed by biological treatment (MF-B), and biological treatment followed by microfiltration (B-MF). Firstly, microfiltration experiments were carried out using Kaolin-HPMC membrane at various applied pressures (69 - 345 kPa) and the maximum removal efficiency values of the parameters such as total suspended solids (TSS) (100%), turbidity (100 %), total organic carbon (TOC) (84%) and chemical oxygen demand (COD) (78 %) were obtained at a low pressure of 69 kPa. Complete removal of TSS and turbidity were observed at all the applied pressure values. However, the COD and TOC removal efficiency decreased with an increase in applied pressure from 69 to 345 kPa. In order to meet the discharge limits of the treated water parameters, other alternative techniques were investigated, such as biological treatment, MF-B and B-MF. The oleaginous bacterium, *Rhodococcus opacus* was used for the biological treatment of produced water. The results revealed that the combined MF-B system was the most effective, showing 99% removal efficiency for TOC and COD compared to all other systems (microfiltration, biological treatment, and B-MF). Cleaning efficiency of the membrane was investigated using different chemical reagents and a mixture containing 0.1 wt% sodium dodecyl sulfate and 1 wt% sodium hypochlorite resulted in a maximum flux recovery of 92.6%. Furthermore, toxicity assessment of the treated water obtained from MF-B system revealed a maximum germination index of 74.3% for *Cicer arietinum* and 71.1% for *Vigna mungo.* After evaluating the potential of the prepared membrane in different liquid phase separation applications, its suitability as a support to prepare composite membrane was examined.

Chabazite (CHA) zeolite composite membrane was prepared through hydrothermal synthesis route for the separation of heavy metal ions from their respective solutions. In order to fabricate zeolite composite membrane, tubular ceramic supports (Kaolin-HPMC) were placed in the suspension with a molar composition of 1 SiO_2: 0.07 Al_2O_3: 0.9 Na_2O: 33.1 H_2O in a Teflon-coated autoclave reactor. The hydrothermal treatment was carried out at 100 ^oC for 24 h. Different strategies were employed to fabricate the composite membrane, such as coating the ceramic support solely on the interior surface, exterior surface, and both sides. The results obtained from XRD, FESEM and FETEM indicated that the hydrothermal synthesis route produced pure, ultrafine and uniform particles of chabazite. The effect of coating on the membrane surface (s) was investigated by measuring the weight increment, porosity, pore size and pure water permeability. The results revealed that the ceramic tube coated on both sides has the highest amount of zeolite loading, i.e., 1.82±0.18 g along with porosity of 30.50±0.50%, water permeability of 4.83×10^{-9} m^3/m^2s kPa and average pore diameter of 36 nm. The ceramic support coated on both sides (CM_B) displayed better characteristics when compared to the membrane coated only inner surface (CM_I) and the membrane coated only on outer surface (CM_O); hence it was used to separate different heavy metals from aqueous solution. Also, the estimated cost of CM_B membrane was found to be 868 USD/m^2.

The performance of the CM_B composite membrane was tested to remove cerium from aqueous solution. The membrane removed more than 99.9% of cerium for the different parameters of feed concentrations and pH studied. Additionally, the performance of the membrane in separating heavy metal ions (Cd^{2+}, Al^{3+}, Mg^{2+}, and Ni^{2+}) from their solutions was evaluated using single, binary and tertiary mixtures in order to mimic real wastewater. The prepared composite membrane demonstrated excellent rejection efficiency (>99%) for all the metal ions at an applied pressure of 276 kPa, feed concentration of 1000 mg/L and pH 3. These findings suggest that the prepared ceramic and zeolite composite membranes have excellent application potential for wastewater treatment and lower cost than commercial ceramic membranes made of α-alumina, zirconia and titania membranes.

भारतीय प्रौद्योगिकी संस्थान गुवाहाटी
Indian Institute of Technology Guwahati

Contents

List of tables

List of Figures

Nomenclature

R^2	Coefficient of determination
Na-CMC	Sodium salt of carboxymethylcellulose
GG	Guar gum
HPMC	Hydroxypropyl methylcellulose
VRF	Volume reduction factor
V_i	Initial volume of feed
V_f	Final volume of feed
R_m	Resistance of membrane
R_t	Total resistance
R_f	Filtration resistance
TSS	Total suspended solids
COD	Chemical Oxygen Demand
TOC	Total Organic Carbon
PES	Polyethylene sulfone
PEI	Polyethyleneimine
TMC	Trimesoyl chloride
MOFs	Metal-organic-frameworks
TMA	Trimesic acid
HPEI	Hyperbranched polyethylenimine
GO	Graphene oxide
EDA	Ethylenediamine
PEUF	Polymer-enhanced ultrafiltration
P(VC-*co*-DMA)	poly (vinyl chloride *co* dimethylaminoethyl methacrylate)
TEAOH	Tetraethyl ammonium hydroxide
TPAB	Tetrapropylammonium bromide
TPAOH	Tetrapropyl ammonium hydroxide
TEOS	Tetraethyl orthosilicate
CTAB	Cetyltrimethylammonium Bromide
MP-AES	Microwave plasma atomic emission spectroscopy
Al-CWs	Aluminium based constructed wet lands
CHA	Chabazite

Notations

V_m	Membrane volume
C	Concentration
ID	Inner diameter of membrane
OD	Outer diameter of membrane
A	Effective area of membrane
J_{pw}	Pure water flux
t	Separation time
L_h	Water permeability
r	Pore radius (m)
l	Pore length
W_i	Initial dry weight of the membrane (g) before dipping acid/base medium
W_f	Final dry weight of the membrane (g) before dipping acid/base medium
W_{wet}	Wet weight of the membrane (g) after dipping in water
W_{dry}	Dry weight of the membrane
J	Permeate flux
J_0	Permeate flux at y-intercept
k	Slope

Greek symbols

ρ_w	Density of water
τ	Membrane tortuosity
ε	Membrane porosity
μ_w	Viscosity of water
μ_p	Viscosity of permeate
α	Alpha

भारतीय प्रौद्योगिकी संस्थान गुवाहाटी
Indian Institute of Technology Guwahati

Chapter 1

Introduction, Literature review and Objectives

Introduction, Literature review and Objectives

This chapter discusses a brief summary of the fundamentals and classifications of membrane technology. Recent advances in the fabrication of low-cost ceramic membrane and zeolite-ceramic composite membrane using various inexpensive sources are elaborated. This chapter also discusses the successful application of membrane technology in various fields. The detailed literature review presented in this chapter shows the possible scope for further research in the aforementioned topics based on which objectives of the research are defined. Lastly, the organization of the thesis is summarized.

1.1. Background investigation

The separation and purification process is an important aspect of downstream operation as it deals with great energy consumption and operational cost in chemical, petrochemical, biochemical, and several other industries. Innovations in separation technologies are critical to achieve high productivity and reducing environmental pollution (Nasef et al., 2012). On the other hand, the need for wastewater treatment has increased alarmingly due to urbanization and industrialization. In particular, the harmful effects associated with discharging untreated heavy metal containing wastewater to water bodies have an adverse impact on mankind and aquatic life (Imdad and Dohare, 2022). Membrane separation is regarded as a clean and simple process, which does not require any addition of coagulants or additives and can be operated with low energy requirement (Hubadillah et al., 2018). Both polymeric and ceramic membranes are applied in the membrane separation process (Malik et al., 2020). Ceramic membranes have superior characteristics for long life-term application and they are now effectively used in a wide range of industries to solve separation, concentration and purification challenges. Due to their technological benefits, viz. better stability, reversible fouling, easy cleaning and high permeate, ceramic membranes are gaining attention on a global scale for use in water and wastewater treatment applications (Asif and Zhang, 2021). In the early 1960s, the use of

ceramic membrane has been first reported for the successful filtration of beer and recovery of extract (Hubadillah et al., 2018). The common materials used in the fabrication of ceramic membranes were metal oxides viz. Al_2O_3, SiO_2, TiO_2, ZrO_2, and their combinations. However, the cost of these raw materials and high sintering processes (~ 1500 ^oC) limits their large-scale application (Mestre et al., 2019). In comparison to polymeric membranes, the cost of industrial use for inorganic membranes is one to three orders of magnitude more per unit area of the membrane. (Abd Aziz et al., 2019). Hence, there is a need to find cheaper raw materials for producing low-cost ceramic membranes with excellent characteristics. Furthermore, as majority of the inorganic pollutants remains charged in water, manufacturing of low-cost membranes with the charged surface can be explored (Sunil et al., 2018; Nayak et al., 2017; Waszak and Gryta, 2016).

1.2. Introduction to membrane technology

The word membrane originates from the Latin word *membrana*, which means skin. It passes materials selectively. *"A membrane is a selective barrier that permits the preferential permeation/retention of one or several components from gaseous and/or liquid mixtures"* (Ravanchi et al., 2009).

Membrane technology is often considered the best available technology owing to its various advantages, such as

- Lower energy consumption, since it involves no phase change
- Linear scale up
- Often simpler than alternative processes
- Easily combined with other separation processes, so-called hybrid processes (Selatile et al., 2018)

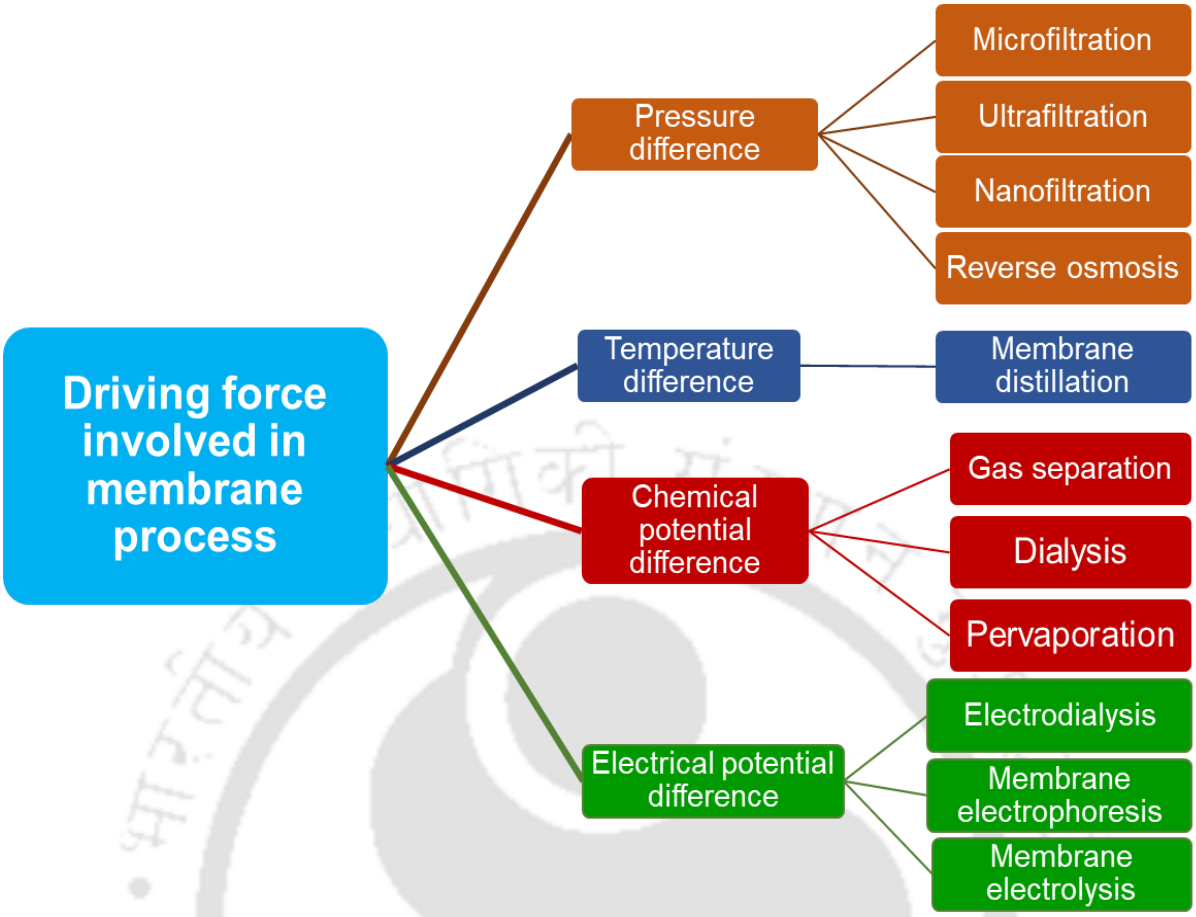

Fig. 1.1 Classification of membrane process based on driving force

1.2.1. Classification of membrane processes

Transport through the membrane takes place when a driving force is applied to the components in the feed. Based on driving force, the membrane processes are classified into pressure-driven membrane process, temperature-driven membrane process, concentration-driven membrane process, and electrical-driven membrane processes. Fig. 1.1 displays the classification of membrane processes based on driving force. Among them, pressure-driven membrane process is gaining more interest, especially in water and wastewater treatment applications (Manni et al., 2020).

1.2.1.1. Pressure-driven membrane process

Most industrial membrane separations are pressure-driven membrane processes (Ravanchi et al., 2009). In this process, the hydraulic pressure exerted on the solution at one side of the

membrane serves as a driving force to achieve separation. Among the various pressure-driven membrane processes, microfiltration (MF) has been extensively used for concentrating fine particles and wastewater treatment (Zhao et al., 2002). It can be used to treat large volumes of water at low transmembrane pressure (≤ 5 bar) and offers high permeate flux compared to ultrafiltration (UF) and nanofiltration (NF) (Manni et al., 2020). Fig. 1.2 displays various types of pressure-driven membrane processes used in membrane technology, such as microfiltration, ultrafiltration, nanofiltration, and reverse osmosis. Apart from the pressure requirement, all these processes differ by their membrane pore sizes.

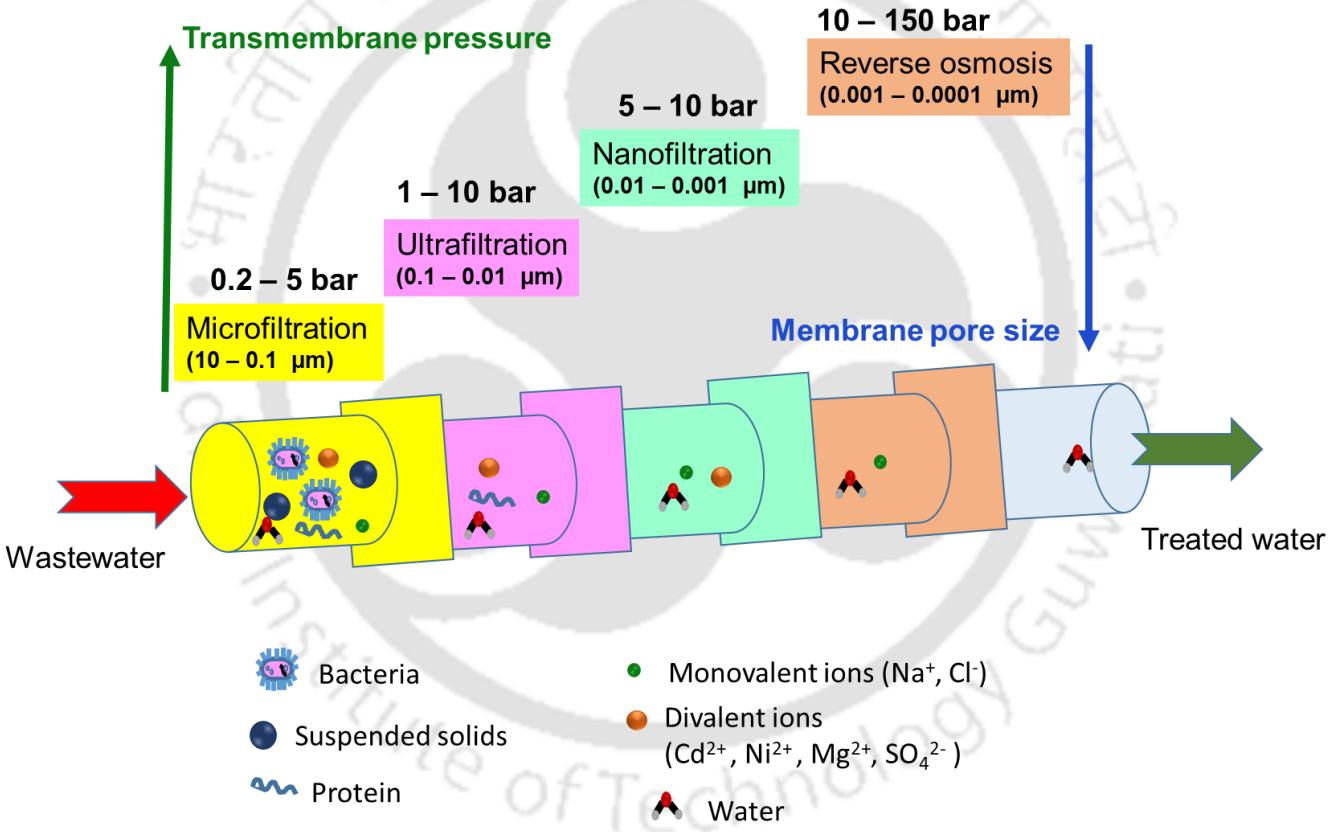

Fig. 1.2 Types of pressure-driven membrane processes

Microfiltration

- Pore size of the membrane ranges from 0.1 – 10 µm and the pressure ranges from 0.2 - 5 bar (Ang et al., 2006).
- The solute particles, which are greater than 0.1 µm size, are separated in this pressure-driven membrane process (Selatile et al., 2018).
- Mainly applicable to remove suspended particles, sediment, algae, protozoa and bacteria from liquid streams (Manni et al., 2020).

Ultrafiltration

- Pore size of the membrane ranges from 10 nm – 0.1 µm and the pressure ranges from 1 – 10 bar.
- The solute particles, which are greater than 10 nm and smaller than 0.1 µm size, are separated in this pressure-driven membrane process.
- Applications are mainly found in the removal of small colloids and viruses from wastewater (Manni et al., 2020).

Nanofiltration

- Average pore diameter of the membrane is around 1 – 10 nm and the pressure ranges from 5 – 10 bar
- This filtration separates divalent ions and dissolved organic matter from wastewater (Selatile et al., 2018).

Reverse osmosis

- A pressure-driven process in which solvent passes through the membrane in the direction of opposite to the osmosis by applying transmembrane pressure.
- Pore size of the membrane is in the range of less than 1 nm and the pressure ranges from 10 – 150 bar
- In the past few years, the utilization of RO membranes increased in purifying drinking water applications (Ang et al., 2006).

1.2.2. Membrane modules

Various types of membrane modules utilized in the industrial application are illustrated in Fig. 1.3 and summarized in Table 1.1. Plate and frame modules are generally useful for the treatment of feed with high solid content (landfill leachate). However, the relative manufacturing cost of this membrane module is significantly very high due to low packing density (Obotey Ezugbe and Rathilal, 2020). Spiral wound configuration offers high packing density; on the contrary highly susceptible to fouling, hence cleaning is difficult (Van der Bruggen et al., 2004). In case of hollow fibre module, major advantage is that it can host large membrane areas in a single module. However, it is very expensive and also requires huge capital requirements. Tubular configuration has a higher surface-to-volume ratio than plate and frame modules, which is advantageous for easy scale up to treat wastewaters containing high suspended solids (Sebastian et al., 2010). Tubular membrane module is less susceptibility towards fouling than hollow fibre and spiral wound modules because of their relatively large diameters. Hence, it is essential to use a suitable module, such as tubular module, that neither requires high manufacturing cost nor is difficult to clean (Van der Bruggen et al., 2004).

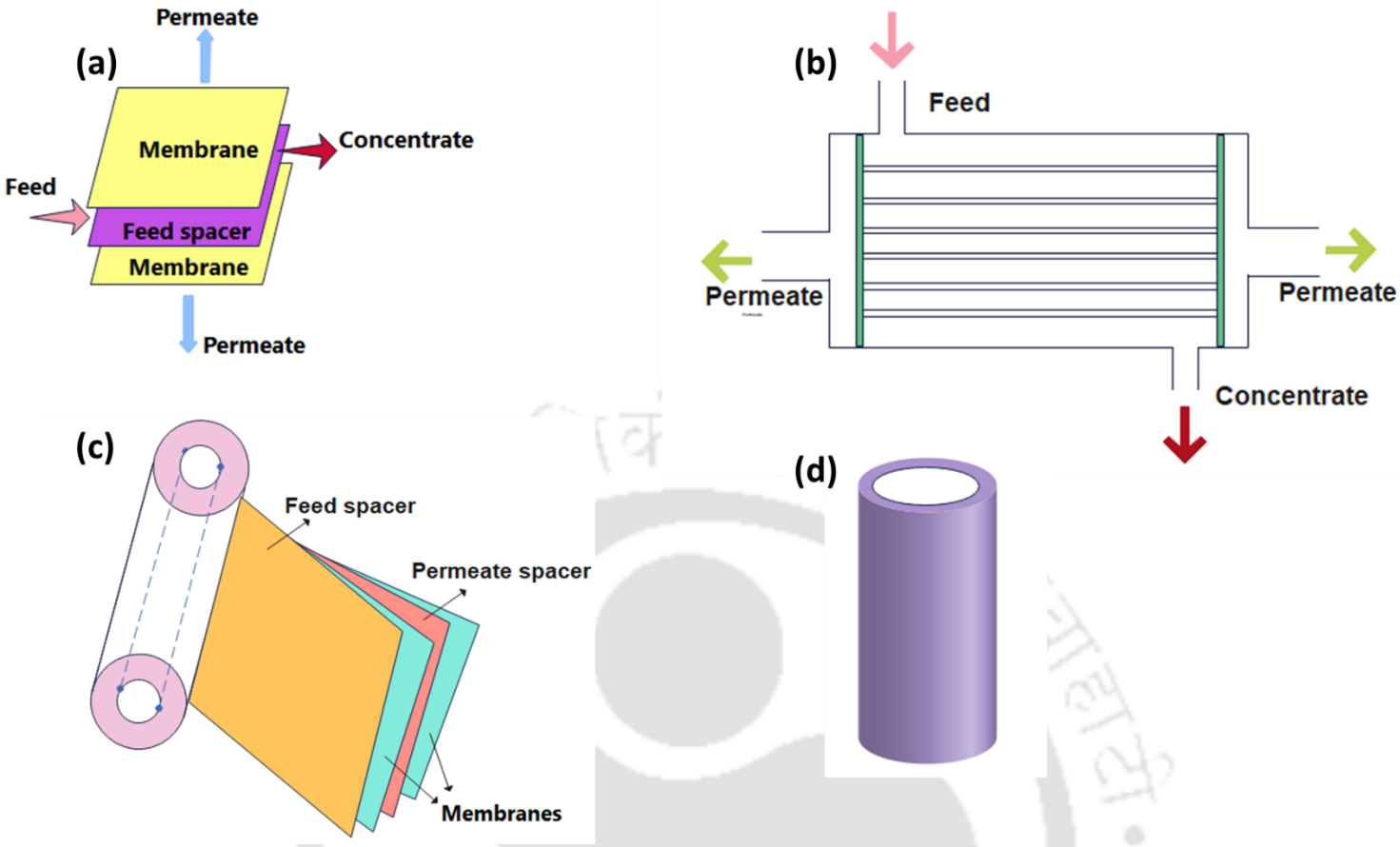

Fig. 1.3 Various membrane modules: (a) plate and frame, (b) hollow fiber, (c) spiral wound, and (d) tubular module

Table 1.1 Different industrial membrane modules for the application of pressure-driven membrane processes

Parameter	Application	Reference
Plate and frame	MF, UF	Obotey Ezugbe and Rathilal, (2020)
Tubular	MF, UF	Sebastian et al., (2010)
Hollow fiber	UF, RO	Van der Bruggen et al., (2004)
Spiral wound	NF, RO	Obotey Ezugbe and Rathilal, (2020)

1.2.3. Membrane materials

Synthetic membranes are commonly classified into two groups such as organic membrane and inorganic membrane. Different inorganic materials such as ceramic, metallic, carbon-based and zeolites are commonly used to prepare inorganic membranes. Organic membranes are made of

synthetic and natural polymers such as cellulose acetate, polypropylene, polysulfone and polyvinylidene fluoride (Tibi et al., 2020).

1.2.4. Merits and demerits of polymeric and ceramic membranes

Recent studies demonstrated that ceramic membranes are remarkable interest for the treatment of industrial wastewater because of their advantages like high flux, better lifetime, higher total suspended solids (TSS) tolerance, ability to utilize harsh chemical and hydraulic cleaning methods, lower risk of irreversible fouling than polymeric membranes (Asif and Zhang, 2021). A pre-treatment step is required to remove the suspended solids from wastewater by using clarification system in the polymeric UF/MF, which increases the overall process cost (Kurth et al., 2018). Table 1.2 displays the benefits and drawbacks of polymeric and ceramic membranes

Table 1.2 Benefits and drawbacks of polymeric and ceramic membranes

Parameter	Polymeric membranes	Ceramic membranes	References
Chemical stability	Poor	Excellent	Achiou et al., (2017)
Mechanical strength	Poor	Excellent	Ebrahimi et al., (2010)
Cleaning	Difficult	Easy	Asif and Zhang, (2021)
Thermal stability	Poor	Excellent	Ebrahimi et al., (2010)
Fouling behaviour	high propensity	less propensity	Asif and Zhang, (2021)
Weight	less	Heavy	Asif and Zhang, (2021)
Cost	Inexpensive	Expensive	Kumar et al., (2015b)

1.3. Raw materials used for the preparation of low-cost ceramic membrane

Fig. 1.4 displays the use of different types of low-cost raw materials for the production of ceramic membranes. Among the raw materials, the usage of kaolin is nearly 33% which is higher than that of other precursors, owing to various advantages, namely high absorption

capacity, high silica to alumina ratio, excellent thermal and rheological properties as well as their abundance in nature. This shows the effective use of kaolin based ceramic membranes over other raw materials for the application of liquid phase separation.

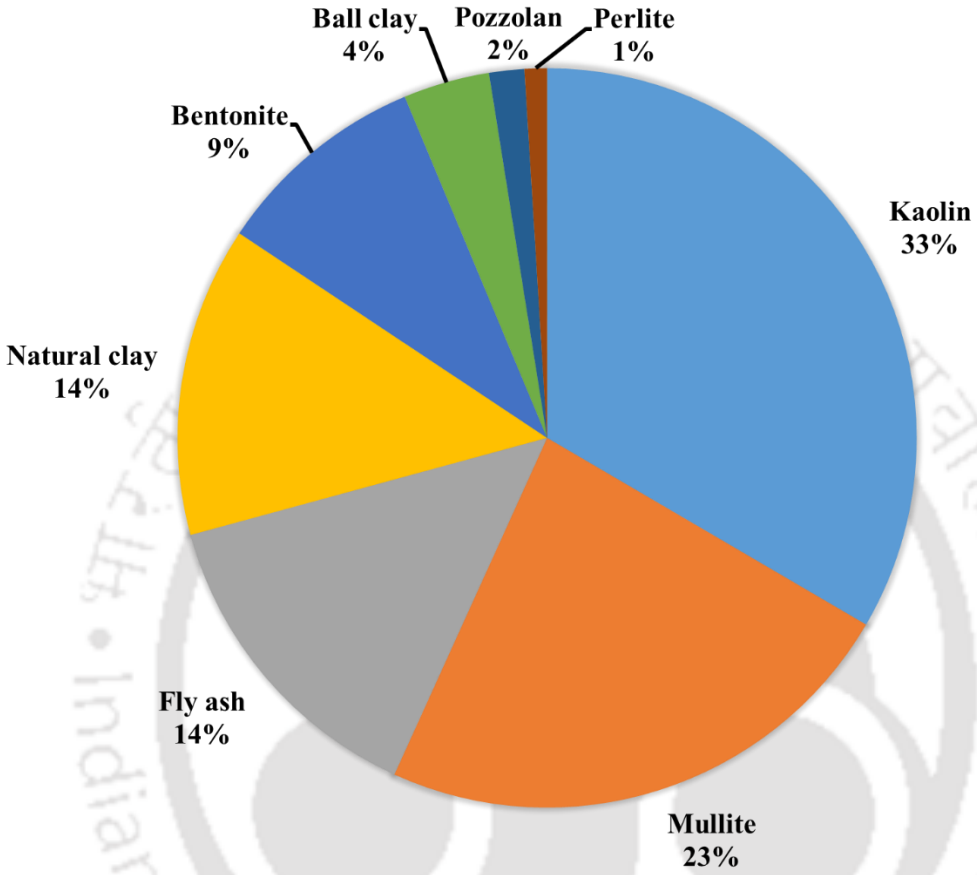

Fig. 1.4 Number of articles published (2010-2022) on fabrication of ceramic membranes using major low-cost ceramic materials (Courtesy: Google Scholar, accessed on 15th May 2022)

1.4. Fabrication techniques involved in the production of ceramic membrane/support

The method of fabrication determines the final product geometry and microstructure, which greatly impacts properties and performance of ceramic membrane (Carretero et al., 2002). Ceramic membranes are generally fabricated in flat and tubular configurations. Various techniques were reported for manufacturing ceramic membranes that include pressing method, tape casting, extrusion, freeze casting and phase-inversion. Among these, extrusion and pressing techniques are the most widely used methods for fabricating ceramic membranes

(Mestre et al., 2019). The schematic of different types of fabrication techniques is displayed in Fig. 1.5.

1.4.1. Extrusion

Extrusion process is used to fabricate tubular ceramic membranes (Fig. 1.5a). Tubular and multichannel ceramic membranes are gaining much interest owing to their high surface to volume ratio (Rani et al., 2021). In case of extrusion process, raw materials are well mixed with binder solution to make a paste with proper rheological properties. Subsequently, the paste will be extruded with the help of piston through a die to get the desired shape and subjected to several thermal treatment steps of drying and sintering to obtain membranes with desirable properties (Mestre et al., 2019). Extrusion pressure and displacement rate of die are the operating parameters that affect the fabrication in this process.

1.4.2. Pressing method

Pressing method is an inexpensive process and suitable for large production volumes. This method is generally used to prepare simple geometries such as circular and flat supports (Fig 1.5b). In this method, the internal frictions are high as particles rub one on another. Hence the energy requirement to form the green support is greater than that of the extrusion process (Mestre et al., 2019).

1.4.3. Tape casting

Tape casting is used to produce flat ceramic sheets (Fig. 1.5c). In this method, a slip with pseudoplastic behaviour can be used to cast a tape. The slip consists of ceramic powder, dispersion medium (water or organic solvent) and organic additives (binders, plasticizers and dispersants). The slurry is loaded in the container, and the green membrane is formed on a moving tape where a levelling doctor's blade controls the thickness of the tape. After that, the green tapes were cut into pieces and sintered to remove organics and to promote densification (Mestre et al., 2019).

1.4.4. Other shaping methods

Freeze casting and phase inversion are some of the other fabrication techniques to prepare ceramic membranes. Freeze casting involves freezing liquid suspension followed by frozen solvent sublimation in the presence of reduced pressure and temperature. During freezing, the growth of solvent crystals rejects ceramic particles in the suspension, which leads to shaping the pores. This method allows control over the size, shape and distribution of pores (Gaudillere et al., 2016). Phase inversion is a rare method to fabricate ceramic membranes (Hubadillah et al., 2016).

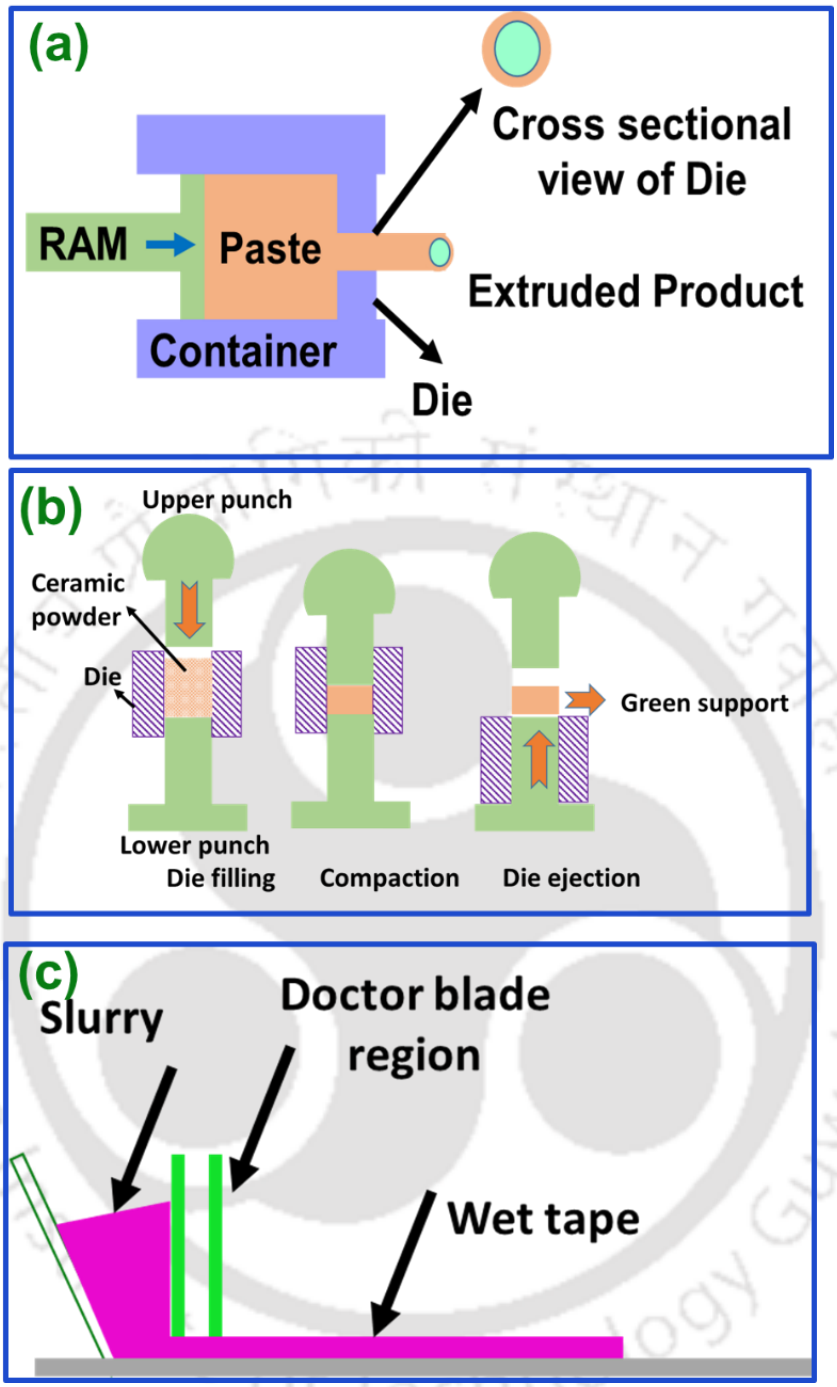

Fig. 1.5 Various fabrication techniques: (a) extrusion method, (b) pressing method and (c) tape casting

1.5. Zeolite membranes

Zeolites are crystalline and hydrated aluminosilicates with cations. Zeolite membranes are a type of inorganic membranes which separate liquid and gas species owing to their defined pore

size at molecular level and high ion exchange capacity (Algieri and Drioli, 2021). The ratio of Si to Al defines properties such as wettability and surface charge in zeolite membranes. Zeolite membranes can be used for the treatment of water and wastewater and desalination processes (He et al., 2019). Zeolite membranes provide a number of benefits over their polymeric counterparts in terms of their ability to survive at high temperatures, high surface charge, and resistance to organic solvents (Shukla and Kumar, 2005). Among all the benefits associated with zeolite membranes, the high surface charge of the membrane can be of great interest to researchers working on heavy metal separation from water (Sunil et al., 2018; Waszak and Gryta, 2016). Generally, direct crystallization and secondary growth method are used to prepare zeolite membranes (Nayak et al., 2017). It is well documented in the literature that direct crystallization, also called in-situ growth, is a simple process and is quite easy to operate (Huang et al., 2012). The major advantages of direct crystallization include high reactivity of reactants, low energy consumption, low air pollution and formation of metastable phases (Johnson and Arshad, 2014). However, there are some limitations of direct crystallization too, that includes the challenge to prepare a dense and phase-pure zeolite membrane due to poor heterogeneous nucleation on the support surface (Huang et al., 2012; Johnson and Arshad, 2014). In this process, the supports are submerged in the synthesis solution, and the zeolite membrane is formed by direct crystallization on support (Huang et al., 2012).

1.6. State of the art

1.6.1. Preparation of ceramic membrane

The manufacturing cost of ceramic membranes is much higher when compared to polymeric membranes (Yang et al., 2017). Though ceramic membranes can be applied even in a harsh environment owing to their excellent mechanical, thermal, and chemical stability when compared with their polymeric counterparts, their use in various fields is way too costly. In general, the cost of raw materials and energy involved in the sintering process are the two

components primarily responsible for the high price of ceramic membranes (Kumar et al., 2015b). Hence, in order to keep the membrane cost low, it has been suggested to use cheaply available raw materials, viz. natural clays (Workneh and Shukla, 2008), feldspar (Bose and Das, 2013), and kaolin (Vasanth et al., 2011) for the production of low-cost ceramic membranes. In comparison to the conventionally used raw materials, including silica (SiO_2), zirconia (ZrO_2), titania (TiO_2), and alumina (Al_2O_3), the afore-mentioned starting materials are inexpensive, abundantly available and require a low sintering temperature for membrane fabrication. It is well reported that the inclusion of natural raw materials lowered the manufacturing cost of ceramic membranes (Malik et al., 2020). Kaolin clay was used to prepare a low-cost disc-shaped microfiltration membrane and the estimated cost was found to be 130 USD/m^2 based on the cost of raw materials used (Nandi et al., 2009). In another study, a low cost tubular ceramic membrane was fabricated using kaolin, feldspar and sawdust. Based on selection of raw materials, preparation and energy consumption, support membrane cost was estimated to be around 250 USD/m^2 (Bose and Das, 2013). Recently, Goswami and Pugazhenthi, (2022) developed a tubular ceramic membrane using fly ash as a key precursor and the estimated membrane cost was 250 USD/m^2. Majouli et al. (2011) developed a flat ceramic membrane with an average pore size of 6.64 µm from Moroccan perlite using extrusion technique and the membrane was tested for the clarification of baking powder suspension. A low-cost ceramic membrane was prepared by Achiou et al. (2017) with an average pore size of 0.36 µm using natural pozzolan clay as a starting material for the pre-treatment of seawater. Tunisian clay-based tubular configuration ceramic membrane was coated by the slip-cast technique and the average pore diameter of the coated layer was calculated to be 0.18 µm (Khemakhem et al., 2011). Majouli et al. (2012) developed tubular ceramic membranes with a mean pore size of 0.27 µm from Moroccan clay as a precursor for microfiltration (MF) of industrial wastewater. Circular-shaped flat ceramic membrane derived from kaolin clay

exhibited excellent water permeability, porosity and good corrosive resistance and was used for the treatment of chromium containing wastewater (Vasanth et al., 2012). As evident from Table 1.3, among the many materials investigated for the production of ceramic membranes, kaolin has delighted many researchers owing to its low cost and unique properties such as high strength, good hydrophilicity and low sintering temperature than alumina (Hedfi et al., 2014; Hubadillah et al., 2018; Bose and Das, 2013; Vasanth et al., 2012). Moreover, the particle size and chemical composition of kaolin aid in manufacturing excellent porous ceramic membranes compared to other expensive raw materials (Bousbih et al., 2020). Besides, the membranes prepared with kaolin as a precursor offered low pore size (Chakraborty et al., 2018; Nandi et al., 2008; Hedfi et al., 2014; Bose and Das, 2013).

In addition to the raw materials used in the manufacture of ceramic membranes, binders play a vital role by enhancing the plasticity of the ceramic paste and improving the flow characteristics, which are very much required for extrusion. It also helps in reducing crack formation induced by changes in volume during thermal treatment (Elbadawi et al., 2017). Besides, binders considerably alter the membrane characteristics, such as porosity, mechanical strength, chemical stability and morphology. Both organic and inorganic binders are generally used in the fabrication of porous ceramic membranes (Bose and Das, 2013; Elbadawi et al., 2017; Cai et al., 2015; Benito et al., 2005). Organic binders include polyvinyl alcohol (PVA), polyethylene glycol (PEG), carboxymethyl cellulose (CMC), etc., whereas inorganic binders are sodium metasilicate, boric acid, etc. Wang et al. (2006) developed circular shaped α-alumina membranes with 2 wt% methylcellulose as a binder and 2 wt% corn starch as a pore forming agent. It was reported that the fabricated membranes possess an average pore diameter of 0.8 µm and porosity of 40 %. In another study, Amin et al. (2020) prepared a flat ceramic membrane by adding 15 wt% of PVA to the raw material, and the membrane showed an apparent porosity and an average pore diameter of 49 % and 0.091 µm, respectively. Two

tubular ceramic supports made from α-alumina and cordierite through the extrusion method were fabricated by Benito et al. (2005). In this study, CMC and PEG were used as binder and plasticizer, respectively in order to get a smooth texture of the green supports. In another work, two different configurations (tubular and flat) of ceramic membranes were fabricated using kaolin and doloma mixture along with 4 wt% methocel (obtained from methylcellulose) as a plasticizer and 4 wt% amijel (derived from starch) as a binder (Bouzerara et al., 2006). The tubular membranes prepared via the extrusion method resulted in a lower porosity than flat membranes. Bose and Das (2014) prepared a tubular ceramic membrane using sodium metasilicate and boric acid as binders and the membrane showed porosity and average pore diameter values of 20 % and 0.21 µm, respectively.

As evident from the afore-mentioned literature (Table 1.3), ceramic membranes fabricated with organic binders have better mechanical strength, chemical stability and lower pore size than membranes prepared using other types of binders (Amin et al., 2020; Bose and Das, 2013; Benito et al., 2005). Notably, organic binders with long chains and polar groups adhere easily to ceramic particles and improve rheological properties (Amin et al., 2020). Table 1.3 displays available literature on the fabrication of ceramic membranes using different raw materials and fabrication techniques.

Table 1.3 Available literature on fabrication of ceramic membranes

Membrane material	Method of membrane fabrication	Sintering temperature (ºC)	Membrane Configuration	Porosity (%)	Pore size (µm)	Mechanical strength (MPa)	Chemical stability (interms of weight loss %)	References
α- alumina, titania, starch and methylcellulose	Pressing	1400	Flat	40	0.8	50	Acid: 0.55 Base: 0.2	Wang et al., (2006)
α- alumina, kaolin, methocel, PVA and Dolapix CE 64	Extrusion	1350	Tubular	48	0.75	37	-	Oun et al., (2017)
Grind waste from kiln rollers and PVA	Pressing	1250	Flat	49	0.091	-	-	Amin et al. (2019)
Pozzolan and phosphate	Pressing	1050	Flat	32.07	1.33	15.69	Acid: 7.1 Base: 0.18	Beqqour et al., (2019)
Pozzolan	Pressing	950	Flat	33	2.36	19.16	Acid: 3.14 Base: 0.7	Achiou et al., (2016)
Pozzolan, starch, amijel and methocel	Extrusion	950	Tubular	41.2	0.36	15.36	-	Achiou et al., (2017)
Perlite, methocel, amijel and starch	Extrusion	1000	Flat	41.8	6.64	1.2	Acid: 0.2 Base: 6	Majouli et al., (2011)
Perlite, methocel, amijel and starch	Extrusion	1000	Tubular	42	6.6	-	-	Majouli et al., (2012)
Cordierite and magnesium carbonate	Extrusion	1380	Tubular	36.2	8.66	31	Acid: 4.5 Base: 0.2	Dong et al., (2007)
Moroccan clay, zirconia, Amidon, Amijel, PVA, PEG, Methocel, and Dolapix	Extrusion	1225	Tubular	43	11	10	-	Saffaj et al., (2006)

Moroccan clay and phosphate	Pressing	1100	Flat	28.11	2.5	17.5	Acid: 7.1 Base: 0.24	Mouiya et al., (2018)
Fly ash, amijel, methocel, and starch	Extrusion	1125	Tubular	51	4.5	18	Acid: 2	Jedidi et al., (2009)
Kaolin, feldspar, sodium metasilicate and boric acid	Pressing	850	Flat	29.98	0.93	8.75	-	Chakraborty et al., (2018)
Kaolin, quartz, calcium carbonate, sodium carbonate, boric acid and sodium metasilicate	Casting	850-1000	Flat	33-42	0.55- 0.81	3-8	Acid: < 4 Base: < 4	Nandi et al., (2008)
Kaolin, quartz and calcium carbonate	Pressing	900	Flat	30	1.3	34	Acid: < 6 Base: 0	Vasanth et al., (2011)
Kaolin, quartz, calcium carbonate, sodium carbonate, boric acid and sodium metasilicate	Pressing	900	Flat	37.4	2.16	73	-	Emani et al., (2014)
Kaolin	Pressing	950	Flat	30	0.1	60	-	Hedfi et al., (2014)
Kaolin, Feldspar, Quartz, and Saw dust	Pressing	850	Flat	36	0.19	2	-	Bose and Das, (2014)
Kaolin, Feldspar, Saw dust, Sodium metasilicate, and Boric acid	Pressing	850	Tubular	21	0.21	11.68	Acid: < 6 Base: < 6	Bose and Das, (2014)

1.6.2. Fabrication of zeolite-ceramic composite membranes

Increasing evidence shows the use of multi-layer ceramic membranes with α-alumina as support and zeolite as a coating material (layer) to treat oily wastewater and water containing heavy metals, etc. Table 1.4 shows the available literature on fabrication of zeolite-ceramic composite membrane. Zeolite composite membranes offer great potential for gas/liquid separation as compared to their counterparts owing to their uniform and molecular sized channels, superior ion-exchange capacity as well as excellent thermal and mechanical strength (Nabavi et al., 2014; Karakiç et al., 2019). However, the longer synthesis duration and high synthesis temperature are still bottlenecks for their large-scale industrial application (Potdar et al., 2002; Wu et al., 2015). Looking at the advantages associated with zeolite membranes, various types of zeolites such as Hydroxy sodalite, Chabazite, Faujasite, etc., are being used for the purpose of ceramic composite membrane fabrication (Nabavi et al., 2014; Basumatary et al., 2016; Sun et al., 2016).

It is worthy to mention that in the synthesis of zeolite, expensive organic structural directing agent (OSDA), namely N, N, N-trimethyl-1- adamantammonium hydroxide (TMADaOH) (Karakiliç et al., 2019), tetrapropylammonium hydroxide (TPAOH) (Zhu et al. 2015), Tetraethylammonium hydroxide (TEAOH) are being used extensively (Araki et al., 2020). However, these templates should be removed from zeolite and for that purpose, an additional calcination process needs to be carried out. During the process of calcination, toxic gases are released into the environment. Besides, the mandatory calcination step also increases the fabrication cost of zeolite (Liu et al., 2019; Pan et al., 2001). Moreover, it was reported that defects and cracks could occur during the calcination process because of variations in thermal expansion between support and zeolite (Dong et al., 2000). It was reported by Pan et al. (2001) that the separation of hydrogen-hydrocarbon using MFI zeolite membrane made without OSDA was superior as compared to the MFI membranes developed with OSDA. Hence, it can

be concluded that the OSDA-free zeolite not only maximizes the advantages of zeolite membrane, but is also quite environment friendly (Zhang et al., 2020).

From Table 1.4, it is evident that extensive literature on template-free synthesis of NaA zeolite is available. It is worth to mention that the acid resistance of NaA zeolite is poor owing to its high aluminium content compared to other zeolites (Hasegawa et al., 2010). Chabazite (CHA) zeolite is similar to that of NaA zeolite with reduced aluminium content. This feature helps the CHA zeolite to be a potential material for acid resistance (Wu et al., 2015; Hasegawa et al., 2010). The CHA-type zeolite has an interconnected three-dimensional pore structure with stacked sequence of six rings and an aperture size of 0.38 × 0.38 nm. Generally, CHA zeolite is coated on α-alumina support, and these membranes are often used for the application of gas separation (Hasegawa et al., 2010; Wu et al., 2015; Karakiliç et al., 2019). Tubular α-alumina membrane was used as a support to prepare a defect-free CHA zeolite coated ceramic composite membrane for the gas separation application (Karakiliç et al., 2019). For this composite membrane fabrication, the synthesis time and temperature were maintained at 18 h and 160 ^{o}C, respectively.

Table 1.4 Literature summary for the preparation of composite membranes

Support material	Coating material	Membrane Configuration	Coating method	Template	Temperature (°C)	Synthesis time	Application	References
α–Al_2O_3	FAU	Tubular	Secondary growth	-	100	6 h	Pervaporation	Kumakiri et al., (2014)
α–Al_2O_3	NaA	Tubular	Hydrothermal	-	65	6-24 h	Pervaporation	Basak et al., (2014)
α–Al_2O_3	NaA	Hollow fiber	Hydrothermal	-	90	12 h	Heavy metal removal	Zhu et al., (2018)
Mullite	NaA	Tubular	Hydrothermal	-	70-130	1-5.5 h	Pervaporation	Kazemimoghadam et al., (2007)
Pozzolan	NaA	Flat	Hydrothermal	-	60	24 h	Dehydration of ethanol	Achiou et al., (2018)
Kaolin, ball clay, feldspar, quartz, pyrophyllite and calcium carbonate	Analcime	Flat	Hydrothermal	TPAB	180	2-5 days	Gas	Potdar et al., (2002)
α–Al_2O_3	MFI	Tubular	Hydrothermal	TPAOH and TEOS	180	16 h	Desalination	Zhu et al., (2015)
α–Al_2O_3	MFI	Flat	Hydrothermal	TPAOH	180	4 h	-	Dong et al., (2000)
Kaolin, ball clay, feldspar, quartz, pyrophyllite and calcium carbonate	MCM-41	Flat	Hydrothermal	TEOS and CTAB	110	4 days	Cr (VI) separation	Basumatary et al., (2015)

α–Al_2O_3	Silicate-1	Tubular	Hydrothermal	TPAOH, TEOS and CTABr	100	48-72 h	Gas separation	Wang et al., (2014)
α–Al_2O_3	MCM-48	Tubular	Hydrothermal	TEOS and CTAB	100	3 days	-	Wu et al., (2008)
Stainless steel	SAPO-34, ZIF	Tubular	Hydrothermal	TEAOH	220 150	24 h 5 h	Desalination	Duke et al., (2016)
α–Al_2O_3	CHA	Tubular	Hydrothermal	TEAOH	160	36 h	Gas separation	Araki et al., (2020)
α–Al_2O_3	CHA	Tubular	Secondary growth	-	140	18 h	Pervaporation	Hasegawa et al., (2010)
α–Al_2O_3	CHA	Tubular	Seeding followed by Hydrothermal	TMAdaOH	160	18 h	Gas separation	Karakiliç et al., (2019)
α–Al_2O_3	CHA	Flat	In-situ crystallization	TMAdaOH and TEOS	150	40 h	Gas separation	Maghsoudi and Soltanieh, (2014)
Mullite	CHA	Tubular	Secondary growth	TMAdaOH and TEAOH	170	3 days	Gas separation	Wu et al., (2015)

1.6.3. Critical industrial application of ceramic membrane in liquid phase separation

Owing to their resistance against chemicals and higher thermal stability as well as robustness, ceramic membranes have been commonly used for different applications, particularly industrial wastewater treatments such as in food industry (juice and wine), pharmaceutical industry, treatment of wastewater and water, and desalination of seawater (Manni et al., 2020; Luque et al., 2008). The first large-scale commercial success of ceramic membranes has been applied in the food and beverages industries (Issaoui et al., 2019). The specific advantages of ceramic membranes include capability to withstand high temperatures, backwashing pressure and non-swelling during filtration of different solvents (Asif and Zhang, 2021). Therefore, in this section, a succinct overview of ceramic membrane performance is provided, which mainly focuses on the applications of ceramic membrane in water and wastewater treatment.

1.6.3.1. Recovery of microalgae from its broth solution

Microalgae based products are of recent interest owing to their use as a potential feedstock for biofuels and value-added products such as carbohydrates, nutraceuticals, cellulose, starch, proteins, antioxidants, lipids and pigments (carotenoids, lutein, etc.) as well as fertilizer and energy-rich crop with high efficiency towards removal of carbon and nutrients (Ummalyma et al., 2017; Gross et al., 2013; Bilad et al., 2012; Mo et al., 2014). However, the main bottleneck for the commercial application of algal products is algal biomass production as well as its harvesting using low-cost techniques (Singh et al., 2018). It has been estimated that the cost of microalgae harvesting is 20-30% of produced biomass cost and the cost of equipment used for harvesting and dewatering is reported to be 90% of the total production cost of biomass in open ponds (Amer et al., 2011). Therefore, an efficient and cost-effective method for the separation of algae from its broth is key to commercial production and application of microalgae based products (Ummalyma et al., 2017; Gross et al., 2013; Mo et al., 2014). Table 1.5 presents different techniques used for recovery of microalgae.

Table 1.5 Literature summary of different technologies for the separation of algae

Algal species	Techniques	Recovery (%)	Operation Mode	References
All algal species	Centrifugation	99	Batch	Shen yet al., (2009)
R. salina	Flocculation	85-90	Batch	Knuckey et al., (2006)
***Scenedesmus* sp.**	Bio-flocculation	95	Batch	Kim et al., (2011)
***Scenedesmus* sp.**	Filtration PVDF membrane	90	continuous	Chen et al., (2012)
***Chlorella* sp.**	Mixed matrix PVDF membrane	100	continuous	Hwang et al., (2015)
***Euglena* sp.**	PVDF and PSF membranes	100	continuous	Lau et al., (2020)

Conventional techniques, such as centrifugation, flocculation, and coagulation, are well suited for separating algae from highly concentrated broth (Barros et al., 2015; Chen et al., 2012, Lau et al., 2020). These methods, however, involve high cost in terms of energy required to separate algal biomass from dilute broth, which contains less than 0.5 kg/m^3 of dry algal biomass (Olguín, 2012). In addition to the high-energy cost involved, these processes use coagulants or additives for separation, which leads to contamination of the final product, thereby necessitating further steps for purification (Knuckey et al., 2006; Giorno et al., 2013). Besides, these methods are not suited for continuous separation of algae from dilute broth. Hence, recent research is focussed on developing energy-efficient and cost effective methods for continuous harvesting of algae from dilute streams (Hung and Liu, 2006). In this regard, membrane technology is proving to be successful for algae separation, which does not produce any unwanted products during the separation process. Moreover, it is regarded as a clean and simple process, which does not require any addition of coagulants. Chen et al. (2012) employed a hollow fiber PVDF membrane for continuous separation of *Scenedesmus* sp. from its broth

solution and the highest recovery was found to be 90%. The literature study regarding microalgae recovery using membrane filtration revealed that research works carried out primarily used polymeric membranes (see Table 1.5).

1.6.3.2. Efficient recovery of fine TiO_2 particles from suspension

Recently, there have been reports on increased nanoparticles (NPs) production in a large scale due to their potential applications in various industries (Weir et al., 2012; Karlsson et al., 2019). In particular, titanium dioxide (TiO_2) is the most frequently used nanomaterial next to silver in consumer products such as paints, pigments, toothpaste, filters, sunscreens, cosmetics, etc. Due to its broad range of applications, TiO_2 nanoparticles are released into wastewater from industries, thereby bringing issues related to environmental release and human exposure (Olabarrieta et al., 2018). This is particularly important because of the cytotoxic, genotoxic and hemolytic effects of TiO_2 NPs on human erythrocyte and lymphocyte cells (Tang et al., 2019). On the other hand, TiO_2 is also used as a catalyst in the photocatalytic process to treat wastewater owing to its high stability and low cost. It is observed that in the above-mentioned process, the reaction efficiency decreases when the catalyst is reused without separation in consecutive runs (Fujishima et al., 2008; Karlsson et al., 2019). Therefore, TiO_2 recovery is challenging in terms of maintaining a constant catalyst concentration as well as avoiding the wash-out of TiO_2 NPs from the system (Fernández-Ibáñez et al., 2003). The separation of TiO_2 NPs from treated water creates another problem to be solved for the commercial application of the process (Li et al., 2019). These two domains compel the separation of TiO_2 from various industrial effluent as well as photocatalytic reactors. In this context, some investigations have focused on the separation of TiO_2 NPs from constituent solution by conventional techniques such as sedimentation, flocculation and coagulation (Ghimici et al., 2013; Wang et al., 2016). The drawbacks of these techniques are low efficiency, prolonged residence time and limitation with batch operation, i.e., continuous recovery of nanoparticles is not possible. Hence, few

studies have dealt with cost-effective and efficient techniques for continuous recovery of TiO_2 NPs from suspension. Weimin et al. (2001) investigated various parameters that affect the recovery of TiO_2 from photocatalytically treated water using polypropylene membrane and the strong influence due to pH indicated the importance of interfacial phenomenon in microfiltration. A complete recovery could be possible owing to the small pore size (0.2 µm) of the membrane than the TiO_2 particles (14 µm) in suspension. Zhao et al. (2002) recovered fine TiO_2 particles (2.89 µm) from acid wastestreams using α-alumina membranes of pore diameters 1 and 0.2 µm and examined the fouling mechanisms involved for regeneration and reuse of the membrane. Ceramic membranes are generally fabricated using metal oxides such as alumina, zirconia, silica and titania (Malmali et al., 2018). The inclusion of these ceramic membranes in industrial processes is limited owing to their high cost associated with raw materials used and processing temperatures (1300 – 1500 ^oC) (Goswami and Pugazhenthi, 2020b). Table 1.6 represents the summary of literature available regarding recovery of TiO_2 nanoparticles from wastewater.

Table 1.6 Summary of available literature regarding TiO_2 separation using different techniques

Technique	Material	Pore size	Feed concentration (mg/L)	Recovery (%)	References
Flocculation	Synthesized cationic polysaccharides	NA	50	50	Ghimici et al., (2013)
Coagulation	PFS, PACl, $FeCl_3$ and alum	NA	30	77	Wang et al., (2001)
Encapsulation followed by adsorption	Lecithin liposomes, Poly (L-Lysine)	NA	1000	58	Taylor et al., (2020)
Cross flow Ultrafiltration	Cellulose acetate	MWCO-30,000 Da	500	-	Lee et al., (2001)
Cross flow microfiltration	α - alumina membrane	0.2 µm	60-80	100	Zhao et al. (2002)
Cross flow microfiltration	Polypropylene (PP)	0.2 µm	500	100	Weimin et al., (2001)

*NA-Not Applicable

1.6.3.3. Produced water treatment

In oil and gas exploration, produced water (PW) is the main wastewater stream from both onshore and offshore wells (Alammar et al., 2020). It consists of a complex mixture of suspended and dissolved hydrocarbons, heavy metals, salts, and production chemicals (Jiménez et al., 2018). Physico-chemical characteristics of PW depend on both well and reservoir's lifetime (Fakhru'l-Razi et al., 2009; Ebrahimi et al., 2010). The amount of PW generated from oil and gas exploration is 39.5 million m^3/day, which is around 3/4th in terms of water to oil ratio (Abdel-Shafy et al., 2020). Disposal, reinjection, and reuse are the common management strategies for handling the produced water. Reusing PW in the process of oil and gas extraction is advantageous as it lowers the PW disposal into the environment. However, PW cannot be directly utilized for reinjection due to its high concentration of oil and total suspended solids (TSS), which need to be reduced to 40 mg/L and 10 mg/L, respectively, in order to avoid plugging and pump damage during the process (Zsirai et al., 2016; Jiménez et al., 2018). According to environment (protection) rules framed by Central Pollution Control Board, Government of India (1992), the chemical oxygen demand (COD) concentration in the treated wastewater should be less than 250 mg/L prior to disposal into surface water (Central Pollution Control Board, Government of India). Currently, less than 1% of total volume of PW has been utilized for reuse purposes from upstream and downstream processes of oil and gas exploration (Kusworo et al., 2018). Therefore, developing a low-cost technique for the removal of suspended solids and oil from PW is crucial to meet the required standard for its safe discharge and reuse purposes. Gas floatation, adsorption, and hydrocyclones are conventionally followed to remove dispersed oil at high concentrations (Fakhru'l-Razi et al., 2009, Al-Ghouti et al., 2019). However, efficiency of these techniques decreases when the oil droplet size is less than 10 µm (Ebrahimi et al., 2010; Ali et al., 2018). Biological methods for treating PW using microalgae, fungi, and bacteria in aerobic and anaerobic systems are beneficial due to low-cost and less energy requirements (Lu et al., 2009). However, at high oil

concentration, biological methods fail due to biomass growth inhibition (Al-Ghouti et al., 2019).

There is an increase in evidence revealing that membrane separation processes play a vital role in PW treatment, owing to high treatment efficiency, ease of operation, less corrosion issues, and easy scaling up (Kusworo et al., 2018, Ali et al., 2018). Depending on reservoir characteristics, produced water may have oil and grease concentrations between 2 to 565 mg/L, salinity or salt concentration ranging from 1000 to 250,000 mg/L, pH ranging from 2.60 to 10.20 and temperatures up to 92 ^{o}C (Weschenfelder et al., 2015a). The oilfield-produced water at the feed temperature of 60 ^{o}C was pre-treated using 0.1 µm pore-size α-alumina ceramic microfiltration membrane by Ebrahimi et al. (2010) and reported a maximum TOC removal efficiency of 38%. The oilfield produced water containing high salinity (98,800 mg/L) was successfully treated using ZrO_2 ceramic membrane with a mean pore size of 0.10 µm in a pilot scale study and found that the permeate was completely free of suspended solids (Weschenfelder et al., 2015b). All these literature reports clearly reveal that ceramic membranes are efficient to treat produced water due to their high thermal and chemical stability (Ebrahimi et al., 2010; Weschenfelder et al., 2015a). Several researchers have used a combined process involving membrane filtration and other processes for the complete removal of organic matter from PW (Abdel-Shafy et al., 2020; Kusworo et al., 2018; Riley et al., 2016). For instance, Campos et al. (2002) reported the application of a combined system consisting of microfiltration with polymeric membrane and airlift bioreactor for the treatment of PW. The hybrid system showed 80% and 65% removal efficiency for TOC and COD, respectively. A hybrid membrane biosystem reported by Riley et al. (2016) successfully removed more than 99% organic matter and 94% TDS from PW. Table 1.7 reports the literature on produced water treatment using various combined techniques.

Table 1.7 Available literature on the treatment of produced water using various combined techniques

Techniques	Membrane	Wastewater	Pore size (µm)	Feed concentration (mg/L)	Removal efficiency (%)	References
Integrated adsorption with microfiltration	Cellulose acetate	Petroleum produced water	0.20	**COD:** 7110	54.3	Abdel-Shafy et al., (2020)
Integrated adsorption and double stage membrane process	Nanohybrid PES–nano silica	Original produced water (Indonesia)	0.002	**COD:** 150	76	Kusworo et al., (2018)
Functionalization of alumina ceramic microfiltration	α- alumina	Petroleum produced water (Utah, USA)	0.22	**TOC:** 356	99.6	Maguire-Boyle et al., (2017)
Ceramic membrane filtration	α- alumina and TiO_2	Oilfield produced water	0.20	**TOC:** 200-2000	38	Ebrahimi et al., (2010)
Combined microfiltration followed by biological treatment	Mixed cellulose ester (MCF)	Offshore oilfield wastewater (brazil)	0.10	**TOC:** 386	85	Campos et al., (2002)

1.6.3.4. Heavy metals separation from aqueous solution

Water is a vital requirement for all living beings existing on this earth, and hence, it must be managed carefully. Rapid urbanization and industrialization over the past few years has drastically increased the contamination level in water. Besides, over exploration of ground water has led to the decreased water table in many areas, thus severely affecting not only human lives, but also the entire ecosystem (Sunil et al., 2018; Carolin et al., 2017; Min et al., 2021). Excessive level of heavy metals in water can be the cause of some serious health hazards. Table 1.8 displays the available literature on different heavy metals separation using various membranes. Among various heavy metal ions found to be present in drinking water, cadmium (Cd^{2+}) is considered as one of the most hazardous ions, even if present in extremely low quantities (Chauvin et al., 2019; Awual 2019). It is a non-essential element to mankind and is also non-biodegradable in nature. However, owing to its high solubility in water, it is easily

bio-accumulated and, thus, moves to the food chain (Shahat et al., 2021; Murthy et al., 2009). It is worth to mention that the Itai-Itai sickness, which severely affected the population of Japan in the 1960s, was caused due to consumption of cadmium contaminated water leading to bone softening and fractures in humans (Carolin et al., 2017). Their accumulation in human can be the cause of kidney failure, bone damage and some other serious illnesses (Sgarlata et al., 2008). Furthermore, another heavy metal, nickel can also induce different diseases in people such as pulmonary fibrosis, contact dermatitis and even cancer (Min et al., 2021). It is found in literature that heavy metals are released into the environment mostly through wastewater discharge. The major sources for these heavy metals are the effluents coming from industries such as paint, mining, dye, plastic, etc., nuclear reactor control rods, electronic waste such as mobile phones, batteries, jewellery, coins, computer circuit boards, just to name a few (Awual 2013; Carolin et al., 2017). According to World Health Organization (WHO), the permissible limit for Cd and Ni in drinking water is 3 - 5 µg/L and 0.1 mg/L, respectively (Gumpu et al., 2015; Sharififard et al., 2018; Maher et al., 2014). Similarly, the effluent discharge limit for Cd and Ni to the marine environment is fixed as 2 mg/L and 5 mg/L, respectively (Central Pollution Control Board, Government of India). Hence, it is utmost necessary to remove these heavy metals from wastewater before discharging them into the environment.

Literature on other metal ions separation, such as aluminium and magnesium, is limited. Aluminium is an abundant metal, found commonly in different in-home equipment. Owing to its widespread use, aluminium generates a considerable quantity of waste (Purwanti et al., 2019). However, Aluminium recycling consists of a series of processes that generate many by-products along with huge quantities of wastewater (Kurniawan et al., 2018). Also, in aluminium based constructed wet lands (Al-CWs), Al release was more and the general guideline according to WHO permissible limit in drinking water is 0.2 mg/L (Babatunde et al., 2011). Aluminium contamination may be the cause of changed color of groundwater, decreased soil

fertility and acute toxicity in contaminated ponds (Purwanti et al., 2019; Slaninova et al., 2014). Like Aluminium, drinking water may contain other metal ions such as calcium, magnesium, etc. High concentrations of calcium and magnesium salts in water symbolize effluents from urban wastewater treatment plants, which ultimately contribute to the hardness of water (Dudziak and Kudlek, 2019).

Cerium (Ce), the most abundant element in the rare earth metals family, is widely used in various fields. The extensive use of cerium can be seen in chemical engineering, metallurgy, nuclear energy, catalysis, agriculture, and microelectronics (Ren et al., 2018; Vijayaraghavan et al., 2010). Ce is often discharged directly into the environment from the aforementioned industries, causing adverse impacts on reproductive and nervous system activities in aquatic animals (Siciliano et al., 2021). As this hazardous substance accumulates in soil and water, its concentration in the human body also rises (Dashtian et al., 2017). Siciliano et al. (2021) reported that Ce compounds inhibit the growth of unicellular green algae by suppressing their photosynthesis reaction. Shahnaz et al. (2022) investigated the acute toxicity of Ce in fish (*Danio rerio*) and reported 100% mortality after 48 hours of Ce(III) exposure at the maximum dosage of 5 mg/L.

To keep a check on water contamination, many conventional technologies have been used over the years to remove metal ions from wastewater. However, owing to various disadvantages associated with these technologies, membrane filtration is receiving much more recognition from researchers. Indeed, in recent times, membrane separation has become the key component in separation and purification processes (Sunil et al., 2018). Because of their high separation efficiency, membrane processes are regarded as an environmentally clean technology for removing a wide range of hazardous contaminants without creating additional pollution (Jamil et al., 2018).

It has been found that use of various nanofiltration and reverse osmosis membranes for the separation of metal ions is well documented in literature (Gao et al., 2016). However, in reality, use of reverse osmosis membranes adds cost to the whole separation process, making the process unaffordable for the weaker sections of society. Though nanofiltration membranes (membrane with pore size ~1 nm and surface charge) improves process economics by performing similar separation at a lower pressure than reverse osmosis, the flux produced by nanofiltration membranes are also quite lesser than the ultrafiltration membranes (Chowdhury et al., 2021; Shukla et al., 2005; Shon et al., 2013). Polymeric composite membranes using polyethylene sulfone, poly vinyl chloride and polyethyleneimine, etc., were used for the separation of different heavy metals (Zhang et al., 2015; Gong et al., 2020; Zhou et al., 2019). Gao et al. (2016) employed a modified polyethylene sulfone nanofiltration composite membrane for cadmium removal from an aqueous solution and observed a maximum permeability of 4.83×10^{-9} m^3/m^2 h kPa with 94% removal efficiency. A positively charged ultrafiltration membrane was developed by Zhou et al. (2019) using poly (vinyl chloride *co* dimethylaminoethyl methacrylate) to remove cadmium from an aqueous solution. A maximum permeability of 233×10^{-9} m^3/m^2 h kPa along with 95.5% removal efficiency was obtained. Therefore, use of ultrafiltration membranes can be considered as a great alternative to achieve metal ion separation from their solutions. Table 1.8 shows available literature for heavy metals separation from water.

Table 1.8 Summary of literature on different metal ion separation using various membranes

Technology	Membrane	Pore size (nm)	Pure water permeability (m^3/m^2 s kPa)×10^{-9}	Heavy metal	Conditions	Rejection (%)	References
Nanofiltration	Chitosan/PES composite membrane	0.347	9.58	Ni	**C_f**: 1000 mg/L **P**: 1000 kPa	96.3	Zhang et al., (2015a)
Nanofiltration	Kraton matrimid composite membrane		6.67	Cd Ni	**C_f**: 1000 mg/L	>98 >98	Thong et al., (2014)
Nanofiltration	PEI/TMC/P84	-	4.83	Cd	**C_f**: 1000 mg/L **P**: 500 kPa	94	Gao et al., (2016)
Nanofiltration	MOFs/PEI/TMA composite membrane	1.5-2.2	33.88	Ni	**C_f**: 1000 mg/L **P**: 400 kPa	90.9	Gong et al., (2020)
Nanofiltration	HPEI modified GO cross linking EDA	-	13.91	Ni Cd	**C_f**: 1000 mg/L **P**: 100 kPa	96 90.5	Zhang et al., (2015b)
Ultrafiltration	P(VC-*co*-DMA)	3.27	233	Cd	**C_f**: 10 mg/L	95.5	Zhou et al., (2019)
Ultrafiltration	PEI PEUF	-		Cd	**C_f**: 1000 mg/L **P**: 300 kPa	73	Hebbar et al., (2016)
Ultrafiltration	γ - Al_2O_3 composite membrane	5.4-13.6	236	Al Mg	**C_f**: 3000 mg/L	88 72	Majhi et al., (2009)
Ultrafiltration	GO/Al_2O_3 composite membrane	430	17.5	Cd	**C_f**: 100 mg/L	100	Liu et al., (2019)

1.6.4. Fouling and cleaning of ceramic membrane

Despite various advantages associated with the membrane process, fouling is a major issue due to particle deposition and cake layer formation on the membrane surface (Lee and Kim, 2014). This results in reduced permeate flux, high operating and maintenance cost. However, ceramic membranes are reported to have less fouling propensity and irreversible fouling in comparison with polymeric membranes (Li et al., 2020; Lee and Kim, 2014). The fouling of ceramic membranes can be analyzed using various filtration models, namely resistance-in-series model and pore blocking models, etc. (Yang et al., 2017; Zhang et al., 2012). In addition to low fouling tendency, aggressive cleaning methods that don't affect the membrane longevity can reduce cleaning time and irreversible fouling for ceramic membranes. Therefore, cleaning the fouled membrane after a certain point of operation is necessary to attain original membrane performance (original permeate flux) during the filtration process. Generally, the fouled membrane is periodically cleaned by physical cleaning (rinse and backwash) or chemical cleaning and both. In the chemical cleaning of fouled membranes, two sequential steps take place: (i) chemical reaction between the cleansing agent and the foulants in the fouling layer and (ii) mass transfer of the foulants from the fouling layer to the bulk solution. The chemical reactivity of the cleansing agent strongly influences the cleaning effectiveness because the second step of mass transfer can occur only when the chemical reaction destabilizes the foulant-foulant interactions (Chakrabarty et al., 2010). As reported in several research articles, effective cleansing agents can considerably reduce the foulant-foulant adhesion forces that bear the structural integrity of the fouling layer on the membrane surface (Chakrabarty et al., 2010; Zhang et al., 2019; Al-Amoudi and Lovitt, 2007). Thus the choice of cleansing agents that exhibit favorable reactions with the fouling substances is crucial. The cleansing agents must be able to dissolve most of the precipitated materials and remove them from the surface of the membrane with no surface damage (Al-Amoudi and

Lovitt, 2007). Various commercially available cleansing agents, categorized into six groups such as surfactants, oxidation agents, enzymes, acids, metal chelating agents, and alkalis, were used to clean fouled membranes (Zhang et al., 2019; Al-Amoudi and Lovitt, 2007). Concentration, pH, applied pressure, cross-flow velocity, temperature, and duration of treatment have been identified as important factors for cleaning of fouled membranes during microfiltration (Chen et al., 2015; Mendoza-Roca et al., 2010). Furthermore, cost-effective and suitable chemical cleansing agents that are safe to use and which, do not affect the membrane porosity and pore size, and do not produce new foulants are highly desired (Garmsiri et al., 2010, Abadi et al., 2011, Abdalla et al., 2019, Wang et al., 2022). Abadi et al. (2011) used a tubular α-alumina membrane with a mean pore size of 0.20 µm for the treatment of oily wastewater and the fouled membrane was efficiently cleaned using 2 wt% sodium hydroxide (NaOH) solution at 70-80 ^{o}C. The cleaning of 0.45 µm pore size ZrO_2-TiO_2 ceramic membrane after microfiltration of oily wastewater was done by flushing with water and then dipping the membrane in 2 wt% NaOH solution at 80 ^{o}C for 30 min, followed by rinsing with water and a similar soak at 80 ^{o}C for 30 min in 0.50 % nitric acid solution (Abdalla et al., 2019). Another study reported a maximum cleaning efficiency of 33 % when the ceramic membrane (0.20 µm) was cleaned using 1 wt% NaOH solution after PW treatment (Ebrahimi et al., 2010). Mendoza-Roca et al. (2010) investigated the cleaning efficiency of membranes contaminated by tannery effluent using various cleansing agents, namely sodium hypochlorite (0.75 to 1 g/L), sodium dodecyl sulfate (0.50-2.00 %), and two separate enzymes (1-10 g/L). They found a maximum flux recovery of 92 % when the membrane was cleaned with 1 g/L sodium hypochlorite. Chen et al. (2015) reported a maximum pure water flux recovery of 77 % for the membranes cleaned using a mixed solution containing NaOH (1 wt%) and sodium dodecylbenzene sulfonate (0.10 wt%).

1.7. Outcome from literature review

Though ceramic membranes offer distinguished advantages compared to polymer membranes, they are expensive due to the utilization of costly metal oxides (alumina, zirconia and titania, etc.) as starting materials. Besides, these membranes need high sintering temperatures (>1200 ^{o}C), which limit their industrial scale usage. Hence, there is a necessity to fabricate low-cost tubular ceramic membranes from inexpensive sources. Even though many researchers have been working on the development of low-cost ceramic membranes using naturally available clays, fabrication of membranes with better characteristics at low sintering temperature is a challenging task.

As evident from literature review, organic binders are vital for improving the properties of ceramic membranes. Three organic binders, namely guar gum (GG), hydroxypropyl methylcellulose (HPMC) and carboxymethylcellulose (CMC), are easily water soluble at room temperature (25 ^{o}C) and do not require the addition of any dispersing agents for the production of ceramic membrane. Moreover, these binders are biocompatible and biodegradable. Guar gum is a naturally available and highly water-soluble polysaccharide, which imparts high viscosity even at a low concentration. High viscosity is also desirable for providing strength to the membrane. On the other hand, a low concentration of such binders ensures a high ceramic solid loading, which reduces the probability of occurrence of defects, particularly during shrinkage (Elbadawi et al., 2017). Despite many advantages, including high water solubility, biocompatibility, biodegradability and requirement of very low concentration, these binders have not been tested for manufacturing kaolin based tubular ceramic membranes.

In the synthesis of zeolite, use of expensive organic structural directing agent (OSDA) requires calcination step to remove the template from zeolite. This mandatory calcination step increases the fabrication cost of zeolite. High synthesis temperature and longer synthesis duration limit the use of zeolite membranes in various industrial processes. It is evident from the literature

review that CHA zeolite is often coated on α-alumina support and these membranes are used for the application of gas separation. Hence, the preparation of inexpensive supported zeolite membranes without using organic template for the liquid phase separation applications can be explored.

The extensive literature review carried out regarding the separation of microalgae from its broth solution reveals that conventional techniques are primarily used for separation. In processes like flocculation and coagulation, coagulants or additives are used for separation, which leads to contamination of the final product, thereby necessitating further steps for purification. Moreover, in case of separating the low biomass concentration of microalgae (0.5 kg/m^3), use of microfiltration membranes is recommended owing to the high separation efficiency and continuous separation of algae. Regarding separation of microalgae from its broth solution, low-cost ceramic membranes can be recommended as they affect the harvesting cost in large-scale applications. Similar is the case for the separation of TiO_2 nanoparticles and treatment of produced water. Hence, the aforementioned three liquid phase separation using kaolin based low-cost ceramic membranes will be targeted as a part of this research work. Further, the available research on the use of membrane filtration in removing heavy metals (cerium, cadmium, nickel) from wastewater shows mainly the application of polymeric membranes.

1.8.Objectives of the thesis

Based on the literature gap, the following objectives were addressed in the thesis.

- Fabrication and characterization of low-cost tubular ceramic membrane using inexpensive clays as the raw materials along with different binders
- Performance evaluation of developed kaolin based tubular ceramic membrane for various liquid phase separation processes, namely, recovery of microalgae from its

broth solution, TiO_2 nanoparticles separation from its suspension and onshore oilfield produced water treatment.

- Facile synthesis of OSDA-free CHA zeolite coated ceramic composite membrane using hydrothermal method
- Continuous removal of heavy metals from aqueous solution using zeolite-ceramic composite membrane

1.9. Thesis outline

The doctoral thesis was organized into six chapters

Chapter 1: **Introduction, Literature review and Objectives**

This chapter elaborates on the introduction of membrane technology and its footprint in water and wastewater treatment. This chapter also covers a detailed review of the literature on various sources to fabricate ceramic membranes and zeolite ceramic composite membranes. Thereafter, the research gap and objectives of this work framed by using kaolin as a key precursor for the fabrication of low-cost ceramic membranes are presented in this chapter.

Chapter 2: **Preparation and characterization of kaolin based tubular ceramic membrane**

Membrane cost has been identified as a key factor in determining the total cost of membrane separation processes. Therefore, tubular ceramic membranes were fabricated using inexpensive precursors, including kaolin, $CaCO_3$ and quartz with different organic binders by extrusion method. Characteristics of kaolin based tubular ceramic membranes prepared with different organic additives such as guar gum (GG), sodium salt of carboxymethyl cellulose (CMC) and hydroxypropyl methylcellulose (HPMC) were compared in this chapter. The raw materials and prepared membranes were characterized using various standard techniques such as X-ray fluorescence analysis, X-Ray Diffraction analysis, Field Emission Scanning Electron Microscope and Thermogravimetric analysis. The average pore size, pure water permeability,

porosity, mechanical strength and chemical stability of the fabricated membranes were evaluated. Finally, the estimation of production cost of the membrane was presented based on raw materials, energy consumption, manpower and equipment cost.

Chapter 3: Application of kaolin based ceramic membrane for liquid phase separation

This chapter discusses the application of indigenous tubular ceramic membrane for harvesting of microalgae, TiO_2 separation from aqueous suspension and produced water treatment. In case of microalgae separation, characterization of microalgae, effect of applied pressure on permeate flux and recovery, influence of additive on volume reduction factor, and extracellular protein and carbohydrate analysis for the collected permeate, fouling mechanism by different pore blocking models were analysed. The effect of applied pressure, cross flow velocity, feed concentration and pH were investigated to check the TiO_2 separation efficiency of kaolin-HPMC membrane. In order to understand the fouling mechanism, Hermia pore blocking models were applied. In case of produced water treatment, experiments were carried out using combined microfiltration and biological processes. The effect of applied pressure on permeate flux, regeneration of fouled membrane using various cleaning agents, and toxicity assessment of best-treated water were examined.

Chapter 4: Facile synthesis of OSDA-free chabazite zeolite coated kaolin ceramic membrane

This chapter discusses the preparation of chabazite zeolite-based ceramic composite membrane by hydrothermal method. In order to find the optimum coating method, different types of coating strategies were employed by coating only on inner surface, only on outer surface and both sides of the membrane. The synthesized zeolite was subjected to X-ray diffraction, fourier transform infrared spectroscopy, thermogravimetric analysis, field emission scanning electron microscope, field emission transmission electron microscope, and surface area analysis. Also,

the fabricated membranes were characterized through field emission scanning electron microscope, porosity, water permeability and pore size measurements. Finally, the estimation of fabrication cost of composite membrane was presented based on raw materials, energy consumption, manpower and equipment cost.

Chapter 5: Continuous removal of heavy metals from aqueous solution using zeolite-ceramic composite membrane

This chapter explicitly describes the application of CHA type zeolite-ceramic composite membrane for the separation of cerium and cadmium from its solution. The influence of applied pressure, feed concentration and feed pH were studied for the separation of cerium. In case of cadmium separation, the effect of applied pressure, feed pH and nature of anions on permeate flux and cadmium rejection were investigated. The present study also aims at the separation of various metal ions from aqueous solutions with binary and tertiary salt mixtures along with the single salted solutions.

Chapter 6: Overall conclusions and Recommendations for future work

This chapter summarizes the overall conclusions from this work. This chapter also provides some useful recommendations for future research.

Chapter 2

Preparation and characterization of kaolin based tubular ceramic membrane

Preparation and characterization of kaolin based tubular ceramic membrane

This chapter discusses the detailed discussion about fabrication of tubular ceramic membrane derived from inexpensive clay kaolin as a major component along with quartz and calcium carbonate. Three different binders, namely guar gum (GG), hydroxypropyl methylcellulose (HPMC), sodium salt of carboxymethylcellulose (CMC), were employed for the fabrication of membranes. All the membranes were characterized using standard methods and techniques. Based on the membrane properties, the optimized membrane was selected for further microfiltration operations.

2.1. Materials

The selection of raw materials is a crucial step for the fabrication of membranes. The significance behind the chosen materials is displayed in Table 2.1. The raw materials utilized for the preparation of tubular ceramic membranes, viz. kaolin and quartz, were obtained in proximity to Kanpur, India. Calcium carbonate, CMC, GG, sodium hydroxide, hydrochloric acid (0.1 mol/L) were obtained from Merck (I) Ltd., Mumbai. HPMC was supplied by N. Shashikant & Co (India). Water required for preparing the binder solutions was collected from Millipore (Elix-3) system.

Table 2.1 Significance of the raw materials used in this study.

Raw material	Significance	References
Kaolin	Contributes low plasticity and high refractory to membrane	Hubadillah et al., (2018)
Quartz	Provides mechanical and thermal strength	Hedfi et al., (2014)
Calcium carbonate	Pore former	Harinkhere et al., (2022)
CMC/ GG/ HPMC	Act as a binder	Falamaki et al., (2006) Elbadawi et al., (2017)

2.2. Fabrication of tubular ceramic membrane

Kaolin-based tubular ceramic membranes with the dimensions of 100 mm length, 11.5 mm outer diameter and 5.5 mm inner diameter were prepared by extrusion technique. The raw material composition (50 wt% kaolin, 25 wt% $CaCO_3$, 25 wt% quartz) used for the fabrication of tubular ceramic membrane was chosen based on our previous work (Vasanth et al., 2011; Singh et al., 2020). In this study, the effect of three different binders (3 wt% aqueous solutions) viz. CMC, GG and HPMC on characteristics of a tubular ceramic membrane was examined. For this, kaolin, quartz and calcium carbonate were exactly weighed based on the composition. After uniform mixing of the basic components with the binder solution, the prepared paste was fed into a tabletop horizontal extruder machine (M/s VB Ceramic Consultants, India) to get a tubular shaped membrane. A stainless steel die was used to manufacture membrane tube with dimensions of 11.5 mm and 5.5 mm of outer and inner diameters. In the case of membrane without any binder, the raw materials were mixed with Millipore water devoid of any binder were prepared to get the paste for extrusion. A series of controlled thermal treatment steps were followed in order to avoid any bend and micro-cracks in the membrane. Firstly, the green membrane was dried at room temperature for 12 h, which was followed by drying at 100 °C and 200 °C in a hot air oven for 12 h each. Further, the membrane was sintered at 950 °C for 6 h in a programmable furnace (M/s VB Ceramic Consultants, India) with a slow heating rate of 0.5 °C per min. After sintering, the furnace was switched off and the membrane was allowed to cool down under ambient room temperature. Both ends of the membrane were smoothened using abrasive paper (C-220) to get 100 mm length. Finally, the membrane was cleaned with water in an ultrasonication bath to remove any loose particles from the membrane and the wet membrane was dried at 100 °C for 12 h and taken for further characterization. The fabricated membranes were named as follows: Kaolin (without additive), Kaolin-CMC (CMC additive), Kaolin-GG (Guar Gum additive) and Kaolin-HPMC (HPMC additive). The entire steps

involved in the fabrication of tubular membrane are depicted in Fig. 2.1. The extruder machine and prepared membrane are shown in Fig. 2.2.

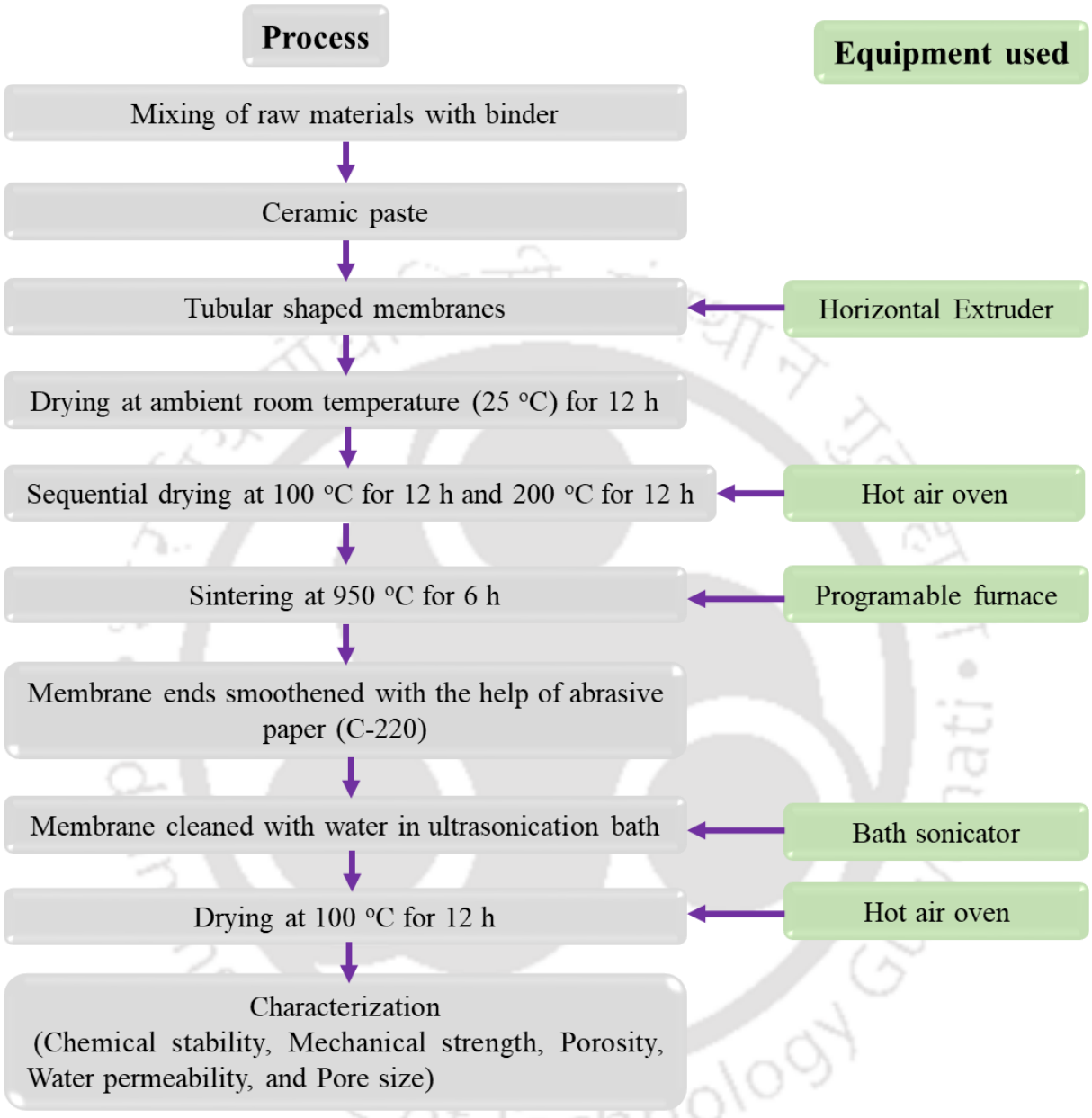

Fig. 2.1 A schematic showing the steps involved in the preparation of tubular ceramic membrane

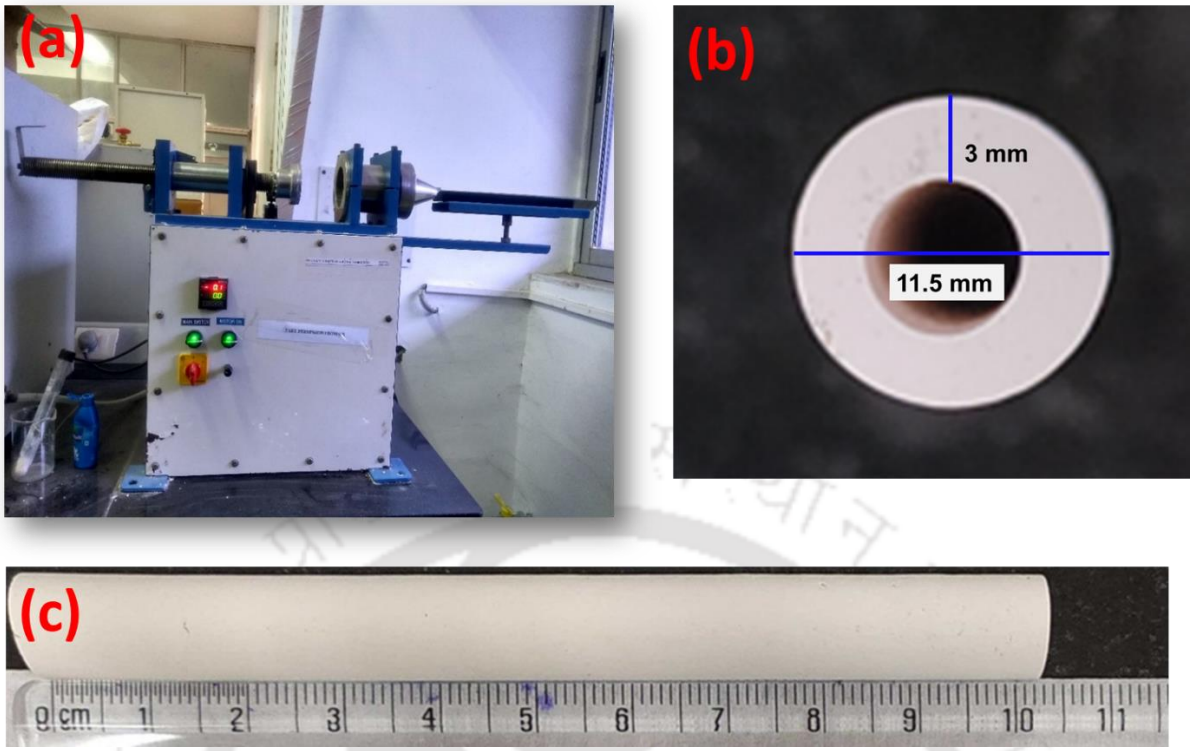

Fig. 2.2 Photograph showing (a) horizontal extruder machine used in this study (b) cross-sectional view of the membrane and (c) fabricated membrane

2.3. Characterization techniques

2.3.1. X-ray fluorescence analysis

X-ray fluorescence (Model: Axios FAST Make: Panalytical) analysis of two clay materials (kaolin and quartz) was performed with boric acid pellets to study their chemical composition. For this analysis, 1 g of sample was mixed with 0.5 g of boric acid and the mixture was pressed in a hydraulic press at 40 kN to make the pellet.

2.3.2. X-ray diffraction analysis

Phase identification of the raw materials (kaolin, quartz and $CaCO_3$), sintered and unsintered membranes were assessed using X-ray diffractometer (Bruker AXS, Netherlands) with Cu Kα radiation source. The operational current and voltage used for analysis were 40 mA and 40 kV, respectively. Measurements were carried out in the 2θ ranges from 1 to 80 with a step size of 0.05 ^{o}/s.

2.3.3. Thermogravimetric analysis

In order to identify the appropriate sintering temperature and thermal stability of the ceramic membranes, thermogravimetric analysis of green membranes (non-calcined) was performed using TGA/DTG instrument (Model: STA449F3A00, Make: Netzsch) under air atmosphere. For this analysis, samples were placed in a platinum crucible of volume 150 µL, and the temperature was steadily raised from 20 to 1000 ^{o}C with a heating rate of 10 ^{o}C/min.

2.3.4. Morphological analysis

Field emission scanning electron microscope (Model: Sigma 300, Make: Zeiss) was used to analyse the morphology of the membrane (inner and outer surface) and any defects on its surfaces. A small portion of the membrane was cut and fixed on the top of a stud with the help of double-sided carbon tape, followed by gold coating of the sample using an auto fine coating instrument to impart conductivity.

2.3.5. Chemical stability

Membrane corrosion tests are generally performed in harsh acidic and basic environmental conditions in order to evaluate their chemical stability in terms of percentage weight loss. Chemical stability of membranes in this study was estimated by measuring the difference in their weight before and after the corrosion resistance test. The test was conducted by placing the membranes individually in basic (NaOH; pH = 13.3) as well as in acidic (HCl; pH = 1.4) solution for 7 days. After one week, these membranes were taken out of the acidic or basic solutions, washed with water, dried in a hot air oven, and weight of the dried membranes was measured. Subsequently, weight loss of the membrane was calculated using the following equation (2.1) (Kumar et al., 2015b):

$$\text{weight loss } (\%) = \frac{W_i - W_f}{W_i} \times 100 \qquad (2.1)$$

Where W_i is the initial dry weight of the membrane (g) and W_f is the final dry weight of the membrane (g) after its suspension in the respective solution.

2.3.6. Mechanical strength

Mechanical stability test of the membranes was conducted to evaluate their strength in terms of compressive strength, for which Universal Testing Machine (UTM) (Model MEDIAN 250, BISS) was used. The membranes were cut in the dimensions of 20 × 11.5 × 5.5 mm according to the ASTM C1424-99 standard, placed inside a support, and then the load (25 KN) was applied vertically till cracks were observed in the membrane. The following expression was used to estimate the compressive strength of all the prepared membranes.

$$\text{Compressive strength (MPa)} = \frac{\textit{Applied load in KN}}{\text{Cross sectional area of the sample } (m^2)} \quad (2.2)$$

2.3.7. Porosity

Archimedes' principle was used to calculate the porosity of the membrane. To determine the porosity of membranes, the membranes were dipped in Millipore water for 24 h. After taking the membrane out of the water and removing excess water from its surface with tissue paper, its final wet weight (W_{wet}) was measured. Then the wet membranes were dried at 120 ^{o}C for 3 h and weighed to get the dry weight (W_{dry}). Finally, the porosity of the membrane was calculated by substituting the values of wet weight (W_{wet}), dry weight (W_{dry}), total volume of the membrane (V_m) and density of water (ρ_w) in the following expression (2.3) (Kumar et al., 2015b):

$$\text{Porosity (\%)} = \frac{W_{wet} - W_{dry}}{V_m \times \rho_w} \times 100 \quad (2.3)$$

All these quantitative experiments (porosity, chemical stability and mechanical strength) were carried out with at least five samples and mean values were reported with standard deviation as final results in this study.

2.3.8. Pure water flux and pore size measurement

Schematic of in-house made cross-flow microfiltration setup is depicted in Fig. 2.3. A lab-scale microfiltration setup was developed by connecting feed tank, dampener, pump, pressure

indicator, membrane module with the tubular arrangement, rotameter and control valves. The feed was supplied to the membrane module by a circulation pump from the feed tank. A lab-scale membrane module for placing a single membrane was constructed using 316 stainless steel (316 SS). For pure water flux measurement, the membrane was placed horizontally inside the membrane module (Fig. 2.3) to get an active filtration area of 17.27×10^{-4} m^2. The applied pressure was regulated by using the control valve connected at by-pass. The flow rate inside the membrane was maintained with a control valve installed on the retentate side. Membranes were compacted prior to the actual experiments by subjecting them to a higher applied pressure. In addition to this, water flux measurements were carried out once the steady-state was reached. The permeate through the ceramic membrane was collected from bottom port of the module and its weight was determined at different intervals using an electronic balance. The permeate sample was collected at an equal time interval upto1 h with various applied pressures and a constant crossflow rate of 6.42×10^{-3} m/s. The water flux (J_{pw}) was measured by substituting volume of permeate (V), active filtration area (A: 17.27×10^{-4} m^2) and time (t), in the following equation (2.4). Pure water permeability was measured using Darcy's law (2.5) by observing permeate flux at different applied pressures. The average pore size of the prepared membranes was then evaluated using Hagen-Poiseuille equation (equation 2.6) (Jana et al., 2010)

$$J_{pw} = \frac{V}{A\times t} \tag{2.4}$$

$$J_{pw} = L_h \times \Delta P \tag{2.5}$$

$$r = \left(\frac{8\mu_w \tau l L_h}{\varepsilon}\right)^{\frac{1}{2}} \tag{2.6}$$

Here, r, ε, L_h and l represent pore radius, membrane porosity, pure water permeability and pore length across the membrane thickness, respectively (assuming that the membrane has continuous pores throughout its cross section). While the symbol τ stands for membrane tortuosity (typically used as 1) (Kumar et al., 2015b), μ_w represents the viscosity of water at room temperature (Jana et al., 2010).

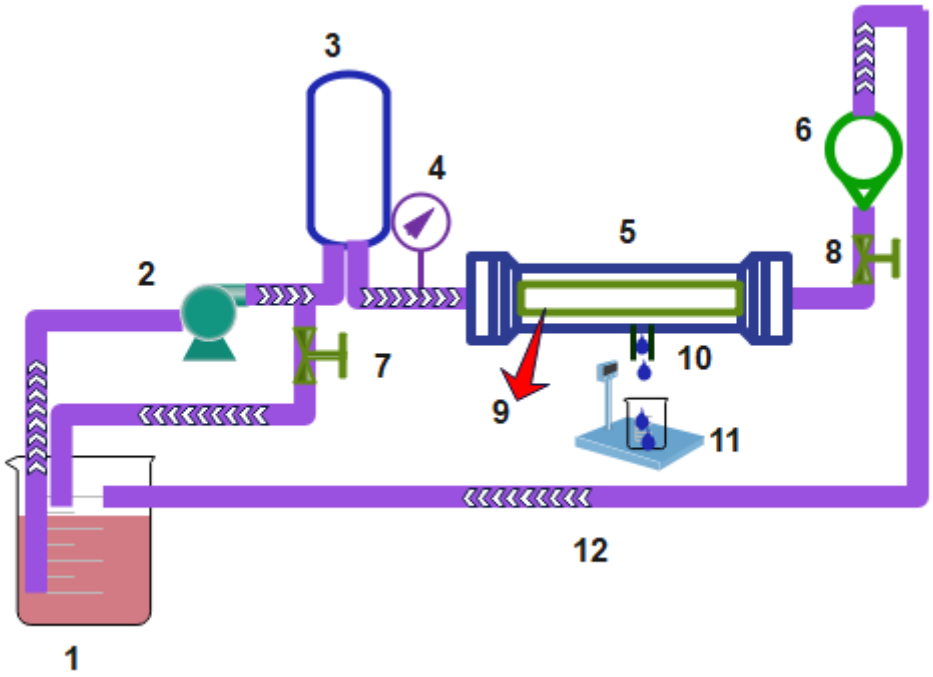

Fig. 2.3 A lab-scale cross flow filtration set up (1 – Feed tank, 2 – Pump, 3 – Dampener, 4 – Pressure gauge, 5 – Stainless steel module, 6 – Rotameter, 7, 8 – Control valves, 9 – tubular membrane, 10 – Permeate tank, 11 – Electronic balance and 12 – Retentate)

2.4. Results and Discussion

2.4.1. Characterization of raw materials

2.4.1.1. X-ray fluorescence analysis

The chemical composition of clay materials (kaolin and quartz) obtained by XRF analysis is presented in Table 2.2. The XRF results confirm that the main chemical composition of kaolin is SiO_2 (50.46 wt%) and Al_2O_3 (35.33 wt%). Traces of impurities present in kaolin clay include K_2O, Fe_2O_3, Na_2O, P_2O_5, CaO, TiO_2, MnO, etc. Quartz is highly rich in SiO_2 (86.97 wt%) along with a considerable quantity of Al_2O_3 (7.59 wt%). Negligible quantity of other oxides (Fe_2O_3, K_2O, TiO_2, CaO, MnO and P_2O_5) present in quartz can be considered as impurities. A high value of SiO_2/ Al_2O_3 ratio is indicative of high purity quartz. The Loss of ignition (LOI) value observed with both clays is attributed to degradation of carbonates and dehyroxylation of clay.

Table 2.2 Chemical composition (wt%) of clays (kaolin and quartz) used in this work

Oxides/raw material	Kaolin	Quartz
SiO_2	50.46	86.97
Al_2O_3	35.33	7.59
CaO	0.24	0.18
Fe_2O_3	0.86	0.49
K_2O	1.05	0.20
Na_2O	0.31	-
P_2O_5	0.02	0.01
TiO_2	0.02	0.02
MnO	0.01	0.02
Loss of ignition (LOI)*	11.72	4.52

* Loss of ignition at 1000 ^oC

As reported in the literature by Saikia et al. (2010), kaolinite from the north-eastern part of India is composed of major oxides of SiO_2 (44.71 wt%) and Al_2O_3 (36.34 wt%) along with a few minor oxides as impurities. P_2O_5 is used as a nucleating agent for ceramics manufacturing industries. It promotes heterogeneous nucleation and produces a fine grained interlocking morphology after heat treatment (Von Clausbruch et al., 2000). Lee et al. (2009) conducted a 90 day-toxicity study with P_2O_5 contained glass-ceramic (BGS-7: 4g in 20 ml) in rat and found no systemic toxicity associated with the treatment. Besides, the P_2O_5 content present in kaolin clay utilized in this work is around 0.02 wt% which is lower than the reported literature (0.311 wt% P_2O_5; Yahaya et al., 2017).

2.4.1.2. X-ray diffraction analysis

Fig. 2.4 shows the XRD profiles of raw materials (kaolin, quartz, and $CaCO_3$) used to prepare the ceramic membrane, which matches with the corresponding JCPDS files. The XRD peaks of kaolin were found to be in agreement with the JCPDS file no #14-164. The peaks at the diffraction angles 20.85° and 26.65° of quartz were well matched with the JCPDS file no 46-1045. Similar patterns were observed by Kumar and Pugazhenthi, (2017) for tubular ceramic membranes made from a mixture of natural clays.

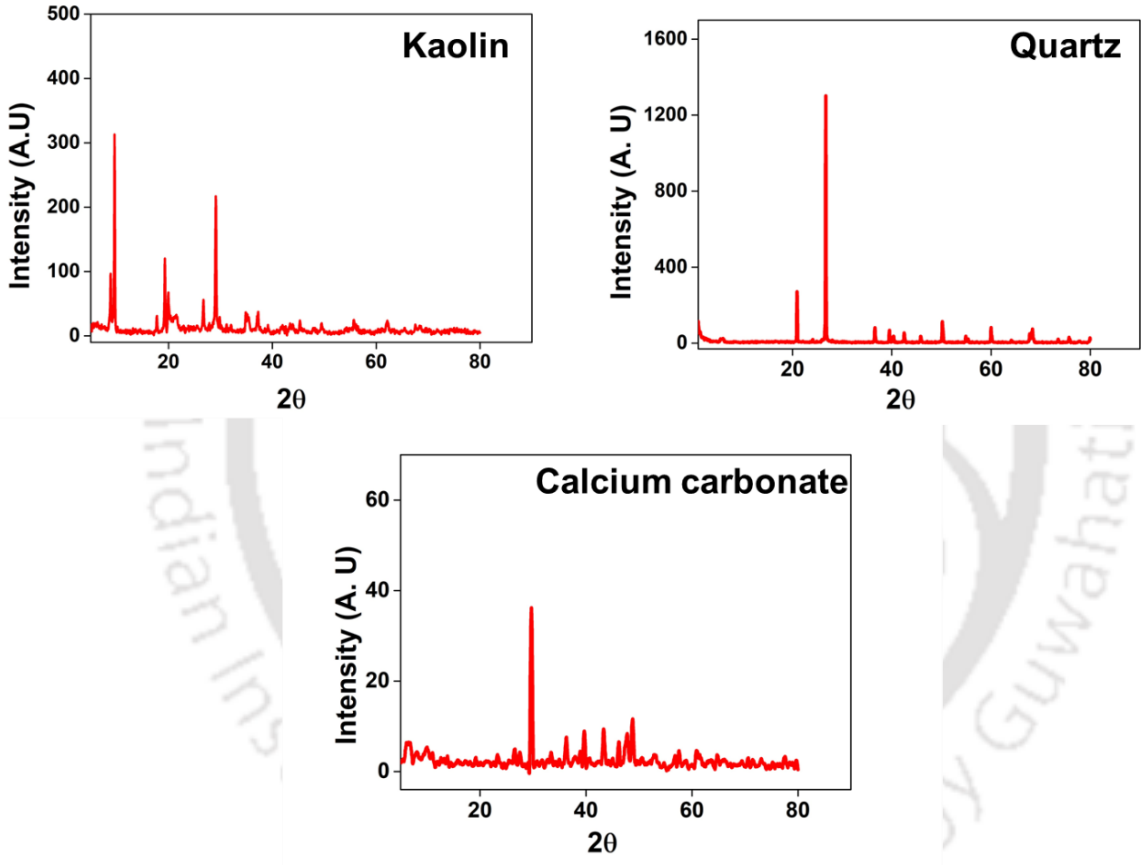

Fig. 2.4 XRD profiles of the raw materials used in this study

2.4.2. Characterization of membrane

The organic additive used as a binder in ceramic membrane fabrication has various advantages such as water retention, binding and good filming. The primary function of additive in membrane fabrication is to provide adhesion and cohesion to raw materials (Falamaki et al., 2006; Guironnet et al., 2019; Ananthakumar et al., 2004; Fan et al., 2016). Accordingly,

cohesion force may be well defined as the internal strength of the fabricated membrane, whereas adhesion is the bonding of different molecules that binds all three raw materials (kaolin, quartz, and $CaCO_3$) together. It was reported in the literature that the addition of boehmite gel in precursor material resulted in a paste having excellent movement in the extruder barrel, which eventually helped in fabricating membrane at low exit pressure (Ananthakumar et al., 2004). Unlike other binders which require dispersing agent, the additives (binders) chosen in the present study viz. CMC, GG and HPMC are readily soluble in water and do not require any dispersing agent. As reported in the literature (Falamaki et al., 2006), these additives act as a binder as well as an effective deflocculant. In comparison with other binders like wood extracts, starches, flours and gums, the membranes fabricated using water soluble polymers such as polyvinyl alcohols and cellulose, possess various distinctive characteristics like high wet strength, high water retention during extrusion and ease of extrusion (Fan et al., 2016). Besides the aforementioned characteristics, the additives (CMC, GG, and HPMC) used in the present study have outstanding adhesive capacity and rheological properties, due to which smooth membranes having very high surface finish were obtained without facing much difficulty. On the other hand, the membrane prepared without any additive (only Millipore water used) offered very low adhesion, leading to separation of precursors and water during the extrusion process (Wu et al., 2013), which resulted in a considerable material loss. For instance, in the present work, only two membranes with poor surface finish were obtained in the absence of additives (when only Millipore water was used); on the contrary, in the presence of additives, a maximum of sixteen membranes with smooth surface finish were obtained for the same quantity of raw material (300 g).

2.4.2.1. X-ray diffraction analysis

The phase changes of the sintered membranes were examined via XRD profiles, as shown in Fig. 2.5. The complete crystalline phase is observed for the sintered membrane, and the most

recognized phases for the sintered membrane are quartz (SiO_2), Wollastonite ($CaSiO_3$), mullite ($3Al_2O_3{\cdot}2SiO_2$), and anorthite ($CaO.Al_2O_3{\cdot}2SiO_2$). The main phase change of kaolin to mullite via meta kaolinite phase occurs between 800 °C and 1000 °C (Kumar et al., 2015b). This happens due to the degradation of kaolin material. Conversely, there is no new peak or shifting of peaks observed in all the XRD patterns of the membranes prepared using additives, which further confirms that the additive plays no role in the phase transformation.

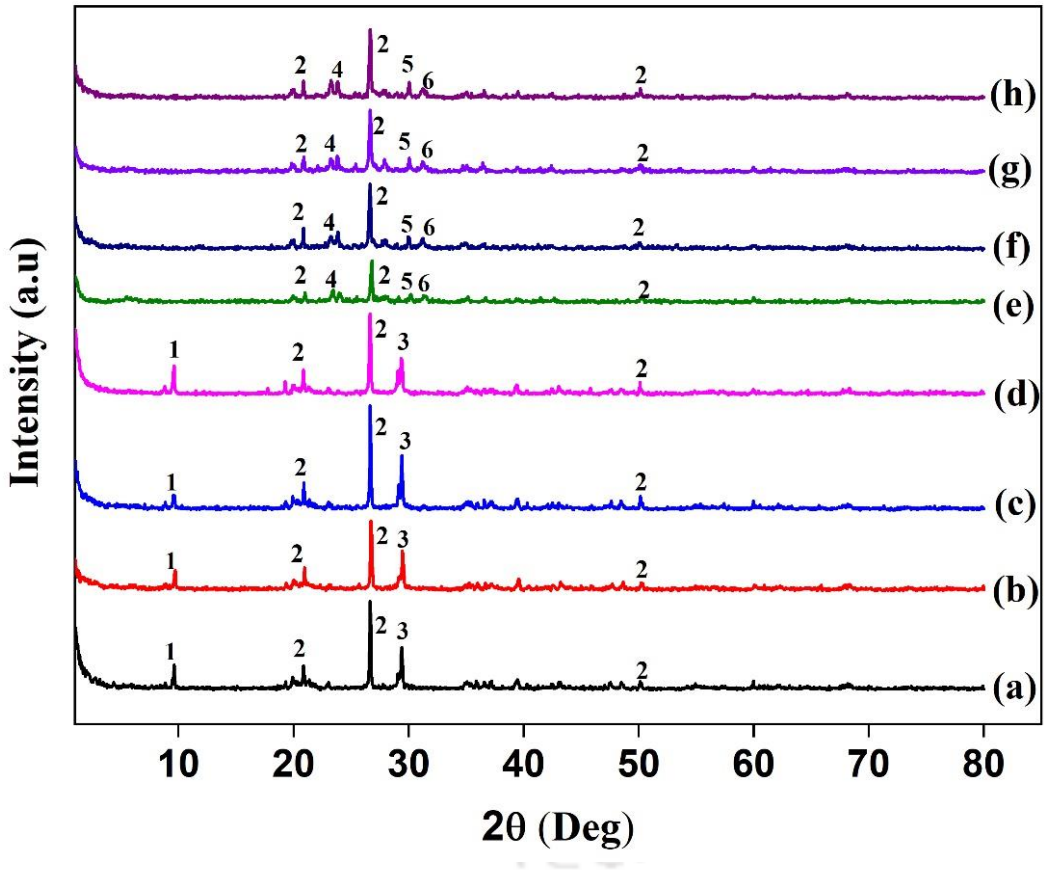

Fig. 2.5 XRD patterns of unsintered (a-d) and sintered (e-h) membrane [1-Kaolin, 2- Quartz, 3- Calcium carbonate, 4-Wollastonite 5-Anorthite, 6- Mullite]

2.4.2.2. Thermogravimetric analysis

TGA and DTG profiles of the additives (Fig. 2.6a-c) and freshly drawn unsintered membrane (Fig. 2.6d-g) are shown in Fig. 2.6. In the TGA curves of additives (Fig. 2.6a-c), the weight

loss before 100 ^{o}C is due to the evaporation of loosely adhered water molecules present in the sample. The major weight loss between 250 ^{o}C and 300 ^{o}C is attributed to the thermal decomposition of the additives. In the TGA profiles of all unsintered membranes (Fig. 2.6d-g), the presence of water is steadily evaporated until a maximum temperature of 200 °C. A weight loss noticed around 300 °C is owing to the thermal degradation of additives (CMC, GG, and HPMC) used in the manufacturing of membranes (Fig. 2.6d-f). The highest weight loss observed in the temperature range of 700-800 ^{o}C is due to the thermal degradation of $CaCO_3$ (pore-forming agent), which leads to the formation of CaO and CO_2 (Kumar et al., 2015b). For all the membranes, a very low or insignificant weight loss is noticed after 760 ^{o}C, which suggests that all the four membranes require a minimum sintering temperature of 760 ^{o}C to achieve membranes having good strength. It is worth to mention that as noticed in our earlier work (Vasanth et al., 2011), the flexural strength of the membranes enhanced steadily with an increase in the sintering temperature from 800 to 950 ^{o}C. Further increase in the sintering temperature resulted in enhancement of flexural strength but at the cost of reduced chemical stability. Hence, in the present study, all the membranes were sintered at 950 ^{o}C.

In connection with the TGA results of the membranes, two endothermic peaks were observed in the DTG plot (see Fig. 2.6d-f). The first endothermic peak explains the degradation of additives used for prepartion of membranes. In case of Kaolin-CMC membrane, the endothermic peak at 300 ^{o}C is attributed to deterioration of the side chain and the release of CO_2 from CMC (El-Sayed et al., 2011). For Kaolin-GG membrane, the endothermic peak appeared around 290 ^{o}C is due to the bond scission in the polymeric backbone of Guar gum. The second endothermic peak observed for all the unsintered membranes at 720 ^{o}C is due to the thermal decomposition of calcium carbonate to CO_2 and CaO.

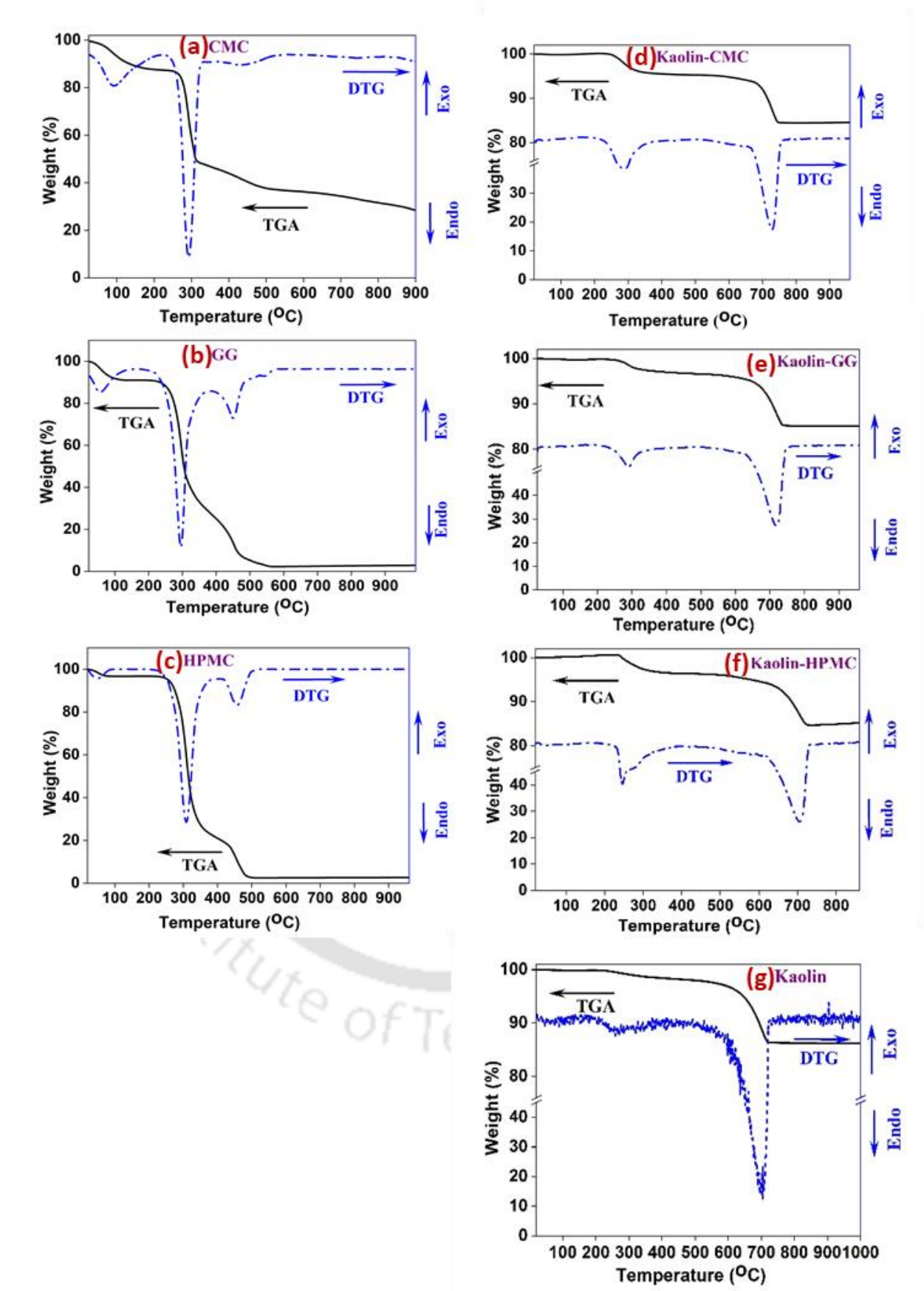

Fig. 2.6 TGA and DTG profiles of additives (a-c) and unsintered membranes (d-g)

2.4.2.3. Morphological analysis

Fig. 2.7 shows the outer surface (a - d) and inner surface (e - h) of the prepared membranes viz. Kaolin-CMC, Kaolin-GG, Kaolin-HPMC, and Kaolin, respectively. It was observed that both outer and inner surface of the membranes in the presence of additives were homogeneous, flawless and smooth with proper distribution of small pores throughout the surface of the ceramic membrane. Nevertheless, in the absence of an additive, prominent pores are evidently seen in the FESEM images (Fig. 2.7 (d) and (h)). This further suggests the increased pore size and porosity of the membrane without any additives added to the membrane.

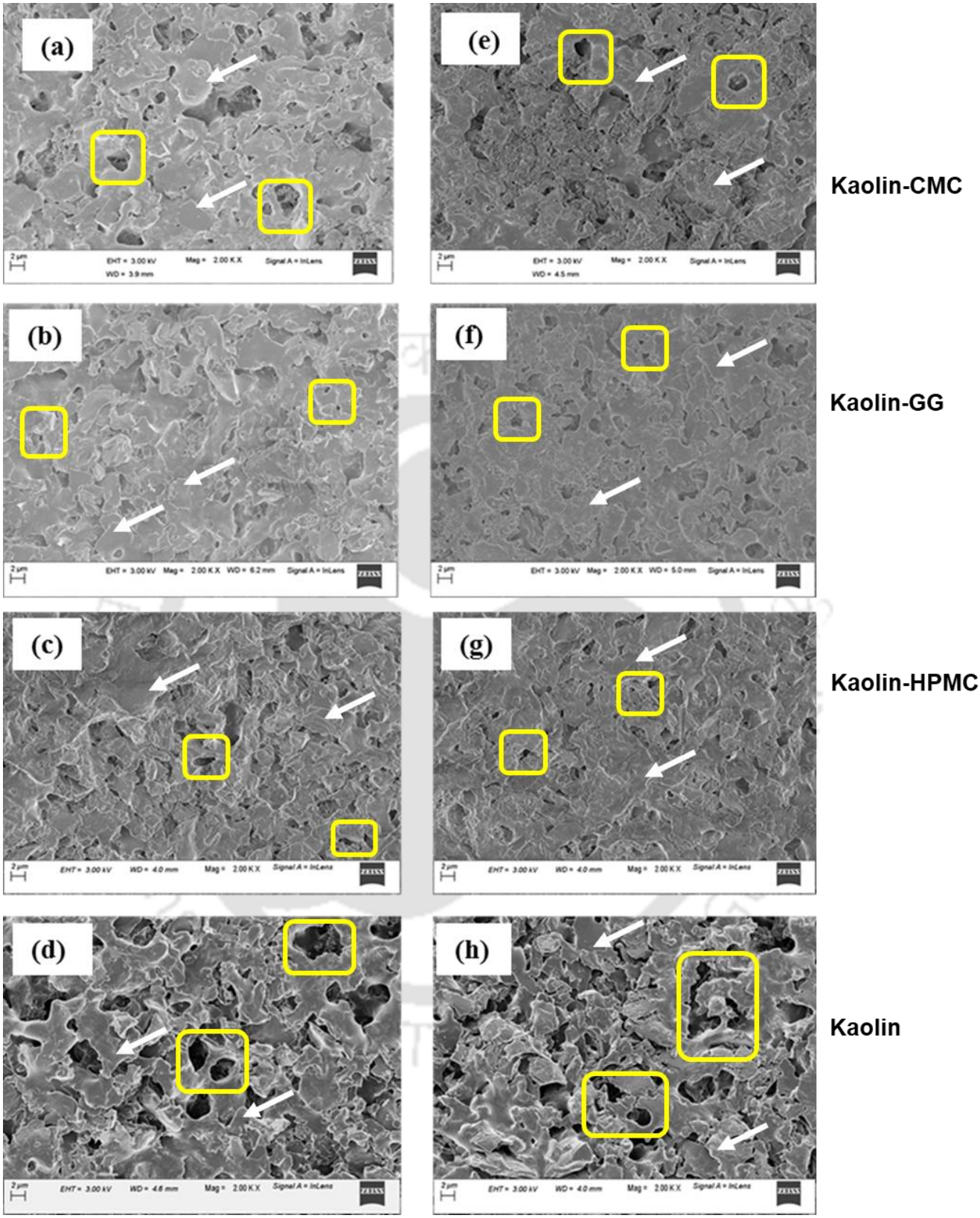

Fig. 2.7 FESEM images of inner surface (a-d) and outer surface (e-h) of membranes (Arrow mark and square symbol represent clay particles and membrane pore, respectively)

2.4.2.4. Chemical stability

The percentage weight loss of various membranes like Kaolin, Kaolin-CMC, Kaolin-GG, and Kaolin-HPMC in acidic solution (HCl, pH=1.4) was 6.5±0.08, 2.9±0.86, 3.28±0.67 and 2.73±0.7%, respectively. In case of alkaline (NaOH, pH=13) environment, these values were greatly reduced to 1.15±0.04, 0.9±0.27, 0.86±0.15, 0.64±0.6%, respectively (see Table 2.3). These results elucidated the suitability of the present membranes in highly acidic and alkaline environments. Further, these results (percentage weight loss of membrane in acid and alkali solutions) are comparable with alumina membrane (Dele-Afolabi et al., 2018).

2.4.2.5. Mechanical strength

The mechanical strength of these Kaolin, Kaolin-CMC, Kaolin-GG and Kaolin-HPMC membranes is 21, 38, 23 and 25 MPa, respectively. The prepared membranes displayed a better strength as compared with other ceramic membranes reported in the literature (Kumar et al., 2015b; Ivanets et al., 2017; Bose and Das, 2014). For instance, ceramic membranes prepared using silicate and aluminosilicate binders yielded a mechanical strength of 18 and 35 MPa, respectively (Ivanets et al., 2017). Mechanical stability of 2 MPa was reported by Bose and Das, 2014 for membrane fabricated using kaolin, saw dust, feldspar sodium metasilicate and boric acid. The high mechanical strength of the present ceramic membranes proposes its suitability for large scale industrial applications (Kumar et al., 2015b)

2.4.2.6. Porosity

The porosity values of Kaolin, Kaolin-CMC, Kaolin-GG and Kaolin-HPMC membranes are estimated to be 48, 36, 42 and 40%, respectively. Thus, nominal porosity obtained for the present ceramic membranes was comparable with the literature (Kumar et al., 2015b; Nalaparaju et al., 2019). Table 2.3 presents the characteristics of various membranes fabricated in the present study.

Table 2.3 Summary of the properties of fabricated ceramic membrane.

Properties		Type of Membrane			
		Kaolin	**Kaolin-CMC**	**Kaolin-GG**	**Kaolin-HPMC**
Mechanical Strength (MPa)		21±1.05	38±4.13	23±4.8	25±1.82
Porosity (%)		48±1.25	36±1.02	42±1.11	40±0.32
Average pore size (µm)		0.182	0.179	0.137	0.178
Water permeability (m^3/m^2s kPa)		1.8583×10^{-7}	1.3624×10^{-7}	0.92619×10^{-7}	1.4945×10^{-7}
Chemical stability (in terms of weight loss)	**In acid (%)**	6.5±0.08	2.9±0.86	3.28 ±0.67	2.73±0.70
	In base (%)	1.15±0.04	0.90±0.27	0.86±0.15	0.64±0.6

2.4.2.7. Pure water flux and pore size measurement

A constant pure water flux for the entire filtration duration at different applied pressures predicts the stable performance of the membrane without any actual damage in the pores (Fig. 2.8a-d). Moreover, as derived from Darcy's law, the pure water flux increased steadily with an increase in the applied pressure (Fig. 2.8e). This advocates that the applied pressure alone is the driving force for water permeation. The water permeability of different membranes like Kaolin, Kaolin-CMC, Kaolin-GG, and Kaolin-HPMC was estimated to be 1.8583×10^{-7}, 1.3624×10^{-7}, 0.92619×10^{-7} and 1.4945×10^{-7} m^3/m^2s kPa, respectively. The estimated average membrane pore size varied from 0.137 to 0.182 µm, where Kaolin-GG membrane was found to be the least and Kaolin membrane was the highest.

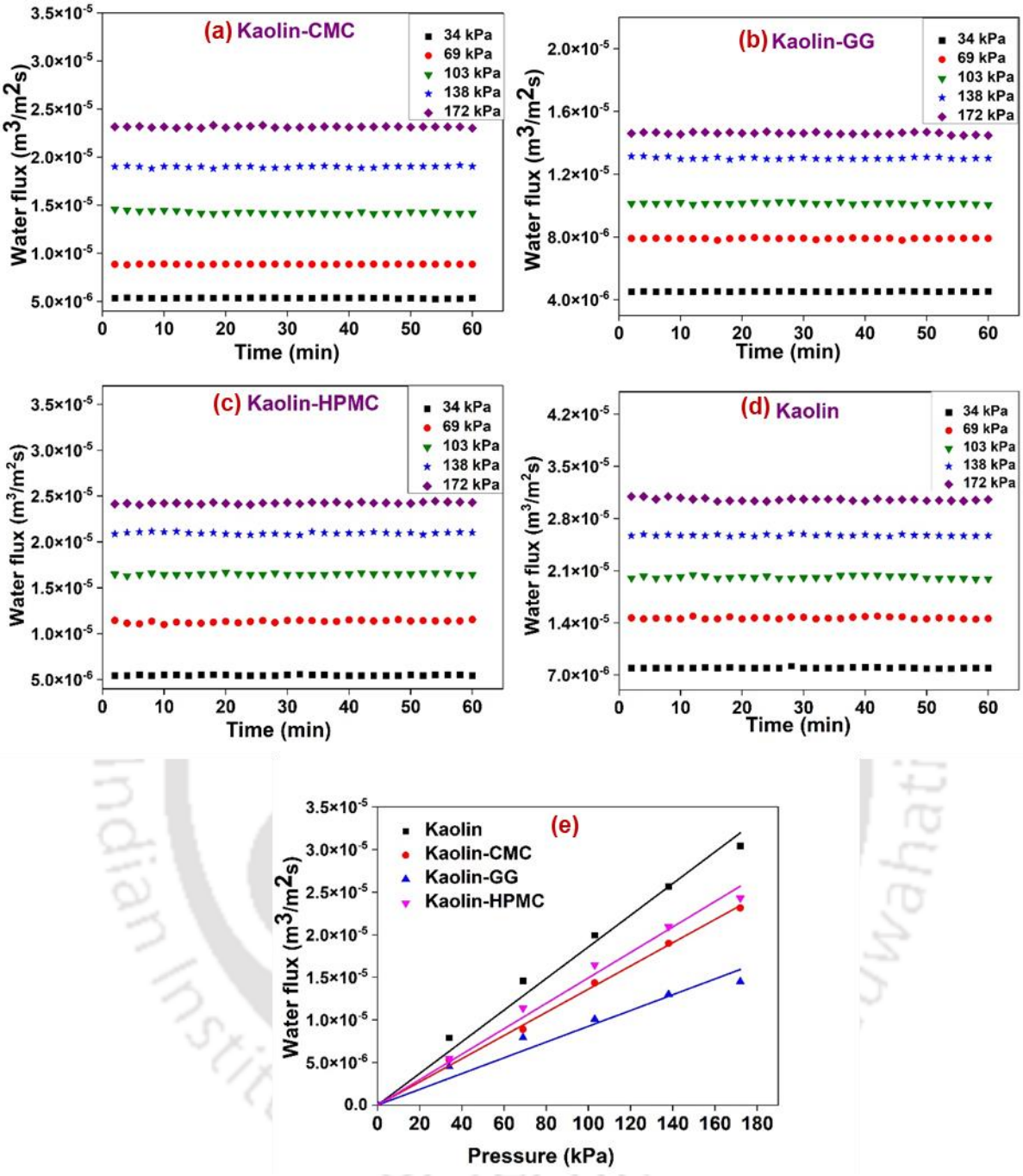

Fig. 2.8 Water flux of fabricated membranes at various pressures: (a) Kaolin-CMC, (b) Kaolin-GG, (c) Kaolin-HPMC, (d) Kaolin and (e) Cumulative water flux of various ceramic membranes as a function of applied pressure.

2.4.3. Estimation of manufacturing cost of membranes

Membrane cost is a key to successful application of membrane technology at an industrial scale. According to some cost estimates presented in the literature, conventional polymeric membranes cost approximately 50-200 USD/m^2 (Nandi et al., 2009). On the other hand, the

cost of commercially available ceramic membranes is in the range of 500-1000 USD/m^2 for alumina and 3000 USD/m^2 for stainless steel membrane (Vasanth et al., 2012). Hence, ceramic membranes are five to ten times more expensive than polymeric membranes. Therefore, majority of industries opt for polymeric membranes in their new installations. Nevertheless, ceramic membranes perform better than polymeric membranes under harsh operational environment for treating wastewater due to their low operational cost. The low operating cost of ceramic membranes is attributed to the ease of cleaning and longer life span over polymeric membranes. A previous study reported that during the treatment of various industrial wastewater using MF/UF membranes, operating expenses of ceramic membranes declined by 55 % compared to polymeric membranes (Al-Anzi et al., 2017).

Primarily, ceramic membranes have a high capital cost due to the high cost of raw materials and the high sintering temperature required to manufacture them. It is worth mentioning that in the present work, the membrane was fabricated using natural clays such as kaolin and quartz, which are less expensive and the membrane is also sintered at a low temperature (950 ^oC) compared to alumina membrane (>1200 ^oC). It is also well documented in the literature that the membranes fabricated using clays, ashes, fly ash, apatite and quartz need relatively low sintering temperatures when compared to conventional ceramic membranes prepared using Al_2O_3, TiO_2 and ZrO_2 (Abdullayev et al., 2019). As a result, membrane cost is reduced drastically compared to conventional ceramic membranes (Abdullayev et al., 2019). Summary of cost estimation of membrane fabrication is presented in Table 2.4. In general, membrane cost is associated with expenses due to raw material, labor, laboratory, equipment, depreciation, repair and maintenance and electricity. The aforementioned expenses included for the fabrication of Kaolin-HPMC membrane are presented in Appendix. A total of 60 membranes produced from each batch was taken as a basis according to the furnace capacity. In the present study, the estimated cost of the fabricated tubular membranes is 248-253 USD/m^2. Thus, the

membranes prepared in this study can be regarded as low cost without compromising the qualities desired for liquid phase separation application. Sushma et al. (2020) reported that the cost of flat ceramic membrane derived from kaolin, boric acid, sodium metasilicate, sawdust, and feldspar was 440.9 USD/m^2. Suresh et al. (2016) used affordable industrial waste fly ash to make three types of disc shaped ceramic membranes and the calculated membrane cost was 462-465 USD/m^2. Based on only raw material and equipment cost, Bose and Das, (2013; 2014) reported the membrane cost as 332 USD/m^2 and 250 USD/m^2 for ceramic membranes developed with binder and without binder, respectively. Recently, Goswami and Pugazhenthi, (2021) developed a tubular ceramic membrane using fly ash as a key precursor and the estimated membrane cost was 250 USD/m^2. The afore-mentioned cost estimation proves that the ceramic membrane prepared using kaolin, quartz and calcium carbonate along with binders is not only competitive to polymeric membranes in terms of cost, but also highly suited for industrial application, even under harsh conditions. Furthermore, the membrane fabricated in this work is less expensive than the other low-cost membranes reported in the literature.

Table 2.4 Detailed cost analysis for the fabricated membranes in this study

Cost type	Calculations for making 60 membranes				USD
Raw material cost	Raw material	Unit price	Material used	Cost (USD)	
	Kaolin	0.16	0.337	0.054	
	Quartz	0.27	0.1687	0.0455	
	Calcium carbonate	8.08	0.1687	1.3635	
	HPMC	34.2	0.015	0.513	
	CMC	32.2	0.015	0.483	
	GG	1.88	0.015	0.0283	
				Total raw material cost for Kaolin-HPMC:	**1.9761**
				Total raw material cost for Kaolin-CMC:	**1.9461**
				Total raw material cost for Kaolin-GG:	**1.4914**
				Total raw material cost for Kaolin:	**1.4631**
Labor cost					**6.75**
Laboratory cost					**1.351**
Electricity cost	Equipment used	Cost for 1 h use (USD)	Time of use (h)	Cost (USD)	
	Extruder	0.051	3.75	0.1912	
	Hot air oven	6.918×10^{-3}	24	0.166	
	Furnace	0.0259	31	0.8	
	Bath sonicator	6.054×10^{-3}	0.33	1.99×10^{-3}	
				Total equipment cost:	**1.1592**
Depreciation cost					**0.72**

Repair and maintenance cost **0.215**

Electricity cost

Equipment used	Power (kW)	Time of use (h)	Cost (USD)
Extruder	0.3725	3.75	0.122
Hot air oven	1.5	24	3.132
Furnace	4	31	10.788
Bath sonicator	0.12	0.33	0.00431

Total electricity cost: **14.046**

Estimated manufacturing cost for one Kaolin-HPMC membrane (USD)	0.437
Estimated manufacturing cost for one Kaolin-CMC membrane (USD)	0.436
Estimated manufacturing cost for one Kaolin-GG membrane (USD)	0.4289
Estimated manufacturing cost for one Kaolin membrane (USD)	0.4284
Estimated manufacturing cost for unit area of Kaolin-HPMC membrane (USD/m^2)	**253**
Estimated manufacturing cost for unit area of Kaolin-CMC membrane (USD/m^2)	**252**
Estimated manufacturing cost for unit area of Kaolin-GG membrane (USD/m^2)	**248.3**
Estimated manufacturing cost for unit area of Kaolin membrane (USD/m^2)	**248**

[#]1 USD = 74.0 INR (8th November 2021)

2.5. Summary

Indigenous low cost tubular ceramic membranes were successfully prepared from kaolin, quartz, calcium carbonate along with different binders. Membranes made with various binders owned an average pore diameter in size range of 0.137–0.182 μm, water permeability of 0.92619×10^{-7} - 1.8583×10^{-7} m^3/m^2 s kPa and porosity of 36 - 48%. Characterization results clearly demonstrated that the prepared membranes possessed excellent characteristics, including strong resistance against alkali, high porosity and high water permeation flux. All the membranes reported in the present study have high mechanical strength, thermal and chemical stability. The cost of the prepared membranes was estimated to be 248 – 253 USD/m^2, which is lower than that of the clay-based ceramic membranes and commercial α - alumina membranes. Thus, the present study emphasizes the use of naturally occurring clays as environmentally friendly and inexpensive precursors for the production of tubular ceramic membranes.

Chapter 3

Application of kaolin based ceramic membrane for liquid phase separation

Application of kaolin based ceramic membrane for liquid phase separation

This chapter discusses the potential application of indigenous kaolin based tubular ceramic membranes in liquid phase separation. The chapter is divided into three parts to discuss microalgae recovery from the culture broth, separation of TiO_2 from aqueous suspension and treatment of produced water. Various pore blocking methods were also discussed in order to find the fouling mechanism in all the cases.

Part A: Recovery of microalgae from its broth solution

3.1. Chemicals and reagents

BG 11 broth with minerals, Bradford Reagent, Anthrone GR, Bovine serum albumin, (+)-Glucose anhydrous and Sodium hypochlorite 4% (w/v) were supplied by HiMedia Laboratories Pvt. Ltd., Mumbai.

3.2. Algae cultivation

The unicellular microalgae, *Chlorella Sorokiniana* used in the present study was procured from the Department of Biosciences and Bioengineering, IIT Guwahati. Identification and characterization of this organism were previously reported in the literature by Arun et al. (2019). Thus, the obtained *Chlorella Sorokiniana* cells were directly grown in expedient BG11 broth mentioned in section 3.1. All the algal growth experiments were carried out in 2L conical flasks with alternating light and dark cycles of 12 h and 12 h, respectively. Further, a light intensity of 3500–3600 lux (cool white light) and the chamber temperature of 25 - 30°C were maintained during the cultivation of algae. The BG11 medium with minerals consisted of 1.5 g/L sodium nitrate, 0.04 g/L dipotassium hydrogen phosphate, 0.075 g/L magnesium sulphate heptahydrate, 0.036 g/L calcium chloride dehydrate, 0.020 g/L sodium carbonate, 0.001 g/L EDTA disodium salt, 0.006 g/L citric acid, 0.006 g/L ferric ammonium citrate and 1 mL trace metal mix. In a 2L

conical flask, 1.642 g of BG 11 medium was added in 1000 mL Millipore water, and this solution pH was measured to be 7.1. Further, the media was sterilized by autoclaving it at 120 ^{o}C for 20 min. A 10 %(v/v) of inoculum of exponentially growing algal culture was inoculated in 2L conical flask and tightly plugged with non-adsorbent cotton to have free air passage. The size distribution of the microalgae was measured by using Laser particle size analyser **(**Model Master sizer 2000, M/s Malvern, UK) at an equal interval of time (24 h) during the entire cultivation period. The growth of microalgae was observed by evaluating the absorbance at λ_{max} 687 nm using a UV/VIS spectroscopy (Model UV-2600, Shimadzu, Singapore). After ending the log growth phase, the microalgae were harvested on 12th day that attained a maximum concentration of 500 – 650 mg/L (on a dry mass basis). This algal biomass culture was diluted with Millipore water to obtain a constant feed concentration of 500 mg/L, which was used thereafter for all microfiltration experiments.

3.3. Microfiltration of algae

All the tests were conducted at ~25°C using a microfiltration system depicted in Fig. 2.3 (Chapter 2). A fixed algae feed concentration (500 mg/L) was used for all the experiments. The performance of the fabricated membrane was tested by inserting it into the membrane module in the microfiltration setup. The algae feed solution was passed to the membrane from the feed tank, and the retentate was recycled back to the feed tank. The permeate was calculated by weighing it under a digital weighing balance. Further, after completion of filtration experiment at a particular pressure, the membrane was cleaned with Millipore water for 30 minutes followed by passing a cleansing agent (NaOCl 4% w/v solution) through the membrane for 2 h to remove algae cells deposited on the membrane surface. After that, Millipore water was passed through microfiltration system for 1 h. With this cleaning procedure, the regenerated membrane regains its original

hydraulic permeability value (within ±2%). Then this membrane was considered for the next run of algae separation. The microfiltration experiment for algae separation was conducted up to 2.5 h at different operating pressures (69 - 345 kPa) with feed concentration of 500 mg/L and a constant flow rate (6.42×10^{-3} m/s). Percentage recovery was calculated from the following expression (Marbelia et al., 2016).

$$\text{Recovery}\ (\%) = \frac{C_0 - C_p}{C_0}\times 100 \qquad (3.1)$$

Where C_0 and C_p are the algae concentration in the feed and permeate (mg/L), respectively. Concentration of microalgae in the feed and permeate solution was measured by using UV/VIS spectroscopy.

3.4. Analysis of extracellular protein, carbohydrate and volumetric reduction factor

A very few literatures were reported on microalgal extracellular polymeric substances (EPS) when compared to bacteria and cyanobacterial EPS. Microalgae generally produce extracellular polymeric substances into the environment during their life cycle. EPS possess excellent stable matrix structure and form 3-D polymer network structure with algae cells to interact each other. Their superior rheological properties attract microalgae EPS for its use in mechanical engineering (bio lubricant and drag reducers) as well as food engineering (thickeners and preservatives). The main components of microalgal EPS are proteins, polysaccharides and lipids. Since these EPS are rich in carbon source, they are helpful to other organisms to grow in the food chain (Xiao and Zheng, 2016). Hence, the presence of EPS in the permeate solution was calculated as carbohydrates and proteins. Besides its use as a value-added product in the microfiltration process, this EPS finding helps to analyze the flux decline mechanism. Protein concentration in the permeate solution was estimated as follows: 0.2 mL of permeate sample was added into 1 mL of Bradford reagent and the solution was incubated at room temperature for 45 min. Subsequently,

absorbance of the sample was estimated at λ_{max} 595 nm using UV/VIS spectroscopy. BSA (Bovine serum albumin) was utilized as the protein standard.

The total carbohydrate concentration in the permeate solution was determined as follows: 1 mL permeate sample was added into 4 mL of anthrone reagent and the mixture was kept in water bath, which was maintained at 100 ^{o}C for 15 min. Then the solution was kept in a refrigerator to cool down to room temperature (~ 25 ^{o}C). Absorbance of the sample was estimated at λ_{max} 620 nm using UV/VIS spectroscopy. Glucose was used as the carbohydrate standard (Kruger, 2009).

Volumetric reduction factor (VRF) was calculated to identify the efficiency of the harvesting process. VRF was estimated using the following equation (Hwang et al., 2015).

$$\mathrm{VRF} = \frac{V_i}{V_f} \qquad (3.\ 2)$$

Where V_i is the initial volume of feed and V_f is the final volume of feed.

3.5. Analysis of fouling mechanisms

For the microfiltration of algae, flux decline was examined using the pore-blocking mechanism. The following four empirical models, such as (1) complete, (2) standard, (3) intermediate pore blocking, and (4) cake filtration model, were utilized (Kumar et al., 2016). The schematic of four pore blocking models is depicted in Fig. 3.1.

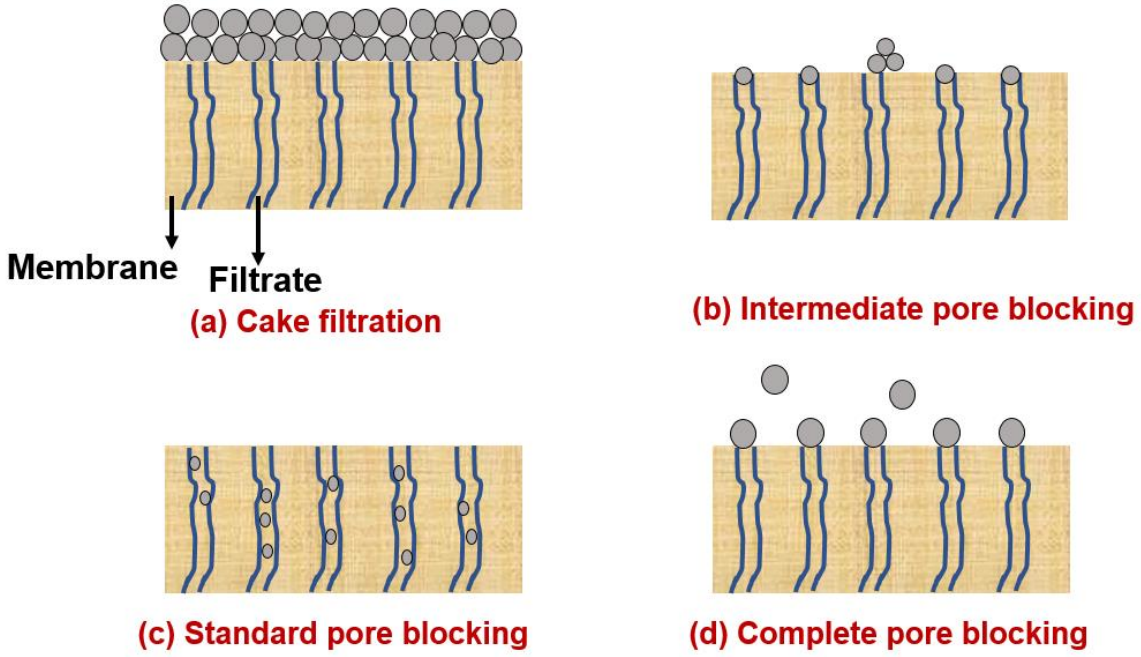

Fig. 3.1 Schematic illustration of four pore blocking models

In compete pore-blocking model, it is recognized that the algae cells present at the inner surface of the ceramic membrane completely block the mouth of the pores without getting stuck into the pore channels of the membrane. Equation 3.3 represents the change of permeate flux with time for complete pore-blocking model.

$$\ln(J^{-1}) = ln(J_0^{-1}) + k_b\, t \qquad (3.\ 3)$$

In case of standard pore-blocking model, it is accepted that the size of the algae cell is smaller as compared to pore mouth of the ceramic membrane, and it promotes the blocking at the channel of the pores in the ceramic membrane. Equation 3. 4 describes the variation of permeate flux with respect to time.

$$J^{-0.5} = J_0^{-0.5} + k_s t \qquad (3.\ 4)$$

In the intermediate pore-blocking model, it is assumed that the size of the algae cells is equal to the pore diameter of the ceramic membrane, and it does not encourage pore blocking in the channel of the pores in the ceramic membrane. Equation 3. 5 explains the changes of permeate flux with respect to time.

$$J^{-1} = J_0^{-1} + k_i t \quad (3.5)$$

In cake filtration model, it is presumed that the size of the algae is more significant than the pore diameter of the ceramic membrane and it induces the creation of cake on the ceramic membrane surface that resists the flow through the permeate side. Equation 3. 6 represents the permeate flux expressed with respect to time.

$$J^{-2} = J_0^{-2} + k_c t \quad (3.6)$$

Where J and J_0 correspond to the flux and flux at y-intercept, respectively. k is the slope and t is separation time. The best fit of experimental flux was analyzed for flux decline data based on the R^2 (coefficient of determination) values found from the linear approach examination by models presented in Equations (3. 3), (3. 4), (3. 5) and (3. 6). All the aforementioned models were screened for its best fit by comparing their R^2 value, which was then used for validating the fouling mechanism in the microfiltration process.

3.6. Results and Discussion

3.6.1. Biokinetic study and characterization of microalgae

Fig. 3.2a clearly shows that both absorbance and concentration enhance with an increase in time (Kholssi et al., 2019). During the cultivation period, the concentration of algal biomass in the broth increased and reached a maximum value of 650 mg/L at the end of the 12th day. Since the concentration of algal biomass was found to be highest at the end of the 12th day, microfiltration experiments were started on the same day to harvest the algal biomass from the broth. Similar

results were also reported in the literature (Kholssi et al., 2019; Kurniawati et al., 2014). For instance, Kholssi et al. (2019), in their study on the fertilizing effect of *Chlorella Sorokiniana* on wheat growth, reported a maximum cell concentration at the end of 12th day. Besides, the particle size distribution revealed that the majority of the algal cells lie in a size range of 2.8 - 6 μm throughout the cultivation period (see Fig. 3.2a). Further, the size distribution of algae cells harvested on the 12th day is shown in Fig. 3.2b. It can be observed that around 42% of the algal cells have a size of 3.31 μm. Therefore, the average size of the algal cells was calculated to be 3.33 μm. The results observed in this work were found to be in line with the results reported by Kurniawati et al. (2014), where the authors harvested the algal cells having an average size of 3.8 μm.

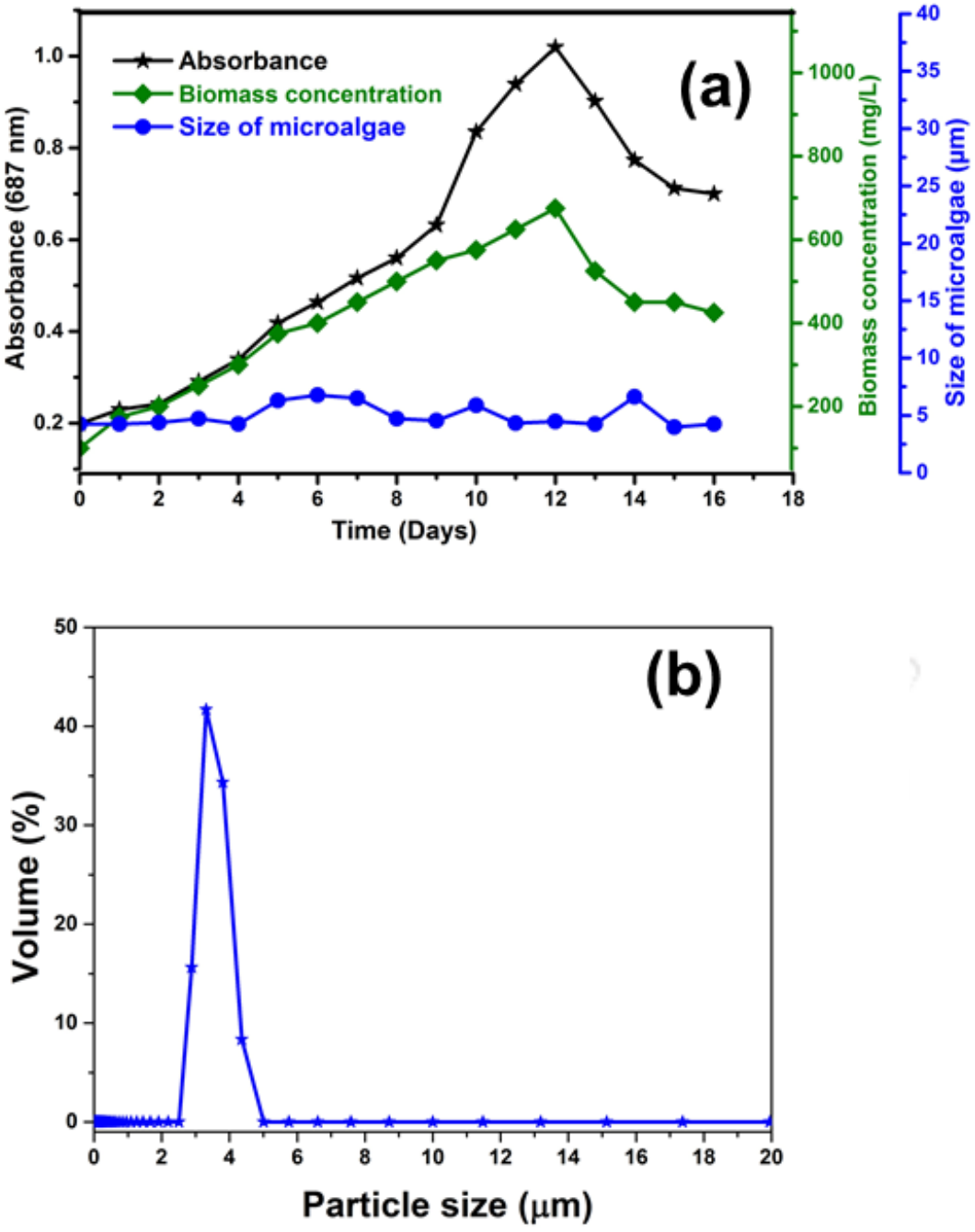

Fig. 3. 2 (a) Biokinetic study on the cultivation of *C. Sorokiniana* and (b) Size distribution of *C. Sorokiniana*

3.6.2. Effect of pressure on algae permeate flux and recovery

Fig. 3.3 depicts the permeate flux pattern of Kaolin-CMC, Kaolin-GG, Kaolin-HPMC and Kaolin membranes as the function of time for five different applied pressures at a constant crossflow rate of 6.42×10^{-3} m/s and an initial algal concentration of 500 mg/L. It can be noticed that the permeate flux decreased rapidly during the initial phase of the microfiltration experiment, and after that, it became steady during the microfiltration experiment. The decrease in the flux observed in the present study is attributed to the pore blockage that arises by the plugging of algal cells on the pore mouth of the membrane and, after that, the steady formation of algal biomass cake layer on the inner surface of the membrane is occurred, which blocks the pore mouth of the membrane. A general trend of increase in permeate flux along with an increase in the applied pressured was noticed till 276 kPa; however, further increase in the pressure to 345 kPa brought no significant enhancement in permeate flux. The initial increase in permeate flux with the rise in pressure is apparent because of the enhancement in the driving force, while the constant value observed after 276 kPa can be attributed to the increase in the total resistance experienced by the membrane during the microfiltration experiment (Hung and Liu, 2006). Nevertheless, a linear increase in the permeate flux with applied pressure (Fig. 3.3) was not observed, which is due to the effect of concentration polarization by the formation of algal layer on the membrane surface during the course of microfiltration experiment (Zou et al., 2011; Hwang et al., 2013). The decrease in permeate flux was found to be maximum at higher pressure because of the quick deposition of the algal cake layer on the ceramic membrane.

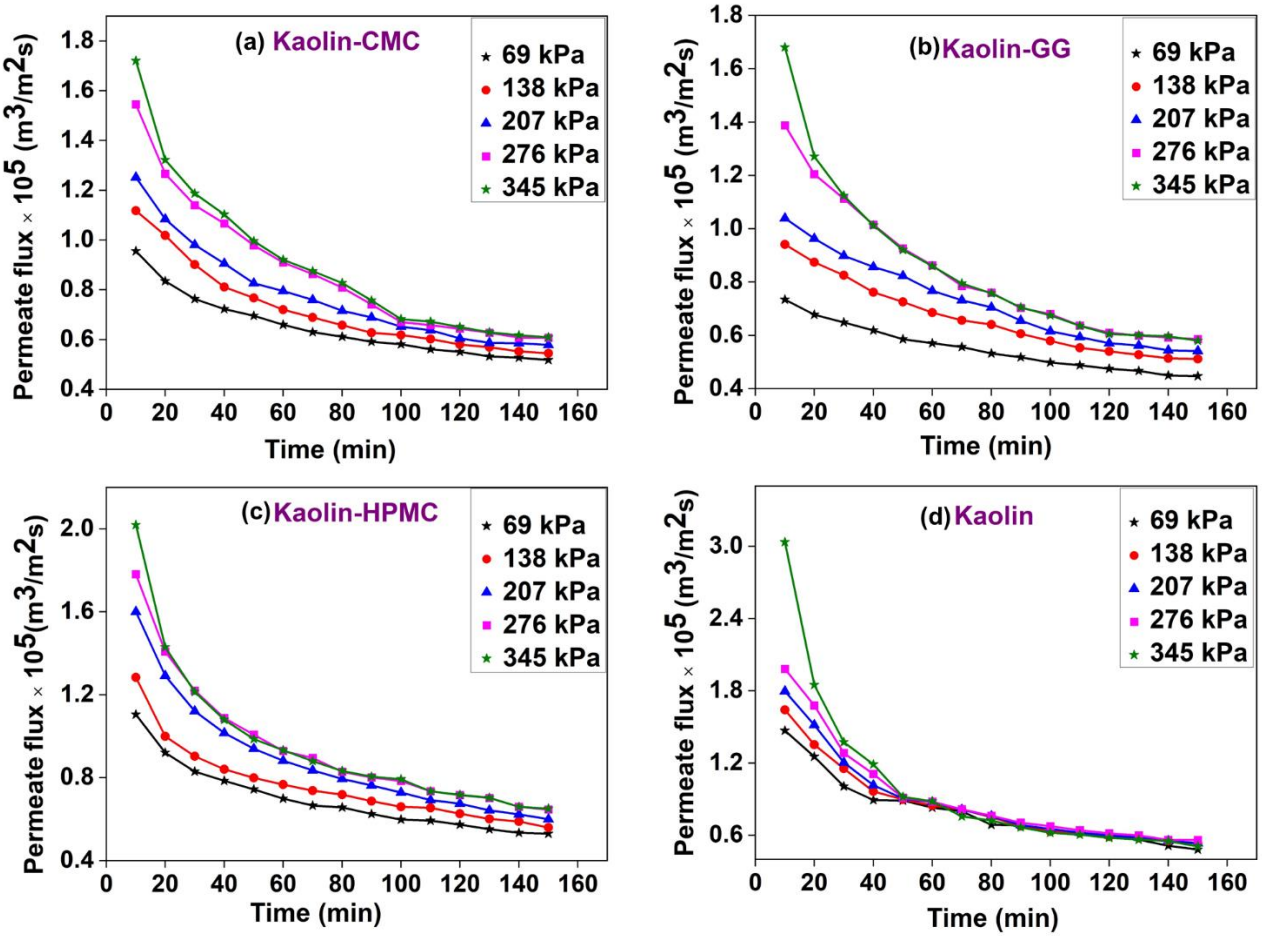

Fig. 3.3 Effect of pressure on permeate flux of (a) Kaolin-CMC, (b) Kaolin-GG, (c) Kaolin-HPMC and (d) Kaolin membrane

The flux decline for the four different membranes tested in the present study follows the order of Kaolin-GG < Kaolin-CMC < Kaolin-HPMC < Kaolin. This pattern can be correlated with the pore size of the respective membrane, where the fouling rate is found to be higher with a larger pore size membrane. At the end of 2.5 h of microfiltration experiment at an applied pressure of 276 kPa, the average permeate flux was estimated to be 0.95×10^{-5}, 0.88×10^{-5}, 0.83×10^{-5} and 0.92×10^{-5} m/s for Kaolin-HPMC, Kaolin-CMC, Kaolin-GG, and Kaolin, respectively.

The variation in algae recovery with respect to pressure for all the four different membranes was depicted in Fig. 3.4(a–d). The recovery percentage was observed to be almost constant for all the pressures. The reason for this trend is that the pore size of all the four different membranes tested in the present study was well below the average size of the algae cells. As evident from Fig. 3.4e, the obtained permeate was clear in colour, indicating complete removal of algae. Based on the results portrayed in Fig. 3.4, it can be concluded that all the fabricated membranes performed well by recovering the algal cells to the retentate stream. All membranes (Kaolin-CMC, Kaolin-GG, Kaolin-HPMC, and Kaolin) produced the maximum recovery of 99.56- 100% for all the applied pressures.

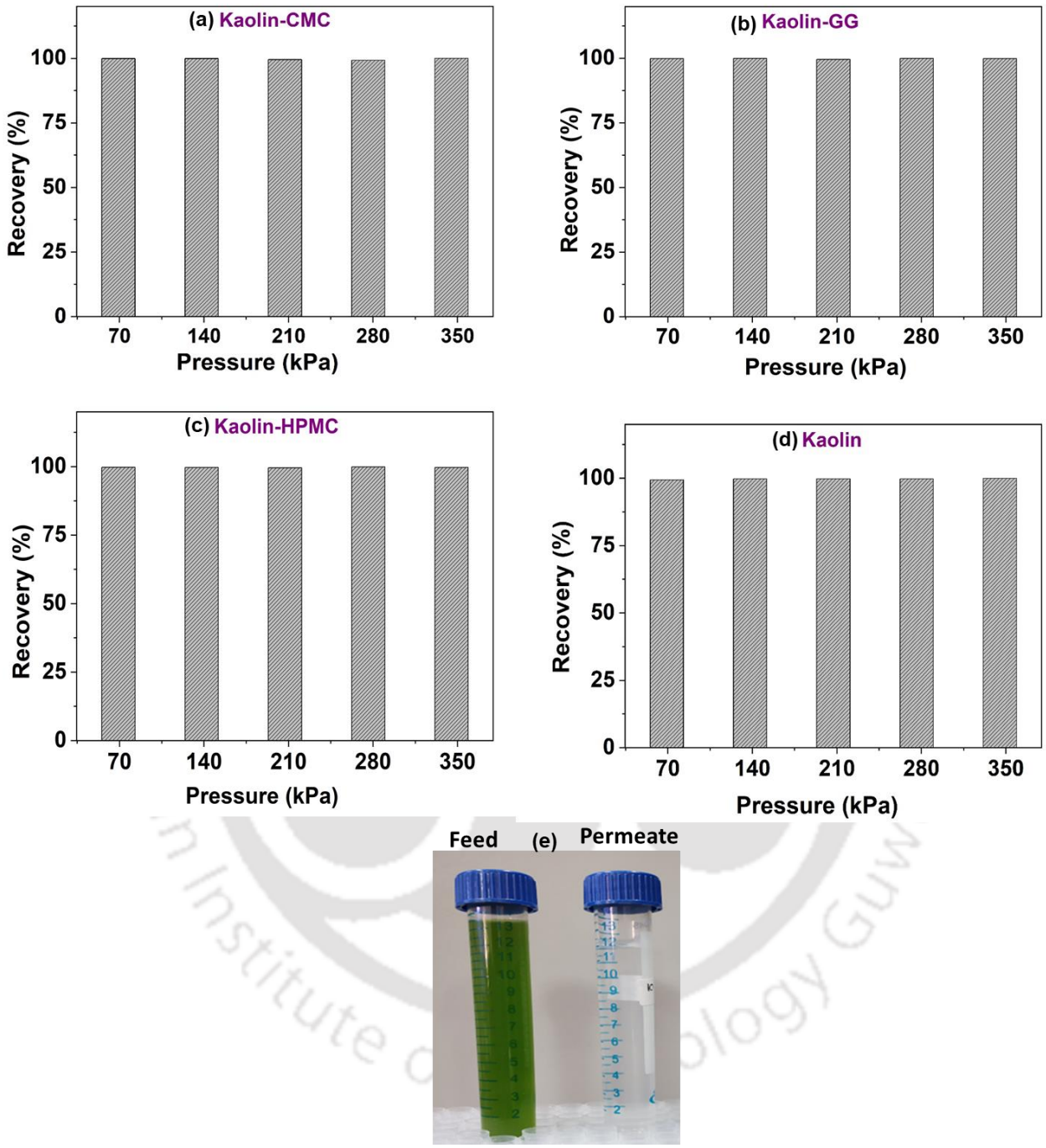

Fig. 3.4 Influence of applied pressure on algae recovery using the membranes ((a) Kaolin-CMC (b) Kaolin-GG (c) Kaolin-HPMC (d) Kaolin) and (e) image of feed and permeate samples

3.6.3. Influence of additive on permeate flux and volumetric reduction factor (VRF)

The performance of all the membranes in terms of average permeate flux is depicted in Fig. 3.5. All the membranes followed the general trend of an increase in total permeate flux with an increase in the pressure. Though the algae recovery value of all membranes is almost the same, it was observed that the average flux of Kaolin membrane is higher than that of other membranes at lower pressures (69-138 kPa). At an optimum pressure of 276 kPa, the average permeate flux of Kaolin-HPMC membrane was found to outperform over all other membranes. The decreased permeate flux of Kaolin membrane at higher applied pressure can be attributed to the pronounced effect of concentration polarization by higher algal deposition on the Kaolin membrane having larger pore size. However, low permeate flux observed for the Kaolin-GG membrane is due to its smaller average pore size (0.137 μm). Amongst all the membranes tested in the present study, Kaolin-HPMC membrane with a porosity of 40% and pore size of 0.178 μm yielded a maximum permeate flux of 1.78×10^{-5} m/s at an applied pressure of 276 kPa and a constant crossflow rate of 6.42×10^{-3} m/s. All the prerequisite needed for the large scale applications of the ceramic membranes in algal separation like smaller pore size, high mechanical strength with less fouling rate, high algae recovery with high permeate flux, are found to be true with the Kaolin-HPMC membrane. It is also to be noted that as mentioned in the characterization section, the fabrication of Kaolin membrane (without any additive) resulted in a huge material loss due to poor adhesion property and yielded only two membranes with good surface finish. Keeping all the above in mind, it can be concluded that Kaolin-HPMC membrane developed in the present study is an excellent option for large scale microfiltration of algal cells.

Fig. 3.6 shows a comparison of VRFs calculated under different applied pressure for all membranes. As it is observed, VRF increases with an increase in the pressure owing to the

enhancement in driving force. The VRF at 276 kPa was 1.08, 1.075, 1.073 and 1.069 for Kaolin-HPMC, Kaolin, Kaolin-CMC and Kaolin-GG membrane, respectively. In this study, the maximum VRF of 1.08 was obtained with Kaolin-HPMC membrane at an applied pressure of 276 kPa. At this operating condition, the algal biomass was concentrated, and the performance of membrane in terms of VRF/m^2 was found to be 635, which is even higher than the PVDF (25 VRF/m^2) (Chen et al., 2012) and microporous membrane (43 VRF/m^2) (Petrusevski et al., 1995). Once again, these results reveal the suitability of the Kaolin-HPMC membrane for the concentration of algal biomass and further, it can be considered as the promising alternative for the other membranes reported in the literature.

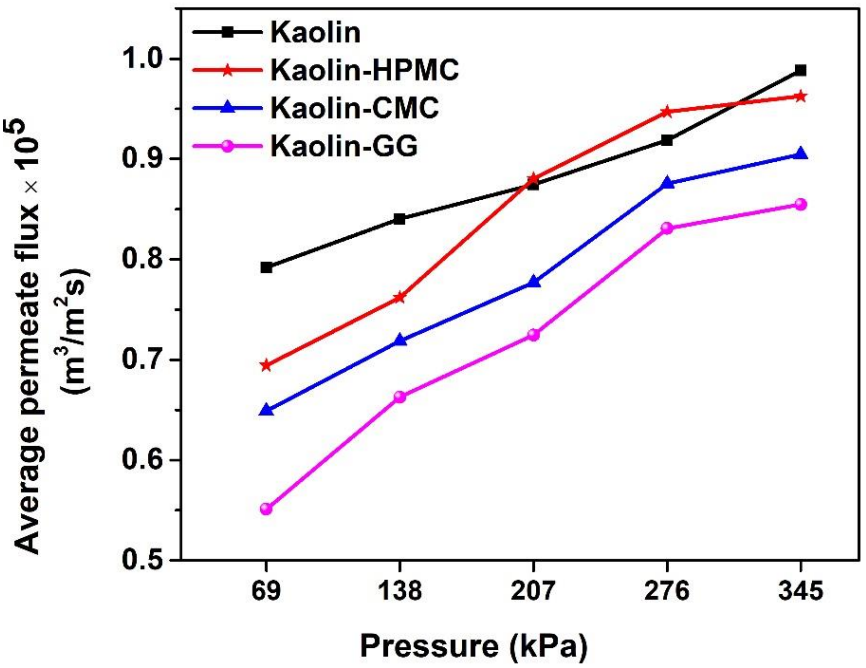

Fig. 3.5 Influence of additive on average permeate flux of different membranes

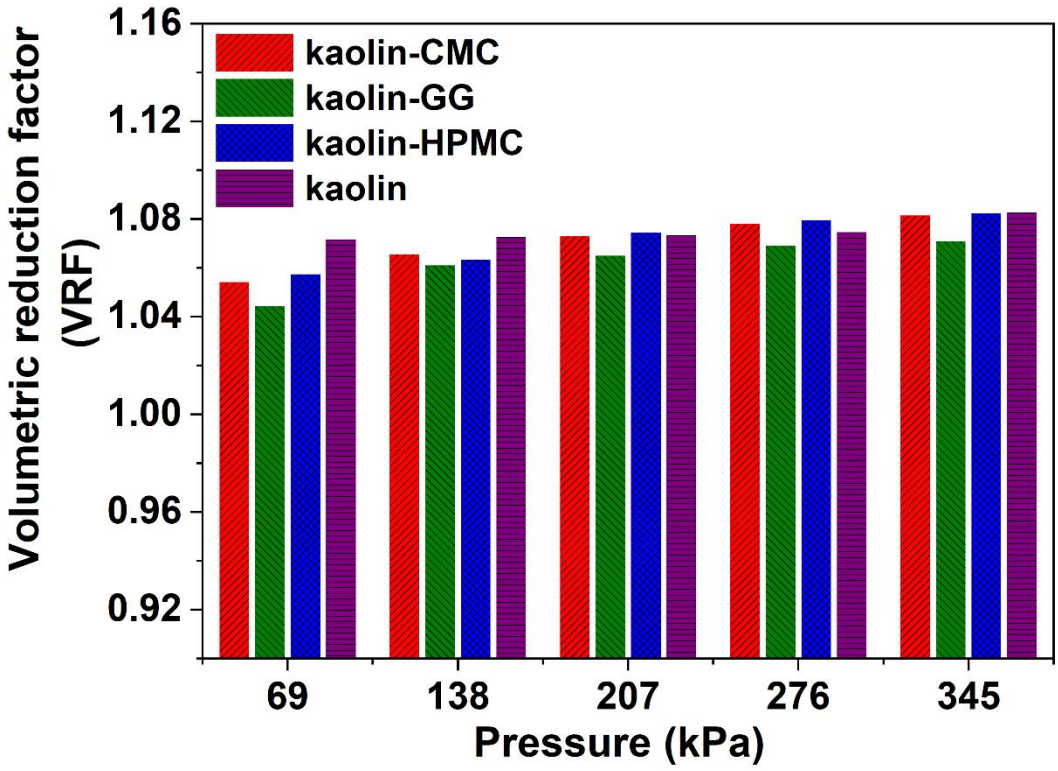

Fig. 3.6 Effect of applied pressure on volumetric reduction factor of different membranes

3.6.4. Extracellular protein and carbohydrate analysis

Though almost a complete recovery of algal cells was obtained through these membranes, in order to gain a better understanding to know the source for pore-blocking, the analysis of extracellular protein and carbohydrate (EPS) concentration in the permeate stream was done and the results were presented in Fig. 3.7. It was noticed from the literature that EPS has a strong effect on the membrane fouling. For instance, Wang et al. (2009) found that EPS played a key role in the fouling of polyether-sulfone membrane having a mean pore size of 0.2 µm. Besides, it was proven in several publications that to isolate the EPS, numerous steps were involved with use of many chemicals (Xiao and Zheng, 2016). In this work, without harming algae cells, EPS was extracted purely in addition to analyse the pore blocking. Further, it was observed in the present study that

some amount of protein concentration (below 0.25 mg/L for all the membranes) and carbohydrate concentration (~114 mg/L) are present in all the experiments. The presence of carbohydrate and protein in permeate stream is due to the extracellular polymeric substances (EPS) formed during the growth phase between polysaccharide chains at the interface of algal cells. The pressure applied on the membrane surface induces the leakage of these EPS from algal cells to permeate side (Larronde-Larretche et al., 2017). Fig. 3.7 portrays the effect of applied pressure on protein and carbohydrate concentration with various membranes. Similar to all other experiments on permeate flux and volume reduction factor, an increase in the applied pressure increased the protein and carbohydrates concentration in permeate as well. With the investigated pressures, the extracellular carbohydrate concentration in permeate stream increased in the following order: 69 kPa < 138 kPa < 207 kPa < 276 kPa < 345 kPa. The increased pressure enhances the build-up of algal cells on the membrane surface, which accelerates the passage of carbohydrate through the membrane in the permeate side, due to increasing convective flux. Since EPS are from the interface of the algal cells and gets leaked out of it, there was no disruption of algal cells observed (see Fig. 3.13). From this, it can be speculated that these extracellular protein and carbohydrates were the one blocking the pores and upon application of excess pressure, these are washed away from the pores of the membrane to enter into the permeate stream. In contrast, protein concentration remains to be constant for all the applied pressures in the Kaolin membrane. This may be because of the larger pores observed in the Kaolin membrane might have made a clear passage for protein to pass into the permeate stream (Zhang et al., 2013). The understanding gained in the present study will be of great use to researchers working in the area of algal research. As the present membrane not only harvest the algal cell but also prepares the filtrate for the next cultivation, it goes one step ahead in

safely extracting the EPS without harming the algal cells, which can in turn be used as a carbon source for the next cycle of algal cultivation.

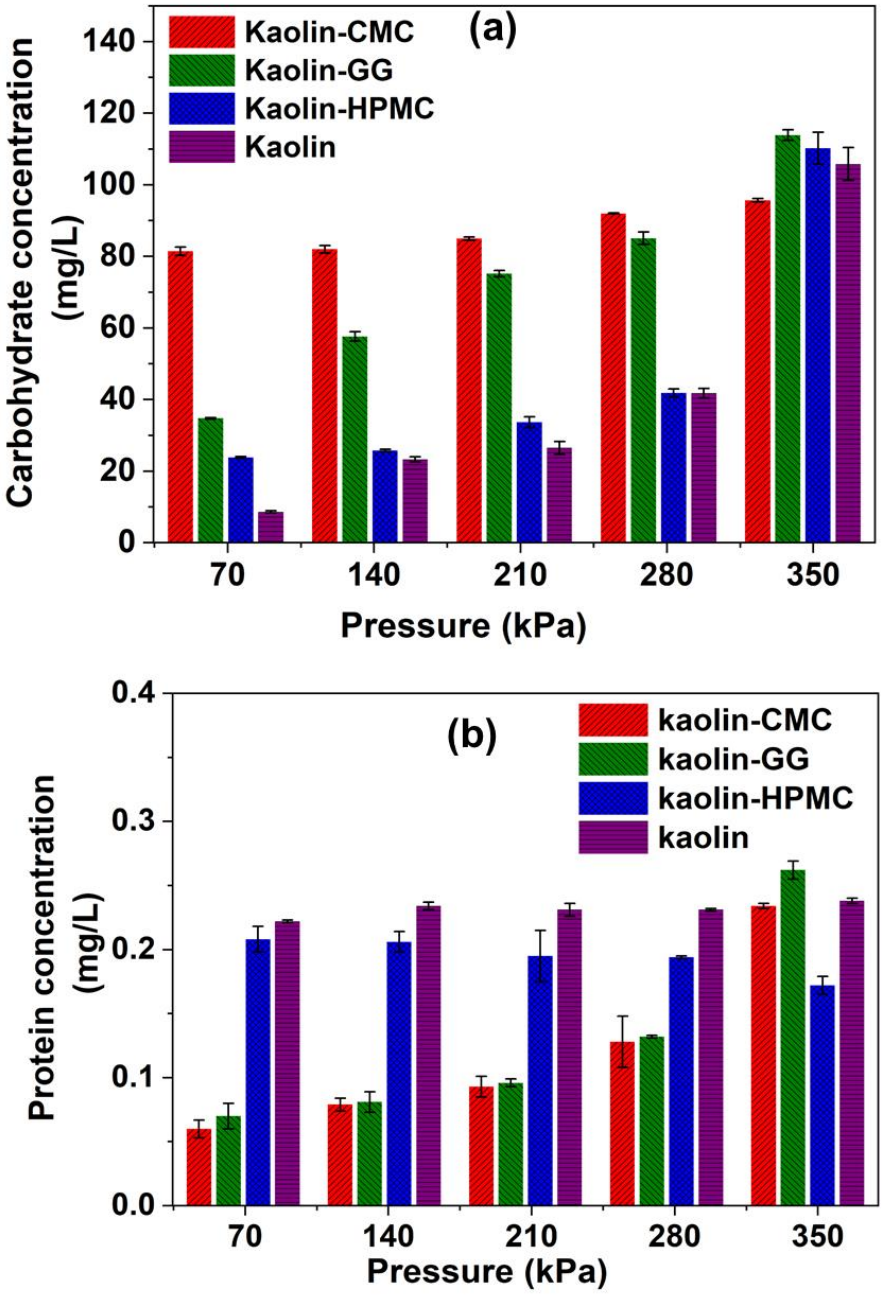

Fig. 3.7 Effect of applied pressure on extracellular (a) carbohydrate and (b) protein content in permeate samples for different membranes

3.6.5. Analysis of membrane fouling

As we observed that the permeate flux decreases with the duration of microfiltration experiment, hence, it is necessary to find the effective flux decline mechanism. The fouling mechanisms were studied with different pore blocking models for the microfiltration of algae. These fouling models present the flux declining mechanism by fitting the flux data of the microfiltration tests with that of the cake filtration or pore-blocking model. Fig. 3.8 depicts the fitted results of Kaolin-HPMC membrane with various pore-blocking models for different applied pressures and Table 3.1 presents the different factors evaluated from the fitted pore blocking models for the separation of algae. Based on the results, it can be illustrated that the cake filtration model fits best with flux data of Kaolin-HPMC membrane. This is ascertained by comparing the R^2 (coefficient of determination) values of different pore-blocking models. For cake filtration model, R^2 value is found to be close to 1 (0.99). The model parameter, k describes the severity of fouling. k_b, the complete pore blocking coefficient, refers to the reduction of membrane surface open to flow. As evidenced from Table 3.1, when the applied pressure increases, k_b also increases. The increased applied pressure enhances the concentration polarization; hence the particles block the passage through the membrane pores. At higher applied pressure, packing density of algal cells increases on the surface of the membrane, thus the membrane pore blocking improves (Zhang and Ding, 2015). In the initial stage of experiment, permeate flux decreases significantly (< 20 min duration) and in the later stage, pressure driven microfiltration leads to a cake layer formation. The k values are higher for the cake filtration model, indicating that the pore blockage happened drastically once the experiment was initiated. It made an understanding that cake layer allows membrane fouling than pore blocking, owing to deposition of large-size algal cells that completely block the membrane pores (Zhu et al., 2016). Similar to the conclusions derived by Kumar et al. (2015b)

and Vasanth et al. (2011), the present study also establishes that the flux decline during the microfiltration of algae followed the cake filtration model. Pore blocking analysis of the other three membranes (Kaolin-CMC, Kaolin-GG and Kaolin) were reported in Figs. 3.9-3.11 and Tables 3.2-3.4.

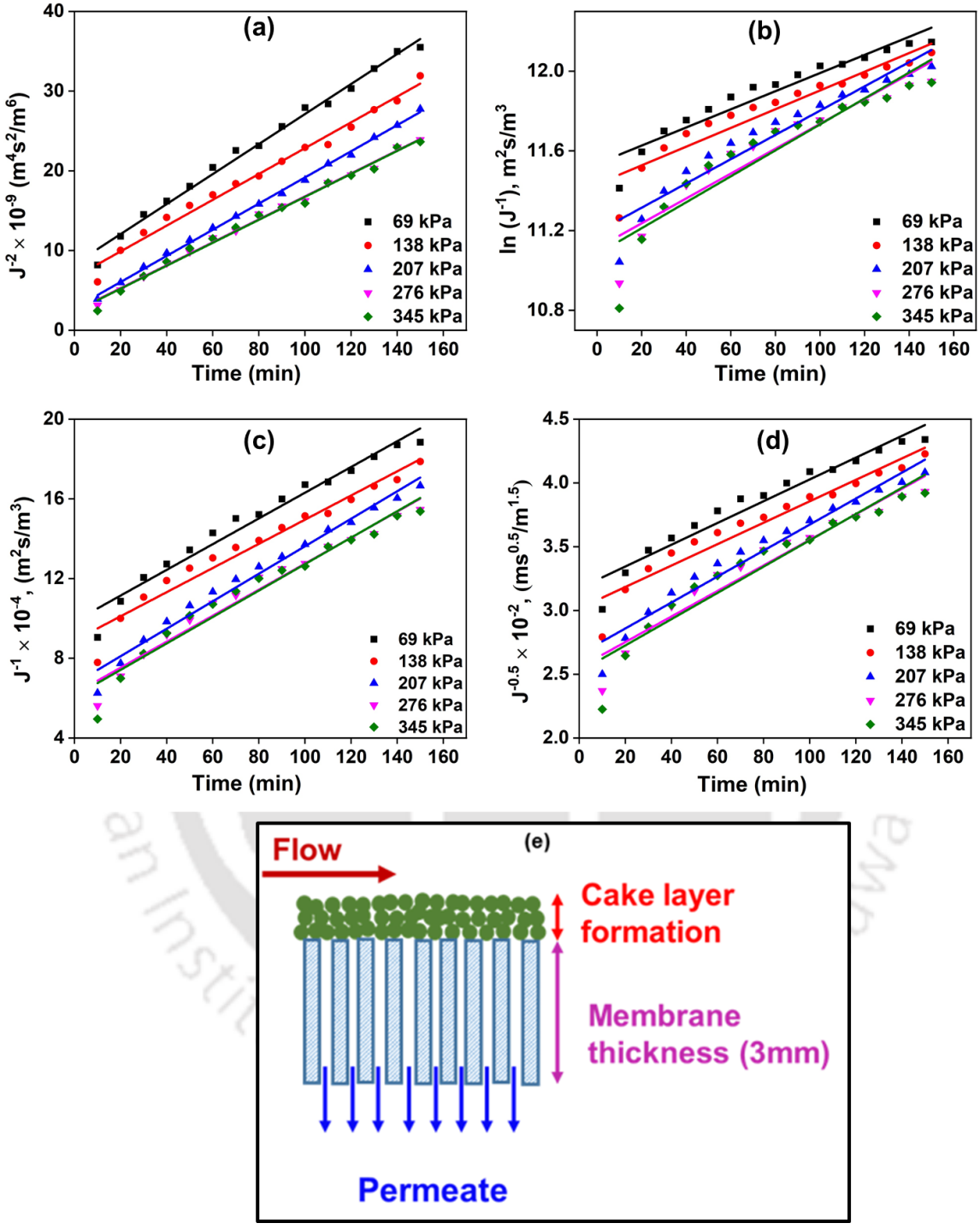

Fig. 3.8 Profiles of permeate flux vs. time for various pore blocking models: (a) Cake filtration model, (b) Complete pore-blocking model, (c) Intermediate pore-blocking model, (d) Standard pore-blocking model and (e) Schematic representation of cake filtration model

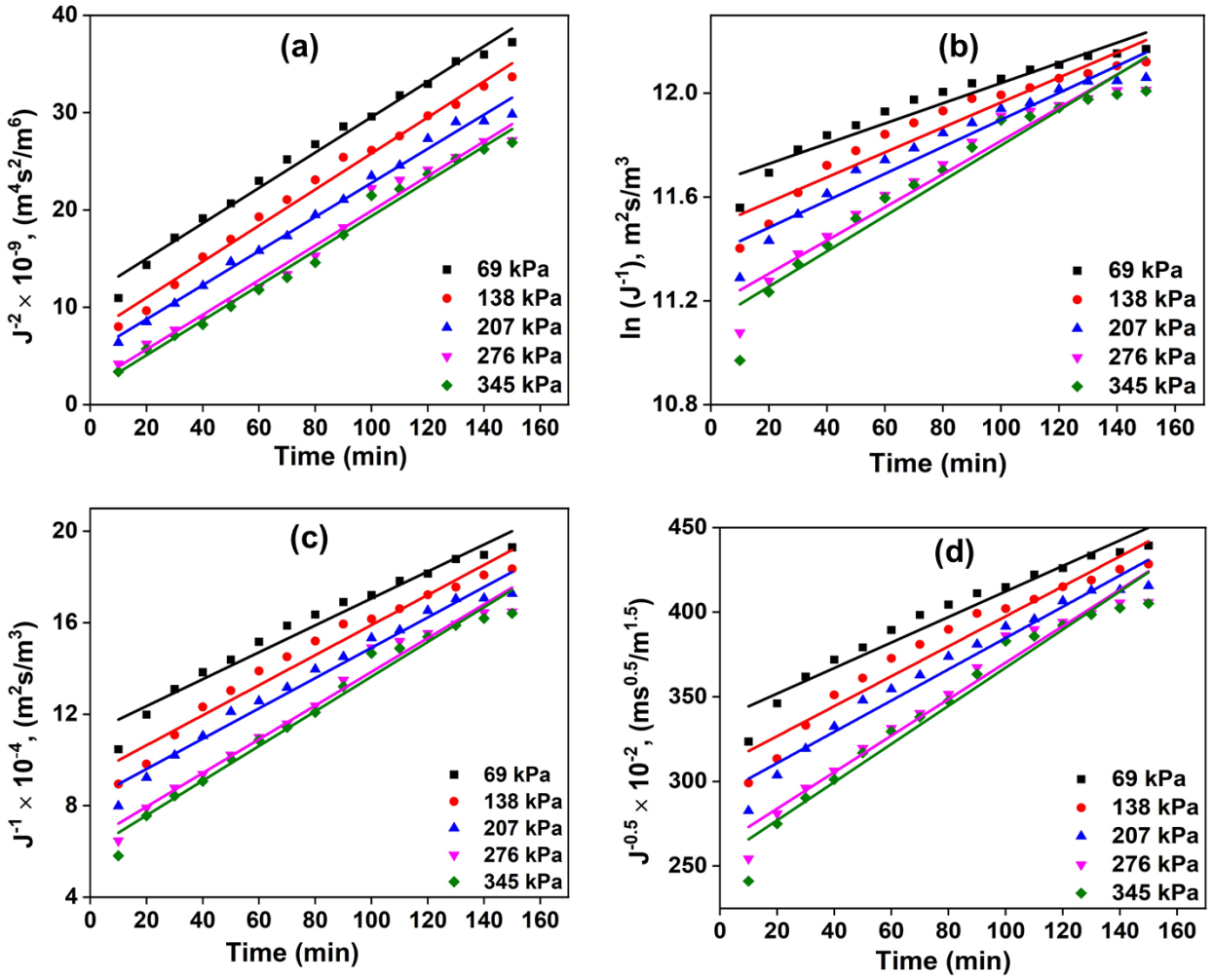

Fig. 3.9 Linearized plots of permeate flux versus time for various pore blocking models of Kaolin-CMC (applied pressures: 69–345 kPa; feed concentration: 500 mg/L; cross flow velocity: 6.42×10^{-3} m/s) (a) Cake filtration model, (b) Complete pore blocking model, (c) Intermediate pore blocking model, (d) Standard pore blocking model.

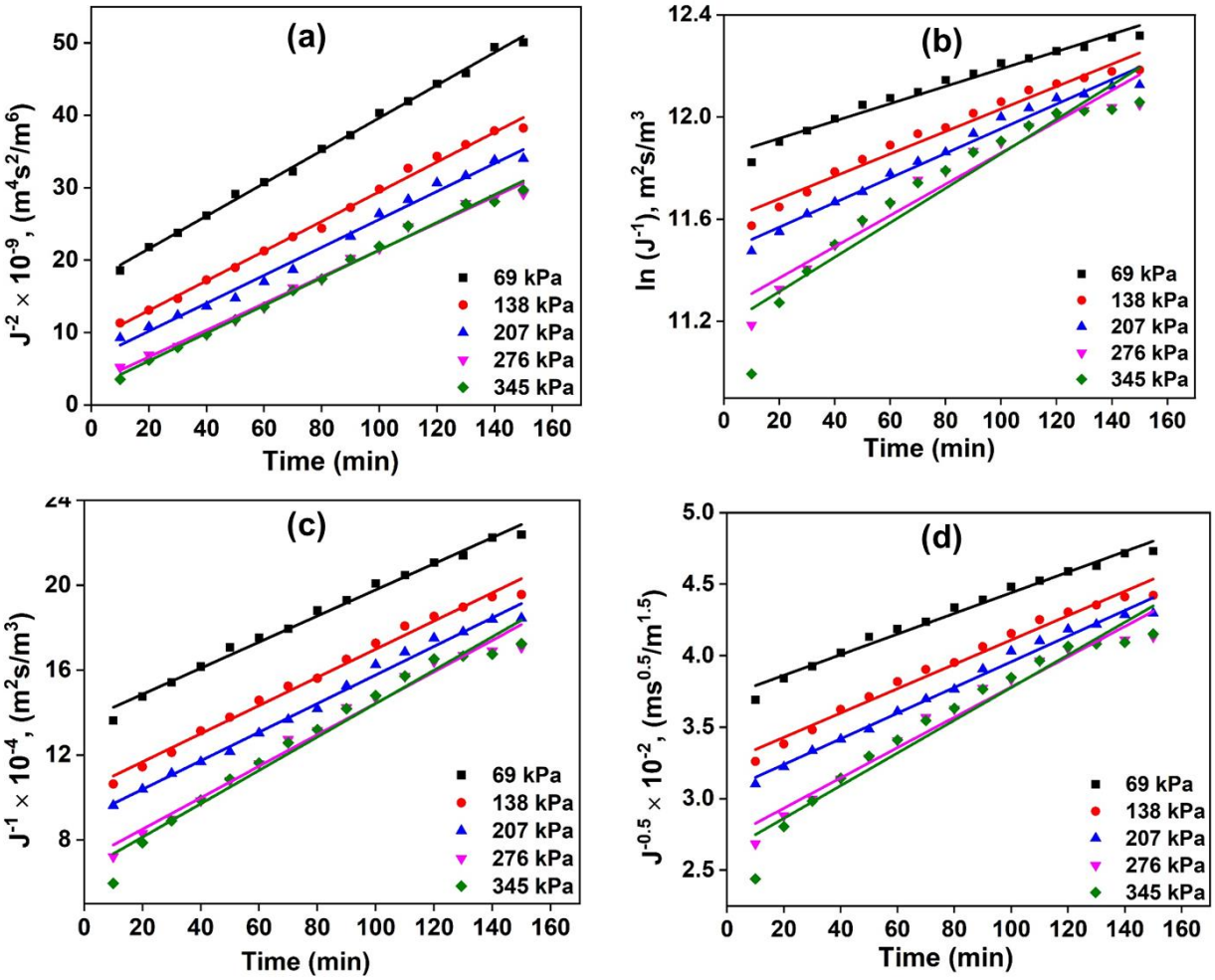

Fig. 3.10 Linearized plots of permeate flux versus time for various pore blocking models of Kaolin-GG membrane (applied pressures: 69–345 kPa; feed concentration: 500 mg/L; cross flow velocity: 6.42×10^{-3} m/s) (a) Cake filtration model, (b) Complete pore blocking model, (c) Intermediate pore blocking model, (d) Standard pore blocking model.

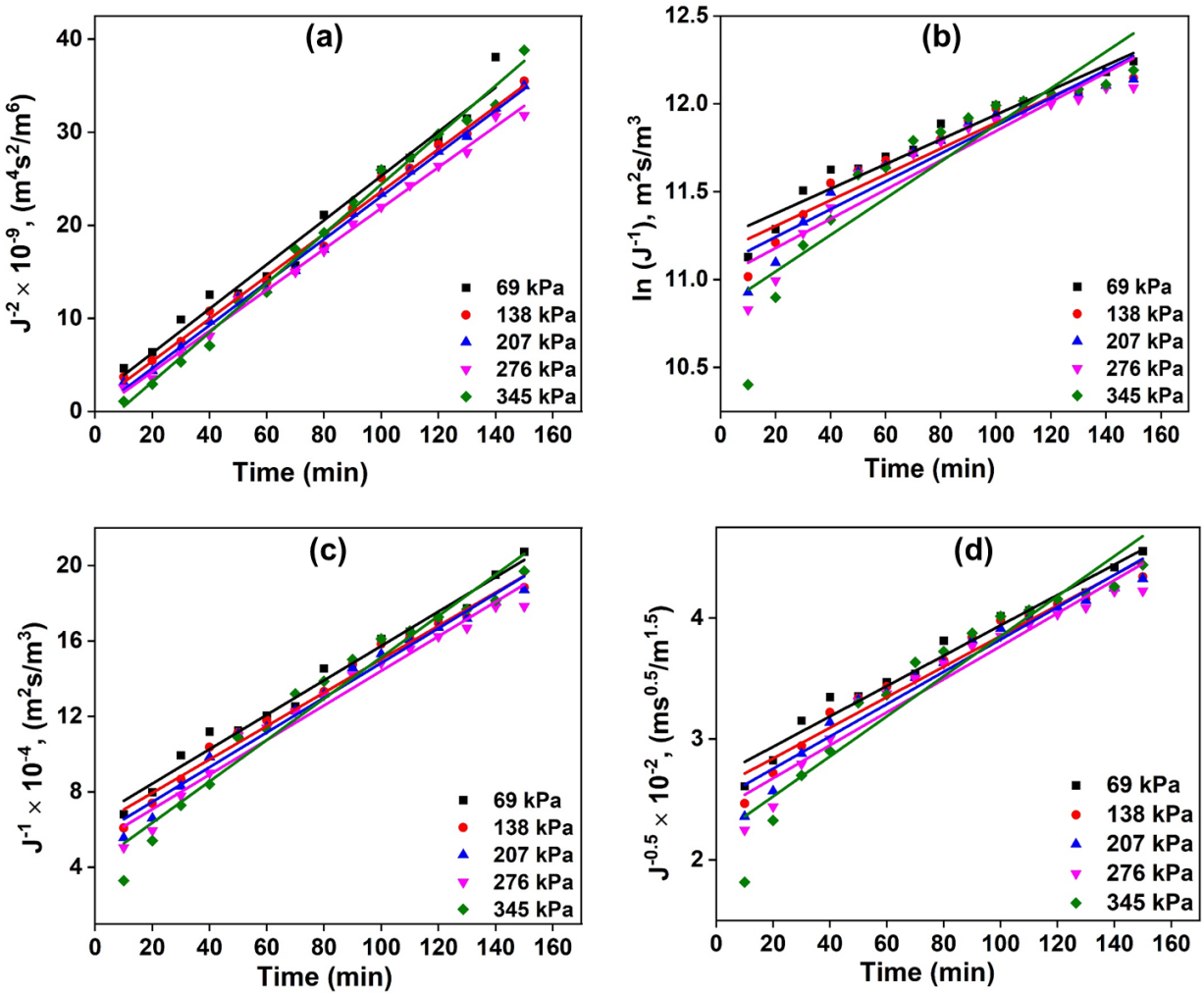

Fig. 3.11 Linearized plots of permeate flux versus time for various pore blocking models for Kaolin membrane (applied pressures: 69–345 kPa; feed concentration: 500 mg/L; cross flow velocity: 6.42×10^{-3} m/s) (a) Cake filtration model, (b) Complete pore blocking model, (c) Intermediate pore blocking model, (d) Standard pore blocking model.

Table 3.1 Summary of parameters associated with various pore blocking models for Kaolin-HPMC membrane.

Applied Pressure (kPa)	**Standard pore blocking**			**Intermediate pore blocking**			**Complete pore blocking**			**Cake filtration**		
	R^2	k_s	$J_0^{-0.5}\times(10^{-2})$	R^2	$k_i \times (10^{-2})$	$J_0^{-1} \times (10^{-4})$	R^2	k_b	$\ln(J_0^{-1})$	R^2	$k_c \times (10^{-8})$	$J_0^{-2} \times (10^{-9})$
69	0.94	0.85	3.17	0.96	6.45	9.85	0.91	0.0045	11.53	0.99	1.88	8.3
138	0.92	0.84	3.01	0.95	6.06	8.89	0.88	0.0047	11.43	0.98	1.61	6.7
207	0.95	1.01	2.65	0.98	6.89	6.72	0.91	0.0060	11.19	0.99	1.64	2.8
276	0.94	1.00	2.55	0.96	6.52	6.22	0.89	0.0062	16.42	0.99	1.44	2.4
345	0.90	1.03	2.51	0.95	6.63	6.09	0.84	0.0065	11.08	0.99	1.44	2.3

Table 3.2 Summary of parameters associated with various pore blocking models for Kaolin-CMC membrane

Applied Pressure (kPa)	**Standard pore blocking**			**Intermediate pore blocking**			**Complete pore blocking**			**Cake filtration**		
	R^2	k_s	$J_0^{-0.5} \times (10^{-2})$	R^2	$k_i \times (10^{-2})$	$J_0^{-1} \times (10^{-4})$	R^2	k_b	$\ln(J_0^{-1})$	R^2	$k_c \times (10^{-8})$	$J_0^{-2} \times (10^{-9})$
69	0.94	0.75	3.4	0.96	5.9	11.2	0.91	0.0039	11.7	0.99	1.82	11.3
138	0.94	0.88	3.1	0.96	6.6	9.3	0.91	0.0048	11.5	0.99	1.85	7.3
207	0.95	0.92	2.9	0.97	6.6	8.3	0.93	0.0052	11.4	0.99	1.75	5.3
276	0.96	1.07	2.6	0.97	7.4	6.5	0.94	0.0064	11.2	0.98	1.78	2.1
345	0.95	1.13	2.5	0.97	7.6	6.1	0.92	0.0068	11.1	0.99	1.78	1.5

Table 3.3 Summary of parameters associated with various pore blocking models for Kaolin-GG membrane

Applied Pressure (kPa)	Standard pore blocking			Intermediate pore blocking			Complete pore blocking			Cake filtration		
	R^2	k_s	$J_0^{-0.5} \times (10^{-2})$	R^2	$k_i \times (10^{-2})$	$J_0^{-1} \times (10^{-4})$	R^2	k_b	$\ln(J_0^{-1})$	R^2	$k_c \times (10^{-8})$	$J_0^{-2} \times (10^{-9})$
69	0.98	0.72	3.7	0.98	6.1	13	0.97	0.0034	11.8	0.99	2.2	17
138	0.98	0.85	3.2	0.98	6.6	10	0.96	0.0043	11.6	0.99	2.0	8.9
207	0.98	0.89	3.0	0.98	6.7	9	0.97	0.0048	11.5	0.99	1.9	6.3
276	0.96	1.06	2.7	0.97	7.4	7	0.94	0.00612	11.2	0.99	1.8	2.9
345	0.93	1.14	2.6	0.96	7.8	6	0.89	0.0068	11.2	0.99	1.9	2.2

Table 3.4 Summary of parameters associated with various pore blocking models for Kaolin membrane

Applied Pressure (kPa)	Standard pore blocking			Intermediate pore blocking			Complete pore blocking			Cake filtration		
	R^2	k_s	$J_0^{-0.5} \times (10^{-2})$	R^2	$k_i \times (10^{-2})$	$J_0^{-1} \times (10^{-4})$	R^2	k_b	$\ln(J_0^{-1})$	R^2	$k_c \times (10^{-8})$	$J_0^{-2} \times (10^{-8})$
69	0.97	1.25	2.68	0.96	9.1	6.6	0.94	0.007	11.23	0.98	2.37	15.1
138	0.95	1.26	2.58	0.98	8.8	6.1	0.91	0.0073	11.15	0.99	2.27	8.37
207	0.95	1.33	2.48	0.97	9.2	5.6	0.90	0.008	11.08	0.99	2.3	0.15
276	0.93	1.36	2.40	0.96	9.2	5.2	0.88	0.0083	11.01	0.99	2.2	-1.46
345	0.90	1.65	2.19	0.95	10.9	4.1	0.81	0.01	10.83	0.99	2.7	-2.13

Fig. 3.12(a-c) shows the morphology of the inner surface and outer surface as well as cross sectional view of the fouled membrane, as observed through FESEM analysis. One can evidently see that the inner surface of the membrane shows the formation of algae layer (cake layer formation). However, there is no algae present on the outer surface of the membrane, which also confirms 100% algae recovery by the membrane. It is also to be noted that as evident from the images (Fig. 3.12a and c), the algal cells are in spherical shape, indicating that there is no damage to the cells even at higher applied pressure. The microscopic image also justifies this fact and the same is presented in Fig. 3.13.

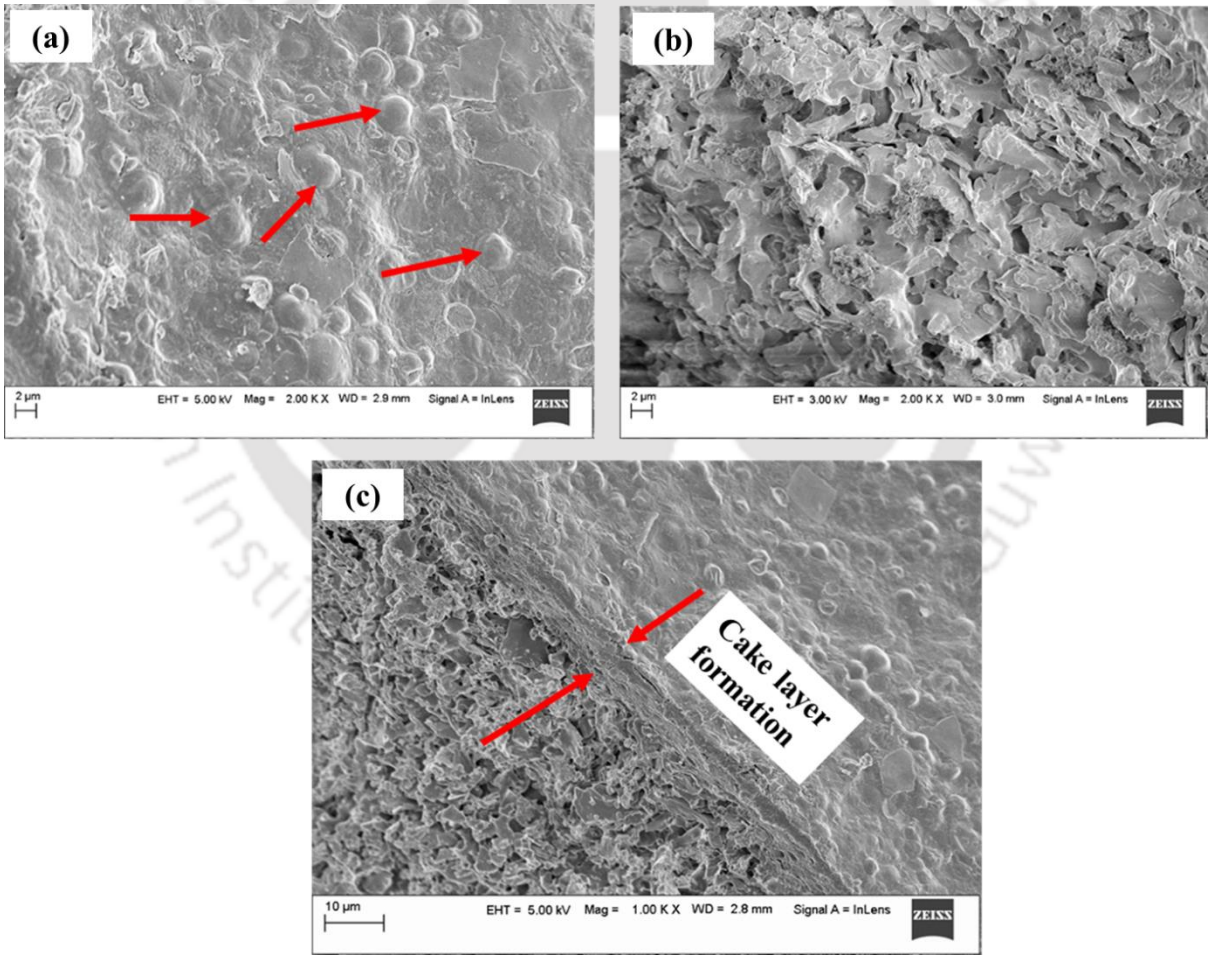

Fig. 3.12 FESEM images of the fouled membrane: (a) inner surface, (b) outer surface and (c) cross-sectional view showing cake formation on the inner surface

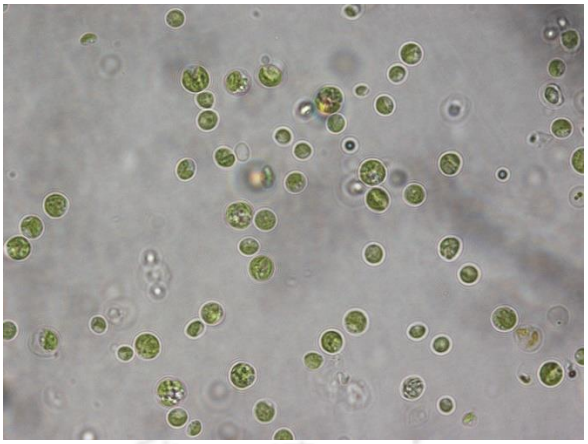

Fig. 3.13 Microscopic image of retentate sample containing microalgae

3.6.2. Comparison of the prepared membranes with other membranes

The performance of the present membranes is evaluated in terms of permeate flux, recovery, VRF/m^2, capacity per volume of reactor (φ) and φ/m^2. Since the average pore diameter of the prepared membranes is smaller than the microalgae size, hence complete recovery of algae is achieved in this work. As evident from Table 3.5, high values of VRF per m^2 and φ per m^2 are observed in this work as compared to the membranes reported in literature (Chen et al., 2012; Petrusevski et al., 1995; Rossi et al., 2004), which once again endorses the outstanding performance of the fabricated membrane. A high VRF per m^2 value reported by Rossi et al. (2004) for commercial PAN membrane (40 kDa) is due to longer filtration time (13 to 20 h). The recovery of algae reported by Chen et al. (2012) for hollow fiber PVDF membrane is 90%. As there is no extensive study reported in the literature on the application of ceramic membranes for algal separation, thus the comparison of the performance of the present membranes is made with the polymeric membranes. It is noteworthy that the present low-cost tubular kaolin-based membranes hold excellent thermal, chemical, and mechanical properties over polymeric membranes. Based on the comparative analysis, it can be concluded that the prepared ceramic membranes are the best alternative to polymeric membranes for the recovery of algae from its culture medium.

Table 3.5 Comparison of performance of the prepared membranes with other membranes reported in the literature

Membrane	Microorganism	Initial feed concentration	VRF	Membrane area (m^2)	VRF /m^2	Capacity per volume of reactor (φ) (min^{-1})	φ / membrane area (min^{-1} m^{-2})	References
Polyacrylonitrile (40 kDa, neutral and hydrophilic)	*Arthrospira platensis*	0.45 g L^{-1}	5	0.01	500	0.001025	0.1025	Rossi et al., (2004)
		1.0 g L^{-1}	5	0.01	500	0.00089	0.089	
			10	0.01	1000	0.00075	0.075	
Hollow fiber PVDF microfiltration membrane	*Scenedesmus sp.*	0.305 g L^{-1}	10	0.4	25	0.036	0.09	Chen et al., (2012)
		0.968	10	0.4	25	0.032	0.08	
Flat sheet microporous membrane	Multiple type of algae	chlorophyll-α < 1 µg/L	40	0.93	43	0.0175	0.019	Petrusevski et al., (1995)
Low cost tubular ceramic membrane	*Chlorella Sorokiniana*	0.5 g L^{-1}	1.08	0.0017	635	0.0005	0.29	This study

[#]Capacity means permeate flow rate; Volume of reactor means initial volume of the feed

Part B: Separation of TiO_2 particles from suspension

3.7. Microfiltration of TiO_2 nanoparticles

Titanium dioxide (TiO_2) used in this work was acquired from Merck (I) Pvt Ltd. For the microfiltration experiments, feed suspensions were prepared by mixing TiO_2 powder with water. According to Weimin et al. (2001), TiO_2 concentrations in the range of 0.05 to 0.5 wt% are generally utilized in slurry reactors to achieve high photocatalytic degradation efficiency. Hence, different feed concentrations (0.05 - 1 wt%) were selected for performing the microfiltration experiments in this study. Cross flow experimental setup depicted in Fig. 2.3 (chapter 2) was used. Kaolin-HPMC membrane was used in this work as it possesses excellent characteristics. In each MF experiment, the feed solution was freshly prepared and the pH was set to 6.5. All the experiments were carried out at an ambient temperature (25 ^oC). Permeate quality was evaluated in terms of percentage recovery (R) based on the removal of TiO_2 by MF. TiO_2 concentration in the permeate and feed solutions was measured in terms of turbidity using a turbidity meter (Model: STI-407, Make: STI, India) and the recovery (%) was calculated using the following relationship (Manni et al., 2020).

$$\text{Recovery, R(\%)} = \left(1-\frac{C_p}{C_f}\right)\times 100 \qquad (3.7)$$

Where C_f and C_p are the TiO_2 concentration value of feed and permeate, respectively

After each experimental run, the membrane was cleaned by passing water for 30 min at a high applied pressure, followed by washing with a detergent solution (1 g/L surf excel solution) for 2 h. After the cleaning step, the membrane was removed from the module and treated in a bath sonicator for 5 minutes by soaking it in water to remove any pore blocking particles. The MF experimental setup was further cleaned by passing water for 1 h to remove any residual cleansing agent. The clean membrane was checked for pure water flux prior to its reuse in the

following experiment in order to confirm restoration of the original flux value of the membrane. The regenerated membrane displayed the water flux within ±5% of its initial value.

3.8. Membrane fouling analysis

The membrane fouling during the course of microfiltration of TiO_2 particles was examined by resistance-in-series model. In microfiltration experiments, the membrane resistance (R_m) was first measured using pure water flux (J_{pw}) data.

$$R_m = \frac{\Delta P}{\eta_w \times J_{pw}} \tag{3.8}$$

where R_m is the resistance of membrane (m^{-1}), η_w is the viscosity of water (Pa·s). Microfiltration using TiO_2 suspension of known concentration was later carried out to determine permeate flux of the membrane. Thus the permeate flux of TiO_2 can be measured using the following equation.

$$J_{pf} = \frac{\Delta P}{\eta_p \times (R_m + R_f)} \tag{3.9}$$

where J_{pf} is steady-state permeate flux, η_p is the permeate viscosity (Pa·s), ΔP is the applied pressure (Pa). The viscosity of permeate is assumed to be the same as the viscosity of water. The initial permeate flux of MF process will depend only on R_m (R_f is zero) at a constant applied pressure. Pore blocking and cake formation will cause R_f to increase when the filtration progresses. Hence, the microfiltration of TiO_2 will change from membrane resistance limited to filtration resistance limited process. The total resistance (R_t) is sum of filtration resistance and intrinsic membrane resistance. The membrane resistance is constant and doesn't vary with process conditions, whereas the filtration resistance will change based on process conditions.

3.9. Characterization of TiO_2 nanoparticles

The raw TiO_2 powder was evaluated for its phase compositions by an XRD (Model: D8 Advance, Make: Bruker, Netherlands). The profiles were acquired using Cu Kα radiation as a source, with a step size of 0.05 recorded in the 2θ values ranging from 5 to 70. The size of TiO_2

NPs was measured using Delsa Nano C particle size analyzer (Model: Delsa Nano C, Make: M/s Beckman Coulter, Switzerland). The zeta potential (or surface charge) of TiO_2 NPs was also measured using Delsa Nano C zeta potential analyzer (Model: Delsa Nano C, Make: M/s Beckman Coulter, Switzerland). For zeta potential measurement, feed suspension was prepared at different pH using either HCl or NaOH solution. The morphology and primary particle size of TiO_2 were analyzed by field emission transmission electron microscope (Model: 2100F, Make: JEOL, Japan) and field emission scanning electron microscope (Model: Sigma 300, Make: Zeiss, Germany). For FETEM analysis, the TiO_2 sample was sonicated for 10 min and immediately, on a conductive copper grid, a small drop of the sample was kept and then dried before analysis. The morphology of the fouled membranes, both inner and outer surfaces and filtration layer formation, was analyzed by FESEM (Model: Sigma 300, Make: Zeiss, Germany) after the end of the MF experiment. The membrane cleaning efficiency was confirmed by energy-dispersive X-ray spectroscopy (Model: Gemini, Make: Zeiss, Germany) analysis.

3.10. Results and Discussion

3.10.1. Characterization of TiO_2 nanoparticles

Fig. 3.14(a) portrays the XRD profile of TiO_2 NPs. The obtained result is in good agreement with JCPDS standard files #21-1276 (for rutile) and #21-1272 (for anatase), confirming that both anatase and rutile phases are present in the TiO_2 powder. Sharp peaks appeared at 2θ values of 25.2^o and 48.01^o, respectively, which correspond to the anatase phase. Anatase phase has a higher degree of hydroxylation, which generates a large number of hydroxyl groups (OH^-) on the surface (Liao et al., 2009). Hence, it will be responsible for more negative zeta potential, which ultimately affects the size of TiO_2 agglomerates. The XRD results are in good agreement with zeta potential measurement. The intensity of the XRD peaks signifies that the nanoparticles are crystalline and their size was calculated to be 55 nm using Scherrer's equation (Wang et al., 2016).

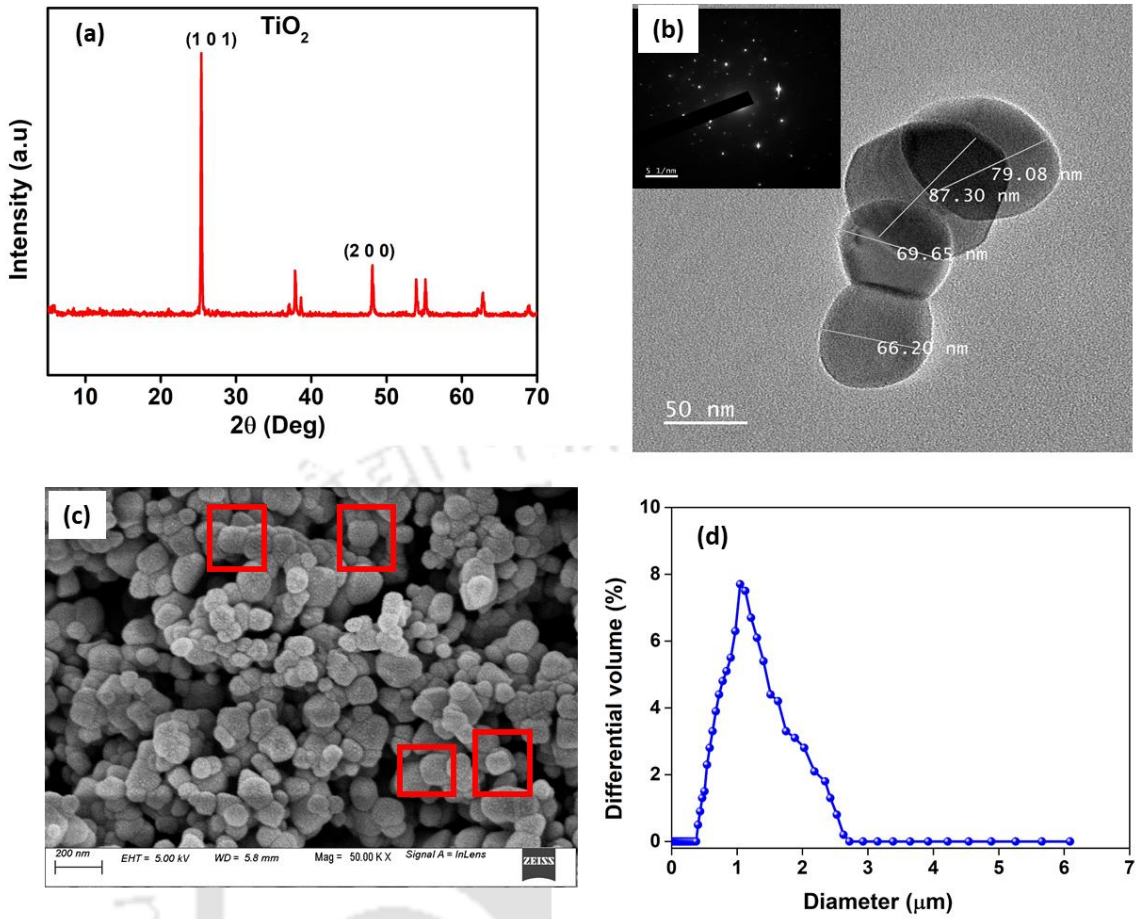

Fig. 3.14 (a) XRD profile, (b) FETEM image and (c) FESEM image of TiO_2 NPs; (d) Aggregation behaviour of TiO_2 NPs measured using particle size analyzer.

The surface morphology and structure of TiO_2 NPs were examined by FESEM and FETEM, respectively. Fig. 3.14(b) shows a bright field TEM image with a selected area electron diffraction (SAED) pattern of TiO_2 NPs agglomerates. The SAED pattern demonstrated that the sample is crystalline. The primary particle size of TiO_2 NPs by FETEM was observed to be 75 nm. Similar patterns are reported for single crystalline CuO nanosized particles prepared with various additives (Dong et al., 2001). The results of TEM were in good agreement with the XRD analysis. As evident from Fig. 3.14(c), TiO_2 nanoparticles possessed a smooth surface with cubic-like structures. The size and shape of the particles were uniform, but a large amount of these particles were also in agglomerated form.

The particle size distribution of TiO_2 NPs measured using particle size analyzer is depicted in Fig. 3.14(d) and the mean size of the particle was estimated to be 1.3 µm. The result clearly demonstrated that agglomerates of TiO_2 NPs with different sizes were present in the feed samples. A similar observation was made by Weimin et al. (2001), who reported that the TiO_2 particle size (i.e., aggregate) ranged from 14 to 3.5 µm. Ghimici et al. (2013) also mentioned the hydrodynamic size of TiO_2 as 401.7 nm at pH 6.2. Based on the above results, it can be said that TiO_2 separation efficiency is strongly influenced by interfacial effects of aggregation rather than by its primary particle size (Weimin et al., 2001). It is worth mentioning that when TiO_2 is dispersed in water, they have different surface groups such as $-TiOH_2$, -TiOH, and $-TiO^-$, depending on the pH of the suspension. These charged groups, in turn, significantly affect particle aggregation (Ghimici et al., 2013). These observations on the TiO_2 NPs further substantiate that microfiltration is an efficient technique to separate the NPs in aggregate form from the water and microfiltration selected in this work to separate TiO_2 from water was justified.

Fig. 3.15 shows the zeta potential and particle size of TiO_2 NPs at different pH. The pH at which the net surface charge density is zero is the isoelectric point (IEP) (Xu et al., 2008). Fig. 3.15(a) elucidates that the IEP of TiO_2 is ~5.1 and TiO_2 NPs aggregate maximum at this pH value. The dispersion of TiO_2 improves with an increase in the surface charge, as clearly evident from Fig. 3.15b. The average size of TiO_2 particles (i. e., aggregates) at IEP (5.1) is found to be 1.58 µm, whereas particles with a greater surface charge are dispersed well. Similar results were observed by Weimin et al. (2001), who reported that TiO_2 particles tend to aggregate near IEP with a maximum particle size of 3.5 µm.

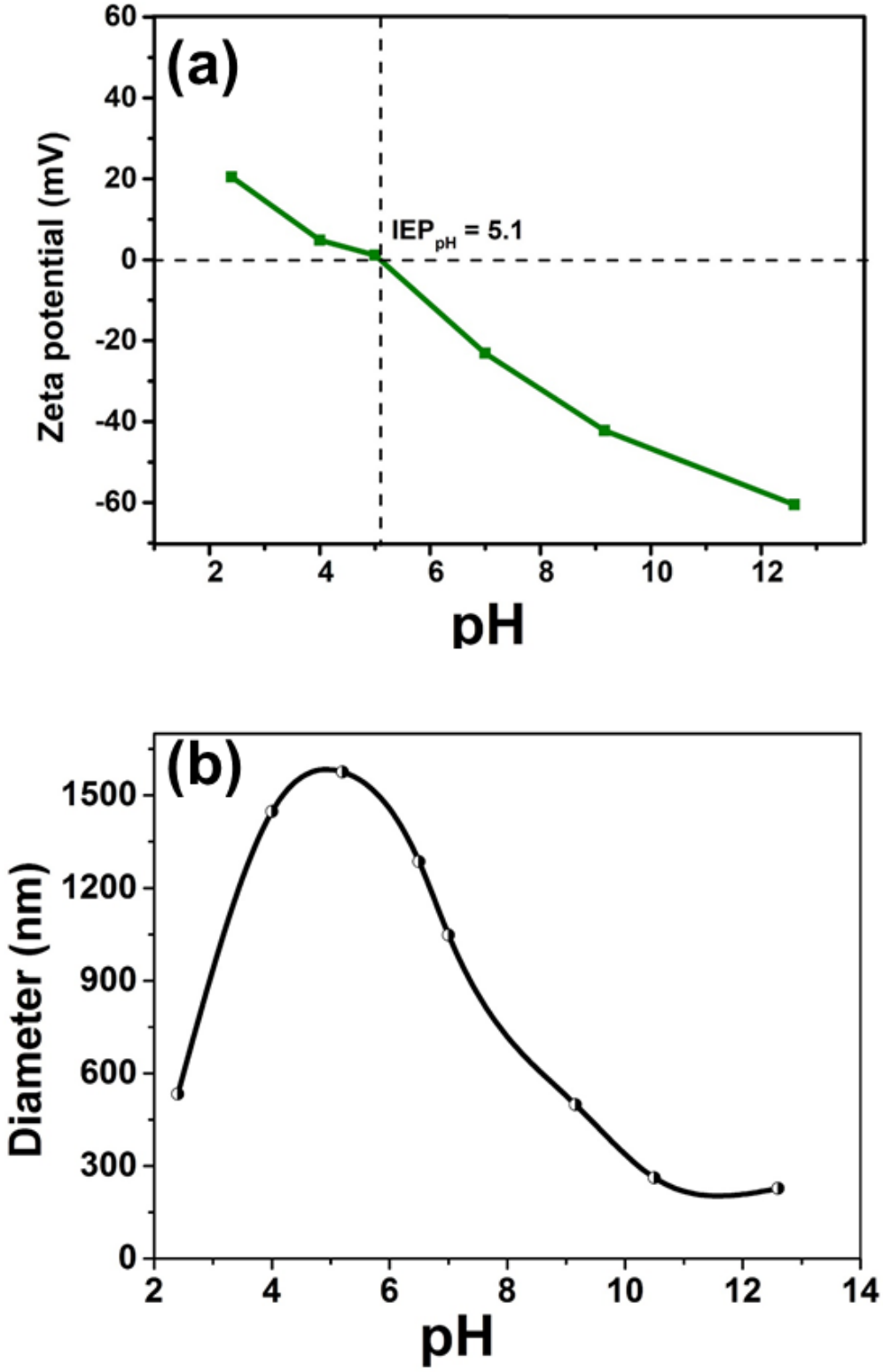

Fig. 3.15 Plots of (a) zeta potential vs. pH of TiO_2 suspension and (b) particle size of TiO_2 vs. pH

3.10.2. Microfiltration of TiO_2 NPs

The agglomeration of TiO_2 NPs in water as dispersion medium is favourable for microfiltration to separate TiO_2 NPs from its suspension. Cross-flow MF is a flow parallel to filter medium, which helps to reduce the formation of a filtration layer. Various parameters that influence cross flow MF performance are applied pressure, cross flow velocity (CFV), filtration layer resistance, membrane resistance, particle size distribution in the feed, agglomeration behaviour of particles, pH of the feed solution, etc. Among these parameters, applied pressure, CFV, feed concentration and pH are the key independent parameters and hence, the influence of these factors was examined in this study.

3.10.2.1. Effect of applied pressure

Interfacial forces between particles as well as that between the particles and membrane surface significantly affect the permeate flux (Kühnl et al., 2010). Fig. 3.16a depicts the variation in permeate flux with various applied pressures for TiO_2 separation. At all the applied pressures, the permeate flux decreased with microfiltration duration due to increased filtration layer thickness on the membrane surface. After a certain time (170-180 minutes), the permeate flux reached a nearly constant value, which may be due to the transport of net deposited particles remaining the same as that of the back transport of particles from the filtration layer (Weimin et al., 2001). However, a sharp decline in permeate flux was not observed in this study, which is advantageous for large-scale applications. A previous study demonstrated that after a specific duration of microfiltration, the increased accumulation of solute particles on the membrane surface results in the layer formation with a very low porosity value (Zhang et al., 2016). Compared to large-sized particles, small-sized nanoparticles usually cause severe fouling. As evident from Fig. 3.16a, the permeate flux augmented with increasing applied pressure from 138 to 414 kPa due to increased driving force. Yang et al. (2017) also noticed an enhancement in permeate flux with an increase in transmembrane pressure from 0.05 to 0.1 MPa during the

filtration of cellulase fermentation broth using attapulgite microfiltration membrane having a mean pore size of 0.12 µm.

Permeate sample collected at each applied pressure was subjected to turbidity measurement to estimate the recovery efficiency of TiO_2 NPs, and the results are presented in Fig. 3.16b. As apparent from the figure, the recovery performance of the membrane is found to be excellent with almost 100% recovery of TiO_2 NPs achieved at all the applied pressures. The possible reason for complete recovery of NPs from its suspension is that the membrane with a small pore size restricts the passage of larger sized TiO_2 agglomerates through the membrane in the permeate side (Shukla et al., 2000). Similar results were observed by Qin et al. (2015), where fly ash based ceramic membranes having mean pore diameters of 1.25 and 0.3 µm displayed complete recovery of suspended particles from kiwi (fruit) juice due to small pore size of the membranes as compared to large-sized suspended particles present in the juice.

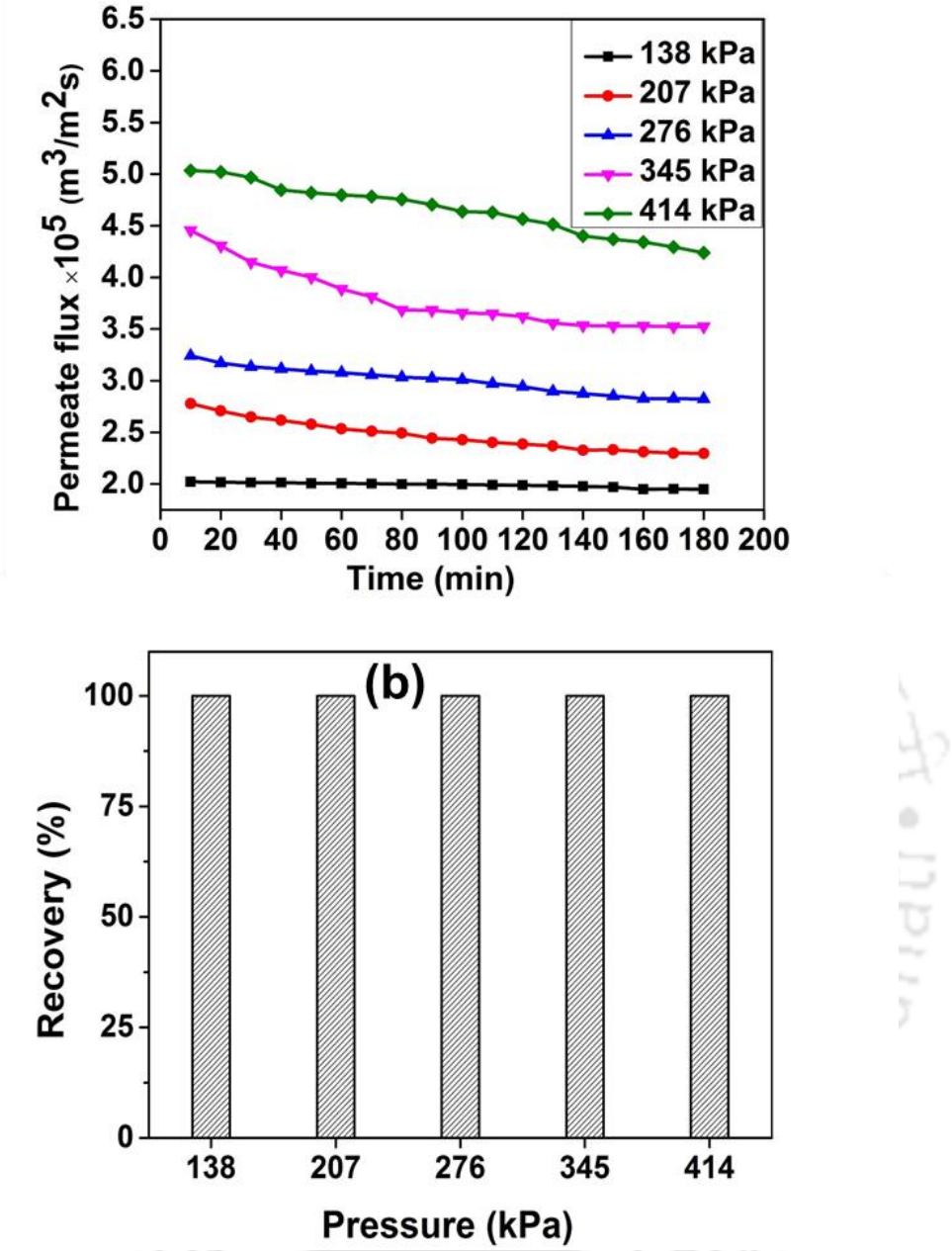

Fig. 3.16 Effect of applied pressure on (a) permeate flux and (b) recovery of TiO_2 NPs (Feed concentration = 0.1 wt%; pH = 6.5; CFV = 2.41×10^{-3} m/s)

3.10.2.2. Effect of cross flow velocity

The membrane performance in terms of flux and recovery at different cross flow velocities (2.41×10^{-3}, 4.02×10^{-3} and 5.63×10^{-3} m/s) for treating TiO_2 NPs suspension is depicted in Fig. 3.17. It is observed from Fig. 3.17 (a and b) that a high cross flow velocity helps in enhancing

the permeate flux almost linearly. An increase in cross flow velocity enhances the shear stress on the surface of the membrane, i.e., increasing sweeping action over the membrane, resulting in a decrease in the thickness of the filtration layer on the membrane surface (Tanudjaja et al., 2017). The permeate flux is only affected by membrane resistance during the initial stages of MF operation, and as the filtration layer grows, the flux decreases. Conversely, mass boundary layers tend to decrease with increasing cross flow velocity and mass transfer coefficients tend to increase (Yang et al., 2017). As evident from Fig. 3.17c, TiO_2 recovery performance of the membrane in terms of turbidity is almost the same and found to be 100% at all the investigated cross flow velocity values. This result indicates that the membrane's recovery performance is not affected by the cross flow velocity as the average size of TiO_2 agglomerates in the feed is significantly greater than the membrane pore size. Hence, complete recovery of TiO_2 from the suspension is attributed to the simple size exclusion mechanism. The obtained result is consistent with the results reported by Zhao et al. (2002) for the removal of TiO_2 particles using α-alumina membrane with an average pore diameter of 0.2 μm, which is substantially smaller than the particle size (2.89 μm).

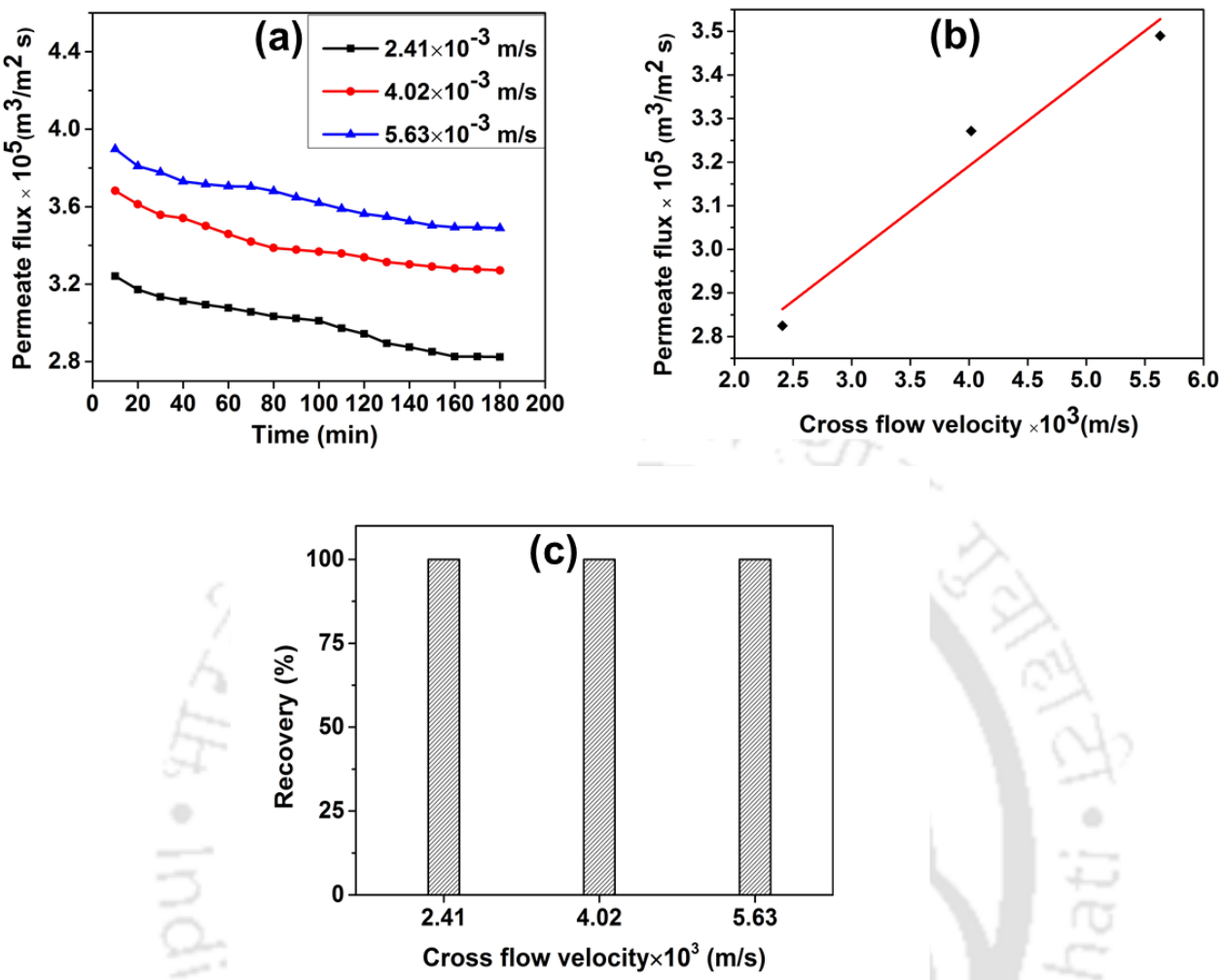

Fig. 3.17 Effect of cross flow velocity on (a) permeate flux (b) linear plot of permeate flux vs. cross flow velocity and (c) recovery of TiO_2 NPs (Feed concentration = 0.1 wt%; pH = 6.5; Applied pressure = 276 kPa)

3.10.2.3. Effect of feed concentration

The permeate flux profile with time for different TiO_2 concentrations (0.05, 0.1 and 1 wt%) at an applied pressure of 276 kPa and cross flow velocity of 2.41×10^{-3} m/s is shown in Fig. 3.18 (a). As expected, the permeate flux decreased with increasing TiO_2 concentration (Fig. 3.18a). Comparison of the flux profile for the three feed concentrations, it was observed that at higher TiO_2 concentration (1 wt%), the flux declined drastically due to rapid formation of filtration layer on the membrane surface at the beginning of microfiltration itself, which compacted

quickly to form a hard and thick filtration towards the end of the MF process. Besides, the quantity of permeate produced was significantly less than that of the other two feed concentrations (0.05 and 0.1 wt% TiO_2) due to the thick and stiff filtration layer formation on the membrane surface. Similar results were reported by Akamatsu et al. (2020) for the microfiltration of Bovine serum albumin (BSA) using polyethylene microfiltration membrane (0.06 µm); the permeate flux decreased when the BSA concentration was increased from 10 to 5000 mg/L. Fig. 3.18 (b) demonstrates 100% recovery at all three feed concentrations. These results also reveal that TiO_2 NPs aggregated at all the studied feed concentrations, which helped to recover TiO_2 completely by microfiltration. Fig. 3.18 (c) shows comparison of the images of feed and permeate samples, which reveals that the permeate obtained is transparent due to complete recovery of TiO_2 particles by microfiltration.

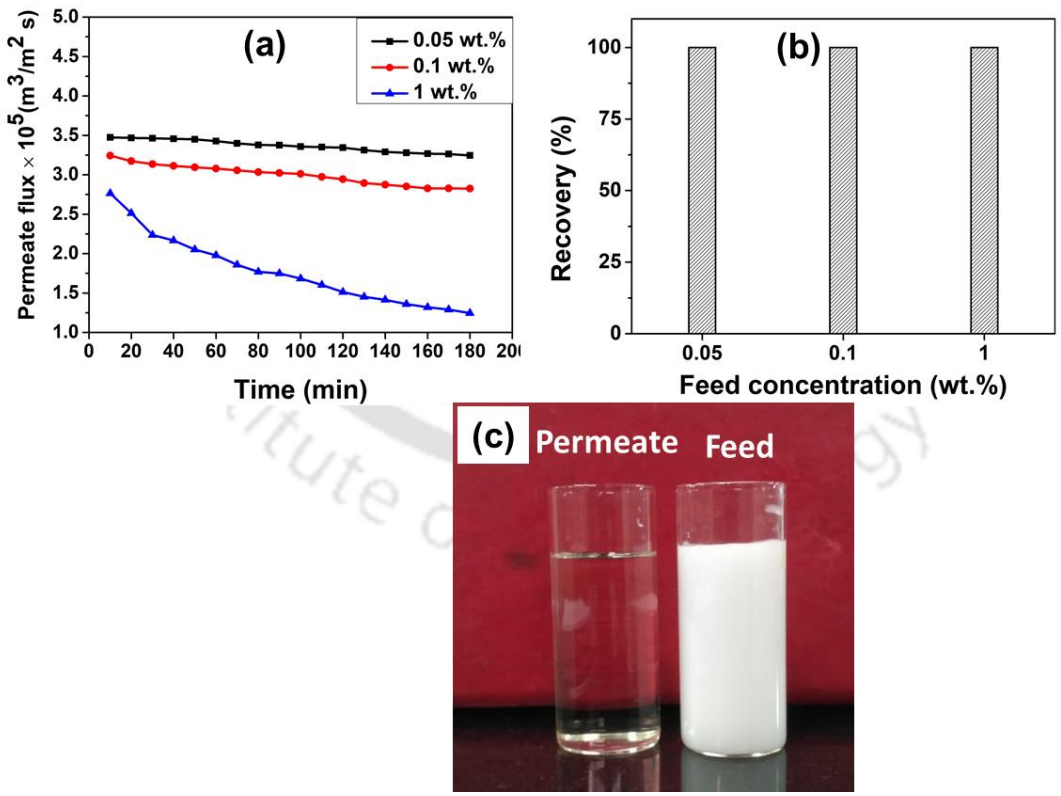

Fig. 3.18 Effect of different feed concentrations (0.05 – 1.0 wt% of TiO_2) on (a) permeate flux and (b) recovery, and (c) images comparing feed and permeate samples (Applied pressure = 276 kPa; pH = 6.5; CFV = 2.41×10^{-3} m/s)

3.10.2.4. Effect of pH

It is well reported that the pH will strongly influence zeta potential, which ultimately influence TiO_2 NPs agglomerate size in the feed (Weimin et al., 2001). Hence, in order to understand the effect of feed pH on the average permeate flux and recovery rate, microfiltration of TiO_2 NPs was examined at five different pH of feed (4, 5.1, 6.5, 9, 11) containing a fixed TiO_2 concentration of 0.1 wt%. The results obtained are presented in Fig. 3.19 (a), which shows that the maximum flux is produced using the feed at pH 5.1. Compared with the experimental condition at pH 4 of the feed, the experiment carried out at feed pH 5.1 resulted in the highest flux. At pH 5.1(IEP), the TiO_2 NPs possessed zero charge and its size (i. e., aggregates) maximum (Fig. 3.15b). Such large particles may produce filtration with high porosity, whereas at a pH above and below the IEP, fine particles offer more resistance to permeate flux. It has been well documented that the permeate flux of various nanoparticles (TiO_2 and SiO_2) through ceramic membrane is enhanced at pH close to its IEP, whereas at a pH above and below its IEP, the permeate flux decreases (Le et al., 2019). Vyas et al. (2000) reported that the permeate flux increased with the large particles owing to scouring of the filtration surface. A previous study also indicated that for the separation of neutral charged nanoparticles by ceramic microfiltration membrane, the filtration layer formed on the membrane surface is thin due to the back transport of particles from the membrane (Le et al., 2019). At all the investigated feed pH values, 100% recovery of TiO_2 NPs was observed (Fig. 3.19 (b)).

Even though the membrane characterization results clearly demonstrated that the developed membrane is stable in the acidic environment (pH 4 and 5.1), it is also equally important to know if any leaching of materials from the membrane occurs when the membranes are used to treat acidic solutions. In this regard, after performing the microfiltration experiment with the feed suspension at pH 4, few characterizations were done to identify any changes in the membranes. FESEM images portrayed in Fig. 3.20 revealed no enlarged pores present after

treating the membrane with the feed suspensions at pH 4. Comparison of XRD results of the fresh and used membrane at feed pH 4 also elucidated that there is no change in its composition as similar peaks appeared in both cases (Fig. 3.20 (c)). Moreover, the turbidity of the permeate was zero. From these observations, it can be concluded that at this experimental condition (feed pH 4; applied pressure 276 kPa; CFV 2.41×10^{-3} m/s), leaching from the membrane was absent. It is clear from the above discussion that the reason for obtaining high flux at feed pH 4 and 5.1 is attributed to the size of TiO_2 NPs at these values.

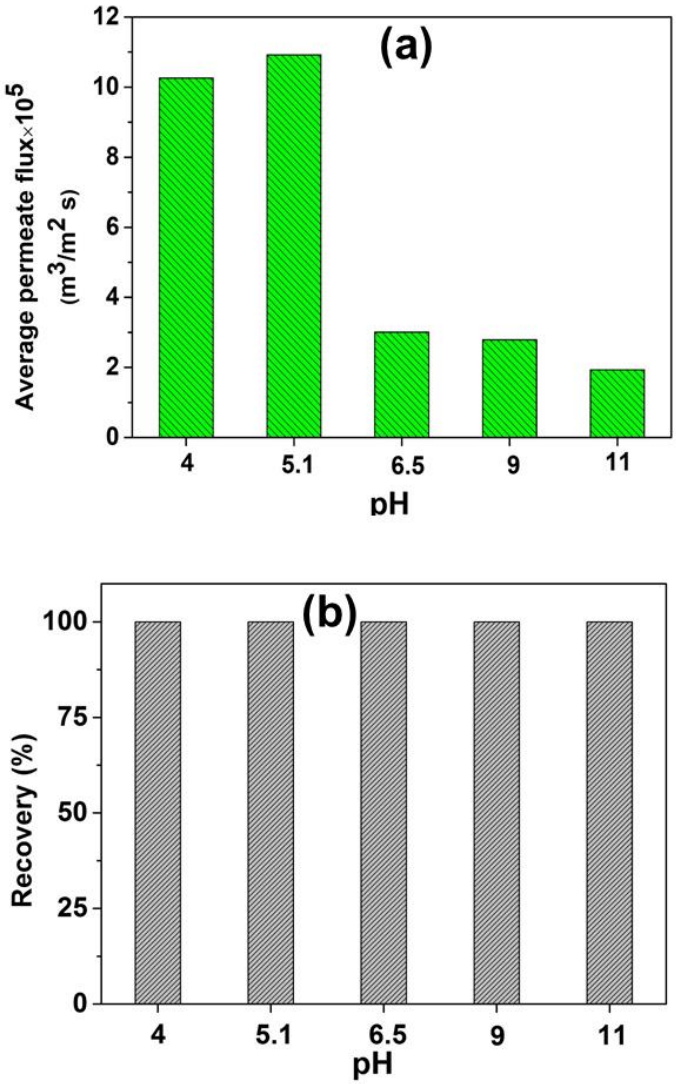

Fig. 3.19 Effect of pH on (a) average permeate flux and (b) recovery of TiO_2 NPs (CFV = 2.41×10^{-3} m/s; Applied pressure = 276 kPa; Feed concentration = 0.1 wt%)

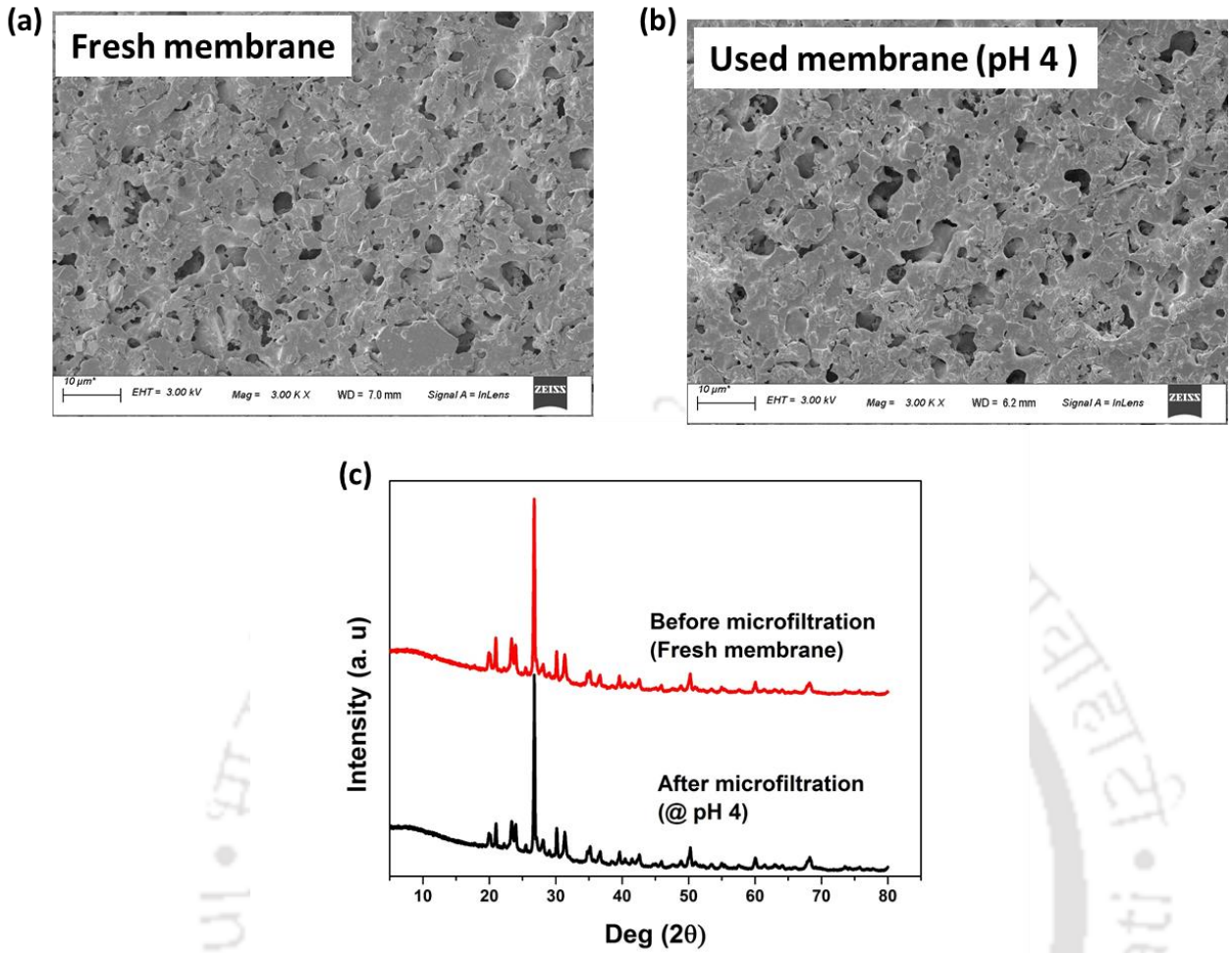

Fig. 3.20 (a-b) FESEM image of inner surface of membrane before and after microfiltration of TiO_2 NPs at pH and (c) XRD analysis

3.10.3. Fouling analysis

The resistances during microfiltration of TiO_2 suspension were examined by using a resistance-in-series model. The influence of operating parameters such as applied pressure and CFV on the fouling of membrane was studied in detail and the results are discussed here.

The hydraulic resistance values of the membrane were determined at various applied pressures in order to study the effect of applied pressure on the fouling mechanism. Fig. 3.21a shows the variation in resistances during microfiltration for different applied pressures ranging from 138 to 414 kPa and a fixed cross flow velocity of 2.41×10^{-3} m/s. Values of membrane resistance (R_m), total resistance (R_t) and filtration resistance (R_f) were calculated using earlier equations

(3.8) and (3.9). As evident from Fig. 3.21a, filtration resistance (R_f) and total resistance (R_t) increased steadily with an increase in applied pressure and remained constant at high applied pressures. The change in R_t is due to a change in R_f value. As the applied pressure increased from 138 to 276 kPa, the value of R_f increased steadily and remained constant above 276 kPa applied pressure. During the course of microfiltration, filtration layer thickness increased and reached a quasi-steady state. The constant values of resistances at higher applied pressures (>276 kPa) indicated the formation of a highly compacted filtration layer with TiO_2 NPs (Manikandan et al., 2019). Yang et al. (2017) also reported a similar trend of resistances during the separation of cellulase from fermentation broth.

Fig. 3.21b depicts the hydraulic resistances and their significance in microfiltration at different cross flow velocities in the range of 2.41×10^{-3} m/s – 5.63×10^{-3} m/s and a fixed applied pressure of 276 kPa. With increasing cross flow velocity, R_f and R_t decreased, which is attributed to the enhancement in shear stress at higher CFV and reduced cake formation on the membrane surface. This positive effect of increasing CFV alleviates the formation of filtration layer on the surface of the membrane (Zhao et al., 2005). Hence, R_f decreased with an increase in CFV due to induced shear stress.

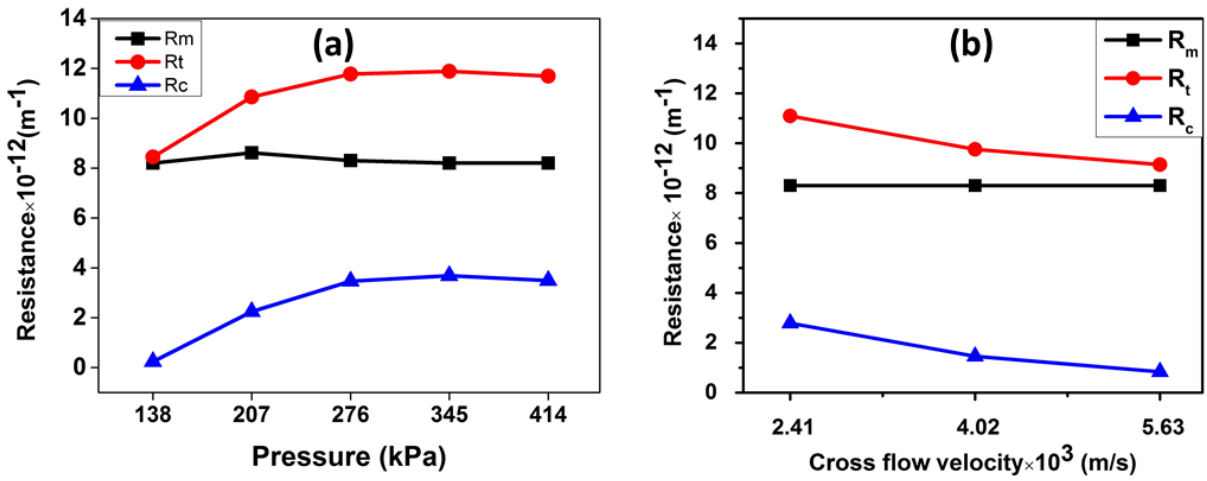

Fig. 3.21 Influence of (a) applied pressure and (b) cross flow velocity on resistances

For the understanding of fouling mechanism in constant pressure microfiltration, four fouling models were examined, which were mentioned in section 3.5. Fig. 3.22 displays the linear plot of all four models for experimental data.

Table 3.6 reports the parameters of each model, including regression coefficient, slope and initial permeate flux. Based on the regression coefficient (R^2) and the initial permeate flux (experimental value 3.246×10^{-5} m^3/m^2 s) values, it can be concluded that the cake filtration is the best model that describes the experimental permeate flux. It indicates that majority of TiO_2 particles size are larger than the pore size of the membrane due to which continuous retention of TiO_2 particles on the membrane surface takes place during microfiltration, leading to formation of cake. This cake layer provides additional resistance to the liquid permeation via membrane. As the flux profile fits with cake filtration model, the fouling is reversible and the membrane cleaning can be easy and efficient (Zhang et al., 2012).

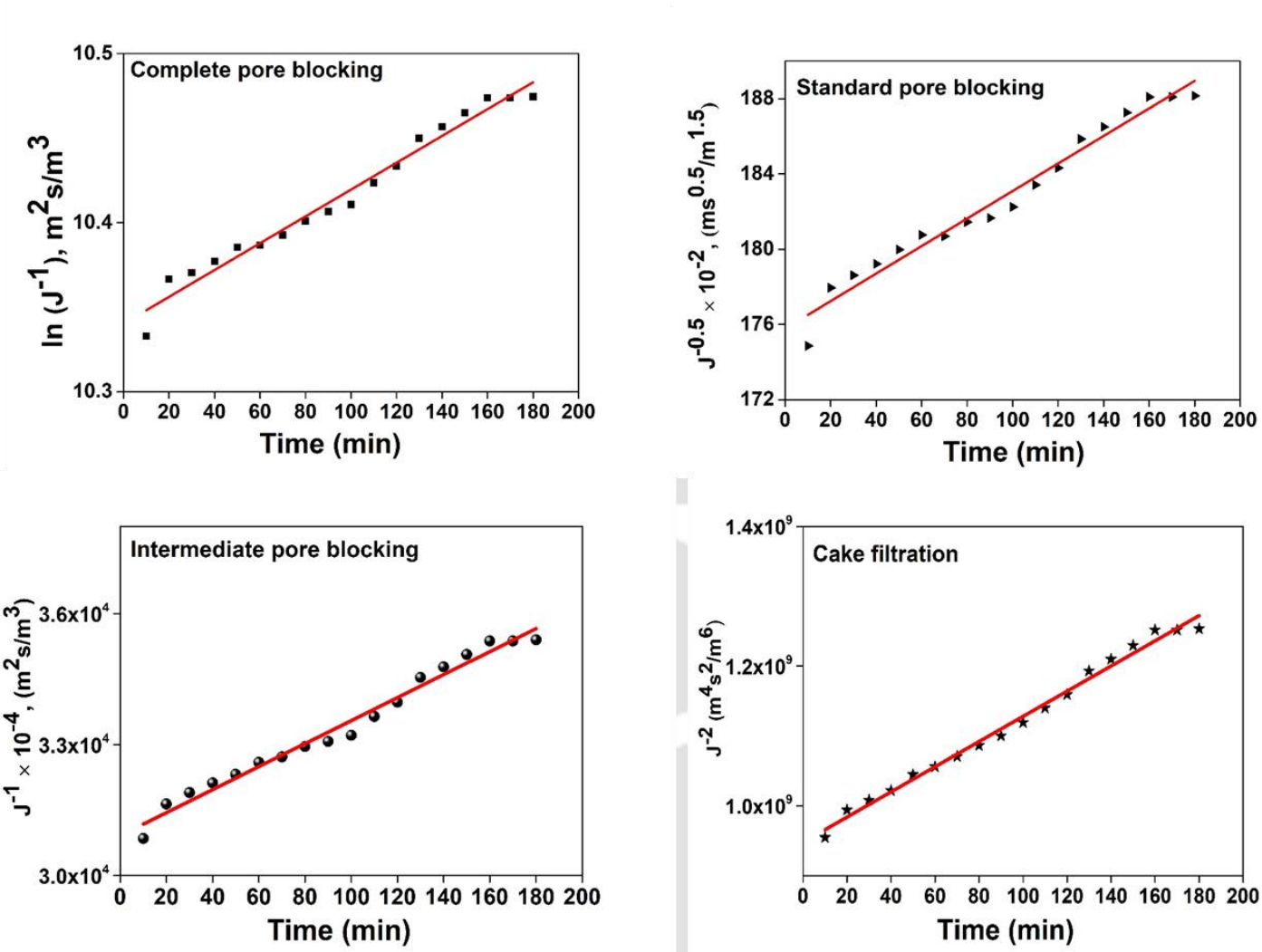

Fig. 3.22 Linear plot of different fouling models applied for the experimental data (Applied pressure = 276 kPa; Cross flow velocity = 2.41×10^{-3} m/s; Feed concentration = 0.1 wt%; pH = 6.5)

Table 3.6 Parameters of different pore blocking models

Type	R^2	Slope (k)	J_0 (m^3/m^2 s)
Standard pore blocking	0.968	7.3×10^{-2}	3.236×10^{-5}
Complete pore blocking	0.972	7.9×10^{-4}	3.230×10^{-5}
Intermediate pore blocking	0.979	2.6×10^{1}	3.234×10^{-5}
Cake filtration	0.99	1.8×10^{6}	3.248×10^{-5}

For understanding the filtration layer formation, it is essential to differentiate the forces acting on streaming particles and deposited particles (Weimin et al., 2001). It is well documented that three forces such as hydrodynamic, adhesive, and frictional forces, will dominate in case of deposited particles, whereas in case of streaming particles, only hydrodynamic force will dominate (Weimin et al., 2001). Electrostatic interactions and van der Waals forces cause the adhesive forces. The attractive van der Waals force is caused by the movement of outer electrons on the interacting particles, which results in flocculating dipoles. The other repulsive electrostatic force is due to the presence of the same charges on the particles. Van der Waals forces are constant for a given suspension, whereas electrostatic repulsive force differs and can be determined by zeta potential measurement.

At the start of filtration, applied pressure and membrane resistance influence the filtration rate. At later stages, convective particle transport to the membrane surface affects the filtrate flow (Weimin et al., 2001). Because of this particle transport, deposition of the particle takes place and the filtration layer grows, resulting in enhancement of filtration layer resistance, thereby reducing the rate of filtration. At the end of microfiltration (after 3 h), the membrane was subjected to FESEM analysis in order to identify the thickness of filtration layer formed and the nature of particle deposition. A cross-section image shown in Fig. 3.23 (a) was used to measure the thickness of the filtration layer, which is found to be ~79 µm. Fig. 3.23b shows FESEM image of the inner surface of the membrane, where feed was supplied. As evident from this image, a bed of TiO_2 NPs was deposited on the membrane surface. TiO_2 NPs completely covered the membrane surface after a certain time of filtration, resulting in a drastic reduction in the permeate flux. Fig. 3.23 (c) shows the outer surface of the membrane with clear pores, indicating complete recovery of TiO_2 NPs during MF and almost no TiO_2 particles passed through the membrane into the permeate side.

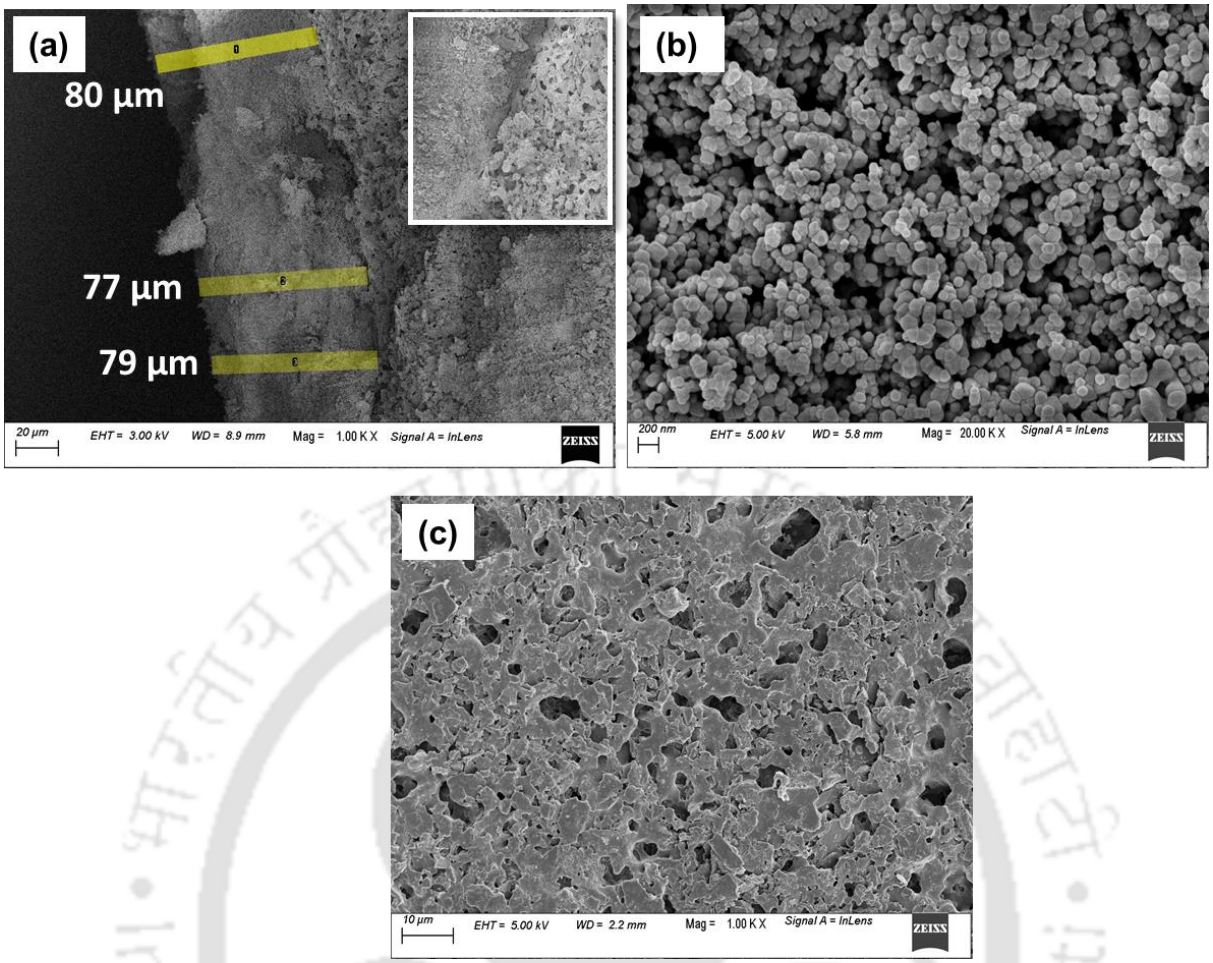

Fig. 3.23 FESEM images of the fouled membrane: (a) cross-section showing filtration layer formation, (b) TiO_2 agglomerates on the inner surface, and (c) outer surface with porous structure

In addition to water flux measurement of the membrane before and after cleaning, elemental composition of the virgin, fouled and cleaned membrane was measured by energy dispersive x-ray (EDX) analysis to check the cleaning efficiency of the membrane. Comparison of the three EDX profiles of the membrane shown in Fig. 3.24 reveals complete removal of the TiO_2 particles deposited in the membrane by cleaning. In case of both the virgin and cleaned membrane (Fig. 3.24a and c), a negligible quantity of Ti was present, which is attributed to the natural clays used as raw material for the membrane fabrication. However, the EDX profile of fouled membrane indicates the presence of a considerable quantity of Ti due to the deposition of TiO_2 NPs on the membrane surface (Fig. 3.24b).

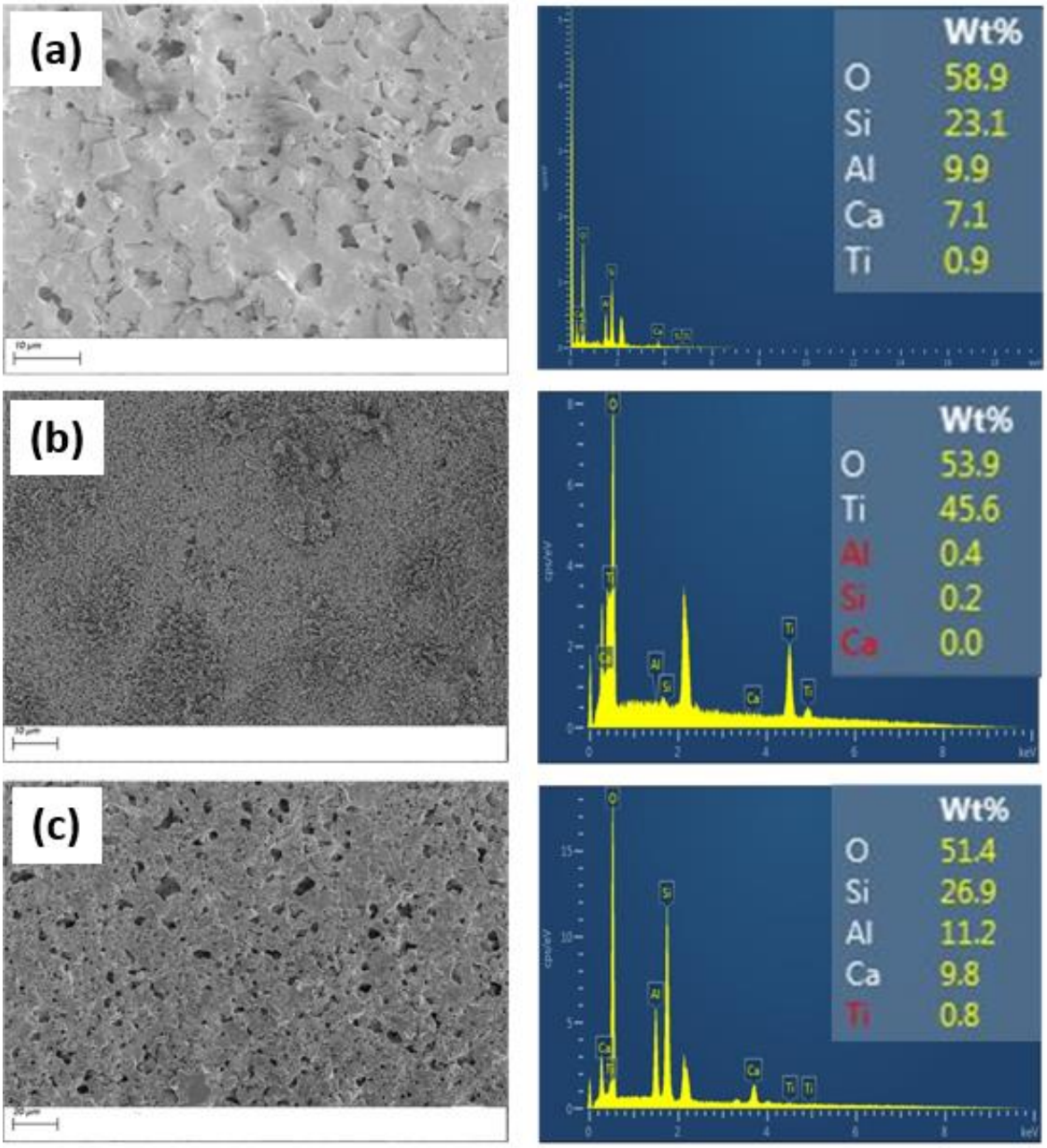

Fig. 3.24 EDX result of (a) virgin (b) fouled and (c) cleaned membrane

3.10.4. Comparison of performance of the membrane with prior arts

Literature on the separation of TiO_2 NPs using tubular ceramic membrane is very limited. Several techniques followed for the separation of TiO_2 NPs from solution are summarized in Table 3.7. As evident from Table 3.7, the developed membrane has a comparable pore size compared to the membranes reported in the literature on microfiltration. The performance of conventional techniques such as flocculation, coagulation and adsorption over the membrane

process is certainly poor in terms of TiO_2 recovery efficiency. Taylor et al. (2020), Ghimici et al. (2013) and Wang et al. (2013) reported the separation of TiO_2 particles using conventional techniques, but the recovery efficiency was very low (50 - 77%). Though polymeric membranes offer high permeability, their long-term industrial use is doubtful due to poor chemical, thermal and mechanical characteristics (Lee et al., 2001). On the other hand, though the alumina-based ceramic membranes reported by Zhao et al. (2002) displayed 100 % recovery of TiO_2 NPs, the high cost of raw material used and high sintering temperature followed for its fabrication are its drawbacks. It is to be noted that the energy cost is directly related to the cross-flow velocity and the transmembrane pressure for microfiltration (Weimin et al., 2001). The required power can be determined by the following relationship (Weimin et al., 2001).

$$P = Q \times \Delta P \tag{3.10}$$

Where, P is Power (Watt), ΔP is pressure drop (Pa) and Q is the flow rate (m^3/s)

As evident from Table 3.7, the required energy cost with the present MF setup is low compared to other MF studies performed using polymeric or alumina membranes. Hence, the low cost due to membrane and energy consumption strongly supports the industrial use of the present low-cost kaolin based tubular membrane for the recovery of TiO_2 NPs from its suspension. In this study, kaolin-based membrane showed that it could overcome the above-mentioned disadvantages and offer complete recovery of TiO_2 without compromising the membrane permeability and the cost involved. Thus, it can be concluded that kaolin-based tubular membranes are superior compared to other membranes for recovery of TiO_2 particles from slurry reactors and effluents of TiO_2 NPs manufacturing industries.

Table. 3.7 Summary of literature on separation of TiO_2 by different methods

Technique	Chemical/ material used	Pore size (µm)	Feed concentration (mg/L)	Time (h)	Power Required (W)	Permeability × 10^{-7} (m^3/m^2 s. kPa)	Recovery (%)	References
Flocculation	Synthesized cationic polysaccharides	-	50	20	NA	NA	50	Ghimici et al. (2013)
Coagulation	PFS, PACl, $FeCl_3$ and alum	-	30	0.5	NA	NA	77	Wang et al. (2001)
Encapsulation followed by adsorption	Lecithin liposomes, Poly (L-Lysine)	-	1000	2	NA	NA	58	Taylor et al. (2020)
Cross flow Ultrafiltration	Cellulose acetate	MWCO-30,000 Da	500	3	188	6.34	-	Lee et al. (2001)
Cross flow microfiltration	α - alumina membrane	0.2	60-80	3	2250	1.5	100	Zhao et al. (2002)
Cross flow microfiltration	Polypropylene (PP)	0.2	500	8	7800	26.3	100	Weimin et al. (2001)
Cross flow microfiltration	Low cost tubular ceramic membrane	0.178	500	3	1.2	1.41	100	This study

*NA- Not applicable, - Not mentioned

Part C: Onshore oilfield produced water treatment

3.11. Chemicals and reagents

Sodium hydroxide (NaOH), sodium hypochlorite (NaOCl), sodium dodecyl sulfate (SDS), sulfuric acid (H_2SO_4), calcium chloride dihydrate ($CaCl_2 \cdot 2H_2O$), magnesium sulfate heptahydrate ($MgSO_4 \cdot 7H_2O$), ferric chloride hexahydrate ($FeCl_3 \cdot 6H_2O$), copper sulfate heptahydrate ($CuSO_4 \cdot 7H_2O$), potassium dihydrogen phosphate (KH_2PO_4), ammonium nitrate (NH_4NO_3), di-sodium hydrogen phosphate dodecahydrate ($Na_2HPO_4 \cdot 12H_2O$), zinc sulfate ($ZnSO_4$), manganese (II) sulfate ($MnSO_4$), cobalt (II) chloride ($CoCl_2$), boric acid (H_3BO_3), and sodium molybdate dihydrate ($Na_2MoO_4 \cdot 2H_2O$) were supplied by Merck (I) Ltd., Mumbai.

3.12. *Rhodococcus opacus* seed culture conditions

In this study, *Rhodococcus opacus* PD360, an oleaginous gram-positive bacterium, obtained from Microbial Type Culture Collection (MTCC), Chandigarh, India, was used for biological tratemment of produced water (PW). In a 250 mL Erlenmeyer flask, the *R. opacus* seed culture was grown with 50 mL sterilized Luria Bertani (LB) broth. Further, the seed culture was incubated at 120 rpm and 30 ^oC until the culture's absorbance at 660 nm reached 0.99. For wastewater treatment, a 1:4 (*v/v*) ratio of Mineral Salt Medium (MSM) to wastewater (produced water) was taken in 250 mL conical flasks (Paul et al., 2019). The composition of the MSM are as follows (g/L): $FeCl_3 \cdot 6H_2O$, 0.0833; $Na_2HPO_4 \cdot 12H_2O$, 6; NH_4NO_3, 1; KH_2PO_4, 1; $CaCl_2 \cdot 2H_2O$, 0.0265; $MgSO_4 \cdot 7H_2O$, 0.409 and 1% of trace metals, which are (g/L): $Na_2MoO_4 \cdot 2H_2O$, 0.3; H_3BO_3, 0.1; $CoCl_2$, 0.8; $MnSO_4$, 0.2; $CuSO_4 \cdot 7H_2O$, 0.2; $ZnSO_4$, 0.2; $CaCl_2$, 0.6 and $FeCl_3$, 1.7. A 10 % (*v/v*) of freshly grown *R. opacus* bacterial culture was added to flasks containing wastewater and MSM in the specified ratio. The flasks were then incubated in an orbital shaker at 30 ^oC and 120 rpm for 72 h for studying the degradation profile of organics and recalcitrant compounds present in the produced water.

3.13. Characterization of produced water

In order to evaluate the physicochemical characteristics of produced water, the pH of the wastewater was determined using a digital pH meter (Model: pH 700, Make: Eutech Instruments). Total suspended solids (TSS) of the wastewater and treated water were measured according to the standard method (APHA, 1998). The particle size of suspended solids in PW was measured using Delsa Nano C particle size analyzer (Model: Delsa Nano C, Make: M/s Beckman Coulter). The total dissolved solids (TDS) and conductivity were measured using a conductivity/TDS meter (Model: CON 2700, Make: Eutech Instruments). For COD estimation, 1.5 mL of potassium permanganate ($KMnO_4$), 2.5 mL of sample (PW/treated water) and 3.5 mL of sulfuric acid (H_2SO_4) were taken into COD vials and the mixture was refluxed in a thermoreactor at 150 ^oC for 2 h. The mixture was then analysed for COD estimation by measuring its absorbance at 600 nm (APHA, 1998). The total organic carbon (TOC) was analyzed by TOC-L instrument (Shimadzu, Japan) with an ASI-L auto-sampler. Turbidity of produced water and treated water were checked using a turbidity meter (Model: HI 142). The following equation (3.11) was used to calculate the treatment efficiency of the membrane (Manni et al., 2020).

$$\text{Removal efficiency (\%)} = \left(1-\frac{C_e}{C_i}\right)\times 100 \tag{3.11}$$

Where C_i and C_e are the physicochemical parameters (turbidity/TSS/COD/TOC) in influent and effluent during the treatment process.

3.14. Onshore oilfield PW treatment by different methods

Oilfield-produced water obtained from Assam-Arakan Fold, India, was used in this study. The collected PW was stored in a refrigerator (~ 4 ^oC) until further use. A schematic of various processes adopted to treat produced water in this study is depicted in Fig. 3.25 (a-d). In this work, four treatment approaches were investigated for the treatment of PW by microfiltration

and biological method: single-step microfiltration (MF), single-step biological treatment (B), hybrid system comprising of MF-B, and B-MF, respectively. In the first treatment method (Fig. 3.25a), microfiltration was carried out using a novel tubular ceramic membrane (Kaolin-HPMC), which was made from inexpensive clay materials collected from the local market. Microfiltration of PW was conducted at a constant cross-flow velocity of 2.41×10^{-3} m/s for different pressures (69 to 345 kPa). To keep the feed concentration constant, the retentate was recycled back to the feed tank. After each experiment, the setup was cleaned by passing 1 g/L detergent solution for 1 h, after cleaning, the membrane was taken out from the module and ultra-sonicated for 10 min to eliminate any pore-blocking material. The cavitation phenomena during ultrasonication remove pollutants from the membrane surface and pores (Goswami and Pugazhenthi, 2020a). Finally, the membrane was flushed with water and the pure water flux was measured. The water flux value was within ±3% of its original water flux, calculated using an un-used membrane value, demonstrating the membrane's reusability in the subsequent experiments.

In the second approach for treating PW, the PW was subjected to biological treatment using a hydrocarbonoclastic and oleaginous bacterium, *R. opacus,* as shown in Fig. 3.25b. In this experiment, the simultaneous biodegradation of toxic hydrocarbons and biomass growth by the bacterium was studied, and the results were obtained by analysis of samples taken at regular interval of time. The wastewater supplemented with MSM as reported earlier in section 3.12 was considered to be essential for supporting the bacterium metabolism for simultaneous COD utilization and its biomass growth. The COD present in the wastewater served as the sole carbon source for biomass growth and metabolism by the bacterium. MSM containing minimal salts provided the additional nutrients required for the bacterium in efficient utilization of COD and, hence, biodegradation of the organics present in the PW. The biodegradation experiments were conducted in a controlled condition of 30 ^{o}C and 120 rpm shaking.

The hybrid microfiltration-biological treatment process (Fig. 3.25c and 3.25d) was evaluated in two different ways; i.e MF-B and B-MF, for achieving maximum COD and TOC removal efficiency. In case of the MF-B system, the PW was subjected to microfiltration (MF) at an applied pressure of 345 kPa, and the collected permeate (COD: 639 mg/L and TOC: 195 mg/L) from the MF process was subsequently treated by the biological method (Fig. 3.25c). Finally, in the last B-MF approach, the raw PW was first subjected to biodegradation using *R. opacus*, and the biologically treated water (COD: 325 mg/L TOC: 112 mg/L) along with the biomass present was subsequently treated by microfiltration. The performance of each system was evaluated by determining the final COD and TOC in the treated water.

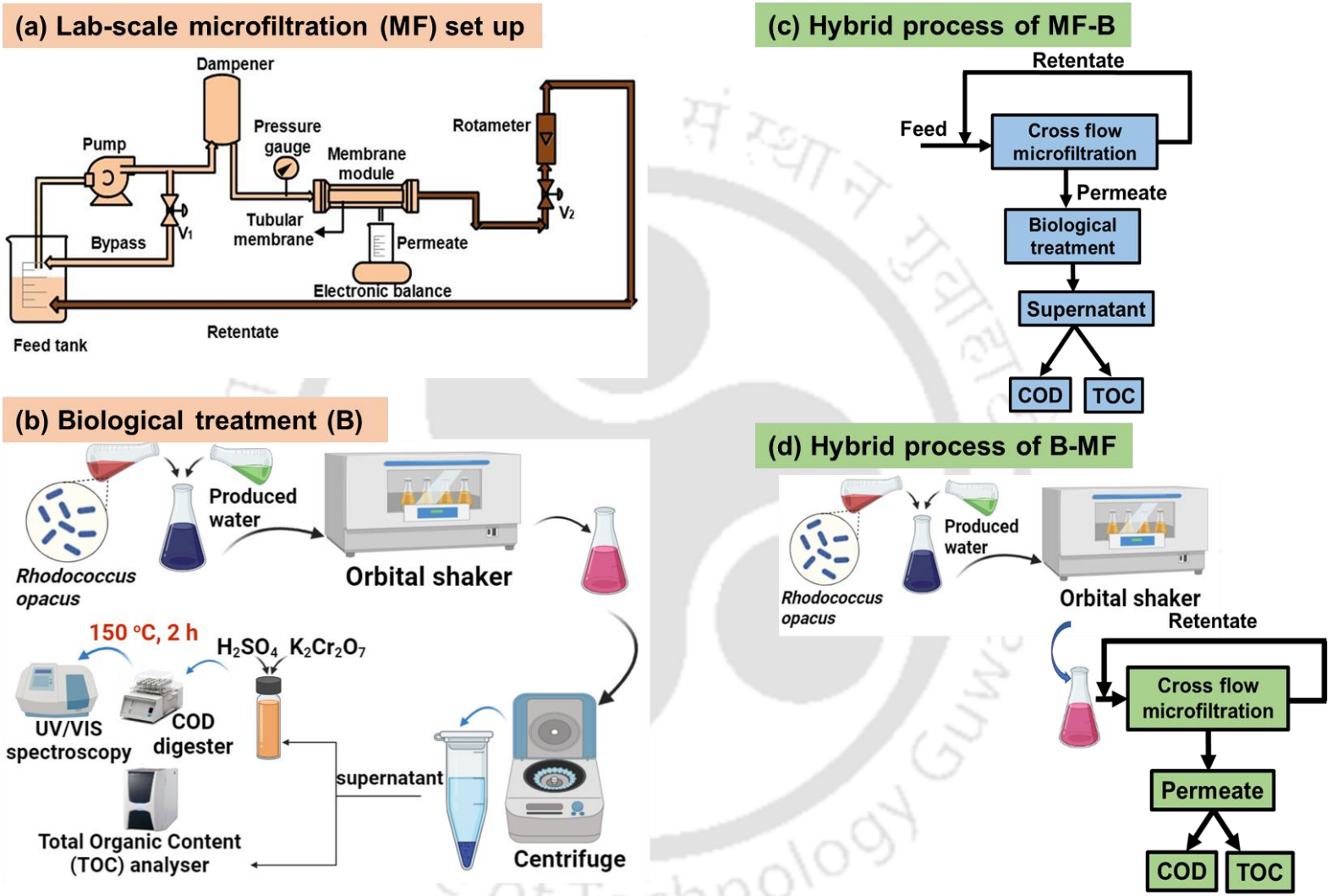

Fig. 3.25 Schematic representation of the different treatment strategies followed in this study

3.15. Membrane cleaning strategies

In order to regenerate the fouled membrane following microfiltration, it was cleaned using different chemical agents in a cross-flow microfiltration setup (see Fig. 3.25a) at room temperature. In this cleaning study, the following chemical agents dissolved in water were evaluated: 2 wt% of NaOH, 2 wt% of NaOCl, 2 wt% of SDS, a combination of 0.1 wt% SDS and 1 wt% NaOH, a combination of 0.1 wt% SDS and 1 wt% NaOCl (See Table 3.5). The cleaning study was conducted with a high cross-flow velocity of 4.82×10^{-3} m/s and a pressure of 207 kPa. Prior to the study, pure water flux (J_{wi}) of the fabricated virgin membrane was determined, and membrane fouling was achieved successfully at a high pressure of 345 kPa and a cross-flow rate of 2.41×10^{-3} m/s. Each fouling experiment was carried out for a duration same as that followed in the microfiltration experiment in order to replicate identical fouling conditions on the membrane surface. Before chemical cleaning, the fouled membrane was rinsed with water by passing water through the microfiltration setup at a constant cross-flow velocity of 4.82×10^{-3} m/s for 10 min, followed by measurement of the pure water flux (J_{ww}). Finally, chemical washing of the fouled membrane at a higher cross-flow velocity of 4.82×10^{-3} m/s for 30 min using different chemical solutions was performed, and then the pure water flux (J_{wc}) was measured. Cleaning efficiency was evaluated in terms of flux recovery (FR) with the help of the following equation (Kazemimoghadam et al., 2007).

$$\text{Flux Recovery, FR (\%)} = \frac{J_{wc} - J_{ww}}{J_{wi} - J_{ww}} \times 100 \qquad (3.12)$$

Where J_{wc} and J_{ww} are the pure water flux after chemical cleaning and after water flush. All the flux measurements were taken at the same operating conditions (applied pressure = 207 kPa; and cross flow velocity = 2.41×10^{-3} m/s; Time = 30 min).

Table 3.8 Chemical reagents utilized in the membrane cleaning study

S. No.	Chemical reagents	Concentration (wt%)
1	NaOH	2
2	NaOCl	2
3	SDS	2
4	NaOH and SDS	1 and 0.1
5	NaOCl and SDS	1 and 0.1

3.16. Seed germination assay for phytotoxicity analysis

Germination index is an important parameter for assessing the phytotoxicity of wastewater. The assay was conducted at room temperature using petri dishes containing raw PW and treated PW along with the required amount of *Vigna mungo* seeds (Black gram) and *Cicer arietinum* L. (Bengal gram). All the four samples, tap water, produced water (feed), treated water (MF-B) and distilled water (control), were added individually into the petridishes containing the seeds, followed by incubation in the dark for 72 h. Seed Germination and Germination Index were calculated by the following equations (3.13) and (3.14) (Luo et al., 2018).

$$\text{Seed Germination (SG)} = \frac{\text{Number of germinated seeds}}{\text{Total seeds}} \times 100 \quad (3.13)$$

$$\text{Germination Index (GI) \%} = \frac{\text{Seed germination (\%)} \times \text{Root elongation (\%)}}{100} \quad (3.14)$$

3.17. Results and Discussion

3.17.1. Characterization of the produced water

Characteristics of PW evaluated in this study are summarized in Table 3.9.

Table 3.9 Characteristics of the produced water used in this study

Parameter	Value	Unit
pH	8.03±0.6	-
Total suspended solids	4475±83	mg/L
Mean particle size	0.6	Mm
Total dissolved solids	2770±68	mg/L
Conductivity	5.5±0.3	mS/cm
Turbidity	49.5±1.5	NTU
Total organic carbon (TOC)	355±0.2	mg/L
Chemical oxygen demand (COD)	951±10	mg/L

The results indicated that the PW contains high level of total suspended and dissolved solids. The mean particle size was found to be 0.6 μm. These characteristics of the PW used in this study are in agreement with the produced water (pH of 8.73 and 316-445 mg/L of TOC) generated from Oil India Limited (OIL), Assam, India (Chakrabarty et al., 2010) and Canada's oil sands (Rashad et al., 2021).

3.17.2. Treatment of produced water by different approaches

The oilfield produced water was treated by four different strategies; (i) single-step microfiltration (MF), (ii) single-step biological treatment (B), (iii) hybrid microfiltration-biological treatment (MF-B) process and (iv) hybrid biological treatment-microfiltration (B-MF) process.

3.17.2.1. Microfiltration

For PW treatment by microfiltration, the indigenously fabricated tubular ceramic membrane (Kaolin-HPMC) was used and the filtration experiments were carried out at room temperature

(25 ^{o}C). The effect of applied pressure on permeate flux was investigated in the range 69–345 kPa and at a constant cross-flow velocity of 2.41×10^{-3} m/s (See Fig. 3.26a). Permeate flux during the microfiltration revealed a drastic decline in flux within an initial period of 20 min, indicating blockage of membrane pores due to TSS and oil droplets. However, as the filtration progressed, the membrane reached a steady flux value in 80-90 min due to cake layer formation on the membrane surface by TSS and oil droplets (Rashad et al., 2021). Judd et al. (2014) reported a maximum suspended solids removal efficiency of 98% from produced water containing 200 mg/L of suspended solids by cross-flow microfiltration. TSS in the PW is due to silt, sediment, and algae, which affect the membrane performance by reducing the permeate flux during microfiltration (Al-Ghouti et al., 2019). Furthermore, from Fig. 3.26b, the steady flux value increased with increasing applied pressure owing to the improved driving force. However, the steady flux value saturated at a high pressure due to concentration polarization of foulant particles on the membrane surface (Kumar et al., 2015b). Hence, up to 138 kPa, the flux increased linearly according to Darcy's law, whereas at higher applied pressure, no significant increase was observed due to quick formation of the cake layer. Owing to the cake layer formation on the membrane surface, the permeability of produced water is less than pure water permeability. Rashad et al. (2021) also observed a similar trend of permeate flux in the treatment of oil-in-water emulsion using a ceramic microfiltration membrane with a mean pore size of 0.3 µm. In another study, a non-linear variation in the flux was reported by Fang et al. (2013) for the microfiltration of oil-in-water emulsion using 2.5 µm pore-sized fly ash-based ceramic membrane.

The treatment efficiency of the membrane was determined by analzying the TSS, turbidity, TOC, and COD of feed and permeate samples. Fig. 3.26 (c) shows the removal efficiency at various applied pressure, which clearly reveals that both TSS and turbidity were removed completely due to the efficient removal of suspended solids by the ceramic membrane (0.178

μm) during microfiltration. At a low applied pressure of 69 kPa, high efficiency of TOC and COD removal was achieved during the microfiltration operation, and the values were 84% and 78%, respectively. However, the removal efficiency values of TOC and COD decreased when the applied pressure was raised from 69 to 345 kPa. This may be attributed to the deformation of oil droplets at higher applied pressures, and subsequent entry into the permeate side, through the membrane pores. The residual COD values of the permeate water collected at 69 and 138 kPa pressures were 200 and 238 mg/L, respectively, which are well-below the discharge standard limit for wastewater into surface water (250 mg/L) (Central Pollution Control Board, Government of India). The images of feed and permeate water collected from the MF experiment (Fig. 3.26d) further confirm that the treated water is clean and free of suspended solids. Though the membrane worked efficiently to treat PW at lower applied pressures, its treatment efficiency at applied pressures greater than 138 kPa was low due to the high COD of the permeate. However, the membrane showed high removal efficiency at low applied pressures, its permeate flux value was low compared to higher applied pressures. Hence, further treatment by low-cost biological method was studied to evaluate the treatment efficiency.

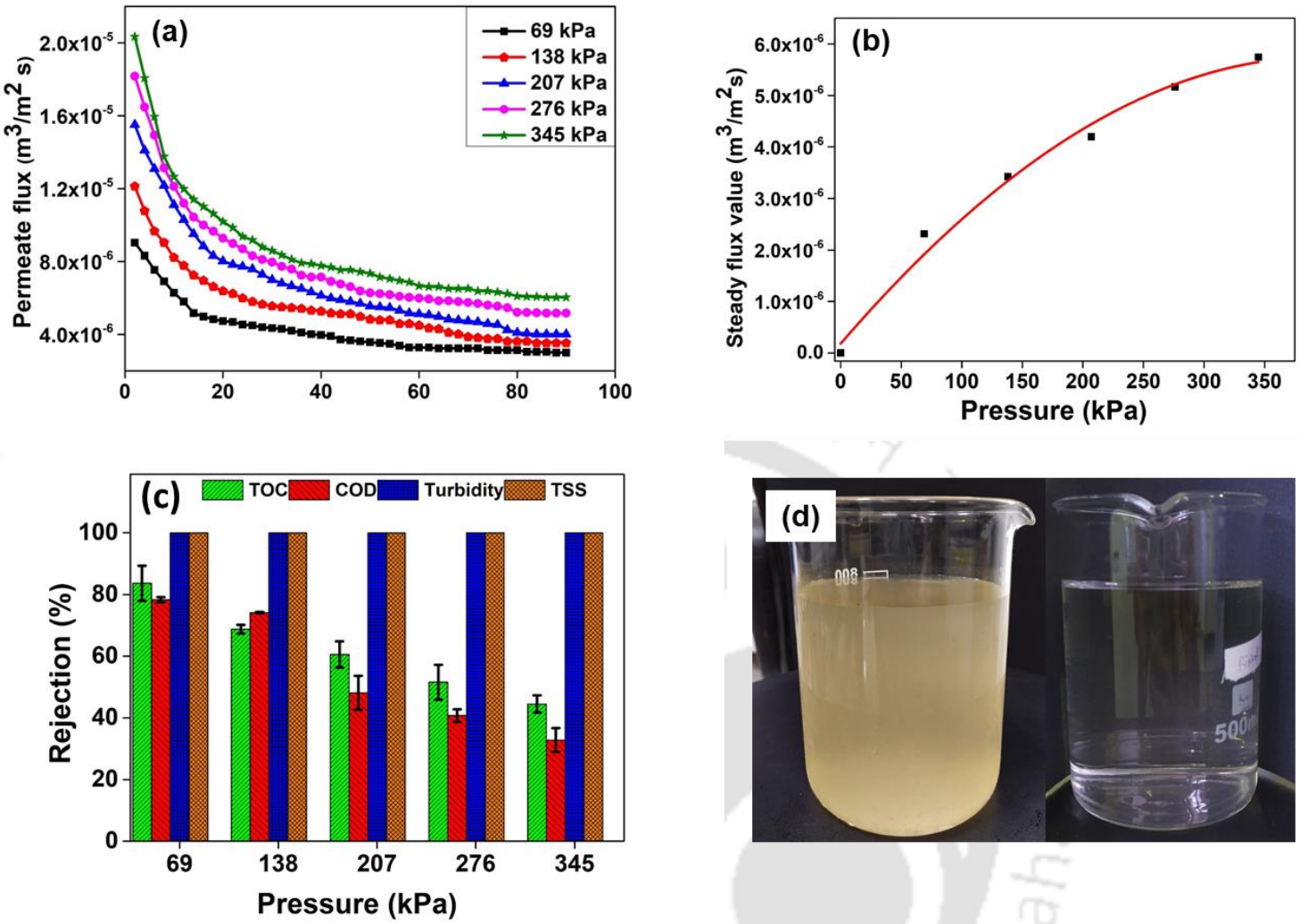

Fig. 3.26 Variation in (a) permeate flux, (b) steady flux and (c) removal efficiency of TOC, COD, Turbidity and TSS as a function of applied pressure. Images comparing feed and permeate samples are shown in (d).

3.17.2.2. Biological treatment

It is well known that certain microorganisms utilize the hydrocarbons present in wastewater as a nutrient source for their growth and metabolism (Al-Ghouti et al., 2019). Hence, biological processes involving such microorganisms are well established and cost effective for the treatment of different industrial wastewaters. In this study, a hydrocarbonoclastic bacterium *R. opacus* was used to treat PW owing to its ability to utilize complex organics present in PW as the sole carbon source (Paul et al., 2021). The biological treatment using *R. opacus* was carried

out in batch shake flasks under controlled temperature and shaking conditions. From Fig. 3.27, significant reduction in COD and TOC of PW are observed by treating the wastewater with *R.opacus*. The COD value of PW decreased from 951 to 325 mg/L after 3 days of batch incubation due to biodegradation of hydrocarbons in PW. Thus, a maximum COD removal of 65% is observed at the end of the batch treatment. The COD removal efficiency value is, however, less efficient when compared to that obtained by microfiltration process (applied pressure: 69 kPa). Li et al. (2005) examined treatment of oilfield-produced water using *Bacillus sp.* in batch shake flasks and achieved 90% COD removal, but after a prolonged incubation time of 30 days. One of the major disadvantages of biological treatment is that it requires more contact time with the wastewater to remove organic pollutants (Al-Ghouti et al., 2019). Nevertheless, it could be concluded that the single-step PW treatment using *R.opacus* was inefficient and the treated water did not match the standards for discharge limits into surface water, necessitating further treatment steps. Hence, in order to improve the PW treatment efficiency hybrid systems were evaluated.

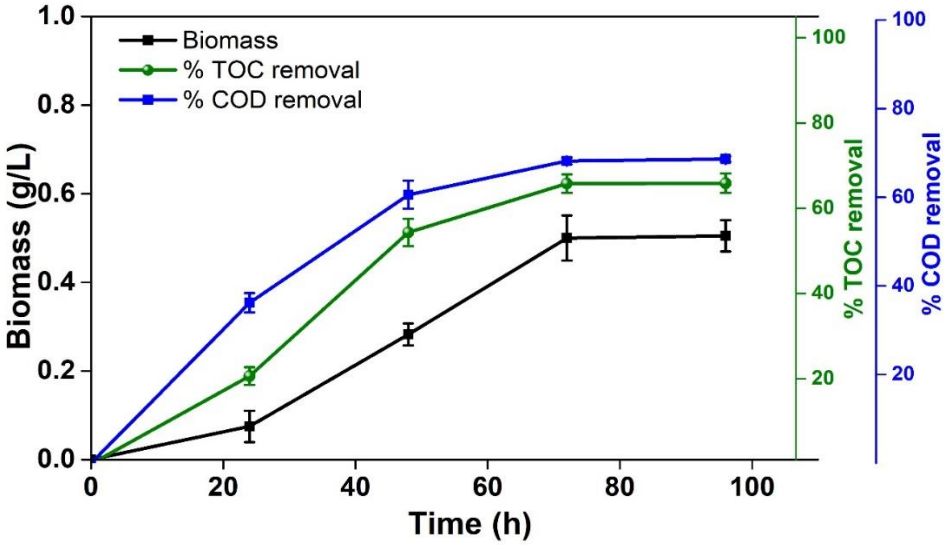

Fig. 3.27 Time profiles of biomass production, TOC and COD removal by *R. opacus* in the batch study

3.17.2.3. Combined microfiltration and biological treatment method

The previous experiments carried out by either microfiltration at high applied pressure or biodegradation showed low COD removal efficiency as the COD of the treated water obtained from both these processes (MF at high applied pressure and biological process) was greater than the discharge limits (COD: 250 mg/L) prescribed by the Central Pollution Control Board, Government of India. Therefore, an integrated or hybrid approach for utilization of recalcitrant compounds by *R. opacus* combined with microfiltration process was employed to achieve high quality effluent and for efficient reuse of the treated PW. Fig. 3.28a depicts the COD removal percentage values obtained in the different approaches: microfiltration, biological treatment, MF-B, and B-MF systems. It is clear from Fig. 3.28 (a) that the removal of both COD and TOC in both the hybrid/combined processes, MF-B (99%) and B-MF (90%), are higher than in the individual experiment on biological treatment or microfiltration process. Between the two hybrid combined processes (MF-B and B-MF), MF-B is found to be more efficient for the treatment of PW because of high COD removal efficiency and very low residual COD concentration (11 mg/L) in the effulent. In case of B-MF system, even though the residual COD concentration of the treated water is 96 mg/L, the microorganism present in the feed to the microfiltration process caused a high risk of membrane fouling, which is however, easily avoided in the MF-B system (see Fig. 3.28b). These results clearly reveal the suitability of MF-B system for the treatment of PW. The high percent removal of COD (99% and 90%) by the hybrid microfiltration and biological treatment systems is comparable with the values reported in previous studies, which further support the feasibility of the hybrid process (Campos et al., 2002; Maguire-Boyle et al., 2017). Campos et al. (2002) investigated combined microfiltration and biological processes to treat PW and found that the maximum COD removal efficiency was approximately 80%. In addition to degrading toxic organics, *R.opacus* biomass used in this study is already known for its ability to accumulate high amount of oil inside, and it is,

therefore, an industrial organism for the treatment of wastewater containing toxic recalcitrant compounds and bio-crude oil production by hydrothermal liquefaction of the lipid-rich biomass (Paul et al., 2021). Thus, by employing MF-B for PW treatment, maximum TOC and COD removal are achieved to produce high quality treated water as well as energy-rich biomass for reuse purpose and bio-oil production.

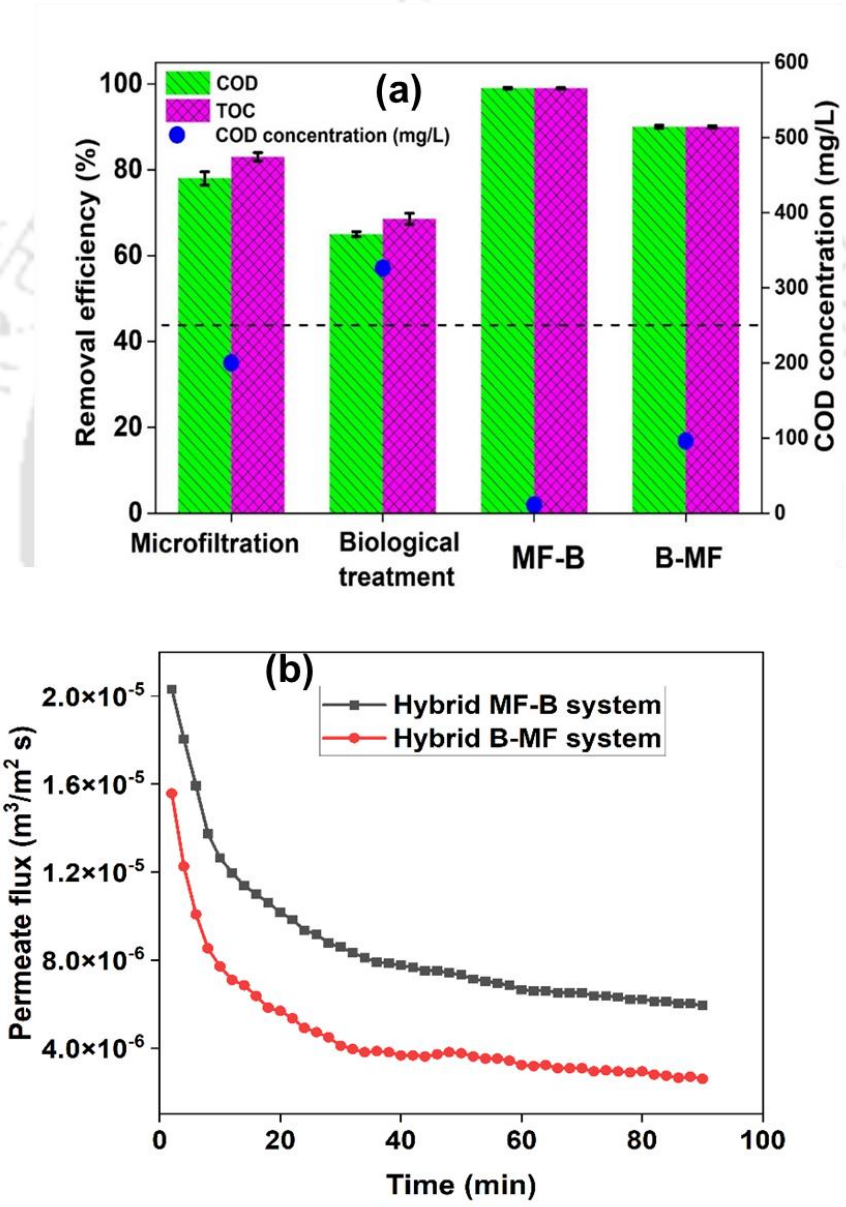

Fig. 3.28 (a) Removal efficiency of COD, TOC and residual COD concentration of treated water by various approaches tested in this study and (b) variation in permeate flux between hybrid MF-B and B-MF systems.

The removal mechanism of TSS, turbidity, TOC and COD involved in this study depends on the suspended solids, dissolved and dispersed oil droplets present in PW. In the MF experiment, a low pore size (0.178 µm) ceramic membrane completely removes the total suspended solids (TSS) present in the PW due to sieving mechanism. Besides, the result of 100% turbidity removal indicates that suspended particles cause the turbidity of PW. The removal efficiency of dispersed organic compounds in terms of COD and TOC is observed to be 78% and 84% by microfiltration at a lower applied pressure of 69 kPa. The removal efficiency is drastically reduced at a higher applied pressure of 345 kPa (33% COD and 45% TOC) owing to the deformation of oil droplets that pass through the permeate side at elevated pressure (Kumar et al., 2015b). It may be noted that water-soluble organic compounds and production chemicals present in PW (which contribute for COD/TOC) cannot be removed by microfiltration. Hence, the permeate obtained from MF process was treated in the biological process to remove the remaining COD/TOC using hydrocarbonoclastic bacterium, R. opacus. The organism degrades the hydrocarbons for their growth and metabolism using different biodegradation or metabolic pathways such as ortho/para and meta pathways (Paul et al., 2019).

3.17.3. Fouling mechanism by different pore blocking models

In order to examine the membrane fouling mechanism involved in this study during microfiltration, the permeate flux data of PW obtained at 345 kPa was fitted with different pore blocking models, and the results are shown in Fig. 3.29. For each model, values of the evaluated parameters, such as regression coefficient (R^2), slope (k), and initial permeate flux at (J_0), are presented in Table 3.10. The predicted value of J_0 by cake filtration model was close to the experimental value (9.54×10^{-5} m^3 m^{-2} s^{-1}) when compared to the other models. From the obtained results, it can be observed that the cake filtration model fitted well with the flux decline. The reason might be owing to lower pore size (0.178 µm) of the ceramic membrane than the mean particle size of suspended solids (0.60 µm) present in PW. Hence, the membrane rejects all the particles, accumulating on the membrane surface and forming a cake layer.

During the microfiltration of PW, the cake layer grows on the membrane surface, giving additional resistance to the permeate to pass through the membrane. Hence, a reduction in permeate flux was observed. The main advantage of this kind of fouling mechanism is easy regeneration of the membrane for repeated use in microfiltration (Manni et al., 2020). Similar results were observed by Kumar et al. (2015b) for microfiltration of synthetic oily wastewater in which the permeate flux data fitted accurately with the cake filtration model.

Table 3.10 Estimated value of parameters of different pore-blocking models for PW treatment by microfiltration at an applied pressure of 345 kPa

Type	R^2	k	J_0 (m^3/m^2 s)
Complete pore blocking	0.83	1.78	7.00×10^{-5}
Standard pore blocking	0.88	1.30×10^{-2}	7.19×10^{-5}
Intermediate pore blocking	0.92	4.02	7.52×10^{-5}
Cake filtration	0.99	1.88×10^{5}	9.12×10^{-5}

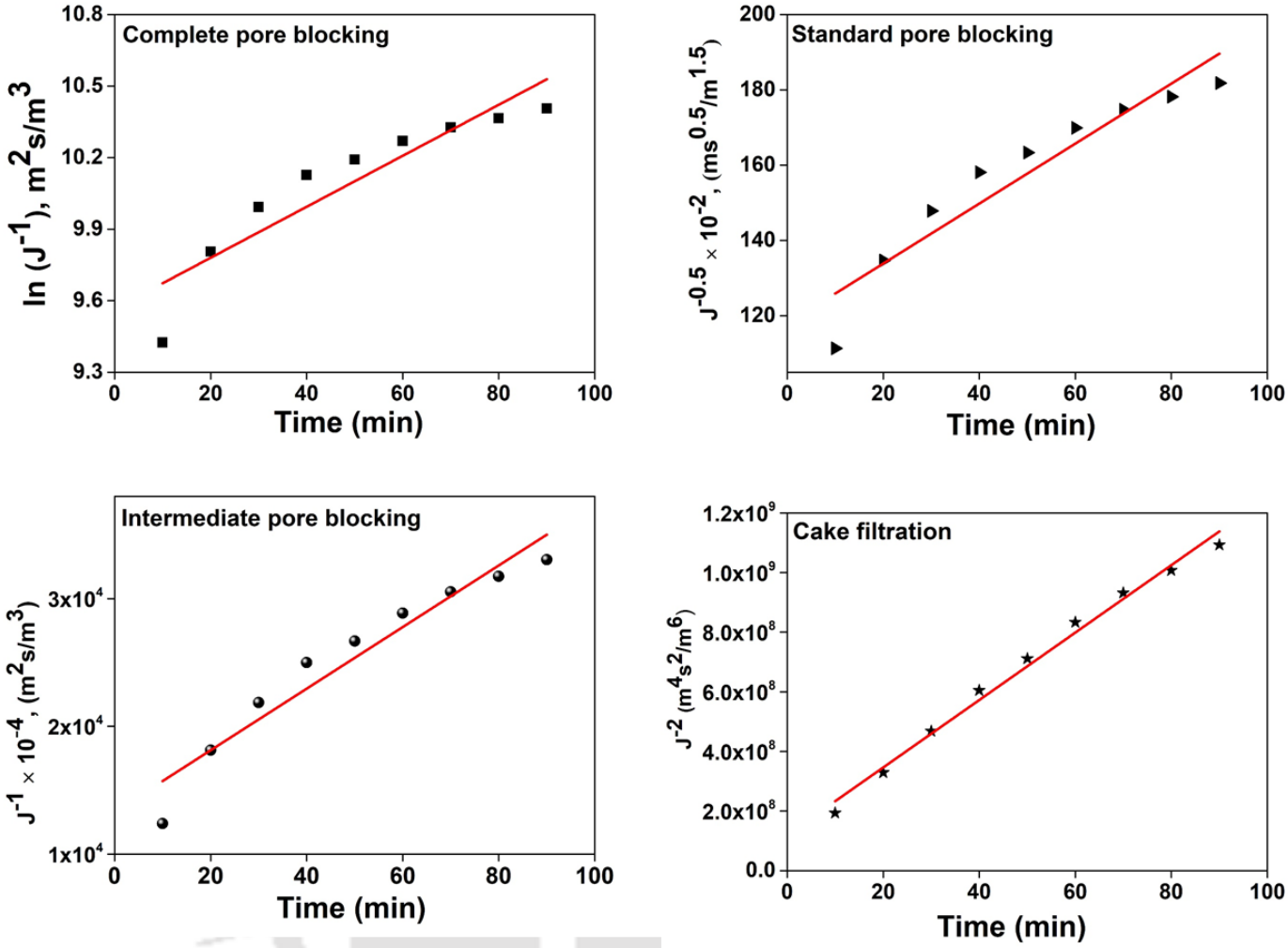

Fig. 3.29 Fouling models applied for the microfiltration of PW (symbols: experimental data; lines: predicted results)

In order to confirm further that the cake layer was formed during MF of PW, the morphology of the membrane was analyzed at the end of the MF experiment using FESEM, and the results are depicted in Fig. 3.30. It is worth to mention that during cross-flow microfiltration of PW, the feed was passed through the tube side of the membrane (see Fig. 3.25a). As evident from FESEM image (Fig.3.30a), the pores of the fouled membrane (inner surface) were completely blocked by suspended solids and oil droplets. On the other hand, pores were visible on the outer surface of the fouled membrane. Clear pores were seen on the exterior surface of the membrane, confirming that both the suspended solids and oil droplets were retained on the inner surface of the membrane. The elemental analysis results demonstrated the enhancement of carbon

content due to fouling on the inner surface of the membrane, which was found to be 47 wt%. In contrast, negligible amount of carbon is seen on the outer surface, confirming that fouling is associated with the inner surface of the membrane. The negligible carbon content on the outer surface of the membrane is attributed to the presence of dissolved oil compounds (see Table 3.9), which escaped through the membrane during microfiltration of PW. Deposition of thick cake layer during microfiltration can be seen in Fig. 3.30 (c). These results clearly demonstrate that most of the oil droplets are retained on the inner surface of the membrane, offering additional resistance to the permeate and hence the decline in the flux. Similar observations were reported by Zarghami et al. (2019) with a modified PES membrane.

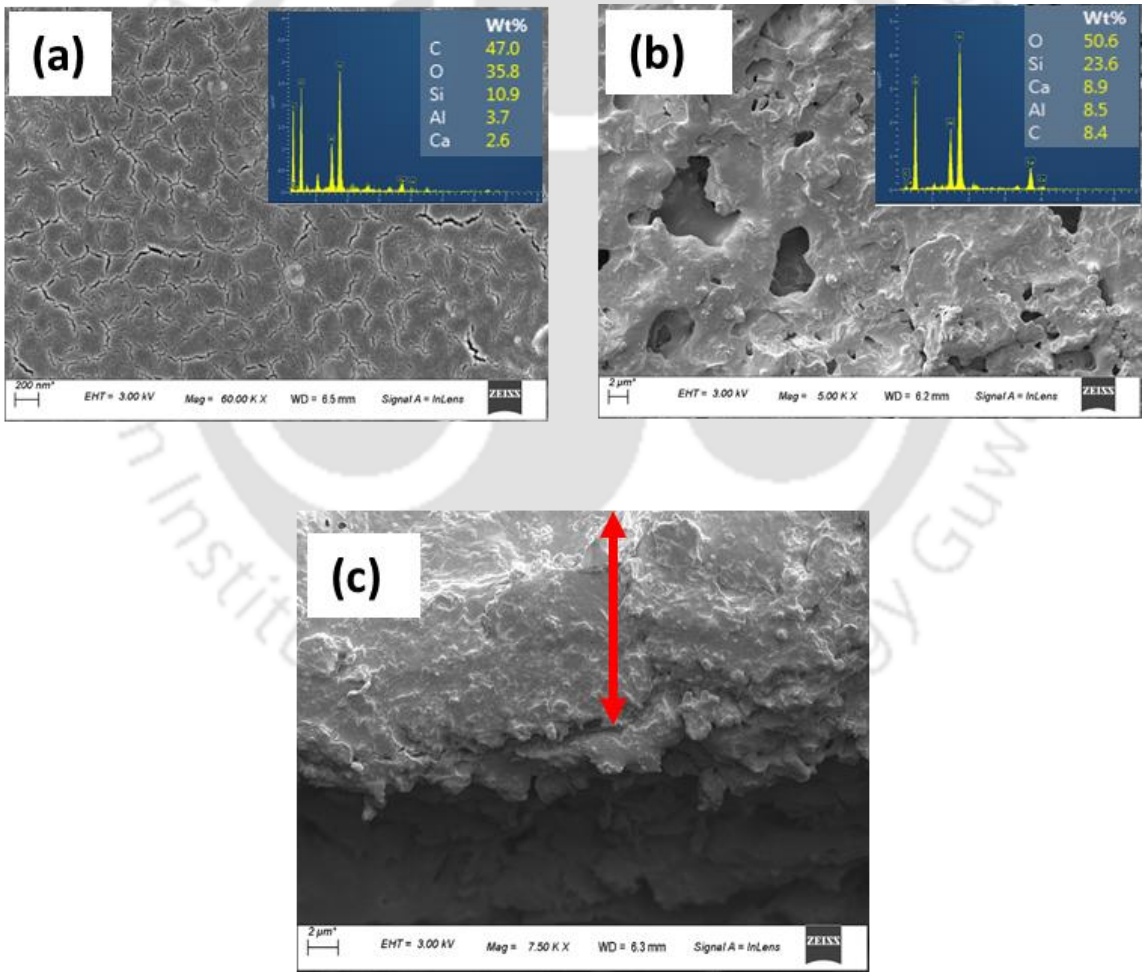

Fig. 3.30 FESEM-EDX images of fouled membrane after microfiltration of produced water: (a) Inner surface of the membrane, (b) outer surface of the membrane, and (c) cross-sectional view of the membrane

3.17.4. Cleaning strategies

In this study, various commercial chemicals such as NaOCl, NaOH, SDS, and a combination of these chemicals, were tested to regenerate the fouled membrane. It is evident from the characterization results of ceramic membrane (Section 2.4.2, Chapter 2) that the corrosion resistance of the membrane in acid is slightly low (2.73±0.7% weight loss). Hence, the acid cleansing agents were not considered in cleaning strategies. Prior to the cleaning experiment, stability of the membrane towards all these chemical agents was tested and the membrane was highly stable with negligible weight loss (<0.6 wt%) in all three cleaning reagents. The cleaning efficiency was evaluated by measuring water flux recovery estimated using Eq. 3.12. As shown in Fig. 3.31, mixture of 1 wt% NaOCl and 0.1 wt% SDS resulted in the highest flux recovery value of 92.6%. The flux recovery for the five chemical solutions tested in the present work followed the order:1 wt% NaOCl and 0.1 wt% SDS > 2 wt% NaOCl > 1 wt% NaOH and 0.1 wt% SDS > 2 wt% NaOH > 2 wt% SDS. NaOH is an alkaline agent that saponifies oils and dissolves them to remove organic foulants by hydrolysis and solubilization mechanism. NaOCl is a swelling agent and solubilizer; also, it can break chemical bonds between foulant and the membrane (Lee et al., 2007). SDS has both hydrophobic and hydrophilic groups. It is well known that surfactants can emulsify macromolecules and remove the foulants from the membrane surface by forming micelles (Chen et al., 2015; Ang et al., 2006). Though all these three reagents were efficient to remove foulants from membrane pores, the membrane displayed good corrosion resistance against NaOCl and SDS solutions than NaOH. Furthermore, the mixture of these two cleaning reagents NaOCl and SDS resulted in very high cleaning efficiency even at their lower concentrations (1 wt% NaOCl and 0.1 wt% SDS) when compared to using the cleaning reagents individually. This is particularly important considering the cost of reagents and preventing the membrane from this corrosive effect at high concentration. Similar results were reported by Chen et al. (2015) that the combination of

sodium dodecylbenzene sulfonate (SDBS) and NaOH was efficient in regenerating the fouled membrane.

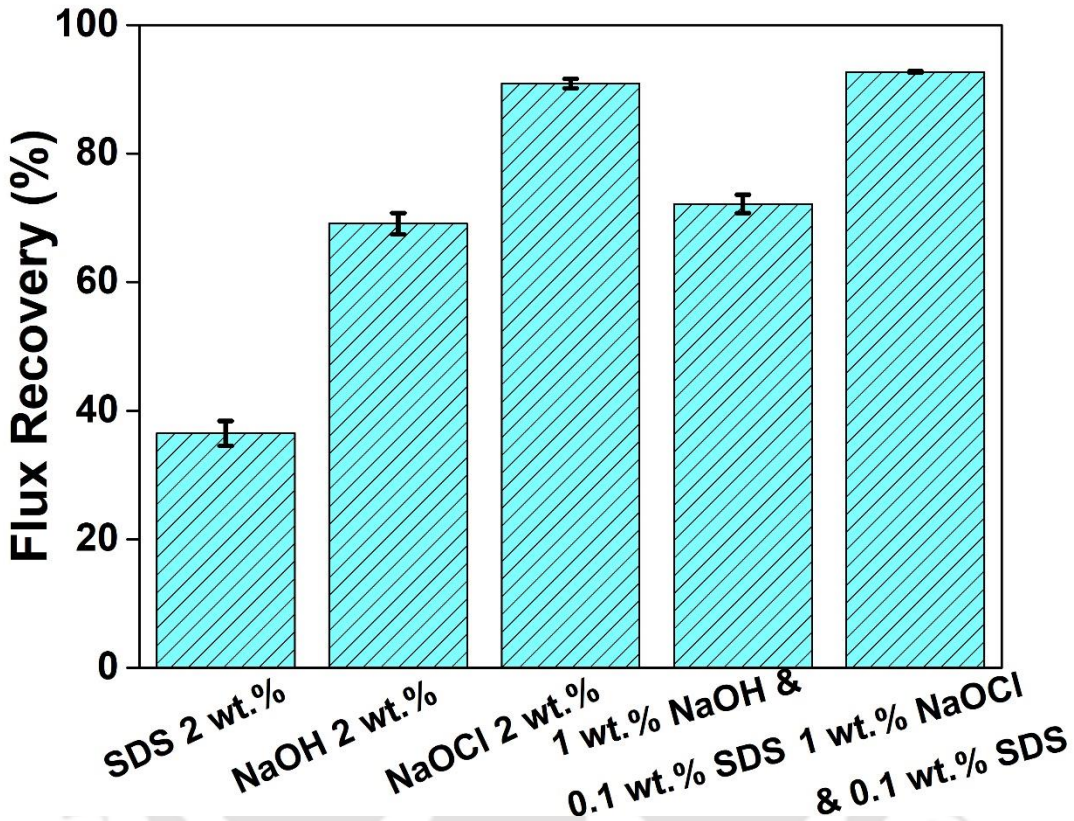

Fig. 3.31 Chemical cleaning of fouled membranes by different chemical reagents

3.17.5. Phytotoxicity assessment of PW and treated water

The GI of *Cicer arietinum* and *Vigna mungo* was analyzed to examine the toxicity of the produced water and treated water obtained using the hybrid MF-B system. The choice of the seeds is based on their high sensitivity to produced water and potential for protein digestibility during germination (Paul et al., 2019; Paul et al., 2021). The germination index can be used to determine the toxic effects of untreated/treated water for assessing the treatment efficiency. Using Eq. (3.13) and (3.14), the germination index of the feed, permeate, and tap water was estimated and the values were compared with that of the control (distilled

water). Fig. 3.32 depicts germination index calculated by using *Cicer arietinum* and *Vigna mungo* seeds. A germination index of 74.3% for *Cicer arietinum* and 71.1% for *Vigna mungo* indicate that the treated water is relatively free from any toxic effects, whereas the raw PW shows a GI of 33.4% and 19.1% for *Cicer arietinum* and *Vigna mungo*, respectively. It is well documented in the literature that GI value of more than 70% is termed as a sample free of phytotoxic substances (Raj and Antil, 2011). Hence, it can be said that the treated water is phytotoxin free and thus can be effectively used for irrigation and other reuse purposes. The corresponding images of germinated seeds of Vigna mungo (Black gram) and Cicer arietinum (Bengal gram) are shown in Fig. 3.33.

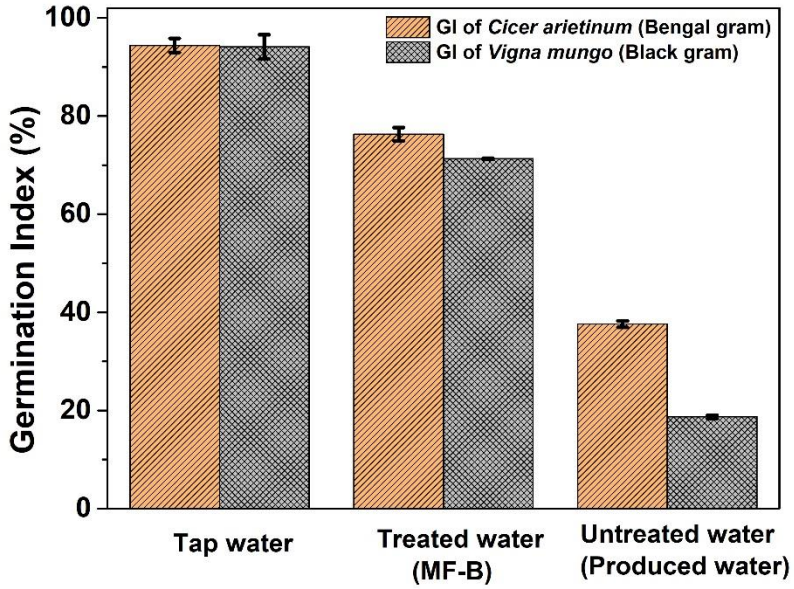

Fig. 3.32 Germination Index of *Vigna mungo* (Black gram) and *Cicer arietinum* (Bengal gram)

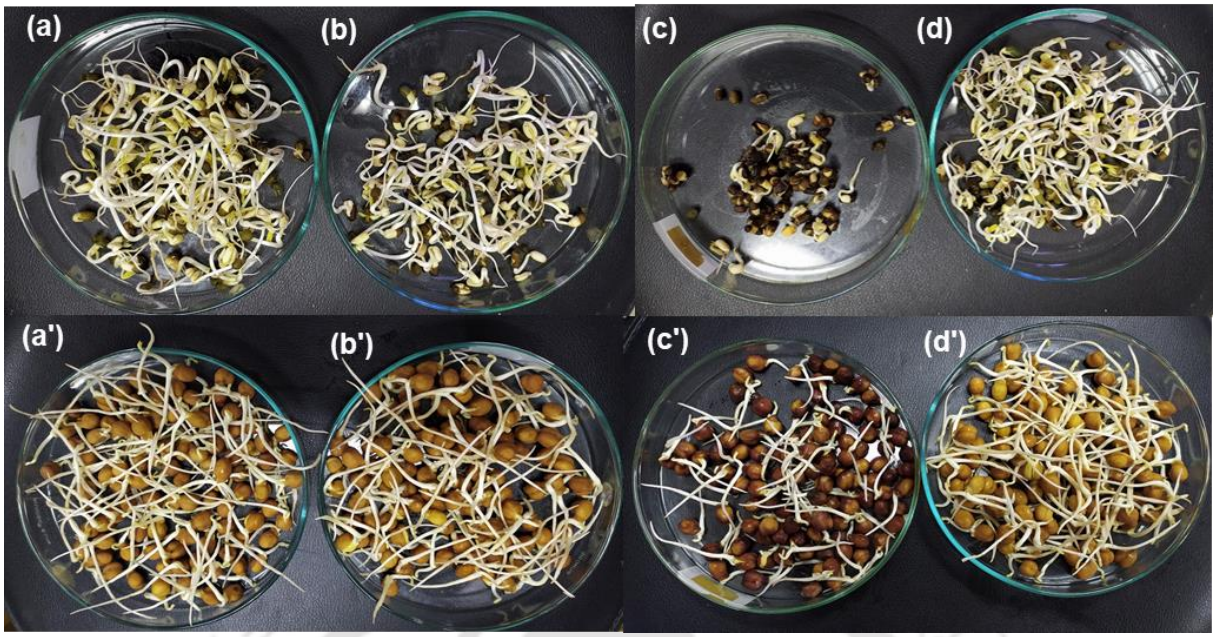

Fig. 3.33 Images of germinated seeds of *Vigna mungo* (Black gram) and *Cicer arietinum* (Bengal gram) incubated with distilled water (a, a'), treated water (b, b'), produced water (c, c') and tap water (d, d').

3.17.6. Distinction over prior arts

Table 3.11 presents the literature on PW treatment using various combined processes. Two α-Al_2O_3 membranes and three polymeric membranes were compared for the microfiltration of PW containing high concentrations of oil (150 to 7110 mg/L). Abdel-shafy et al. (2020) reported 54.3% COD removal efficiency and the highest permeability of 4.7×10^{-9} m^3 m^{-2} s^{-1} kPa^{-1} using a hybrid process comprising of adsorption followed by microfiltration using cellulose acetate membrane (0.2 µm) at 100 kPa. Combined microfiltration and biological treatment of produced water were performed by Campos et al. (2002), and the total efficiency of TOC removal was reported to be 85%. As the produced water contains complex organics, polymeric membranes are considered unsuitable for long-term applications because of their poor chemical stability (Goswami and Pugazhenthi, 2020a). Additionally, polymeric membranes are more sensitive towards cleaning reagents and temperature (>50 ^oC) (Shams Ashaghi et al., 2007). Highly stable α- alumina ceramic membranes having various pore size (0.75 kDa to 0.1 µm) were used by Ebrahimi et al. (2010) to treat oilfield-produced water, and

the maximum TOC removal efficiency of 38% was achieved using the microfiltration membrane. However, because of its high cost, alumina membranes are not commercially viable.

Among the different strategies studied for treating real oilfield produced water, this study found that either individual microfiltration or biological treatments are inefficient individually to achieve desired reduction in COD level of the wastewater. However, combining microfiltration and biological treatment (MF-B or B-MF) is more efficient than the individual systems to keep the COD of the treated water well below the desired discharge COD limit of the water. On the other hand, biological treatment followed by microfiltration (B-MF) may not be desired due to fouling caused by the deposition of the microbial biomass on the membrane surface. Hence, microfiltration using the indigenous tubular ceramic membrane followed by biological treatment using *R.Opacus* (MF-B) is the best strategy to remove COD from the wastewater, maintaining a maximum permeability of 18.7 $\times 10^{-9}$ m^3 m^{-2} s^{-1} kPa^{-1}, which is being reported for the first time in literature. Hybrid and integrated systems are now in high demand, which mainly governs the wastewater treatment systems. Hence, the results obtained in this study could be beneficial for scale up of such systems for industrial use.

Table 3.11 Various literature reports on the treatment of produced water

Techniques	Membrane type	Wastewater	Pore size (µm)	Feed concentration of TOC (mg/L)	Feed concentration of COD (mg/L)	Permeability ($m^3\ m^{-2}\ s^{-1}\ kPa^{-1}$) $\times 10^{-9}$	TOC or COD removal efficiency (%)	References
Integrated adsorption with microfiltration	Cellulose acetate	Petroleum produced water	0.20	NA	7110	4.70	54.30	Abdel-Shafy et al., (2020)
Integrated adsorption and double stage membrane process	Nanohybrid PES–nano silica (Polymeric membrane)	Original produced water (Indonesia)	0.002	NA	150.82	30.50	76	Kusworo et al., (2018)
Functionalization of alumina ceramic microfiltration	α- alumina	Petroleum produced water (Utah, USA)	0.22	356	NA	402	99.60	Maguire-Boyle et al., (2017)
Ceramic membrane filtration	α- alumina and TiO_2	Oilfield produced water	0.20	200-2000	NA	75	38	Ebrahimi et al. (2010)
Combined microfiltration followed by biological treatment	Mixed cellulose ester (MCF)	Offshore oilfield wastewater (brazil)	0.10	386	NA	5.50	85	Campos et al., (2002)
Ceramic membrane microfiltration followed by biological treatment	Kaolin	Onshore oilfield produced water	0.178	355±0.20	951±10	18.70	99 (COD)	This study

*NA – Not available

3.18. Summary

The potential performance of membranes was tested by conducting crossflow microfiltration experiments to separate microalgae from the culture broth, TiO_2 NPs from water and treatment of produced water. In case of microalgae separation, among all the membranes studied (Kaolin, Kaolin-GG, Kaolin-CMC and Kaolin-HPMC), the Kaolin-HPMC membrane yielded a 100% recovery of algae with a high permeate flux of 1.78×10^{-5} m^3/m^2s at an applied pressure of 276 kPa. The investigation of flux decline mechanism using various pore-blocking models showed the best fit for the cake filtration model. In case of TiO_2 NPs separation, among the effect of different operating parameters studied (cross flow velocity, applied pressure, pH of feed TiO_2 suspension), pH strongly influenced the microfiltration of TiO_2 and the highest flux was obtained at the feed pH 5.1. Furthermore, the membrane displayed an excellent performance in terms of reduction in turbidity by 100% under all experimental conditions. While treating produced water, the effect of applied pressure on membrane performance in microfiltration showed that the permeate flux increased as the pressure increased from 69 to 345 kPa. Complete removal of TSS and turbidity was obtained at all the applied pressures. However, the COD removal efficiency at higher applied pressures was not satisfactory as the COD concentration exceeded the dischargeable limits for such wastewater into surface water. The hybrid microfiltration-biodegradation system (MF-B) developed in this study using low-cost ceramic membrane and *R. opacus* was found efficient to treat real oilfield-produced water. The combined system is found to be superior in producing high-quality effluent with COD value below the permissible limit as prescribed by Central Pollution Control Board, India. Among the different chemical reagents tested for cleaning the fouled membrane, the mixture of 1 wt% NaOCl and 0.1 wt% SDS was found to be effective with the maximum flux recovery. Furthermore, toxicity assessment of MF-B system treated PW with *Cicer arietinum*, *Vigna mungo* seeds indicated that the treated water is toxic-free and can be reused for irrigation

purpose. Overall, this study unveiled the potential of ceramic membranes in the field of microalgal separation and TiO_2 NPs separation from water. In addition, the studies demonstrated the capability of hybrid microfiltration using low-cost ceramic membrane and biological treatment using *R.opacus* as a viable option for the treatment of PW.

Chapter 4

Facile synthesis of OSDA-free chabazite zeolite coated kaolin ceramic membrane

Facile synthesis of OSDA-free chabazite zeolite coated kaolin ceramic membrane

This chapter discusses the preparation of chabazite zeolite coated ceramic composite membrane by hydrothermal method. Different strategies were followed to fabricate the composite membranes through the organic template-free hydrothermal synthesis method, such as coating the ceramic tubes solely on the interior surface, exterior surface and both sides. The synthesized zeolite composite membranes were subjected to X-ray Diffraction, Fourier transform infrared spectroscopy (FTIR), thermogravimetric analysis, field emission scanning electron microscope (FESEM), field emission transmission electron microscope (FETEM), BET surface area analysis, porosity, water permeability and pore size measurements.

4.1. Chemicals

Sodium aluminate (anhydrous) and fumed silica were purchased from Sigma Aldrich (India). HCl, NaOH and the chemicals required for measuring cation exchange capacity, ethylenediaminetetraacetic acid (EDTA), Eriochrome Black-T, ammonium chloride (NH_4Cl), ammonia solution (25%) were obtained from Merck (I) Ltd, Mumbai. All the chemicals were used as received and Millipore water was used in all the experiments.

4.2. Synthesis of CHA zeolite – ceramic composite membrane

Synthesis procedure of CHA zeolite was adopted from the literature (Chen et al., 2020), and used a molar composition of 0.9 Na_2O: 0.07 Al_2O_3: 1 SiO_2: 33.1 H_2O. Firstly, 22.26 g of sodium hydroxide pellets were mixed with 200 mL water. This solution was then divided into two equal parts, A and B. To prepare the silicate solution, 20.14 g of fumed silica was completely dissolved in solution A at 90 ^oC temperature and under continuous stirring at 500 rpm. To prepare aluminate solution, 3.85 g of sodium aluminate was dissolved in solution B at room temperature (25 ^oC) by stirring the solution continuously at 500 rpm. Then, the aluminate solution was added dropwise to silicate solution and stirred continuously for 1 h to get a homogeneous solution. The resulting precursor was then crystallized along with the ceramic

support (Kaolin-HPMC) in a Teflon-lined autoclave reactor at 100 ^{o}C for 24 h under static hydrothermal condition. Three different composite membranes were prepared as follows. In the first case, only the inner surface of the ceramic tube (Kaolin-HPMC) was coated with the zeolite layer by wrapping Teflon tape on the outer surface of the support. In the second case, the inner surface of the ceramic tube (Kaolin-HPMC) is entirely blocked by Teflon material while allowing the outer surface of the ceramic tube to be coated with zeolite layer. In the third case, the ceramic tube (Kaolin-HPMC) was kept as it was to allow the zeolite layers to deposit on both sides of the tube. After the hydrothermal reaction, the ceramic tube and zeolite powder were collected and washed with water until the pH of water reached 7 and subsequently dried for 24 h at 100 ^{o}C. The inside, outside, and both side coated tubular ceramic supports were named as CM_I, CM_O and CM_B, respectively. Fig. 4.1 displays the various steps involved in the preparation of the ceramic composite membranes.

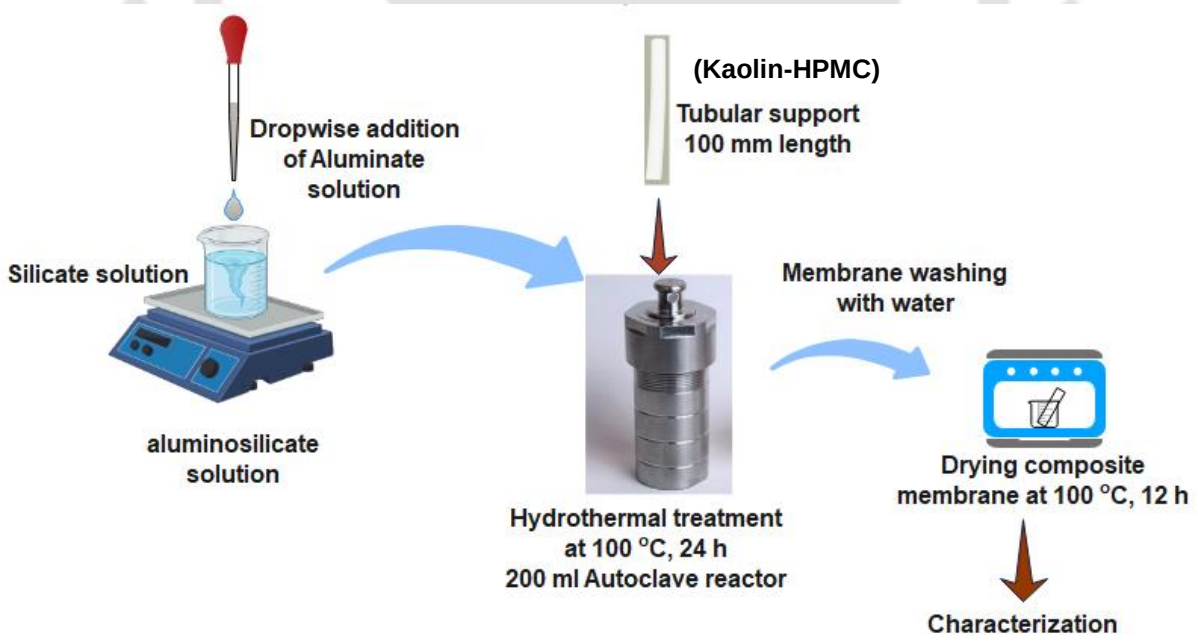

Fig. 4.1 Schematic of the steps involved in the fabrication of CHA zeolite ceramic composite membranes

4.3. Characterization techniques

The prepared CHA zeolite powder was characterized using powder X-ray diffraction (XRD) (Model: Micromax-007HF, Make: Rigaku) at room temperature with monochromated Cu-Kα radiation as a source. The measurements were taken in the 2θ range of 5-45^{o} with a step size of 0.02 to determine the zeolite powder crystallinity and crystallite size. The percentage crystallinity was calculated from the following equation (Iqbal et al., 2019).

$$\% \text{ Crystallinity} = \frac{\text{Sum of the relative intensities of most intense peaks of the sample}}{\text{Sum of the relative intensities of most intense peaks of standard CHA zeolite}} \times 100 \quad (4.1)$$

The average crystallite size was estimated using the Scherrer's equation (Nassar and Abdelrahman, 2017).

$$\text{Crystallite size (D)} = \frac{K \times \lambda}{\beta \times \cos\theta} \quad (4.2)$$

Where K, λ, β, θ are the Scherrer's constant, wavelength of X-ray radiation, full width at half maximum of the XRD diffraction peaks, and diffraction angle in radians, respectively.

The functional groups present in the zeolite powder were analyzed using Fourier Transform Infrared Spectroscopy (FTIR) (Model: IRAffinity-1; Make: M/s Shimadzu). The FTIR spectrum of CHA zeolite powder was recorded using the KBr pellet method at a wavelength range of 4000-400 cm^{-1}. Thermogravimetric analyzer (TGA) (Model: TG 209 F1 Libra; Make: M/s Netzsch) was used to perform thermogravimetric and derivative thermogravimetric analysis (TGA and DTA) of the zeolite powder sample in the temperature range of 25 – 1000 ^{o}C with a heating rate of 10 ^{o}C/min. Morphology of zeolite powder and the surface of zeolite coated membranes were examined by FESEM (Model: Sigma 300, Make: Zeiss). For studying zeolite morphology by FESEM, 0.1 wt% zeolite suspension prepared with water was ultrasonicated for 10 min, immediately after which a small drop of the sample was kept on carbon tape and dried. For the analysis, the sample was placed on the FESEM stub, and the

gold coating was done to impart conductivity to the sample. The particle size distribution of zeolite particles was analyzed by FETEM (Model: 2100F, Make: JEOL). The same instrument was also used for taking Selected Area Electron Diffraction (SAED) patterns. For FETEM analysis, 0.1 wt% zeolite suspension was ultrasonicated for 10 min, immediately following which, a small drop of the sample was kept on a conductive copper grid and dried. Zeta potential of the zeolite composite membrane at different pH was recorded using the Delsa Nano C zeta potential analyzer (Model: Delsa Nano C, Make: M/s Beckman Coulter) to know the surface charge of the membrane. The pH of the samples was adjusted by using NaOH and HCl. The cation exchange capacity (CEC) of CHA zeolite particles was determined using the following procedure (Greenberg et al., 1992; Kumar et al., 2015a). Initially, 1 g of calcium chloride dihydrate was dissolved in 1100 mL water, and the pH of the solution was adjusted to 9 using NaOH solution. From this test, 100 mL of solution was kept aside to determine Ca^{2+} concentration. Dry zeolite powder (1 g) was dispersed in the remaining Ca^{2+} solution (1000 mL), and the suspension was stirred for 1 h. The filtrate was then recovered by passing the suspension through a Whatman filter paper (No. 1). The cation exchange capacity in milliequivalent per gram of dry zeolite was determined by calculating the difference in Ca^{2+} concentration in the original and the filtrate. The concentrations of Ca^{2+} in the respective solutions were determined by titrating 50 mL of sample, after adjusting its pH to 10 using a buffer solution (a combination of NH_4Cl and ammonia water). The titration of the samples was carried out against 0.01 M ethylenediaminetetraacetic acid (EDTA) using Eriochrome Black-T as the indicator. The end point of the titration was noted when the color of the solution changed from wine-red to blue. The cation exchange capacity of the zeolite was then calculated using the following expression (Kumar et al., 2015a).

$$\text{CEC (meq/g)} = \frac{(V_1 - V_2)}{(S \times W)} \times 20 \qquad (4.3)$$

Where V_1 and V_2 are the volumes (mL) of 0.01M EDTA solution consumed by the original and exchanged calcium ion solutions, respectively. On the other hand, S and W represent the sample volume (mL) used for titration and weight (g) of dry zeolite, respectively.

The N_2 adsorption and desorption isotherms of zeolite powder and zeolite composite membrane (CM_B) were determined by using N_2 gas sorption. Prior to the analysis, each sample was degassed for 3 h at 150 ^oC under a continuous flow of N_2 gas. The specific surface area and the pore size distribution were then derived from the BET (Brunauer-Emmett-Teller) technique and the BJH (Barrett-Joyner-Halenda) model, respectively.

The amount of zeolite grown in membrane was quantified by the weight gain of the membrane. The porosity, pure water flux and pore size measurements of the composite membranes were measured using methods reported in Section 2.4.2. (Chapter 2). All the aforementioned quantitative experiments were investigated for at least five samples, and the mean values, including standard deviations, were presented as the final results in this study.

4.4. Results and discussion

4.4.1. Characterization of CHA zeolite powder

4.4.1.1. X-ray diffraction analysis

The synthesized zeolite crystals were characterized for evaluating the crystallinity and crystallite size using X-ray diffraction analysis. Fig. 4.2 displays the crystallographic patterns of the prepared zeolite powder. The XRD patterns accurately matched with JCPDS file #34-0137 of the reference material chabazite (CHA), indicating the formation of high quality pure CHA crystals at the synthesis conditions (Section 4.2). As presented in Table 4.1, the experimentally calculated d-spacing values of the prepared CHA zeolite matched with those of the reference chabazite zeolite material. The occurrence of sharp peaks signifies that synthesis temperature promotes a series of processes, such as transformation of amorphous gel to nucleation and then crystal growth through fusion of nucleus (Le et al., 2019). The percentage

crystallinity of the synthesized zeolite was found to be 98%. The probable reason for obtaining such high crystallinity might be the high intensity of respective peaks. The occurrence of these highly intense peaks illustrates the formation of uniform sized CHA crystals, which is clearly evident from Fig. 4.2. It needs to be mentioned here that the presence of uniform sized zeolite layer has a positive impact in separation experiments owing to absence of defects (Eterigho-Ikelegbe et al., 2021). During the synthesis of composite membrane, a maximum crystallinity of 75% for sodalite nanoparticles was reported by Eterigho-Ikelegbe et al. (2021).

The crystallite size of the synthesized zeolite was calculated to be 16.7±2 nm using Scherrer's equation (Eq. 4.2). These small sized particles lead to easy and heavy deposition of the zeolites on the membrane matrix as they can easily penetrate inside the pores of ceramic support, a feature highly desired from separation point of view.

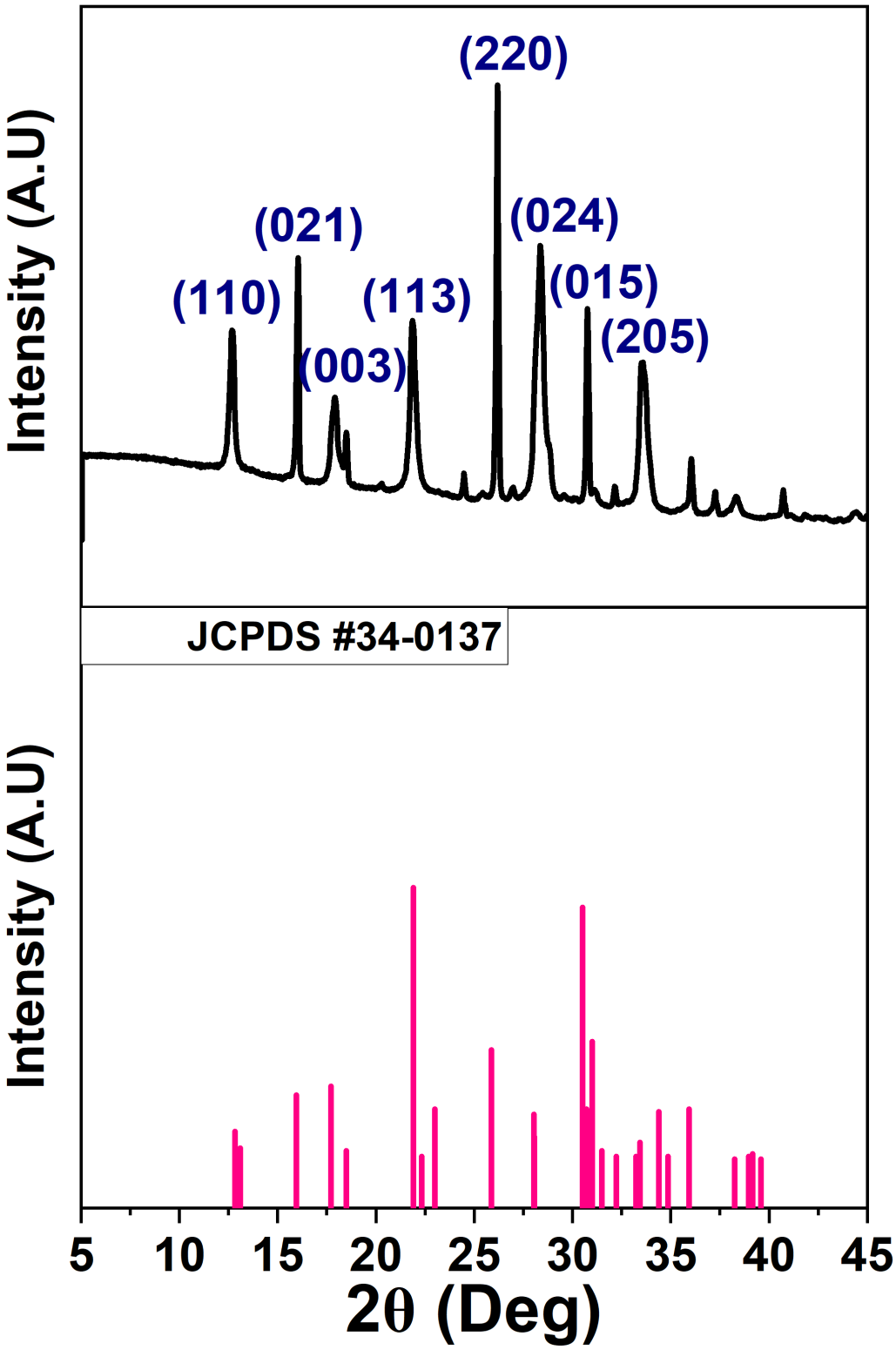

Fig. 4.2 XRD profile of CHA zeolite

Table 4.1 Analysis of XRD patterns of CHA zeolite

2Θ (in degrees)	**d (Å) of Fig. 3a**	**d (Å) of JCPDS file #34-0137**	***h k l* from file #34-0137**
12.62	7.0092	6.89	1 1 0
15.97	5.5460	5.552	0 2 1
17.84	4.9676	5.001	0 0 3
18.43	4.8110	4.667	2 0 2
21.83	4.0688	4.053	1 1 3
26.12	3.4084	3.446	2 2 0
28.28	3.1527	3.176	0 2 4
30.71	2.9092	2.908	0 1 5
33.55	2.6692	2.678	2 0 5
35.99	2.4937	2.497	0 0 6

4.4.1.2. FTIR analysis

The FTIR spectrum of the prepared CHA zeolite is depicted in Fig. 4.3. The spectrum displays a wide band at 3450 cm^{-1} owing to the presence of silanol OH group (Si-OH). A sharp peak at 1010 cm^{-1} represents the asymmetric stretching vibration of T-O-T (T = Al or Si). On the other hand, the band detected at 743 cm^{-1} is because of the symmetric stretch of T-O-T (T = Al or Si). This band is less intense than the band at 1010 cm^{-1}. This might be because of the lesser feasibility of symmetric stretching of the T-O band in the zeolite framework compared to asymmetric stretching (Sharma et al., 2012). The band at 1635 cm^{-1} represents the bending vibration of H-O-H, in which the hydrogen is bound to the framework's oxygen ions.

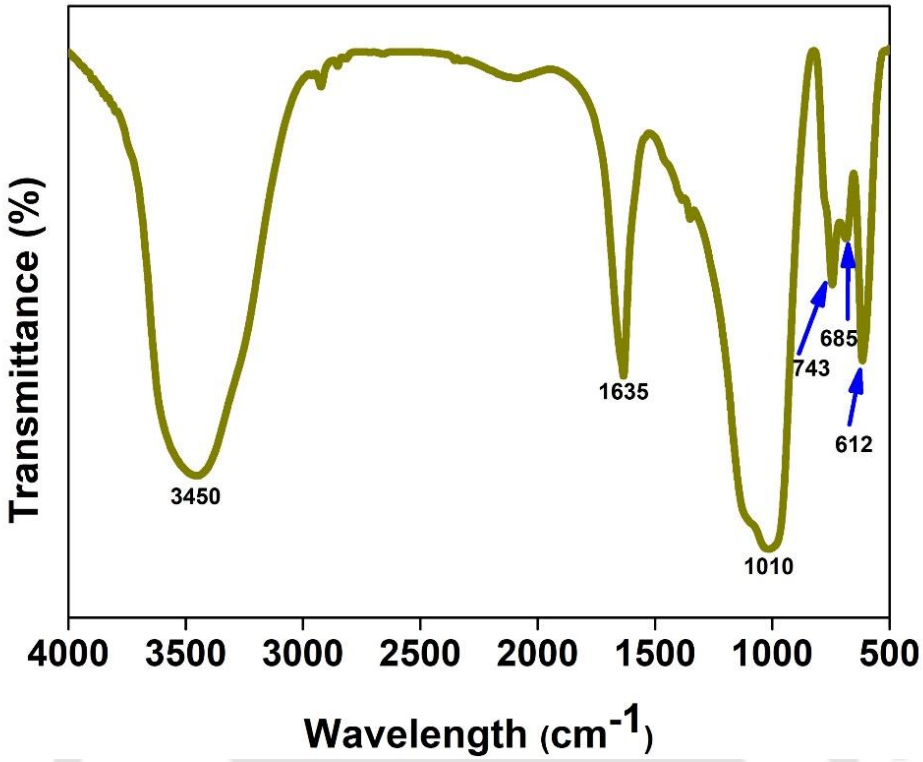

Fig. 4.3 FTIR spectrum of CHA zeolite

The bands at 612 and 685 cm^{-1} indicate the presence of six membered structural unit rings, which are recognized as CHA zeolite features (Aysan et al., 2016). Therefore, it can be inferred that the FTIR spectrum of prepared CHA zeolite contains similar chemical moieties and structural units as those mentioned in literature (Aysan et al., 2016, Basumatary et al., 2015).

4.4.1.3. Energy dispersive X-ray analysis

From the EDX analysis (See Fig. 4.4), the primary constituents in the CHA zeolite were found to be aluminium and silicon, which have tetrahedral connections with sodium and oxygen ions present in the zeolite framework (Salim and Malek, 2016). Besides, it needs to mention that the oxide forms of all the elements described above are responsible for the presence of oxygen in greater quantities (Zhu et al., 2016; Goswami and Pugazhenthi, 2021).

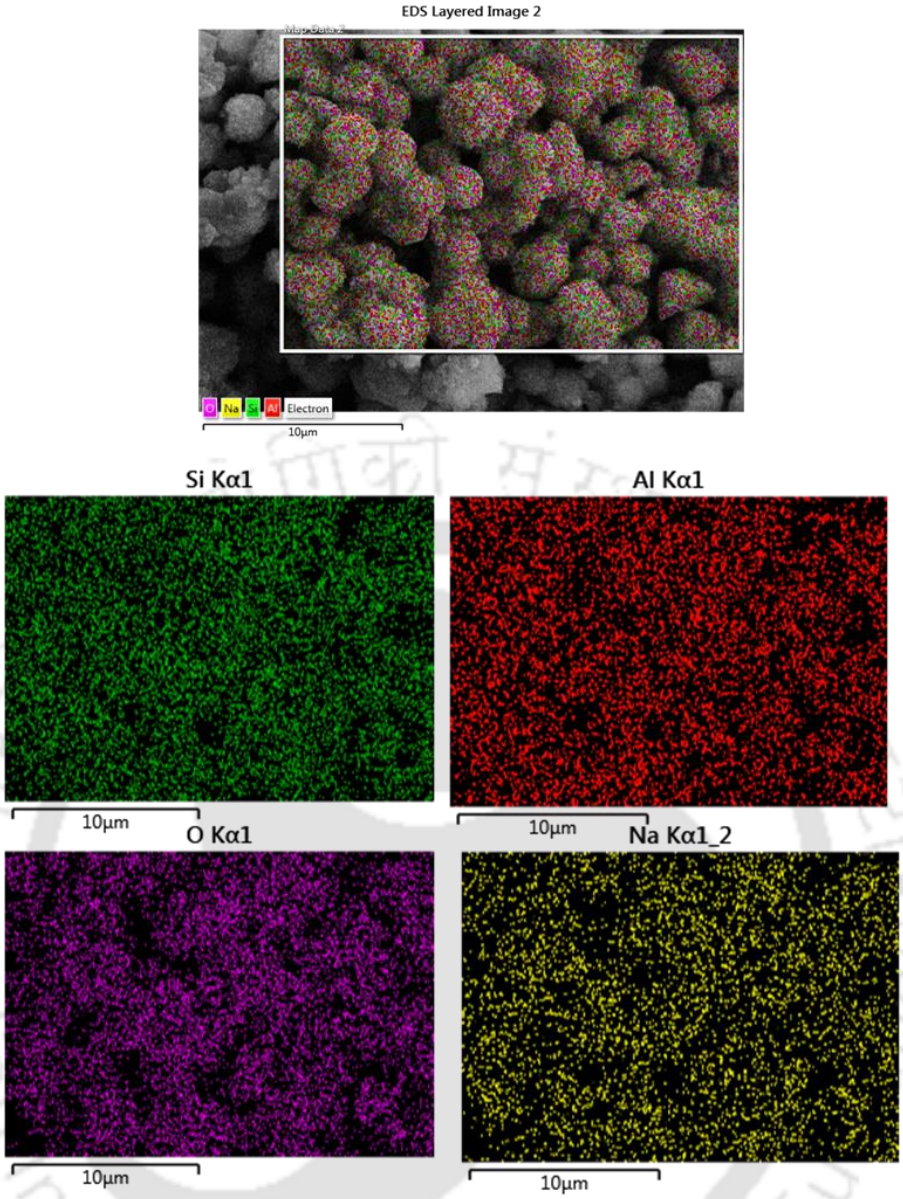

Fig. 4.4 EDX mapping of CHA zeolite powder

4.4.1.4. Morphological study

The morphology of CHA zeolite was examined by FESEM and FETEM analysis to determine its crystalline nature and particle size distribution. Fig. 4.5 depicts the morphology of the zeolite powder synthesized by the hydrothermal method. The prepared zeolite powder consists of small sized homogeneous spherical shaped particles, which are further re-assembled into flowers with a highly rough exterior surface, as seen in FESEM images of Fig. 4.5 (a) and 4.5(b). It is known that the small spheres (see Fig. 4.5b inset) can grow inside the pores of the membrane. Chen et al. (2020) reported that the hydrothermally synthesized CHA zeolite used

to separate copper from drinking water was spherical in shape with a highly rough surface. As evident from the FETEM image (Fig. 4.5c), zeolite powder comprised of many nano-crystallites. The mean size of these synthesized particles was calculated using Image J software and found to be 17.8±2.5 nm (Fig. 4.5d). Furthermore, the SAED image (Fig. 4.5c inset) of the prepared zeolite indicates the diffraction rings confirming the polycrystalline nature of the zeolite. Similar results were obtained by Zhang et al. (2013) for the synthesis of ZSM-5 nanocrystals, which revealed nanocrystals with a highly rough surface exhibiting single crystal-like diffraction

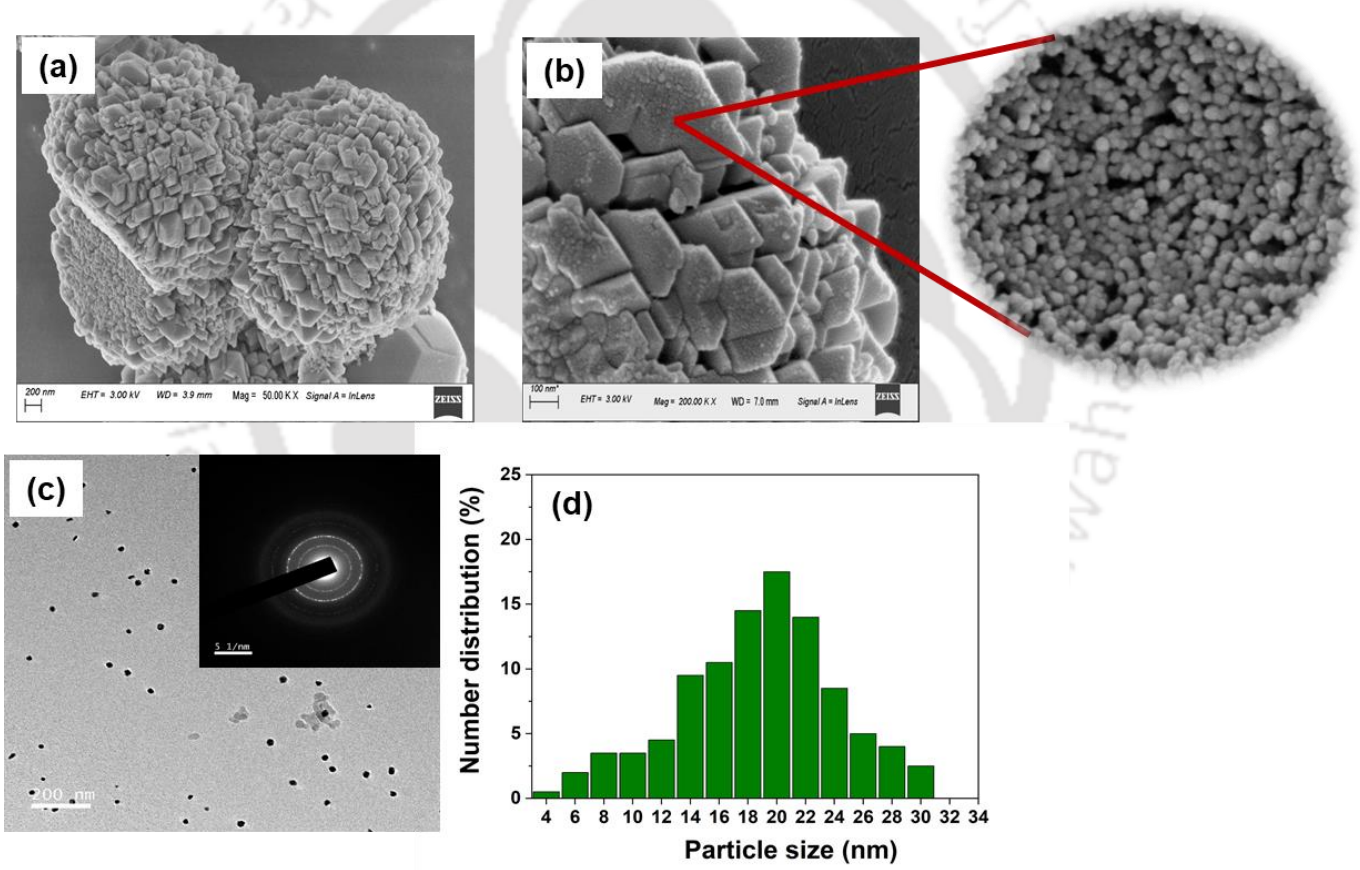

Fig. 4.5 FESEM images of CHA zeolite particles at (a) lower and (b) higher magnification, (c) FETEM images of CHA zeolite with SAED pattern (inset) and (d) number distribution of zeolite particles from the FETEM images

4.4.1.5. TGA and DTG analysis

Fig. 4.6 represents the TGA and DTG analyses of the synthesized CHA zeolite powder. The TGA analysis displayed a total weight loss of 8 % in two different stages for the zeolite powder. Weight loss between 50 and 160 ^{o}C represents the removal of physisorbed water from the surface of the material. From 170 to 370 ^{o}C, another minor weight loss was observed due to thermal desorption of strongly bonded water molecules. DTG curve also represents a similar thermal decomposition of zeolite powder. The endothermal peak at 70 ^{o}C and 240 ^{o}C correspond to the removal of moisture and strongly bonded water molecules, respectively. A similar observation was made by Fan et al. (2020) for the organic template-free synthesis of silicoaluminophosphate (SAPO) zeolite under hydrothermal conditions. The zeolite displayed the removal of weak and strongly bonded water molecules before reaching 200 ^{o}C and in the temperature range 300-400 ^{o}C, respectively. It is reported that at high operating temperatures, the interaction of water molecules leads to structural changes in the zeolite molecules. Therefore, synthesis temperature is considered as one of the important factors that controls the thermal desorption of strongly bonded water molecules (Resasco et al., 2021). Coudert et al., (2009) studied the effect of Si/Al ratio on water present in zeolite framework by considering three zeolites with the same structure (LTA) but with different Si/Al ratios. It was observed that water in hydrophobic zeolite (high Si/Al) behaves as a nanodroplet trying to close its hydrogen bonds onto itself. In contrast, water in hydrophilic zeolite (low Si/Al) opens up to form hydrogen bonds with the oxygen atoms of the framework. It is reported that the synthesis of zeolite in alkaline media is preferable as it affects the Si/Al ratio (Resasco et al., 2021). Hence, from the aforementioned discussion, it can be concluded that low synthesis temperature, high Si/Al ratio, alkaline medium, and ionic strength are important parameters to consider to prevent thermal desorption of strongly bonded water molecules.

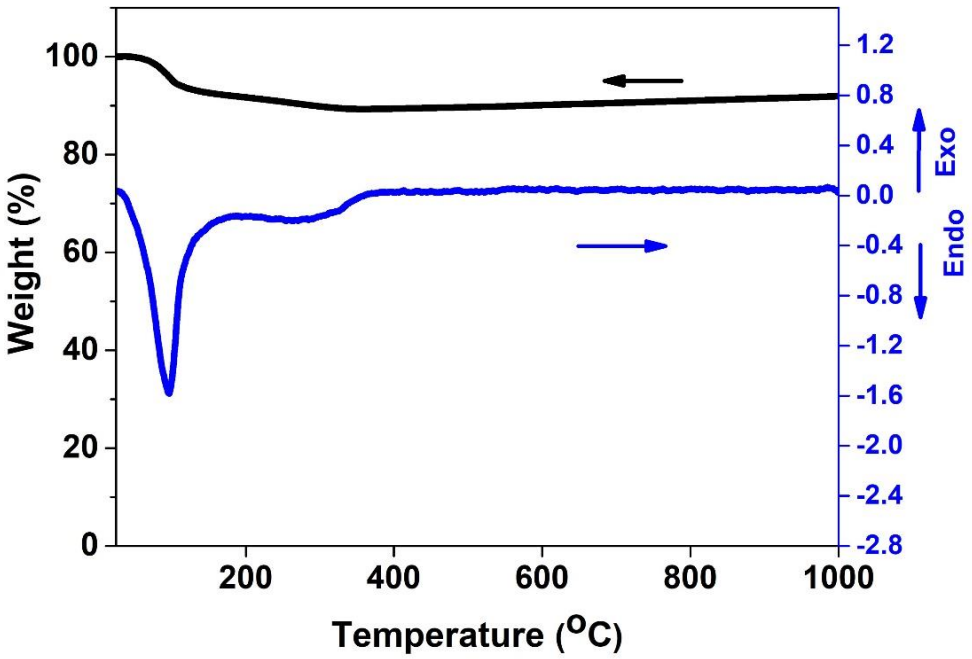

Fig. 4.6 TGA and DTG profiles of CHA zeolite

4.4.1.6. Zeta potential measurement

The variation of zeta potential of the CHA zeolite powder with pH is presented in Fig. 4.7. The isoelectric point (IEP) of the zeolite was found to be 4.3, which implies that the zeolite remains positively charged below a pH value of 4.3 owing to the presence of a significantly high number of H^+ ions. On the contrary, the zeolite gets negatively charged above pH 4.3 due to the presence of a high number of OH^- ions. In the literature, Van Heyden et al. (2008) reported a value of isoelectric point equal to 4.0 of the SAPO-34 zeolite particles (CHA framework) prepared by the hydrothermal method.

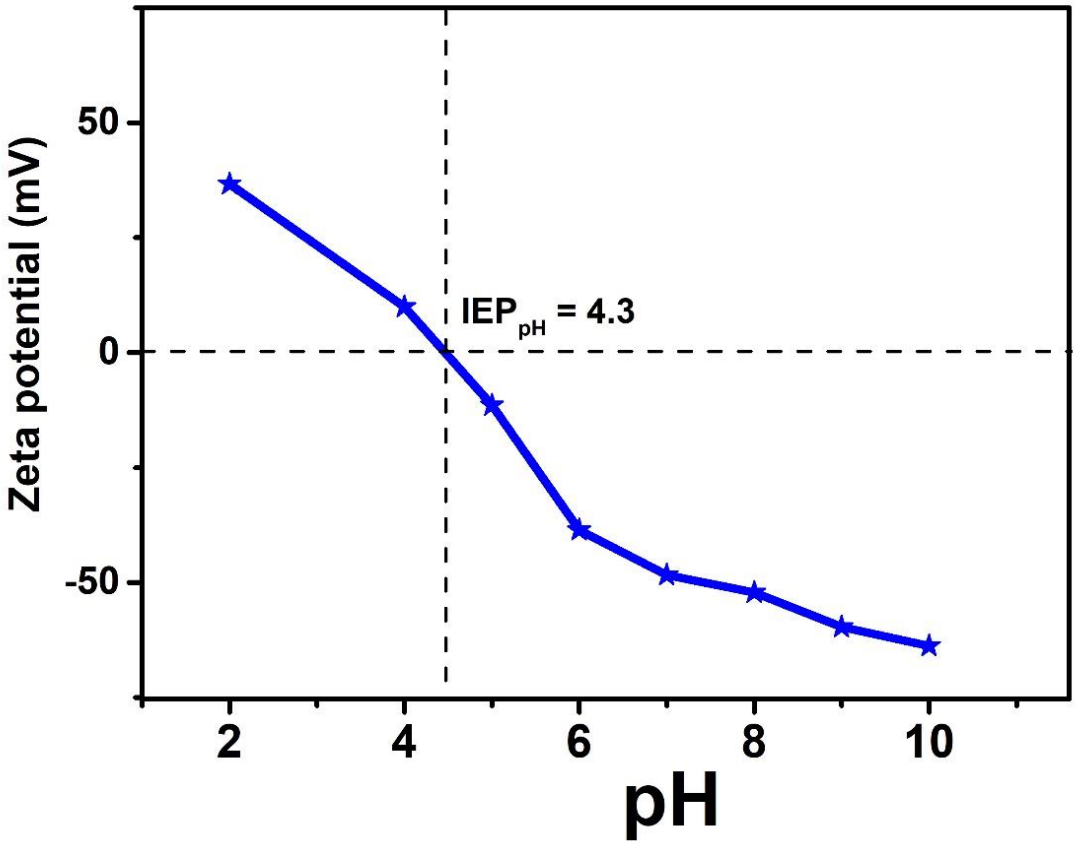

Fig. 4.7 Zeta potential measurement for CHA zeolite at various pH

4.4.1.7. Cation exchange capacity

It is well known that zeolites are aluminosilicates with a tetrahedral framework that holds a cation with enough flexibility to allow cation exchange. The cation exchange capacity of zeolites is used to classify the zeolites for different industrial applications (Singh et al., 2002). The synthesized zeolite showed a high cation exchange capacity of 3.96 meq/g as determined from equation (Eq. 4.3). Singh et al. (2002) studied the fly ash-water interaction (zeolitization) of lagoon ash in wet disposal. The zeolitization process confirmed the formation of zeolites and reported that chabazite zeolite has a high CEC of 4 meq/g. Also, the zeolitized ash was applied for different environmental applications, viz., removal of heavy metals from the

industrial sludge. H-USY is another synthetic zeolite displayed a high cation exchange capacity of 3.63 meq/g which was reported in Zola et al., (2012) study.

4.4.2. Characterization of zeolite-ceramic composite membrane

4.4.2.1. Morphology study of membranes

To further validate the results presented in Table 4.2, the morphology of the prepared ceramic support and composite membranes was observed through FESEM. As seen in Fig. 4.8, the composite membranes are completely covered by zeolite particles and the coverage of CHA zeolite crystal layer can be positively related to weight gain (Cao et al., 2016). The small-sized zeolite particles penetrate through the support pores, while the larger ones get deposited on the support surface, forming the coated layer. The membrane was less coated in case of CM_I than CM_O and CM_B membranes owing to its lower surface area. In the case of CM_B membrane, zeolite particles are uniformly distributed on the membrane surface. During the hydrothermal treatment, the CHA zeolite particles totally covered the inner and outer surfaces of the support. These FESEM results further confirm the weight increment results mentioned in Table 4.2: CM_B membrane was coated with the highest amount of zeolite, followed by CM_O and CM_I membrane, respectively.

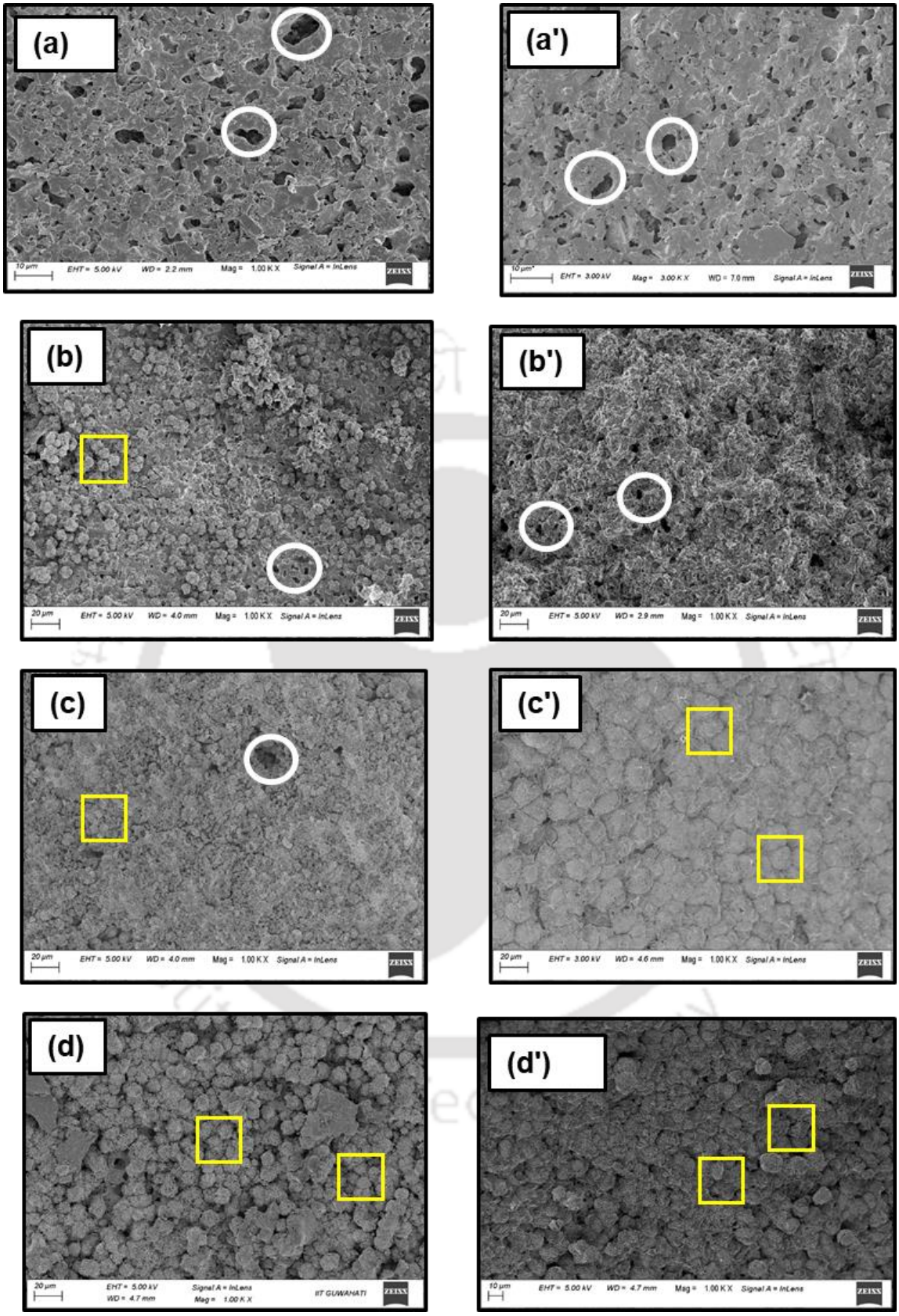

Fig. 4.8 FESEM images of prepared membranes: (a, a′) inner and outer surface uncoated support membrane, (b, b′) inner and outer surface of CM_I composite membrane, (c, c′) inner and the outer surface of CM_O composite membrane, (d, d′) inner and the outer surface of CM_B composite membrane (□: zeolite; ○: pore).

The mechanical strength analysis revealed that the compressive strength of the dual-side coated membrane is 23.8±1.5 MPa, which is similar to the support membrane (25.0±1.8 MPa, section 2.3.6, Chapter 2), thus indicating that the membrane is stable even when zeolite synthesis conducted in a highly alkaline environment (H_2O/Na_2O: 36.8). A fact worth mentioning here is that the mechanical strength of the membrane is quite responsible for the long-term stability or strength of ceramic membrane in the full-scale application along with other characteristics of the membrane such as good chemical resistance (acid and alkali) and high thermal stability (Li et al., 2020). In this study, the achieved mechanical strength of the composite membrane (23.8±1.5 MPa) is found to be comparable with the commercially available silicon carbide (COMEM®) ceramic membrane (average pore size of 40 nm) for ultrafiltration in the full scale by LiqTech International, Inc company, which is reported to have a mechanical strength of 17.2 MPa.

4.4.2.2. Surface area and pore size distribution analysis

Fig. 4.9 displays the specific surface area and pore size distribution of CHA zeolite and CM_B composite membrane. The isotherm in Fig. 4.9a and 4.9c represents type IV isotherm according to IUPAC classification, where the pore size of the zeolite and composite membrane is in the micro and the mesoporous range (Bardestani et al., 2019). This type of isotherm has interactions between N_2 gas and sample (zeolite powder/composite membrane) owing to capillary condensation. Hence, the desorption path is different from that of adsorption, resulting in the formation of hysteresis, thus indicating the pore geometry. In this study, the zeolite and composite membranes show type H1 hysteresis, indicating that the pores have cylindrical geometry. The surface area from the BET plot was measured using the linear fit of N_2 adsorbed branch at relative pressures P/P_o ranging from 0.05 to 0.35, and it was found to be 10.91 m^2/g and 12.43 m^2/g for composite membrane (CM_B) and zeolite powder, respectively. Figs. 4.9b and 4.9d represent the pore size distribution of zeolite powder and composite membrane,

respectively, which were derived from the desorption isotherm data using the BJH model. In the case of composite membrane, which displayed two distribution peaks, it can be said that the membrane matrix has a bimodal pores structure. In this case, the occurrence of peaks at 3.72 nm and 33.4 nm represents the presence of micropores and mesopores in the membrane matrix. The peak at 3.72 nm indicates zeolite pore distribution, as confirmed by the peak appearance at the same pore diameter for zeolite powder (see Fig. 4.9b). It should be mentioned here that the average pore diameter of the membrane is found to be 34 nm.

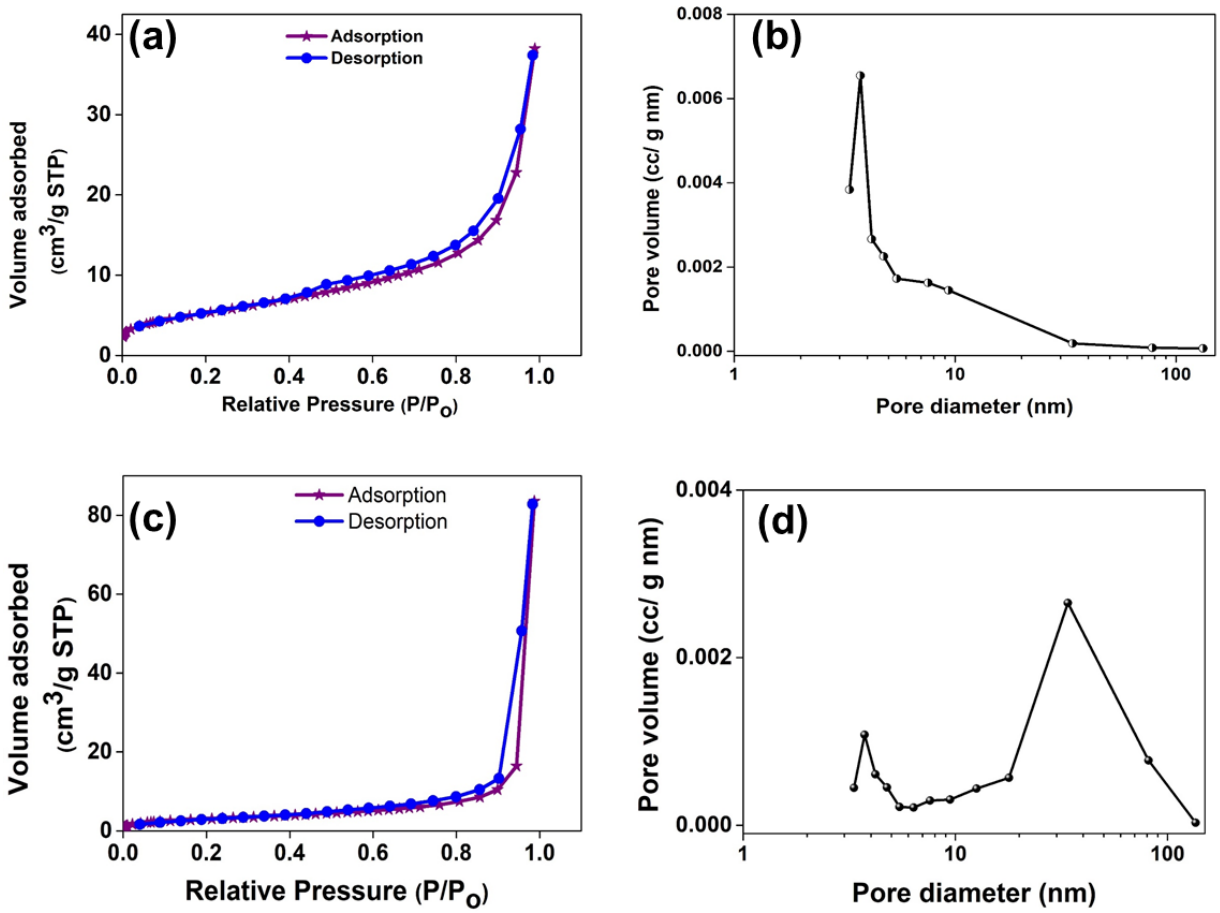

Fig. 4.9 N_2 adsorption and desorption isotherms of (a) CHA zeolite powder and (b) CM_B membrane; BJH pore size distribution of (c) CHA zeolite powder and (d) CM_B membrane.

4.4.2.3. Porosity, pure water flux and pore size measurement

With an applied pressure ranging between 69 and 345 kPa, the pure water flux was measured for all the three membranes (Fig. 4.10). As the applied pressure increased, flux increased in all the cases and in accordance with Darcy's law. Among the three types of coating performed, the membrane coated only inside (CM_I) offered the highest permeate flux owing to the comparatively small amount of zeolite coating. On the other hand, the membrane coated on both sides (CM_B) showed the least permeate flux because of high penetration and growth of zeolite through both sides of the membrane. The increased penetration and subsequent growth of zeolite can be related to the reduced availability of membrane pores, which ultimately aided in lowering the permeate flux in case of CM_B membrane. The permeability of all the coated

membranes was less than that of the support due to the deposition of zeolite particles. Basumatary et al. (2015) prepared a composite membrane by coating MCM-41zeolite on flat ceramic support to separate chromic acid from aqueous solution. It was observed that as the number of coating cycles was increased from 1 to 3, the water permeability reduced from 1.26×10^{-6} to 6.05×10^{-8} m^3/m^2 s kPa owing to the reduced availability of pores.

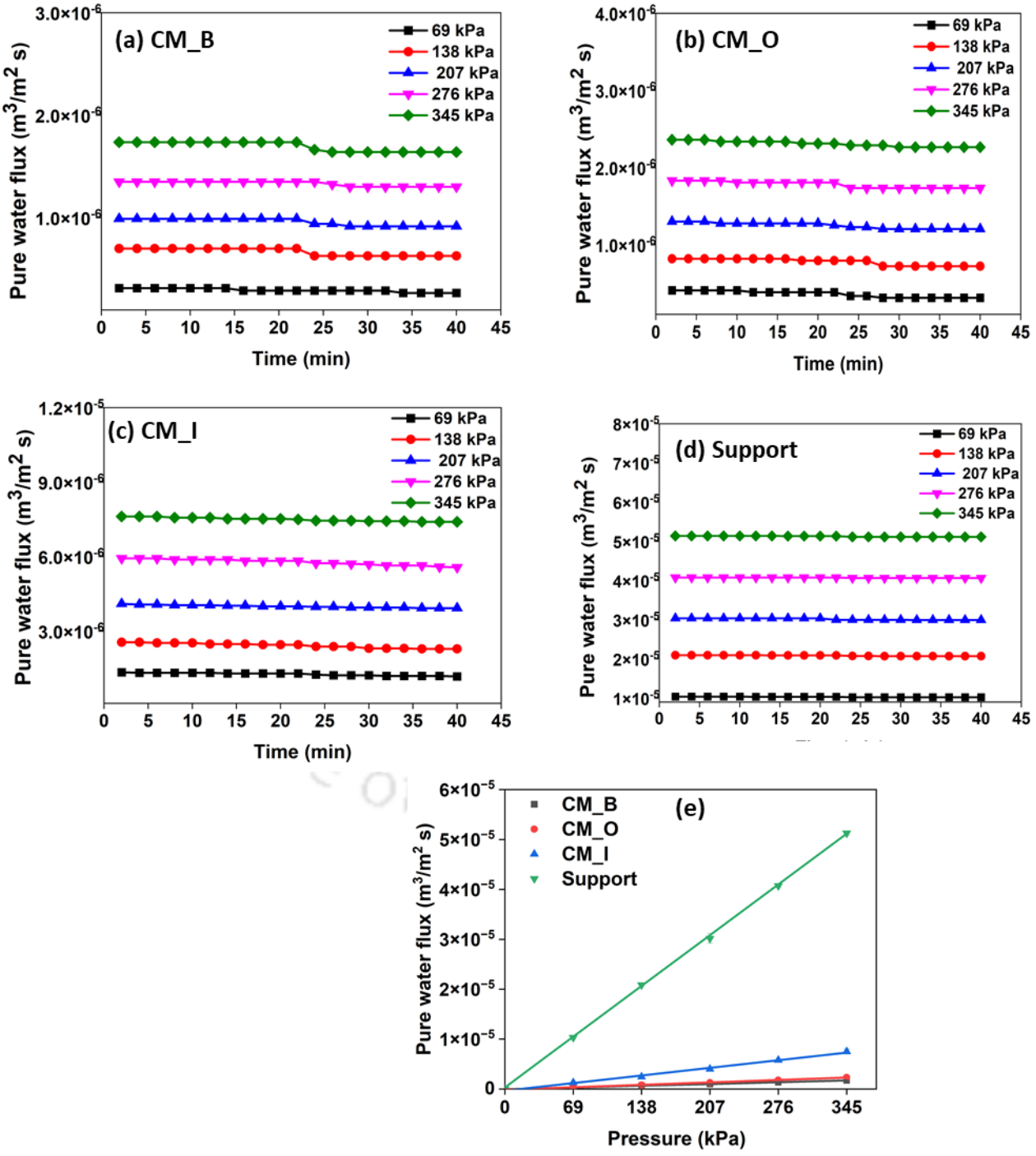

Fig. 4.10 Pure water flux as a function of time at various applied pressures for all membranes: (a) CM_B; (b) CM_O (c) CM_I; (d) support, and (e) pure water permeability versus pressure for all membranes

As can be observed from the experimental results depicted in Table 4.2, the values of water permeability and average pore size of the coated membranes were less than that of the support membrane (support > CM_I > CM_O > CM_B). The porosity of the CM_B membrane was reduced to 30.5±0.5 % from 40±0.3 % (Kaolin-HPMC support). The average pore size of all the membranes reported in Table 4.2 was calculated using equation (2.5) (Chapter 2), and amongst all the membranes, CM_B membrane showed the least pore size of 36 nm. The result is in good agreement with the average pore size calculated from the BJH method (see Fig. 4.9).

While considering the performance of single side coated and both side coated membranes, it has been observed that the water permeability of both sides coated membrane (CM_B) was very low (4.83×10^{-9} m^3/m^2 s kPa) in comparison with single-side inside coated membrane (20.1×10^{-9} m^3/m^2 s kPa) and single-side outer coated membrane (6.42×10^{-9} m^3/m^2 s kPa), which is also evident from the data mentioned in Table 4.2. Besides, the long-term performance of the membrane can be assessed by its ability to separate any metal ion in a large number of operation cycles and for that the increase in weight gain of the membrane due to deposition of zeolite particles can be taken into account. In this case, the weight gain by both side coated membrane (CM_B) is found to be very high (1.82±0.18 g) as compared to the single side coated membranes (1.32 ±0.11 g), which will lead to enhanced separation performance. In this regard, the work of Basumatary et al., (2015) can be mentioned as they reported that the separation performance of the membrane showed significant improvement when the number of cycles of coating was increased from 1 to 3 due to weight gain from 0.45g to 0.89g zeolite.

Table 4.2 Characteristics of support and composite membranes

Membrane	Porosity (%)	Average pore size (nm)	Pure water permeability (m^3/m^2 s kPa)×10^{-9}	Weight gain (g)
Support (Kaolin-HPMC)	40±0.3	178	149	-
CM_I	32.3±0.5	74	20.1	1.32 ±0.11
CM_O	30.7±0.7	43	6.42	1.53 ±0.1
CM_B	30.5±0.5	36	4.83	1.82±0.18

4.4.3. Estimation of manufacturing cost for prepared membranes

The fabrication cost of zeolite-ceramic composite membrane was estimated based on raw material cost, labor cost, laboratory cost, equipment cost, depreciation cost, electricity cost, repair and maintenance cost. The cost of the prepared CM_B membrane was calculated according to the procedure described in Section 2.4.3 and Appendix. The estimated cost was found to be 868 USD/m^2. Another similar kind of ceramic ultrafiltration membrane with ZrO_2 as an active layer costs 2000 USD/m^2, as reported by Dilaver et al. (2018). Hence, it can be inferred that the composite membrane prepared as a part of this study is much cheaper than the one reported in the literature. Besides, it has also been reported that the polymeric NF and RO membranes cost around 40 – 100 USD/m^2 (Panagopoulos et al., 2021). However, the operating cost associated with polymeric membranes is very high. It has been mentioned in earlier literature that the annual operating cost of a ceramic membrane system is almost 55% less than a similar capacity polymeric membrane system due to the lower maintenance cost associated with ceramic membranes (Cabrera et al., 2021).

4.5. Summary

CHA-zeolite was successfully grown on kaolin-based tubular ceramic membrane support by hydrothermal synthesis method. The organic template-free synthesis of CHA zeolite reduced the synthesis time and was found to be environmental friendly as it involves no calcination step for removing the template. The results obtained from XRD, FESEM and FETEM indicated that the hydrothermal synthesis route produced pure, ultrafine and uniform particles of chabazite zeolite. The prepared zeolite displayed a high percentage crystallinity of 98%. The prepared zeolite had a high cationic exchange capacity. Among the three different coating strategies, the zeolite coated on both sides of the membrane (CM_B) was loaded with a maximum quantity of zeolite particles, followed by CM_O and CM_I, respectively. The porosity, pure water permeability and pore size of the composite membrane were found to be lesser than that of the support membrane.

Chapter 5

Continuous removal of heavy metals from aqueous solution using zeolite-ceramic composite membrane

Continuous removal of heavy metals from aqueous solution using zeolite-ceramic composite membrane

This chapter presents the investigation on the performance of both sides zeolite coated composite membrane (CM_B) to remove different heavy metals from aqueous solution. The chapter is divided into two parts. Part A describes the removal of cerium metal ions from aqueous solution in single salt system. The effect of applied pressure, feed concentration, and feed pH on the membrane performance was studied systematically. In Part B, the potential of the membrane in separating different heavy metal ions (Cd^{2+}, Ni^{2+}, Al^{3+} and Mg^{2+}) from their solutions was examined using single, binary and tertiary salt mixtures.

Part A: Separation of cerium from its aqueous solution

In order to evaluate the separation efficiency of the zeolite composite membrane, a synthetic feed solution of cerium was made by dissolving ceric (IV) ammonium nitrate salt in water. Ceric (IV) ammonium nitrate was supplied by HiMedia Laboratories Pvt. Ltd., Mumbai. Cross-flow filtration tests (see Fig. 2.3 of Chapter 2) were performed at different operating conditions by varying applied pressure from 69 to 345 kPa, pH from 2 to 4, and feed concentration from 100 to 1000 mg/L. It is to be noted that the pH of the feed was adjusted by using HCl and NaOH solution. After each experiment, the system along with membrane was cleaned by passing water through the system for a duration of 2 h. The usability of the membrane for the next run was assessed by measuring the hydraulic permeability value after membrane cleaning. A pure water permeability value lying within ±2% of the original value justifies the reusability of the membrane for further separation operations.

It is worth mentioning that the removal efficiency of cerium was determined by using the following expression (Kumar et al., 2021).

$$\text{Removal efficiency (\%)} = \frac{C_f - C_p}{C_f} \times 100 \tag{5.1}$$

Where, C_f and C_p are cerium concentration in feed and permeate solution, respectively. The concentration of cerium required for evaluating the metal removal was measured using microwave plasma atomic emission spectroscopy (Model: Varian, 4210 MP-AES Make: Agilent Technologies, India).

5.1. Results and Discussion

5.1.1. Effect of applied pressure

The effect of applied pressure on permeate flux and removal efficiency of cerium was investigated for the pressure range of 69-345 kPa by keeping a constant cross flow rate of 2.41×10^{-3} m/s, feed concentration of 1000 mg/L and natural pH of 3.3. It has been observed from Fig 5.1 (a) that the permeate flux of the composite membrane increased linearly with increasing applied pressure, all thanks to the enhanced driving force. Murthy et al. (2011) reported a similar observation regarding removal of cerium ions from its aqueous solution where with enhanced applied pressure, the permeate flux through nanofiltration membrane was found to increase linearly. However, the permeate flux obtained is found to be lesser than the pure water flux, owing to the osmotic pressure created by the retained ions that reduces the adequate pressure across the membrane (Basumatary et al., 2016). Although the membrane pore size is significantly larger than Ce ion, high removal efficiency is possible because of the Donnan exclusion mechanism. The rejection is predominantly affected by the electrostatic interaction (Donnan exclusion effect) between the ions and surface of the membrane in the solution (Peydayesh et al., 2020). The schematic of separation mechanism is presented in Fig. 5.2. In case of Donnan Exclusion effect, when the charged membrane is in contact with feed, the concentration of oppositely charged ions will be more near the membrane surface, and the concentration of similar charged ions will be more in solution. Hence, to maintain the electrochemical equilibrium, Donnan potential will develop at the interface between solution and membrane owing to the above-mentioned concentration difference. This potential is the

prime reason because of which the membrane repels ions with similar charge (Gong et al., 2020; Basumatary et al., 2017). This separation mechanism ultimately helped in achieving high retention of Ce >99.7 % at all values of applied pressure for an initial feed concentration of 1000 mg/L. However, a small reduction in the removal performance of the membrane was observed as the pressure increased from 69 to 345 kPa (Fig. 5.1b). This may be because of the fact that as applied pressure increases, the concentration of ions at the surface increases and subsequently, the removal efficiency decreases. Basumatary et al. (2016) also found that the rejection of Fe^{3+} decreased as the applied pressure increased from 69 to 345 kPa using MCM-48 zeolite ceramic membrane for a feed concentration of 3000 mg/L, and pH of 2.45. It is worth mentioning that the concentration of Ce in the permeate at different applied pressures (69 to 2.07 kPa) was less than 5 mg/L for a feed concentration of 1000 mg/L. This ultimately indicates the efficiency of the prepared zeolite composite membrane for removal of Ce ions from its solution and subsequent safe discharge of wastewater into the environment (Shahnaz et al., 2022).

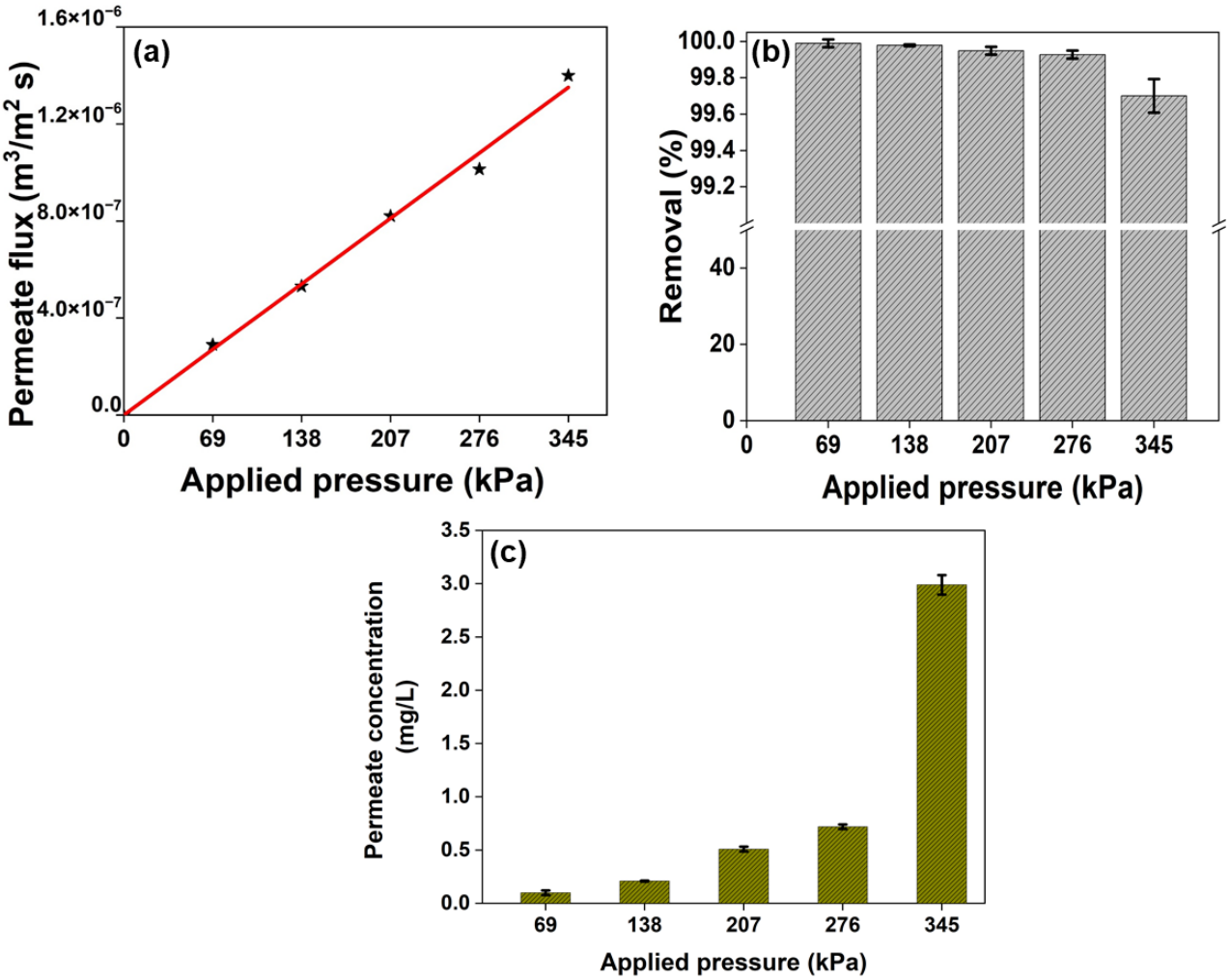

Fig. 5.1 Effect of applied pressure on (a) permeate flux, (b) removal efficiency and (c) permeate concentration (CFV = 2.41×10^{-3} m/s; Feed concentration = 1000 mg/L and Feed pH = 3.3)

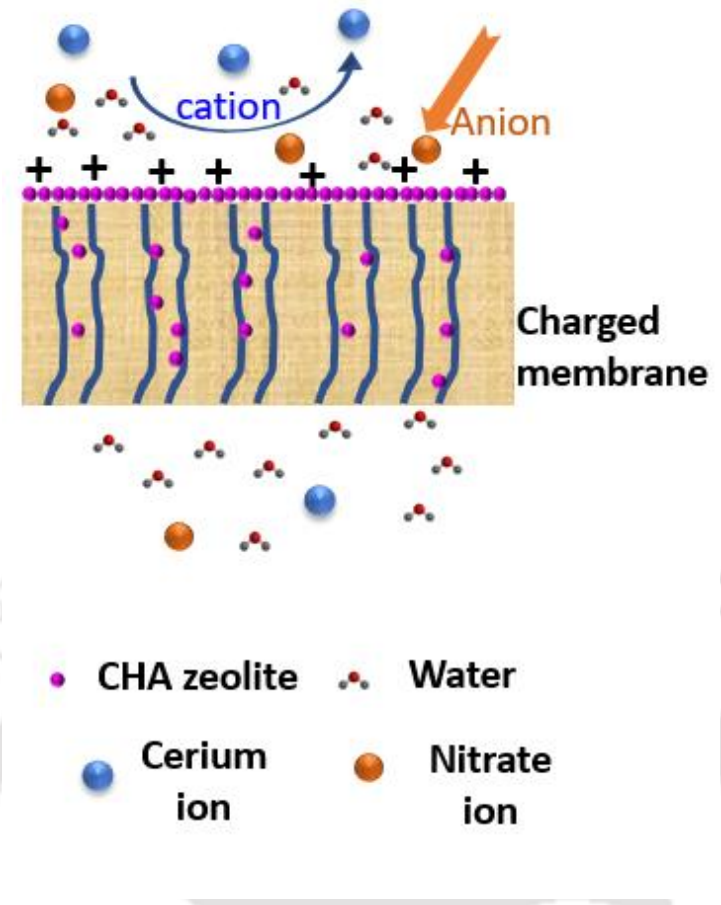

Fig. 5.2 Schematic representation of cerium ion separation

5.1.2. Influence of pH

Experiments were carried out to examine the influence of pH on permeate flux for pH values ranging between 2 and 4 at an applied pressure of 207 kPa and CFV of 2.41×10^{-3} m/s. It is well known that at a higher pH value, majority of the salts will hydrolyze. In this study, the ceric ammonium nitrate salt is observed to get precipitated above pH 4. As a result, the study was done up to a pH value of 4. Fig. 5.3 shows the influence of pH on permeate flux and removal efficiency of Ce from its solution. As already mentioned, the isoelectric point (IEP) of the CHA zeolite is 4.3 and therefore, the membrane will be positively charged at pH values below 4.3 and will be negatively charged at pH values above 4.3. It has been found in literature that the species distribution of Ce(IV) in water is $Ce(OH)_2^{2+}$, $Ce(OH)^{3+}$, and Ce(IV) (Abellan et al., 2017). According to the available scientific research, Ce(IV) ions are stable at negative pH.

The species distribution diagram indicates that $Ce(OH)^{3+}$ species dominate from the pH range of 0 to 1. The $Ce(OH)_2^{2+}$ species present in the pH range of 1 – 4 and at above pH 4, cerium ions will be precipitated as $Ce(OH)_4$ (Abellan et al., 2017).

The rigorous experiment conducted to study the influence of pH on membrane performance revealed that the impact of pH on permeate flux was marginal. However, a significant influence of pH can be seen on membrane's rejection performance. It has already been mentioned that a potential difference is created when charged membrane comes in contact with the metal ion solution. The co-ions will be more concentrated in the solution, whereas counter ions will be more concentrated at the surface of the charged membrane. Owing to this concentration difference, Donnan's potential will be generated at the interface of the membrane and the solution to maintain electrochemical equilibrium by allowing the co-ions to be repelled from the membrane (Basumatary et al., 2016). Along with co-ions, counter ions also will get separated to maintain electroneutrality. It is known that the membrane surface charge decreases when the pH increases from 2 to 4 (Fig. 4.7, Chapter 4). Hence, the decrease in repulsive forces leads to lower removal efficiency of cerium ions. As a result, cerium concentration in the permeate increased from 0.127 to 1.24 mg/L when the pH of the solution shifted from 2 to 4. Muthukrishna et al. (2008) investigated the influence of pH on permeate flux and rejection of Cr(VI) using nanofiltration membrane and found that the change in quantity of permeate flux obtained in acidic pH was marginal. Again, Basumatary et al. (2016) reported a decrease in rejection when pH of the solution increased to IEP of the membrane owing to the lesser amount of repulsive forces available to remove Fe^{3+} ions from its solution using MCM-48 zeolite ceramic membrane.

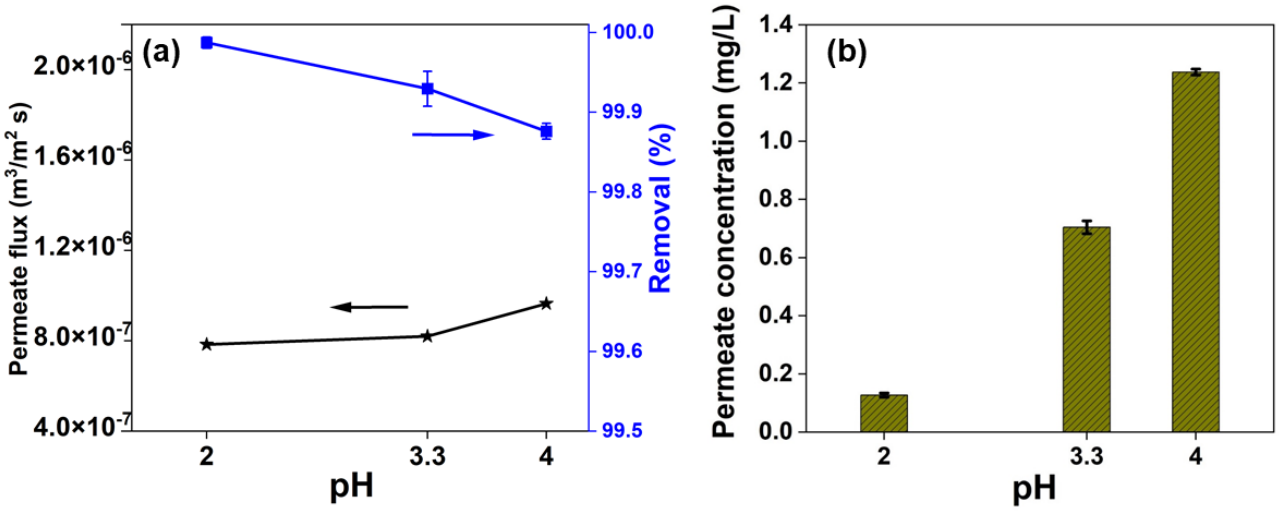

Fig. 5.3 Influence of pH on (a) permeate flux and removal efficiency, (b) permeate concentration vs. pH (Applied pressure = 207 kPa; CFV = 2.41×10^{-3} m/s and Feed concentration = 1000 mg/L)

5.1.3. Effect of feed concentration

Fig. 5.4 illustrates the influence of concentration on permeate flux and removal efficiency of cerium ion at varied feed concentrations ranging from 100 to 1000 mg/L with a constant applied pressure of 207 kPa and natural feed pH ~3.3. As the concentration of the feed increased from 100 to 1000 mg/L, the removal efficiency of the membrane got decreased. This is because with increasing feed concentration, the shielding effect of cations towards the negatively charged groups on the membrane surface gradually increases and Donnan exclusion becomes less effective, leading to lesser removal of cerium ions. It is to be mentioned that complete removal efficiency was achieved only for feed concentrations of 100 and 250 mg/L. Also, as the concentration increases, the osmotic pressure generated by the solutes present in the solution increases, leading to a decrease in the quantity of permeate flux obtained. Besides, the reduction in the quantity of permeate flux can also be related to partial plugging of pores of the membrane and concentration polarization (Basumatary et al., 2016). Peydayesh et al. (2020) studied the effect of Mg^{2+} ion concentration on membrane performance by changing the feed concentration

from 500 to 2000 mg/L and observed a downward trend in both permeate flux and Mg^{2+} rejection. It is to mention here that the profile for variation in permeate concentration at different time intervals was also studied for a feed concentration of 500 mg/L and is reported in Fig. 5.4c. It is quite evident from the figure that because of the effect of concentration polarization, the permeate concentration was gradually decreased (removal efficiency increased) over time until a steady state was obtained on the membrane surface (Kumar et al., 2017).

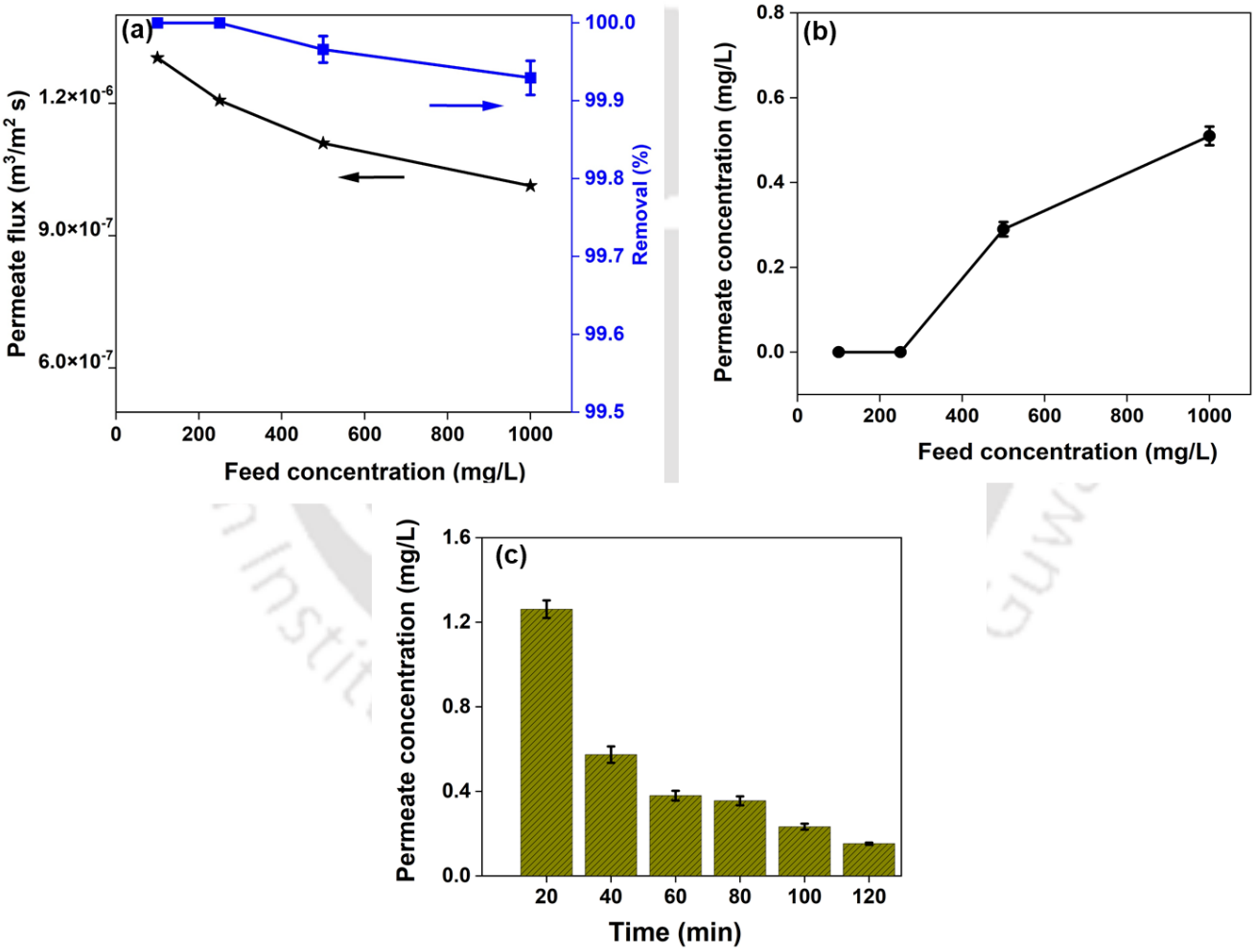

Fig. 5.4 Influence of feed concentration on (a) permeate flux and removal efficiency and (b) permeate concentration (Applied pressure = 207 kPa; CFV = 2.41×10^{-3} m/s and pH = 3.3), (c) Permeate concentration vs. time (Applied pressure = 207 kPa; CFV = 2.41×10^{-3} m/s, pH = 3.3 and Feed concentration = 500 mg/L)

5.1.4. Contrast over prior arts

The literature regarding separation of cerium ions from its solution primarily describes about conventional techniques such as adsorption and biosorption (Dashtian et al., 2017; Awual et al., 2013; Sert et al., 2008; Vijayaraghavan et al., 2010). Although the adsorption technique is quite simple, the adsorbents used for separation generate hazardous sludge, creating another disposal problem (Murthy et al., 2011). Because of their weak selectivity and waste sludge generation, researchers' attention gets driven towards alternative options such as membrane technology, which offers an outstanding quality of permeate without generating any waste sludge (Sadegh and Ali, 2021; Muthukrishnan et al., 2008). Murthy et al. (2011) separated cerium from its aqueous solution using a flat sheet polymeric nanofiltration membrane. The removal efficiency was found to be 94.37% for an initial concentration of 10 mg/L. It is worth mentioning that the feed concentration used in the aforementioned literature was too low. Besides, owing to poor mechanical and chemical stability, polymeric membranes cannot be used for long-term separation (Goswami and Pugazhenthi, 2020a; Kaur et al., 2016). However, in this work, the prepared CM_B composite membrane overcomes the disadvantages mentioned above as it not only offers higher removal efficiency of cerium (99.7-100%), but also uses membrane support prepared from inexpensive clays. Therefore, it can be concluded that this research work has tremendous potential compared to its earlier prior arts towards separating metal ions from their respective aqueous solutions.

Part B: Separation of cadmium from its aqueous solution

Salts, namely $CdSO_4$, $NiSO_4$, $Al_2(SO_4)_3$, $MgSO_4$, $CdCl_2$ required for feed preparation were obtained from Merck (I) Ltd. Water required for preparing the feed solutions for the experiments was collected from the Millipore (Elix-3) system.

For carrying out the separation experiments, the synthetic wastewater samples were prepared by adding required amount of salts to the water. The pH of the feed samples was adjusted using either HCl or NaOH. In this work, the binary system that contains $CdSO_4$, $NiSO_4$ and $CdSO_4$, $Al_2(SO_4)_3$ were named as Cd-Ni and Cd-Al, respectively. Again, the tertiary system containing $CdSO_4$, $NiSO_4$, $MgSO_4$ and $CdSO_4$, $NiSO_4$, $Al_2(SO_4)_3$ were named as Cd-Ni-Mg and Cd-Ni-Al, respectively. The concentration of metal ions in the feed and permeate samples was characterized using Microwave Plasma Atomic Emission Spectroscopy (Model: Varian, 4210 MP-AES Make: Agilent Technologies, India). The removal efficiency was calculated using the equation (5.1). After each experiment, the system was cleaned with Millipore water for 20 min, which followed by measurement of pure water flux again in order to ensure restoration of the original pure water permeability.

5.2. Results and discussion

5.2.1. Influence of applied pressure

The influence of applied pressure on permeate flux and rejection of Cd^{2+} was studied by varying the applied pressure between 69-345 kPa at a constant crossflow rate of 2.41×10^{-3} m/s, natural pH of 6, and feed concentration of 1000 mg/L (See Fig. 5.5). The permeate flux of zeolite composite membranes was enhanced with an increase in the applied pressure owing to an increase in the driving force. The permeate flux varies linearly with increasing applied pressure for the composite membrane, thus signifying Darcy's law behavior (Fig. 5.5b). This might be because of the absence of an additional transport resistance resulting from adsorption and concentration polarization (Basumatary et al., 2015). However, it is observed that the

permeate flux through the zeolite composite membrane is slightly lower than the pure water flux obtained using the same membrane. This might be because of the osmotic pressure generated by the retained ions in the solution that lowers the effective pressure across the membrane, leading to lesser permeate flux (Kumar and Pugazhenthi, 2017).

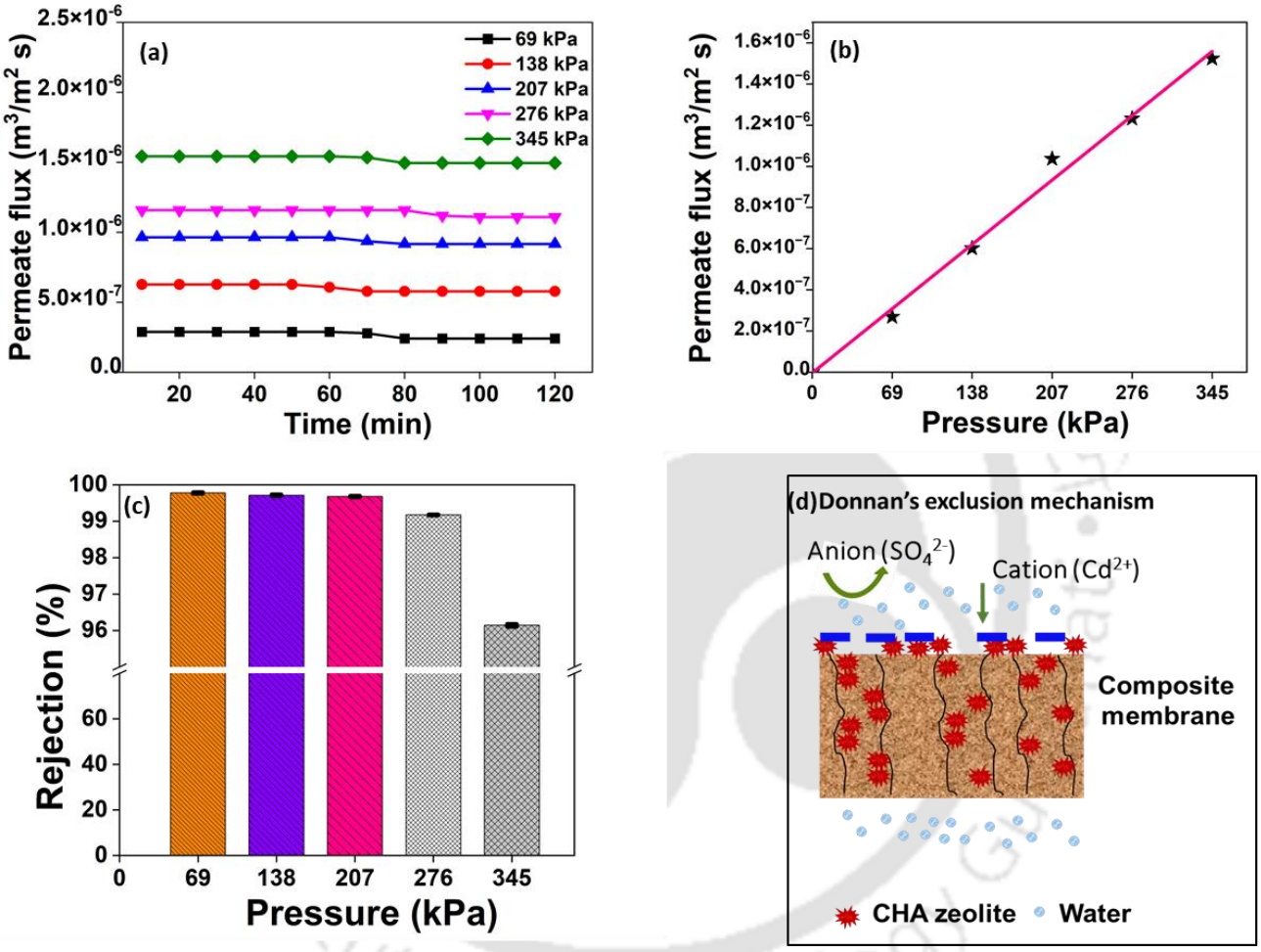

Fig. 5.5 Effect of applied pressure on separation of Cd^{2+} ions from aqueous solution [(a) permeate flux as a function of time, (b) permeate flux as a function of applied pressure, (c) Membrane rejection at different applied pressures (CFV = 2.41×10^{-3} m/s; pH = 6; C_{CdSO4} = 1000 mg/L) and (d) schematic representation of rejection mechanism of Cd^{2+} ions at pH 6]

While discussing about membrane rejection, from Fig. 5.5c, it is clearly evident that the membrane showed more than 99.1% rejection at all applied pressures (except 345 kPa) for an

initial concentration of 1000 mg/L. This is because at solution pH value of 6, the membrane is negatively charged (IEP: 4.3). Therefore, owing to the higher electrostatic interaction, the SO_4^{2-} ions will be repelled by the membrane surface and according to Donnan Exclusion principle, the Cd^{2+} ions will also be retained by the membrane in order to maintain electroneutrality in the solution. The schematic representation of the rejection mechanism is presented in Fig. 5.5d (Liu et al., 2019). However, with increasing value of applied pressure, a slight decrease in rejection was observed, which might be due to the increased convective flux at higher applied pressures that led to the high concentration of ions on permeate side (Shukla et al., 2005).

5.2.2. Effect of pH

According to their pKa values, the majority of heavy metals produce hydroxides as the solution pH rises over 9 (Awual, 2019). Keeping this point in mind, pH values of 3 to 8 were employed in this work so that the influence of Cd^{2+} ion precipitation can be nullified. The species distribution of $CdSO_4$ at various solution pH values is as follows: (Huang, 2016)

Cd^{2+}	2<pH<8
$CdOH^{+}$	8< pH<12
$Cd(OH)_2$	10<pH<14
HSO_4^{-}	pH<2
SO_4^{2-}	2<pH<10
HS^{-}	10< pH<13
S^{2-}	pH>13

The influence of pH on permeate flux and rejection of Cd^{2+} was investigated at a constant applied pressure of 276 kPa, crossflow rate of 2.41×10^{-3} m/s and feed concentration of 1000 mg/L. As evident from Fig. 5.6a, the permeate flux was increased when the feed pH was reaching towards IEP value. This might be because of the decreased electro-viscous forces that reduced additional resistance for permeate flow across the membrane, thereby increasing the quantity of permeate obtained. A similar observation was noticed by Basumatary et al. (2016)

during separation of Fe^{3+} from its aqueous solution. They noticed that increasing the pH from 2 to 3.2 (towards IEP) enhanced the quantity of permeate collected.

As previously mentioned, the rejection performance of the membrane is solely dominated by the electrostatic principle. As the membrane used in this study has an IEP of 4.3, the membrane is positively charged below the IEP (pH < 4.3) and negatively charged above the IEP (pH > 4.3). When this charged membrane comes in contact with cadmium sulphate solution, the concentration of ions opposite to that of the membrane surface will be more near the membrane surface. On the contrary, the concentration of same charged ions will be more in the solution. Owing to this concentration difference, a Donnan potential will be generated at the membrane – solution interface for maintaining the electrochemical neutrality of the system. Development of this potential will make the membrane reject the ions approaching the membrane with an opposite charge so that electrochemical neutrality of the solution is sustained. Therefore, as the pH of the solution increases from 4.3 to 8, an increased intensity of electrostatic repulsion is observed between the negatively charged SO_4^{2-} ions in the solution and the membrane surface and to maintain the electrochemical neutrality, Cd^{2+} ions are also equally get rejected by the membrane surface (Liu et al., 2019). Similarly, when the pH of the solution was reduced to 3 from 4.3, the positive charge on the membrane surface increased, leading to an increased intensity of the electrostatic repulsion between the membrane surface and positively charged Cd^{2+} ions in the solution. Hence, rejection is seen to increase in both the cases, i.e., either changing the feed pH from 4.3 to 8 or from 4.3 to 3 (moving away from IEP). At IEP of the membrane, the observed rejection was zero, which strongly emphasizes that the rejection was completely dependent upon electrostatic interactions between the charged membrane surface and metal ions present in the solution (Basumatary et al., 2015).

5.2.3. Effect of anions

The impact of anions on permeate flux and rejection of Cd^{2+} was investigated at an applied pressure of 276 kPa, cross flow rate of 2.41×10^{-3} m/s, and pH 6. For this, two types of feed solutions, namely 1000 mg/L $CdSO_4$ and a cocktail feed with 500-500 mg/L $CdSO_4$-$CdCl_2$ were prepared for carrying out this experiment. As seen in Fig. 5.6b, the permeate flux was less for the system containing only $CdSO_4$ than the cocktail solution. This is probably due to the presence of more number of divalent ions (SO_4^{2-}) in the solution containing only $CdSO_4$ than the cocktail solution. The increased number of higher valency anions led to higher electrostatic interaction between the anions present in the solution and the negatively charged membrane surface, causing additional resistance for the permeate to flow across the membrane (Murthy et al., 2009; Isawi et al., 2016; Majhi et al., 2009). In a similar way, the rejection performance of the composite membrane also got enhanced with an increase in the valency of the anion, owing to the greater electrostatic repulsion between the membrane surface charge and anion ($SO_4^{2-} > Cl^-$). Additionally, it has also been reported that the hydrated radius of chloride ions is lesser than that of the sulphate ions (3.32 and 3.8 Å), which ultimately resulted in lesser rejection of cations associated with the chloride ions. Similar observation was found by Peydayesh et al. (2020). In their study, a positively charged nanofiltration membrane employed for removal of heavy metal ions from drinking water showed lesser rejection of salts associated with monovalent ions (Cl^-) as compared to the divalent ions (SO_4^{2-}).

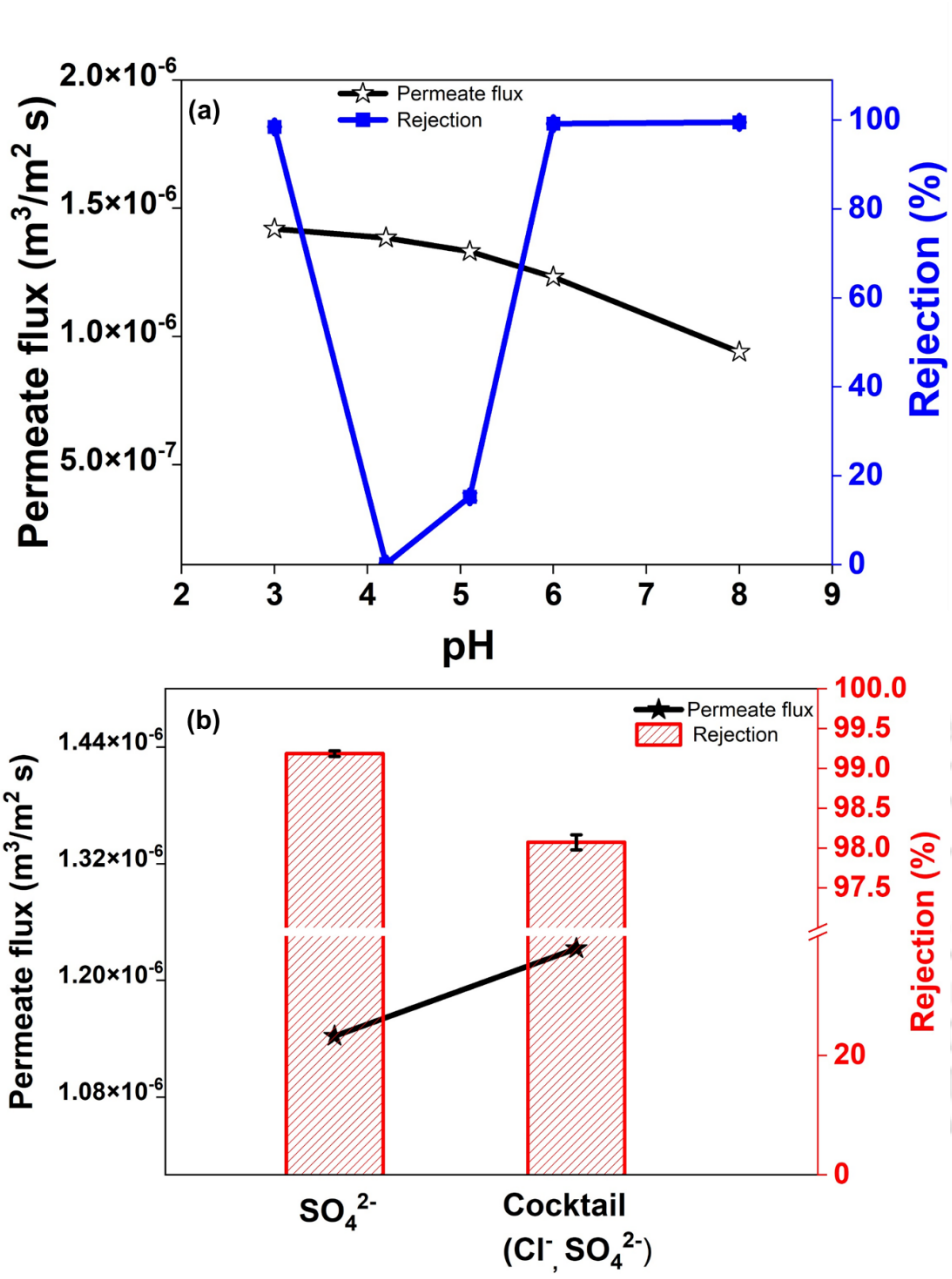

Fig. 5.6 (a) Effect of pH on permeate flux and rejection (Applied pressure: 276 kPa; CFV = 2.41×10^{-3} m/s; C_{CdSO4}: 1000 mg/L) and (b) effect of different anions on permeate flux and rejection (Applied pressure = 276 kPa; CFV = 2.41×10^{-3} m/s; pH = 6; C_f = 1000 mg/L)

5.2.4. Single component system

The concentration of heavy metals such as Ni and Cd in electroplating wastewater usually varies from 5.82-1550 mg/L and is even higher in some cases (Rajoria et al., 2022). Therefore, to check the performance of the membrane in treating water with such concentrated content of

heavy metal, a high concentration (1000 mg/L) was chosen in this study. It is known that, natural water/ wastewater contains ions with different valencies, such as divalent and trivalent ions (Maher et al., 2014). Hence the mixed salt solution was used in this study. The performance of the membrane was tested for single, binary, and tertiary salt aqueous solutions. The optimum conditions such as applied pressure of 276 kPa and cross flow rate of 2.41×10^{-3} m/s were maintained for all three systems. Also, the feed pH of 3 was adjusted by using 0.1 N HCl solution.

Fig. 5.7 illustrates the performance of the composite membrane in the removal of a single metal ion from its aqueous solution at constant operating parameters such as applied pressure of 276 kPa, cross flow rate of 2.41×10^{-3} m/s, pH 3 and feed concentration of C_{CdSO_4} = C_{NiSO_4} = $C_{Al_2(SO_4)_3}$ = C_{MgSO_4} = 1000 mg/L. The species distribution of each metal at different pH of their aqueous solution is as follows (Dubey et al., 2019; Wei et al., 2009).

Al^{3+}, $AlOH^{2+}$, $Al(OH)_2^{+}$	3<pH<6
$Al(OH)_3$(aq)	pH>6
Mg^{2+}	2 <pH<9
$Mg(OH)_2$	pH>9
Ni^{2+}	0<pH<8
$NiOH^{+}$	5.5<pH<10
$Ni(OH)_2$	8<pH<14

The permeate flux of trivalent ions ($J_{Al^{3+}}$) is lower than the divalent ions ($J_{Cd^{2+}}$, $J_{Mg^{2+}}$, and $J_{Ni^{2+}}$) owing to their electrostatic interaction between the positively charged membrane surface and the cations. The higher repulsive forces gave additional resistance to the flow of permeate in the case of the system containing Al^{3+} ions. Among divalent ions, the permeate flux follows as $J_{Ni^{2+}} > J_{Cd^{2+}} > J_{Mg^{2+}}$, according to the hydrated radius (Peydayesh et al., 2020). The rejection performance of the membrane was strongly influenced by the valency and diffusion coefficient of the metal ion (Table 5.1). A higher valency and a lower diffusion coefficient are

always preferable for increased retention of salts by the membrane. Amongst all the four salts used in this study, the diffusion coefficient of Cd^{2+} is the highest and is followed by Ni^{2+}, $Mg^{2+,}$ and Al^{3+}, respectively (Table 5.1), leading to the following salt rejection trend of the membrane : $R_{Al^{3+}}$ (99.9%) >$R_{Mg^{2+}}$ (99.7%) > $R_{Ni^{2+}}$ (99.5%) > $R_{Cd^{2+}}$ (98.5%) (Arshadi et al., 2014; Majhi et al., 2009). A similar result was obtained by Majhi et al. (2009) when they employed a low-cost γ-Al_2O_3 clay composite membrane for the separation of electrolytes from their solutions ($MgCl_2$, $AlCl_3$). In that study, it was observed that permeate flux for $MgCl_2$ was higher than $AlCl_3$ owing to their electrostatic interaction between the positively charged membrane surface and the cations. On the contrary, rejection was found to be higher for $AlCl_3$ solution than $MgCl_2$, which was solely based on the Donnan exclusion principle.

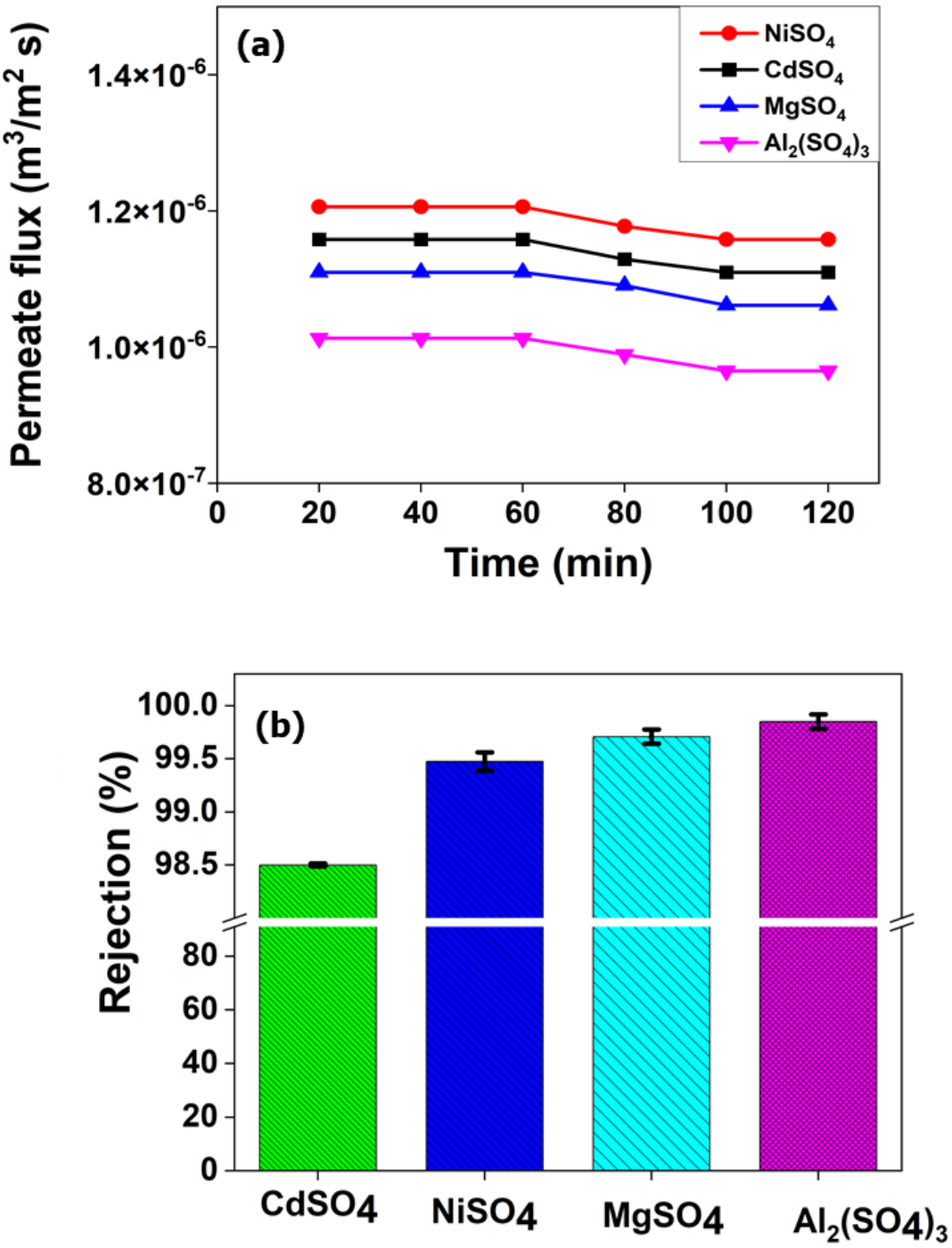

Fig. 5.7 Performance of membrane in single salt system: (a) permeate flux vs. time and (b) rejection (Applied pressure = 276 kPa; CFV = 2.41×10^{-3} m/s; pH = 3; C_{CdSO_4} = C_{NiSO_4} = $C_{Al_2(SO_4)_3}$ = C_{MgSO_4} = 1000 mg/L)

Table 5.1 Properties of selected metal ions (Murthy and Chaudhari, 2009)

Target	Ionic radius (Å)	Hydrated radius (Å)	Diffusion coefficient in water (10^{-9} m^2/s)
Cd^{2+}	1.03	4.26	1.44
Ni^{2+}	0.71	4.04	1.32
Mg^{2+}	0.86	4.28	0.7
Al^{3+}	0.65	4.3	0.46
$*SO_4^{2-}$	2.9	3.8	1.06
$*Cl^-$	1.81	3.32	2.03

*associated co-anions

5.2.5. Binary system

The potential of CHA zeolite composite membrane in removing Cd^{2+} heavy metals from aqueous solution of binary salt mixture (Cd^{2+} with divalent metal ion (Ni^{2+}) and Cd^{2+} with trivalent metal ion (Al^{3+})) was also tested and the obtained results are presented in Fig. 5.8. The operating parameters in both the systems (Cd-Ni and Cd-Al) were kept constant at an applied pressure of 276 kPa, the cross flow rate of 2.41×10^{-3} m/s, feed pH 3 and feed concentration of $C_{CdSO_4} = C_{NiSO_4} = C_{Al_2(SO_4)_3} =$ 1000 mg/L, respectively. The feed pH was adjusted to 3 using 0.1 N HCl solution. It has been observed from the experiments that the permeate flux for Cd-Ni system is higher than the Cd-Al system. This is because of the larger electrostatic interaction between the membrane surface and the electrolyte in case of Cd-Al system that generated additional resistance for flow of permeate across the membrane (Majhi et al., 2009).

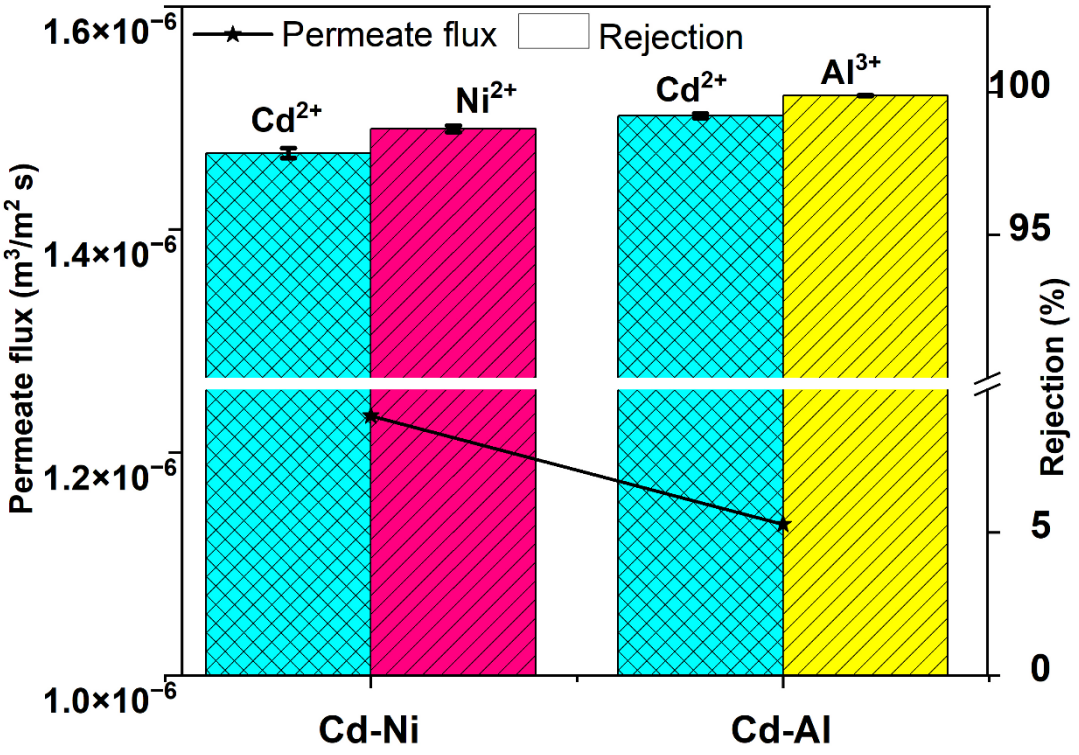

Fig. 5.8 Performance of membrane in binary system (Applied pressure = 276 kPa; CFV = 2.41×10^{-3} m/s; pH = 3; C_{CdSO_4} = C_{NiSO_4} = $C_{Al_2(SO_4)_3}$= 1000 mg/L)

A study of the rejection performance of the membrane reveals that for a positively charged membrane surface, a higher cationic charge will lead to stronger rejection of salts. At a pH value of 3, the membrane remains positively charged, and the exclusion of Al^{3+} will be more compared to Ni^{2+} due to increased electrostatic repulsion. This is the reason for getting increased rejection of Al^{3+} than Ni^{2+} from their respective binary aqueous salt solutions. Moreover, as previously mentioned in Table 5.1 and section 5.2.2.5, the higher diffusion coefficient of Cd^{2+} is another reason, which makes Cd^{2+} ion to pass through permeate side, hence a decrease in retention of Cd^{2+} ions over Ni^{2+} and Al^{3+} was observed (Arshadi et al., 2014; Majhi et al., 2009). A similar observation was noticed by Murthy and Chaudhari, (2009) while assessing the performance of a commercial nanofiltration membrane on the separation

of metal ions (Ni^{2+} and Cd^{2+}) from binary solutions. There too, higher rejection of Ni^{2+} was observed as compared to Cd^{2+} owing to the higher diffusion coefficient of the later.

5.2.6. Tertiary system

Fig. 5.9 illustrates the performance of zeolite composite membrane in terms of rejection and permeate flux obtained during the removal of metal ions from their tertiary aqueous solutions (Cd^{2+} with two divalent metal ion (Ni^{2+}, Mg^{2+}) and Cd^{2+} with one divalent and one trivalent metal ion (Ni^{2+}, Al^{3+})). In both the cases (Cd-Ni-Al and Cd-Ni-Mg), the operating conditions were maintained constant at an applied pressure 276 kPa, cross flow rate of 2.41×10^{-3} m/s, pH 3 and feed concentration of C_{CdSO_4} = C_{NiSO_4} = $C_{Al_2(SO_4)_3}$= C_{MgSO_4} = 1000 mg/L, respectively. The feed pH was adjusted to 3 using 0.1 N HCl solution. The permeate flux profile obtained after rigorous experiments revealed that the flux of Cd-Ni-Mg system is comparatively higher than the Cd-Ni-Al system owing to the less repulsive forces causing the permeate to flow through the membrane easily (Majhi et al., 2009).

The rejection performance of the membrane, in this case too, follows a similar trend as that of the earlier systems. With the membrane being positively charged at the feed pH 3 (IEP 4.3), Al^{3+} ions will be excluded more than the Mg^{2+}, resulting in increased Al^{3+} rejection from its aqueous solution. Additionally, as evident from Table 5.1, the lower diffusion coefficient of Al^{3+} than Mg^{2+} is another reason for increased rejection of the former from its aqueous solution (Majhi et al., 2009).

Within the Cd-Ni-Mg system, the rejection followed the trend $R_{Mg^{2+}} > R_{Ni^{2+}} > R_{Cd^{2+}}$. From this observation, it can be inferred that for all the metal ions being divalent, the rejection is solely dependent on the diffusion coefficient. As mentioned earlier, Cd^{2+} has the highest diffusion coefficient among all other existing ions; hence, in the Cd-Ni-Mg system, the least rejection was recorded for Cd^{2+}. A similar justification can also be applied for the increased

rejection of Mg^{2+} over Ni^{2+}. Similarly, for the Cd-Ni-Al system, the rejection achieved for Al^{3+} was the highest, followed by Ni^{2+} and then Cd^{2+} owing to the highest repulsive forces. Efome et al. (2019) used MOF- 808 embedded polyacrylonitrile membrane for the separation of cadmium from its aqueous solution and reported that the heavy metal (Cd^{2+}) rejection was dropped to 37% in presence of coexisting cations (Na^{+}, Ca^{2+}, Mg^{2+}). However, in this study, the presence of multi-metal ions increased the cadmium separation efficiency, which might be because of an increase in electrostatic repulsions in the Cd-Ni-Al system (Majhi et al., 2009).

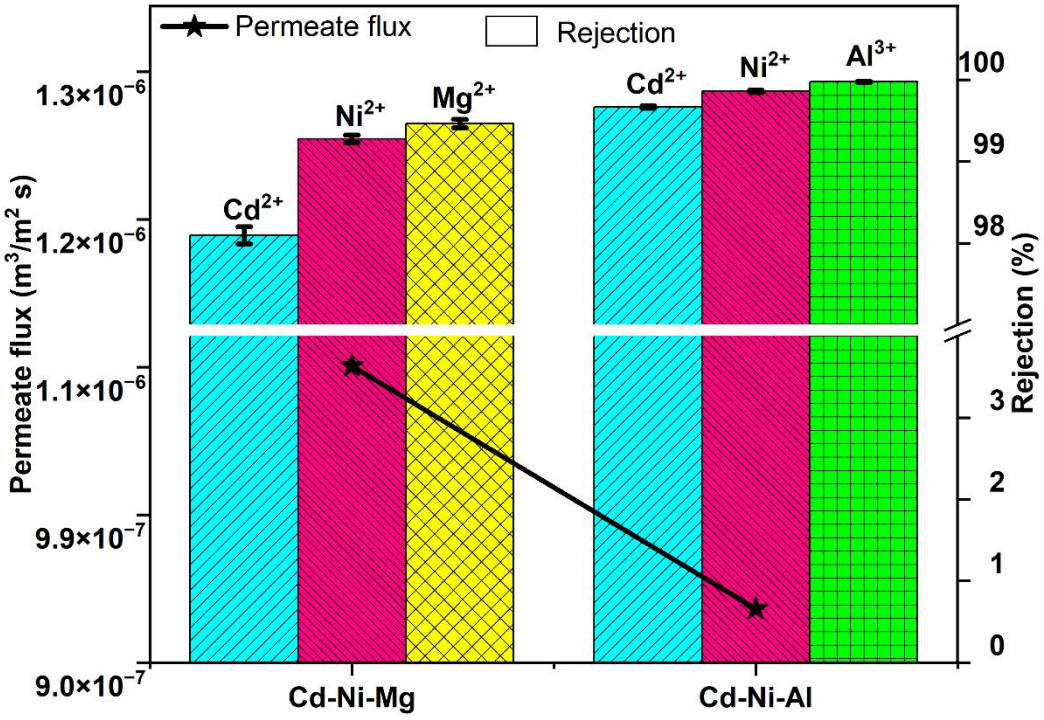

Fig. 5.9 Performance of membrane in tertiary system (Applied pressure = 276 kPa; CFV = 2.41×10^{-3} m/s; pH = 3; C_{CdSO_4} = C_{NiSO_4} = $C_{Al_2(SO_4)_3}$= C_{MgSO_4} = 1000 mg/L)

The permeate concentrations of all three salt systems (single, binary and tertiary) are reported in Fig. 5.10-5.13. The permeate collected from Cd-Ni-Al system contains Ni^{2+} concentration

of 1.4 mg/L, which is well below the discharge standard limit for wastewater into surface water (5 mg/L) (Central Pollution Control Board, Government of India). Also, aluminium concentration (0.17 mg/L) in the same permeate is found to be within WHO guidelines (0.2 mg/L in drinking water). However, the permeate cadmium concentration (3.3 mg/L) still needs another treatment method for safe disposal (Fig. 5.12).

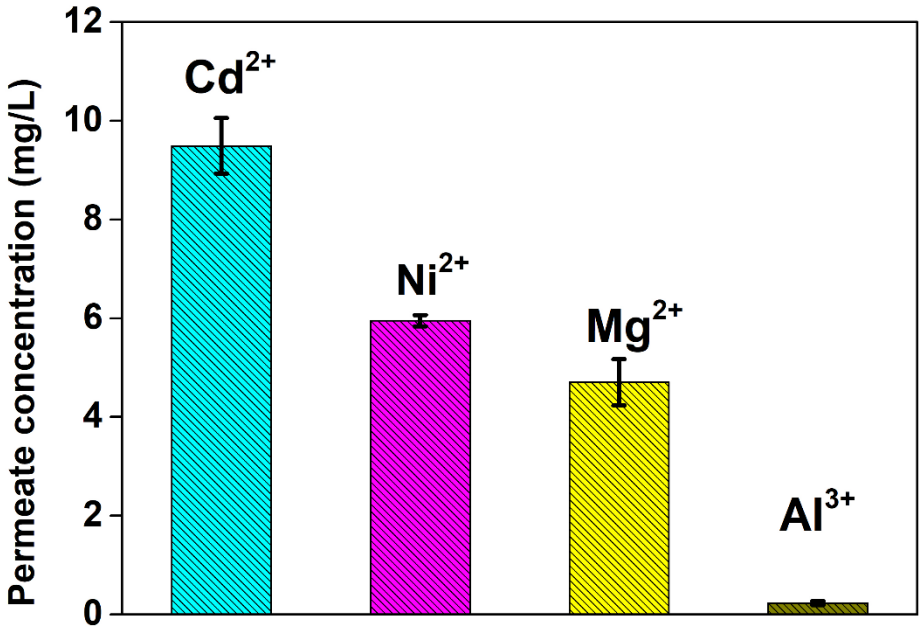

Fig. 5.10 Permeate concentration of metal ions in single salt system

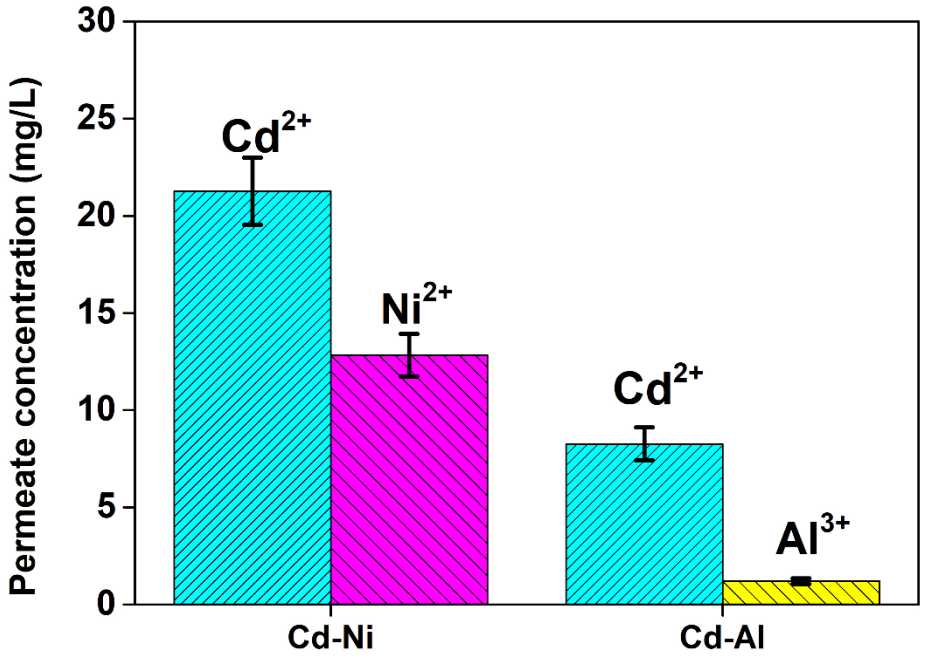

Fig. 5.11 Permeate concentration of metal ions in binary system

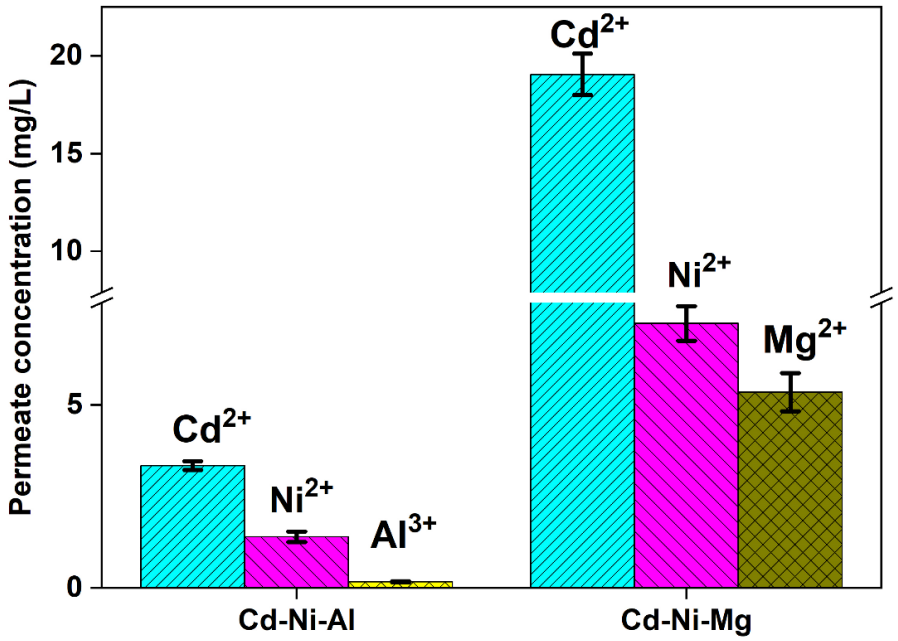

Fig. 5.12 Permeate concentration of metal ions in ternary system

5.2.7. Contrasts over prior arts

The comparison of heavy metal ion removal efficiency of different membranes with the membrane fabricated as a part of this research work is demonstrated in Table 5.2. It is a well-known fact that RO and NF membrane technologies are highly effective in removing heavy metals from water. However, a lower filtering ratio and requirement of high pressure by these processes lead to increased cost as well as high energy consumption, thereby limiting the application of the aforementioned processes in everyday life (Zhou et al., 2019). Also, most of the NF membranes were polymer-based membranes, which are not suitable for long-term applications (Goswami and Pugazhenthi, 2021). It is quite evident from Table 5.2 that the commercial or lab-made NF membranes have very low permeability. Moreover, these membranes offer higher rejection of heavy metals at the cost of very high applied pressure. NF operation, therefore, demands a substrate with robust mechanical properties for sustaining such high applied pressure (Thong et al., 2014). On the contrary, ultrafiltration membranes offer high flux but only give medium rejection of heavy metal ions from their solutions (Hebbar et al., 2016; Majhi et al., 2009). Observing the above mentioned facts, it can be said that the prepared ulfiltration composite membrane showed better metal ion removal efficiency than its counterparts and provided a reasonably good permeate flux at low applied pressure (Table 5.2).

Table 5.2 Literature comparison for different metal ion separation using various membranes

Technology	Membrane	Pore size	Pure water permeability (m^3/m^2 s kPa)×10^{-9}	Heavy metal	Conditions	Rejection (%)	References
Nanofiltration	Chitosan/PES composite membrane	0.347 nm	9.58	Ni	**C_f** : 1000 mg/L **P**: 1000 kPa	96.3	Zhang et al. (2015a)
Nanofiltration	PEI/TMC/P84	-	4.83	Cd	**C_f** : 1000 mg/L **P**: 500 kPa	94	Gao et al. (2016)
Nanofiltration	Polyamide commercial membrane	300 Da	-	Cd Ni	**C_f** : 5 mg/L **P**: 2030 kPa	82.69 98.94	Murthy et al. (2009)
Nanofiltration	MOFs/PEI/TMA composite membrane	1.5-2.2 nm	33.88	Ni	**C_f** : 1000 mg/L **P**: 400 kPa	90.9	Gong et al. (2020)
Nanofiltration	HPEI modified GO cross linking EDA	-	13.91	Ni Cd	**C_f** : 1000 mg/L **P**: 100 kPa	96 90.5	Zhang et al. (2015b)
Ultrafiltration	P(VC-*co*-DMA)	3.27 nm	233.33	Cd Ni	**C_f** : 10 mg/L	95.5 94.5	Zhou et al. (2019)
Ultrafiltration	γ - Al_2O_3 composite membrane	5.4-13.6 nm	236.11	Al Mg	**C_f** : 3000 mg/L	88 72	Majhi et al. (2009)
Ultrafiltration	GO/Al_2O_3 composite membrane	430 nm	17.50	Cd	**C_f** : 100 mg/L	100	Liu et al. (2019)
Ultrafiltration	CHA/kaolin composite membrane	36 nm	4.83	Cd Ni Mg Al	**C_f** : 1000 mg/L **P**: 276 kPa	99 99.5 99.7 99.9	This work

PES: Polyethylene sulfone; PEI: Polyethyleneimine; TMC: Trimesoyl chloride; MOFs: Metal-organic-frameworks; TMA: Trimesic acid; HPEI: Hyperbranched polyethylenimine; GO: Graphene oxide; EDA: Ethylenediamine; PEUF: Polymer-enhanced ultrafiltration; P(VC-*co*-DMA): poly (vinyl chloride *co* dimethylaminoethyl methacrylate; CHA: Chabazite; P: Pressure; C_f : Feed concentration

5.3. Summary

The potential of both sides coated composite membrane (CM_B) was tested towards the separation of rare earth element cerium and cadmium from aqueous solution. Owing to the Donnan exclusion mechanism, the membrane showed remarkable performance interms of high removal of cerium. It was understood that the composite membrane doesn't have the tendency of cake layer formation during filtration. The highest 100% removal of cerium was obtained for the feed concentration of 100 and 250 mg/L at an applied pressure, CFV, natural pH of 207 kPa, 2.41×10^{-3} m/s, and 3.3, respectively. In case of cadmium removal, the effect of applied pressure, pH and anions on permeate flux and rejection was investigated. The results revealed that the rejection is strongly dependent on feed pH and the highest Cd^{2+} rejection of 99.8% was observed at natural feed pH 6 with an applied pressure of 69 kPa, cross flow rate of 2.41×10^{-3} m/s and feed concentration of 1000 mg/L. The study on the effect of anions on membrane performance revealed that the rejection performance was low for monovalent anion (Cl^-) than divalent anion (SO_4^{2-}). The study to evaluate the separation performance of the composite membrane was further extended by incorporating the membrane in removal of metal ions (cadmium, nickel, aluminium and magnesium) from single, binary and tertiary aqueous solution mixtures, where the rejection sequence was observed as $R(Al^{3+}) > R(Mg^{2+}) > R(Ni^{2+}) > R(Cd^{2+})$. Membrane performed comparatively better in terms of rejection for feed samples containing a mixture of different ions. This is quite beneficial as it mimics the actual scenario of water contamination.

Chapter 6

Conclusions and Recommendation for future work

Conclusions and Recommendations for future work

This chapter summarizes the interference drawn from the research work presented in the thesis. Also, some suggestions towards the scope for future research are outlined. The main aim of this research work is to fabricate low-cost tubular ceramic and zeolite ceramic composite membrane by simple and cost effective fabrication techniques and their application in liquid phase separation. The potential performance of the prepared membrane was tested by carrying out experiments in recovery of microalgae from its culture broth, TiO_2 separation, onshore oilfield produced water treatment, heavy metal separation. In this thesis, highly interesting results and discussion were presented, which are summarized in the following section.

6.1. Major conclusions

- An indigenous low-cost kaolin-based tubular ceramic microfiltration membrane was successfully developed using naturally available clays, including kaolin (50 wt%), quartz (25 wt%), and calcium carbonate (25 wt%) along with different organic binders (CMC, GG and HPMC).
- Considering the fabrication ease and membrane properties, Kaolin-HPMC membrane was found to be the best as it offers high water permeability of 1.4945×10^{-7} m^3/m^2s kPa, porosity of 40%, pore size of 0.178 µm and good corrosion resistance. Also, the estimated cost of Kaolin-HPMC membrane was found to be 253 USD/m^2
- Potential performance of all fabricated membranes was tested for the separation of microalgae from its culture broth, and Kaolin-HPMC membrane was found to be the best as it provides the greatest combination of recovery (100%) and permeate flux (1.78×10^{-5} m^3/m^2 s) at an applied pressure of 276 kPa.
- Kaolin-HPMC membrane was further tested for TiO_2 separation and produced water treatment. The maximum permeate flux of 4.24×10^{-5} m^3/m^2s with 100% separation

efficiency was observed at 414 kPa for the separation TiO_2 nanoparticles from its suspension.

- In case of produced water treatment, microfiltration studies using kaolin-HPMC membrane displayed maximum removal efficiency values of TSS (100 %), turbidity (100 %), TOC (84 %) and COD (78 %) at a low applied pressure of 69 kPa.
- However, the COD removal efficiency at higher applied pressures was not satisfactory as the COD concentration of the permeate exceeded the dischargeable limits into surface water. In order to meet the discharge limits of the treated water parameters, combined microfiltration and biological method were employed. The microfiltration followed by biological treatment (MF-B) was the most effective, showing 99% removal efficiency for TOC and COD, thus satisfying the reuse and discharge norms as prescribed by Central Pollution Control Board, India.
- Cleaning efficiency of the fouled membrane which was used for the microfiltration of produced water was tested using different chemical reagents, and a mixture containing 0.1 wt% sodium dodecyl sulfate and 1 wt% sodium hypochlorite resulted in a maximum flux recovery of 92.6%.
- Toxicity assessment of the treated water obtained from MF-B system revealed the treated water is toxin-free and can be reused for irrigation purpose.
- CHA type zeolite ceramic composite membranes were successfully synthesized without using organic structural directing agent by hydrothermal synthesis route. The organic template-free synthesis of CHA zeolite reduced the synthesis time and made the process more environmental friendly as it involves no calcination step for removing the template.
- Among all three strategies of coating, the membrane coated on both sides (CM_B) was loaded with a large quantity of zeolite particles, i.e., 1.82±0.18 g along with porosity of

30.50±0.50%, water permeability of 4.83×10^{-9} m^3/m^2 s kPa and average pore diameter of 36 nm followed by CM_O and CM_I, respectively.

- The CM_B composite membrane was used for the separation of heavy metals and the highest removal of cerium (100 %) was obtained for 100 and 250 mg/L feed concentrations at an applied pressure, CFV, natural pH of 207 kPa, 2.41×10^{-3} m/s, and 3.3, respectively.
- Also, the CM_B membrane performed comparatively better in terms of rejection for feed samples containing a mixture of different ions (Cd^{2+}, Ni^{2+}, Mg^{2+} and Al^{3+}). This is quite beneficial as it mimics the actual scenario of water contamination.

In summary, using inexpensive clays as raw material for tubular ceramic membranes and excellent membrane properties helps in recovering valuable materials and treating wastewater. In addition, the zeolite-ceramic composite membrane synthesized without an organic structural directing agent is better for heavy metal removal owing to high removal efficiency and cost effectiveness as there is no requirement of calcination step for its synthesis.

6.2. Recommendation for future work

- As the support membrane displayed outstanding performance in different liquid phase separations, the potential of the membrane can be extended to treat different industrial sources, namely tanneries, paper and textile industries.
- Economic evaluation of all the separation processes can be appraised to endorse the application for commercial usage in industries.
- Pilot plant study can be considered before recommending it for commercialization.

References

Abd Aziz, M.H., Othman, M.H.D., Hashim, N.A., Adam, M.R. and Mustafa, A., 2019. Fabrication and characterization of mullite ceramic hollow fiber membrane from natural occurring ball clay. Appl. Clay Sci., 177, 51-62. DOI: 10.1016/j.clay.2019.05.003

Abdalla, M., Nasser, M., Fard, A.K., Qiblawey, H., Benamor, A. and Judd, S., 2019. Impact of combined oil-in-water emulsions and particulate suspensions on ceramic membrane fouling and permeability recovery. Sep. Purif. Technol., 212, 215-222. DOI: 10.1016/j.seppur.2018.11.017

Abdel-Shafy, H.I., Mansour, M.S. and El-Toony, M.M., 2020. Integrated treatment for oil free petroleum produced water using novel resin composite followed by microfiltration. Sep. Purif. Technol., 234, 116058. DOI: 10.1016/j.seppur.2019.116058

Abdullayev, A., Bekheet, M.F., Hanaor, D.A.H., Gurlo, A., 2019. Materials and applications for low-cost ceramic membranes. Membr., 9, 105. DOI: 10.3390/membranes9090105.

Abellan, P., Moser, T.H., Lucas, I.T., Grate, J.W., Evans, J.E. and Browning, N.D., 2017. The formation of cerium(III) hydroxide nanoparticles by a radiation mediated increase in local pH. RSC Adv., 7, 3831-3837. DOI: 10.1039/C6RA27066B

Achiou, B., Elomari, H., Bouazizi, A., Karim, A., Ouammou, M., Albizane, A., Bennazha, J., Younssi, S.A. and El Amrani, I.E., 2017. Manufacturing of tubular ceramic microfiltration membrane based on natural pozzolan for pretreatment of seawater desalination. Desalin., 419, 181-187. DOI: 10.1016/j.desal.2017.06.014

Achiou, B., Beqqour, D., Elomari, H., Bouazizi, A., Ouammou, M., Bouhria, M., Aaddane, A., Khiat, K. and Younssi, S.A., 2018. Preparation of inexpensive NaA zeolite membrane on pozzolan support at low temperature for dehydration of alcohol solutions. J. Environ. Chem. Eng., 6, 4429-4437. DOI: 10.1016/j.jece.2018.06.049

Adeleye, A.S. and Keller, A.A., 2016. Interactions between algal extracellular polymeric substances and commercial TiO_2 nanoparticles in aqueous media. Environ. Sci. Technol. 50, 12258-12265. DOI: 10.1021/acs.est.6b03684.

Adler, P., Fadel, A. and Rabasso, N., 2015. Cerium (IV) ammonium nitrate mediated 5-endo-dig cyclization of α-amino allenylphosphonates to spirodienones. Chem. Commun., 51, 3612-3615. DOI: 10.1039/C5CC00281H

Akamatsu, K., Kagami, Y. and Nakao, S.I., 2020. Effect of BSA and sodium alginate adsorption on decline of filtrate flux through polyethylene microfiltration membranes. J. Membr. Sci., 594, 117469. DOI: 10.1016/j.memsci.2019.117469

Alammar, A., Park, S.H., Williams, C.J., Derby, B. and Szekely, G., 2020. Oil-in-water separation with graphene-based nanocomposite membranes for produced water treatment. J. Membr. Sci., 603, 118007. DOI: 10.1016/j.memsci.2020.118007

Ali, A., Quist-Jensen, C.A., Drioli, E. and Macedonio, F., 2018. Evaluation of integrated microfiltration and membrane distillation/crystallization processes for produced water treatment. Desalin., 434, 161-168. DOI: 10.1016/j.desal.2017.11.035

Al-Amoudi, A. and Lovitt, R.W., 2007. Fouling strategies and the cleaning system of NF membranes and factors affecting cleaning efficiency. J. Membr. Sci., 303, 4-28. DOI: 10.1016/j.memsci.2007.06.002

Al-Anzi, B.S. and Siang, O.C., 2017. Recent developments of carbon based nanomaterials and membranes for oily wastewater treatment. RSC Adv., 7, 20981-20994. DOI: 10.1039/C7RA02501G.

Al-Ghouti, M.A., Al-Kaabi, M.A., Ashfaq, M.Y. and Da'na, D.A., 2019. Produced water characteristics, treatment and reuse: A review. J. Water Process Eng., 28, 222-239. DOI: 10.1016/j.jwpe.2019.02.001

Algieri, C. and Drioli, E., 2021. Zeolite membranes: Synthesis and applications. Sep. Purif. Technol., 278, 119295. DOI: 10.1016/j.seppur.2021.119295

Amer, L., Adhikari, B. and Pellegrino, J., 2011. Technoeconomic analysis of five microalgae-to-biofuels processes of varying complexity. Bioresour. Technol., 102, 9350-9359. DOI: 10.1016/j.biortech.2011.08.010

Amin, S.K., Roushdy, M.H., Abdallah, H.A., Moustafa, A.F. and Abadir, M.F., 2020. Preparation and characterization of ceramic nanofiltration membrane prepared from hazardous industrial waste. Int. J. Appl. Ceram. Technol., 17, 162-174. DOI: 10.1111/ijac.13311

Ananthakumar, S., Manohar, P. and Warrier, K.G.K., 2004. Effect of boehmite and organic binders on extrusion of alumina. Ceram. Int., 30, 837-842. DOI: 10.1016/j.ceramint.2003.09.019

Ang, W.S., Lee, S. and Elimelech, M., 2006. Chemical and physical aspects of cleaning of organic-fouled reverse osmosis membranes. J. Membr. Sci., 272, 198-210. DOI: 10.1016/j.memsci.2005.07.035

APHA, Standard Methods for the Examination of Water and Wastewater (20th Ed.) American Public Health Association, Washington DC (1998)

Araki, S., Okubo, Y., Maekawa, K., Imasaka, S. and Yamamoto, H., 2020. Preparation of a high-silica chabazite-type zeolite membrane with high CO_2 permeability using tetraethylammonium hydroxide. J. Membr. Sci., 613, 118480. DOI: 10.1016/j.memsci.2020.118480

Arshadi, M., Amiri, M.J. and Mousavi, S., 2014. Kinetic, equilibrium and thermodynamic investigations of Ni (II), Cd (II), Cu (II) and Co (II) adsorption on barley straw ash. Water Resour. Ind., 6, 1-17. DOI: 10.1016/j.wri.2014.06.001

Arun, S., Manikandan, N.A., Pakshirajan, K. and Pugazhenthi, G., 2019. Novel shortcut biological nitrogen removal method using an algae-bacterial consortium in a photo-sequencing batch reactor: Process optimization and kinetic modelling. J. Environ. Manage., 250, 109401. DOI: 10.1016/j.jenvman.2019.109401

Asif, M.B. and Zhang, Z., 2021. Ceramic membrane technology for water and wastewater treatment: A critical review of performance, full-scale applications, membrane fouling and prospects. Chem. Eng. J., 418, 129481. DOI: 10.1016/j.cej.2021.129481

Atallah, C., Tremblay, A.Y. and Mortazavi, S., 2017. Silane surface modified ceramic membranes for the treatment and recycling of SAGD produced water. J. Pet. Sci. Eng., 157, 349-358. DOI: 10.1016/j.petrol.2017.07.007

Au, P.I. and Leong, Y.K., 2013. Rheological and zeta potential behaviour of kaolin and bentonite composite slurries. Colloids surf., A 436, 530-541. DOI: 10.1016/j.colsurfa.2013.06.039.

Aysan, H., Edebali, S., Ozdemir, C., Karakaya, M.C. and Karakaya, N., 2016. Use of chabazite, a naturally abundant zeolite, for the investigation of the adsorption kinetics and mechanism of methylene blue dye. Microporous Mesoporous Mater., 235, 78-86. DOI: 10.1016/j.micromeso.2016.08.007

Awual, M.R., Yaita, T. and Shiwaku, H., 2013. Design a novel optical adsorbent for simultaneous ultra-trace cerium (III) detection, sorption and recovery. Chem. Eng. J., 228, 327-335. DOI: 10.1016/j.cej.2013.05.010

Babatunde, A.O., Kumar, J.L. and Zhao, Y., 2011. Constructed wetlands using aluminium-based drinking water treatment sludge as P-removing substrate: should aluminium release be a concern? J. Environ. Monit., 13, 1775-1783. DOI: 10.1039/C1EM00001B

Barros, A.I., Gonçalves, A.L., Simões, M. and Pires, J.C., 2015. Harvesting techniques applied to microalgae: a review. Renewable Sustainable Energy Rev., 41, 1489-1500. DOI: 10.1016/j.rser.2014.09.037

Bardestani, R., Patience, G.S. and Kaliaguine, S., 2019. Experimental methods in chemical engineering: specific surface area and pore size distribution measurements—BET, BJH, and DFT. The Canadian J. Chem. Eng., 97, 2781-2791. DOI: 10.1002/cjce.23632

Barredo-Damas, S., Alcaina-Miranda, M.I., Iborra-Clar, M.I. and Mendoza-Roca, J.A., 2012. Application of tubular ceramic ultrafiltration membranes for the treatment of integrated textile wastewaters. Chem. Eng. J., 192, 211-218. DOI: 10.1016/j.cej.2012.03.079

Basumatary, A.K., Kumar, R.V., Ghoshal, A.K. and Pugazhenthi, G., 2015. Synthesis and characterization of MCM-41-ceramic composite membrane for the separation of chromic acid from aqueous solution. J. Membr. Sci., 475, 521-532. DOI: 10.1016/j.memsci.2014.10.055

Basumatary, A.K., Kumar, R.V., Ghoshal, A.K. and Pugazhenthi, G., 2016a. Cross flow ultrafiltration of Cr (VI) using MCM-41, MCM-48 and Faujasite (FAU) zeolite-ceramic composite membranes. Chemosphere, 153, 436-446. DOI: 10.1016/j.chemosphere.2016.03.077

Basumatary, A.K., Kumar, R.V., Ghoshal, A.K. and Pugazhenthi, G., 2016b. Removal of $FeCl_3$ from aqueous solution by ultrafiltration using ordered mesoporous MCM-48 ceramic composite membrane. Sep. Sci. Technol., 51, 2038-2046. DOI: 10.1080/01496395.2016.1187168

Basak, S., Kundu, D. and Naskar, M.K., 2014. Low temperature synthesis of NaA zeolite membranes: The effect of primary and secondary crystallizations. Ceram. Int., 40, 12923-12930. DOI: 10.1016/j.ceramint.2014.04.152

Benito, J.M., Conesa, A., Rubio, F. and Rodriguez, M.A., 2005. Preparation and characterization of tubular ceramic membranes for treatment of oil emulsions. J. Eur. Ceram. Soc., 25, 1895-1903. DOI: 10.1016/j.jeurceramsoc.2004.06.016

Beqqour, D., Achiou, B., Bouazizi, A., Ouaddari, H., Elomari, H., Ouammou, M., Bennazha, J. and Younssi, S.A., 2019. Enhancement of microfiltration performances of Pozzolan membrane by incorporation of micronized phosphate and its application for industrial wastewater treatment. J. Environ. Chem. Eng., 7, 102981. DOI: 10.1016/j.jece.2019.102981

Bilad, M.R., Vandamme, D., Foubert, I., Muylaert, K. and Vankelecom, I.F., 2012. Harvesting microalgal biomass using submerged microfiltration membranes. Bioresour. Technol., 111, 343-352. DOI: 10.1016/j.biortech.2012.02.009

Bose, S. and Das, C., 2013. Preparation and characterization of low cost tubular ceramic support membranes using sawdust as a pore-former. Mater. Lett., 110, 152-155. DOI: 10.1016/j.matlet.2013.08.019

Bose, S. and Das, C., 2014. Role of binder and preparation pressure in tubular ceramic membrane processing: design and optimization study using response surface methodology (RSM). Ind. Eng. Chem. Res., 53, 12319-12329. DOI: 10.1021/ie500792a

Bousbih, S., Errais, E., Darragi, F., Duplay, J., Trabelsi-Ayadi, M., Daramola, M.O. and Ben Amar, R., 2020. Treatment of textile wastewater using monolayered ultrafiltation ceramic membrane fabricated from natural kaolin clay. Environ. Technol. 1-12. DOI: 10.1080/09593330.2020.1729242.

Bouzerara, F., Harabi, A., Achour, S. and Larbot, A., 2006. Porous ceramic supports for membranes prepared from kaolin and doloma mixtures. J. Eur. Ceram. Soc., 26, 1663-1671. DOI: 10.1016/j.jeurceramsoc.2005.03.244

Cabrera, S.M., Winnubst, L., Richter, H., Voigt, I. and Nijmeijer, A., 2021. Industrial application of ceramic nanofiltration membranes for water treatment in oil sands mines. Sep. Purif. Technol., 256, 117821. DOI: 10.1016/j.seppur.2020.117821

Cai, Y., Wang, Y., Chen, X., Qiu, M. and Fan, Y., 2015. Modified colloidal sol–gel process for fabrication of titania nanofiltration membranes with organic additives. J. Membr. Sci., 476, 432-441. DOI: 10.1016/j.memsci.2014.11.034

Cao, Y., Wang, M., Xu, Z.L., Ma, X.H. and Xue, S.M., 2016. A novel seeding method of interfacial polymerization-assisted dip coating for the preparation of zeolite NaA membranes on ceramic hollow fiber supports. ACS Appl. Mater. Int., 8, 25386-25395. DOI: 10.1021/acsami.6b08092

Campbell, D.O. and Buxton, S.R., 1970. Rapid ion exchange separations. Chromategraphic lanthanide separations using a high-pressure ion exchange method. Ind. Eng. Chem. Process Des. Dev., 9, 89-94.

Campos, J.C., Borges, R.M.H., Oliveira Filho, A.M.D., Nobrega, R. and Sant'Anna Jr, G.L., 2002. Oilfield wastewater treatment by combined microfiltration and biological processes. Water Res., 36, 95-104. DOI: 10.1016/S0043-1354(01)00203-2

Carretero, M.I., Dondi, M., Fabbri, B. and Raimondo, M., 2002. The influence of shaping and firing technology on ceramic properties of calcareous and non-calcareous illitic–chloritic clays. Appl. Clay Sci., 20, 301-306. DOI: 10.1016/S0169-1317(01)00076-X

Carolin, C.F., Kumar, P.S., Saravanan, A., Joshiba, G.J. and Naushad, M., 2017. Efficient techniques for the removal of toxic heavy metals from aquatic environment: A review. J. Environ. Chem. Eng., 5, 2782-2799. DOI: 10.1016/j.jece.2017.05.029

Chang, Q., Zhou, J.E., Wang, Y., Liang, J., Zhang, X., Cerneaux, S., Wang, X., Zhu, Z. and Dong, Y., 2014. Application of ceramic microfiltration membrane modified by nano-TiO2 coating in separation of a stable oil-in-water emulsion. J. Membr. Sci., 456, 128-133. DOI: 10.1016/j.memsci.2014.01.029

Chakrabarty, B., Ghoshal, A.K. and Purkait, M.K., 2010. Cross-flow ultrafiltration of stable oil-in-water emulsion using polysulfone membranes. Chem. Eng. J., 165, 447-456.DOI: 10.1016/j.cej.2010.09.031

Chakraborty, S., Uppaluri, R. and Das, C., 2018. Optimal fabrication of carbonate free kaolin based low cost ceramic membranes using mixture model response surface methodology. Appl. Clay Sci., 162,101-112. DOI: 10.1016/j.clay.2018.06.002

Chakraborty, S., Das, C. and Uppaluri, R., 2020. Feasibility of low-cost kaolin–based ceramic membranes for organic Lagernaria siceraria juice production. Food Bioprocess. Technol., 13, 1009-1023. DOI: 10.1007/s11947-020-02455-4

Chauvin, D., Bell, J., Leray, I., Ledoux-Rak, I. and Nguyen, C.T., 2019. Label-free optofluidic sensor based on polymeric microresonator for the detection of cadmium ions in tap water. Sens. Actuators, B, 280, 77-85. DOI: 10.1016/j.snb.2018.10.53

Chen, X., Yu, L., Zou, S., Xiao, L. and Fan, J., 2020. Zeolite cotton in tube: A simple robust household water treatment filter for heavy metal removal. Sci. Rep., 10, 1-9. DOI: 10.1038/s41598-020-61776-8

Chen, H., Ma, N., Cheng, C., Zhang, H., Yuan, W., Liu, P., Feng, X., Liu, J., Yang, Q. and Zhou, S., 2020. Hydrogen activation on aluminium-doped magnesium hydride surface for methanation of carbon dioxide. Appl. Surf. Sci., 515, 146038. DOI: 10.1016/j.apsusc.2020.146038

Chen, C.Y., Yeh, K.L., Aisyah, R., Lee, D.J. and Chang, J.S., 2011. Cultivation, photobioreactor design and harvesting of microalgae for biodiesel production: a critical review. Bioresour. Technol., 102, 71-81. DOI: 10.1016/j.biortech.2010.06.159

Chen, P., Zhong, Z., Liu, F. and Xing, W., 2015. Cleaning ceramic membranes used in treating desizing wastewater with a complex-surfactant SDBS-assisted method. Desalin., 365, 25-35. DOI: 10.1016/j.desal.2015.01.037

Chen, X., Huang, C. and Liu, T., 2012. Harvesting of microalgae Scenedesmus sp. using polyvinylidene fluoride microfiltration membrane. Desalin. Water Treat., 45, 177-181. DOI: 10.1080/19443994.2012.692034

Chowdhury, T., Chowdhury, H., Miskat, M.I., Rahman, M.S., Hossain, N., Membrane-based technologies for industrial wastewater treatment and resource recovery, in: Shah, M. & Rodriguez-Couto, S. (Eds.), Membrane-Based Hybrid Processes for Wastewater Treatment, Elsevier, Amsterdam, 2021, 403-421.

Clément, L., Hurel, C. and Marmier, N., 2013. Toxicity of TiO_2 nanoparticles to cladocerans, algae, rotifers and plants–effects of size and crystalline structure. Chemosphere. 90, 1083-1090. DOI: 10.1016/j.chemosphere.2012.09.013.

Coudert, F.X., Cailliez, F., Vuilleumier, R., Fuchs, A.H. and Boutin, A., 2009. Water nanodroplets confined in zeolite pores. Faraday discuss., 141, 377-398. DOI: 10.1039/B804992K

CPCB (1992) Standards for water quality. Central Pollution Control Board, New Delhi, India (https://www.cpcb.nic.in/GeneralStandards.pdf)

Da Silva, F.S., De Melo, H.G., Benedetti, A.V. and Suegama, P.H., 2019. Influence of Ce (IV) ions amount on the electrochemical behavior of hybrid films in 0.1 mol L-1 NaCl solution. Eclética Química J., 44, 27-56. DOI: 10.26850/1678-4618eqj.v44.4.2019.p27-56

Dele-Afolabi, T.T., Hanim, M.A., Norkhairunnisa, M., Sobri, S., Calin, R. and Ismarrubie, Z.N., 2018. Tensile strength and corrosion resistance properties of porous Al_2O_3/Ni composites prepared with rice husk pore-forming agent. Ceram. Int., 44, 11127-11135. DOI: 10.1016/j.ceramint.2018.03.124

Dilaver, M., Hocaoğlu, S.M., Soydemir, G., Dursun, M., Keskinler, B., Koyuncu, İ. and Ağtaş, M., 2018. Hot wastewater recovery by using ceramic membrane ultrafiltration and its

reusability in textile industry. J. Cleaner Prod., 171, 220-233. DOI: 10.1016/j.jclepro.2017.10.015

Dickhout, J.M., Virga, E., Lammertink, R.G. and de Vos, W.M., 2019. Surfactant specific ionic strength effects on membrane fouling during produced water treatment. J. Colloid Interface sci., 556, 12-23. DOI: 10.1016/j.jcis.2019.07.068

Dohnalová, Ž., Svoboda, L. and Šulcová, P., 2008. Characterization of kaolin dispersion using acoustic and electroacoustic spectroscopy. J. Min. Metall. B. Metall. 44, 63-72. DOI: 10.2298/JMMB0801063D.

Dong, J., Lin, Y.S., Hu, M.Z.C., Peascoe, R.A. and Payzant, E.A., 2000. Template-removal-associated microstructural development of porous-ceramic-supported MFI zeolite membranes. Microporous Mesoporous Mater., 34, 241-253. DOI: 10.1016/S1387-1811(99)00175-4

Dong, Y., Feng, X., Dong, D., Wang, S., Yang, J., Gao, J., Liu, X. and Meng, G., 2007. Elaboration and chemical corrosion resistance of tubular macro-porous cordierite ceramic membrane supports. J. Membr. Sci., 304, 65-75. DOI: 10.1016/j.memsci.2007.06.058

Dong, Y., Li, Y., Wang, C., Cui, A. and Deng, Z., 2001. Preparation of cuprous oxide particles of different crystallinity. J. Colloid. Interface. Sci., 85-89. DOI: 10.1006/jcis.2001.7857.

Dong, Y., Zhou, J.E., Lin, B., Wang, Y., Wang, S., Miao, L., Lang, Y., Liu, X. and Meng, G., 2009. Reaction-sintered porous mineral-based mullite ceramic membrane supports made from recycled materials. J. Hazard. Mater., 172, 180-186. DOI: 10.1016/j.jhazmat.2009.06.148

Donnan, F.G., 1995. Theory of membrane equilibria and membrane potentials in the presence of non-dialysing electrolytes. A contribution to physical-chemical physiology. J. Membr. Sci., 100, 45-55. DOI: 10.1016/0376-7388(94)00297-C

Dos Santos Barbosa, A., dos Santos Barbosa, A., Barbosa, T.L.A. and Rodrigues, M.G., 2018. Synthesis of zeolite membrane (NaY/alumina): Effect of precursor of ceramic support and its application in the process of oil–water separation. Sep. Purif. Technol., 200, 141-154. DOI: 10.1016/j.seppur.2018.02.001

Druchok, M., Holovko, M. and Bryk, T., 2004. A molecular dynamics study of Al^{3+} in water: hydrolysis effects. Condensed Matter Physics.

Dudziak, M. and Kudlek, E., 2019. Removal of hardness in wastewater effluent using membrane filtration. Archit. Civil Eng. Environ., 12, 141-147. DOI : 10.21307/ACEE-2019-030

Duke, M.C., Zhu, B., Doherty, C.M., Hill, M.R., Hill, A.J. and Carreon, M.A., 2016. Structural effects on SAPO-34 and ZIF-8 materials exposed to seawater solutions and their potential as desalination membranes. Desalin., 377, 128-137. DOI: 10.1016/j.desal.2015.09.004

Dubey, S., Sharma, G.C. and Sharma, Y.C., 2019. Optimization of Reclamation of Ni (II)-Rich Solutions by γ-Alumina Nanoparticles. J. Hazard., Toxic and Radioact. Waste, 23, 04019005. DOI: 10.1061/(ASCE)HZ.2153-5515.0000400

Durdureanu-Angheluta, A., Dascalu, A., Fifere, A., Coroaba, A., Pricop, L., Chiriac, H., Tura, V., Pinteala, M. and Simionescu, B.C., 2012. Progress in the synthesis and characterization of magnetite nanoparticles with amino groups on the surface. J. Magn. Magn. Mater. 324, 1679-1689. DOI: 10.1016/j.jmmm.2011.11.062.

Eterigho-Ikelegbe, O., Bada, S., Daramola, M.O. and Falcon, R., 2021. Synthesis of high purity hydroxy sodalite nanoparticles via pore-plugging hydrothermal method for inorganic membrane development: Effect of synthesis variables on crystallinity, crystal size and morphology. Mater. Today:. Proc., 38, 675-681. DOI: 10.1016/j.matpr.2020.03.693

Ebrahimi, M., Willershausen, D., Ashaghi, K.S., Engel, L., Placido, L., Mund, P., Bolduan, P. and Czermak, P., 2010. Investigations on the use of different ceramic membranes for efficient oil-field produced water treatment. Desalin., 250, 991-996. DOI: 10.1016/j.desal.2009.09.088

Elbadawi, M., Mosalagae, M., Reaney, I.M. and Meredith, J., 2017. Guar gum: A novel binder for ceramic extrusion. Ceram. Int., 43, 16727-16735. DOI: 10.1016/j.ceramint.2017.09.066

El-Sayed, S., Mahmoud, K.H., Fatah, A.A. and Hassen, A.D.S.C., 2011. DSC, TGA and dielectric properties of carboxymethyl cellulose/polyvinyl alcohol blends. Physica B, 406, 4068-4076. DOI: 10.1016/j.physb.2011.07.050

Erdem, I., 2017, February. Sol-gel applications for ceramic membrane preparation. In AIP Conference proceedings. 1809, 020011. https://doi.org/10.1063/1.4975426.

Fang, J., Qin, G., Wei, W., Zhao, X. and Jiang, L., 2013. Elaboration of new ceramic membrane from spherical fly ash for microfiltration of rigid particle suspension and oil-in-water emulsion. Desalin., 311, 113-126. DOI: 10.1016/j.desal.2012.11.008.

Fakhru'l-Razi, A., Pendashteh, A., Abdullah, L.C., Biak, D.R.A., Madaeni, S.S. and Abidin, Z.Z., 2009. Review of technologies for oil and gas produced water treatment. J. hazard. Mater., 170, 530-551. DOI: 10.1016/j.jhazmat.2009.05.044

Falamaki, C., Naimi, M. and Aghaie, A., 2006. Dip-coating technique for the manufacture of alumina microfilters using PVA and Na-CMC as binders: a comparative study. J. Eur. Ceram. Soc., 26, 949-956. DOI: 10.1016/j.jeurceramsoc.2004.11.018

Fan, D., Barrier, N., Vicente, A., Gilson, J.P., Clevers, S., Dupray, V., Coquerel, G. and Valtchev, V., 2020. Organic template-free synthesis of an open framework silicoaluminophosphate (SAPO) with high thermal stability and high ionic conductivity. Inorg. Chem. Front., 7, 542-553. DOI: 10.1039/C9QI01223K.

Fang, J., Qin, G., Wei, W. and Zhao, X., 2011. Preparation and characterization of tubular supported ceramic microfiltration membranes from fly ash. Sep. Purif. Technol., 80, 585-591. DOI: 10.1016/j.seppur.2011.06.014

Fan, P.M., Zhen, K.F., Zan, Z.Y., Chao, Z., Jian, Z. and Yun, J.Z., 2016. Preparation and development of porous ceramic membrane supports fabricated by extrusion technique. Chem. Eng. Trans., 55, 277-282.

Fernández-Ibáñez, P.1., Blanco, J., Malato, S. and De Las Nieves, F.J., 2003. Application of the colloidal stability of TiO_2 particles for recovery and reuse in solar photocatalysis. Water. Res. 37, 3180-3188. DOI:10.1016/S0043-1354(03)00157-X.

Fujishima, A., Zhang, X. and Tryk, D.A., 2008. TiO_2 photocatalysis and related surface phenomena. Surf. Sci. Rep. 63, 515-582. DOI: 10.1016/j.surfrep.2008.10.001.

Gaeta-Bernardi, A. and Parente, V., 2016. Organic municipal solid waste (MSW) as feedstock for biodiesel production: A financial feasibility analysis. Renew. Energy. 86, 1422-1432. DOI: 10.1016/j.renene.2015.08.025.

Gao, J., Sun, S.P., Zhu, W.P. and Chung, T.S., 2016. Green modification of outer selective P84 nanofiltration (NF) hollow fiber membranes for cadmium removal. J. Membr. Sci., 499, 361-369. DOI: 10.1016/j.memsci.2015.10.051

Gao, Y., Zhang, Y., Dudek, M., Qin, J., Øye, G. and Østerhus, S.W., 2021. A multivariate study of backpulsing for membrane fouling mitigation in produced water treatment. J. Environ. Chem. Eng., 9, 104839. DOI: 10.1016/j.jece.2020.104839

Garmsiri, E., Rasouli, Y., Abbasi, M. and Izadpanah, A.A., 2017. Chemical cleaning of mullite ceramic microfiltration membranes which are fouled during oily wastewater treatment. J. Water. Process Eng., 19, 81-95. DOI: 10.1016/j.jwpe.2017.07.012

Gaudillere, C. and Serra, J.M., 2016. Freeze-casting: Fabrication of highly porous and hierarchical ceramic supports for energy applications. Boletín de la Sociedad Española de cerámica y vidrio, 55, 45-54. DOI: 10.1016/j.bsecv.2016.02.002

Ghimici, L. and Nichifor, M., 2013. Separation of TiO_2 particles from water and water/methanol mixtures by cationic dextran derivatives. Carbohydr. Polym. 98, 1637-1643. DOI: 10.1016/j.carbpol.2013.07.085.

Giorno, F., Mazzei, R. and Giorno, L., 2013. Purification of triacylglycerols for biodiesel production from Nannochloropsis microalgae by membrane technology. Bioresour. Technol., 140, 172-178. DOI: 10.1016/j.biortech.2013.04.073

Goswami, K.P. and Pugazhenthi, G., 2020a. Treatment of poultry slaughterhouse wastewater using tubular microfiltration membrane with fly ash as key precursor. J. Water Process Eng., 37, 101361. DOI: 10.1016/j.jwpe.2020.101361

Goswami, K.P., Pugazhenthi, G., 2020b. Credibility of polymeric and ceramic membrane filtration in the removal of bacteria and virus from water: A review. J. Environ. Manage. 268, 1-18. DOI: 10.1016/j.jenvman.2020.110583.

Goswami, K.P. and Pugazhenthi, G., 2021. Effect of binder concentration on properties of low-cost fly ash-based tubular ceramic membrane and its application in separation of glycerol from biodiesel. J. Cleaner Prod., 319, 128679. DOI: 10.1016/j.jclepro.2021.128679

Gong, X.Y., Huang, Z.H., Zhang, H., Liu, W.L., Ma, X.H., Xu, Z.L. and Tang, C.Y., 2020. Novel high-flux positively charged composite membrane incorporating titanium-based MOFs for heavy metal removal. Chem. Eng. J., 398, p.125706. DOI: 10.1016/j.cej.2020.125706

Greenberg, A.E., Clesceri, L. S., and Eaton, A. D., 1992.Standard Methods for the Examination of Water and Wastewater, American public health association, Washington, 18th edn, Ch. 1, 3-57.

Gross, M., Henry, W., Michael, C. and Wen, Z., 2013. Development of a rotating algal biofilm growth system for attached microalgae growth with in situ biomass harvest. Bioresour. Technol., 150, 195-201. DOI: 10.1016/j.biortech.2013.10.016

Guirgis, A., Gay-de-Montella, R. and Faiz, R., 2015. Treatment of produced water streams in SAGD processes using tubular ceramic membranes. Desalin., 358, 27-32. DOI: 10.1016/j.desal.2014.12.007

Guironnet, L., Geffroy, P.M., Jouay, F., Pagnoux, C., Richet, N. and Chartier, T., 2019. La0. 6Sr0. 4Fe0. 8Co0. 2O3-δ electrophoretic coating for oxygen transport membranes. Chem. Eng. Sci.: X, 1, 100008. 10.1016/j.cesx.2019.100008

Gumpu, M.B., Sethuraman, S., Krishnan, U.M. and Rayappan, J.B.B., 2015. A review on detection of heavy metal ions in water–an electrochemical approach. Sens. Actuators B., 213, 515-533. DOI: 10.1016/j.snb.2015.02.122

Hanaor, D.A. and Sorrell, C.C., 2011. Review of the anatase to rutile phase transformation. J. Mater. Sci. 46, 855-874. DOI: 10.1007/s10853-010-5113-0.

Harinkhere, D., Kaurav, N. and Okram, G.S., 2022. Preparation and characterization of membranes supports for filtration application. Mater. Today: Proc., 54, 937-940. 10.1016/j.matpr.2021.10.508

Hasegawa, Y., Hotta, H., Sato, K., Nagase, T. and Mizukami, F., 2010. Preparation of novel chabazite (CHA)-type zeolite layer on porous α-Al_2O_3 tube using template-free solution. J. Membr. Sci., 347, 193-196. DOI: 10.1016/j.memsci.2009.10.024

Hassan, R.M., Tirkistan, F.A., Zaafarany, I.A., Asghar, B.H. and Takagi, H.D., 2014. Oxidation of Some Anionic Polyelectrolytes. Kinetics and Mechanism of Oxidation of Carboxymethyl Cellulose Polysaccharide by Cerium (IV) in Aqueous Perchlorate Solutions. Curr. Adv. Chem. Res, 1, 15-24.

He, Z., Lyu, Z., Gu, Q., Zhang, L. and Wang, J., 2019. Ceramic-based membranes for water and wastewater treatment. Colloids Surf. A:, 578, 123513. DOI: 10.1016/j.colsurfa.2019.05.074

Hebbar, R.S., Isloor, A.M., Ananda, K. and Ismail, A.F., 2016. Fabrication of polydopamine functionalized halloysite nanotube/polyetherimide membranes for heavy metal removal. J. Mater. Chem. A, 4, 764-774. DOI: 10.1039/C5TA09281G

Hedfi, I., Hamdi, N., Srasra, E. and Rodríguez, M.A., 2014. The preparation of micro-porous membrane from a Tunisian kaolin. Appl. Clay Sci., 101, 574-578. DOI: 10.1016/j.clay.2014.09.021

Hermia, J., 1982. Constant pressure blocking filtration laws: application to power-law non-Newtonian fluids.

https://cpcb.nic.in/displaypdf.php?id=SW5kdXN0cnktU3BlY2lmaWMtU3RhbmRhcmRzL0VmZmx1ZW50L0R5ZWFuZER5ZV9JbnRlcl9JbmR1cy5wZGY=

Hubadillah, S.K., Harun, Z., Othman, M.H.D., Ismail, A.F. and Gani, P., 2016. Effect of kaolin particle size and loading on the characteristics of kaolin ceramic support prepared via phase inversion technique. J. Asian Ceram. Soc., 4, 164-177. DOI: 10.1016/j.jascer.2016.02.002

Hubadillah, S.K., Othman, M.H.D., Matsuura, T., Ismail, A.F., Rahman, M.A., Harun, Z., Jaafar, J. and Nomura, M., 2018. Fabrications and applications of low cost ceramic membrane from kaolin: A comprehensive review. Ceram. Int. 44, 4538-4560. DOI: 10.1016/j.ceramint.2017.12.215

Hung, M.T. and Liu, J.C., 2006. Microfiltration for separation of green algae from water. Colloids Surf., B, 51, 157-164. DOI: 10.1016/j.colsurfb.2006.07.003

Huang, A., Wang, N. and Caro, J., 2012. Seeding-free synthesis of dense zeolite FAU membranes on 3-aminopropyltriethoxysilane-functionalized alumina supports. J. Membr. Sci., 389, 272-279. DOI: 10.1016/j.memsci.2011.10.036

Huang, H.H., 2016. The Eh-pH diagram and its advances. Metals, 6, 23. DOI: 10.3390/met6010023

Hwang, T., Park, S.J., Oh, Y.K., Rashid, N. and Han, J.I., 2013. Harvesting of Chlorella sp. KR-1 using a cross-flow membrane filtration system equipped with an anti-fouling membrane. Bioresour. Technol., 139, 379-382. DOI: 10.1016/j.biortech.2013.03.149

Hwang, T., Kotte, M.R., Han, J.I., Oh, Y.K. and Diallo, M.S., 2015. Microalgae recovery by ultrafiltration using novel fouling-resistant PVDF membranes with in situ PEGylated polyethyleneimine particles. Water Res., 73, 181-192. DOI: 10.1016/j.watres.2014.12.002

Imdad, S. and Dohare, R.K., 2022. A critical review on heavy metals removal using ionic liquid membranes from the industrial wastewater. Chem. Eng. Process. Process Intensif., 108812. DOI: 10.1016/j.cep.2022.108812

Iqbal, A., Sattar, H., Haider, R. and Munir, S., 2019. Synthesis and characterization of pure phase zeolite 4A from coal fly ash. J. Cleaner Prod., 219, 258-267. DOI: 10.1016/j.jclepro.2019.02.066

Isawi, H., El-Sayed, M.H., Feng, X., Shawky, H. and Mottaleb, M.S.A., 2016. Surface nanostructuring of thin film composite membranes via grafting polymerization and incorporation of ZnO nanoparticles. Appl. Surf. Sci., 385, 268-281. DOI: 10.1016/j.apsusc.2016.05.141

Ivanets, A. and Agabekov, V., 2017. Preparation and characterization of microfiltration ceramic membranes based on natural quartz sand. Chem. J. Moldova., 12, 67-73. DOI: 10.19261/cjm.2017.407

Jamil, T.S., Mansor, E.S., Abdallah, H., Shaban, A.M. and Souaya, E.R., 2018. Novel anti fouling mixed matrix CeO2/Ce7O12 nanofiltration membranes for heavy metal uptake. J. Environ. Chem. Eng., 6, 3273-3282. DOI: 10.1016/j.jece.2018.05.006

Jana, S., Purkait, M.K. and Mohanty, K., 2010. Preparation and characterization of low-cost ceramic microfiltration membranes for the removal of chromate from aqueous solutions. Appl. Clay Sci., 47, 317-324. DOI: 10.1016/j.clay.2009.11.036

Jedidi, I., Khemakhem, S., Larbot, A. and Amar, R.B., 2009. Elaboration and characterisation of fly ash based mineral supports for microfiltration and ultrafiltration membranes. Ceram. Int., 35, 2747-2753. DOI: 10.1016/j.ceramint.2009.03.021

Jiménez, S., Micó, M.M., Arnaldos, M., Medina, F. and Contreras, S., 2018. State of the art of produced water treatment. Chemosphere, 192, 186-208. DOI: 10.1016/j.chemosphere.2017.10.139

Johnson, E.B.G. and Arshad, S.E., 2014. Hydrothermally synthesized zeolites based on kaolinite: A review. Appl. Clay Sci., 97, 215-221. DOI: 10.1016/j.clay.2014.06.005

Karakiliç, P., Wang, X., Kapteijn, F., Nijmeijer, A. and Winnubst, L., 2019. Defect-free high-silica CHA zeolite membranes with high selectivity for light gas separation. J. Membr. Sci., 586, 34-43. DOI: 10.1016/j.memsci.2019.05.047

Kaur, H., Bulasara, V.K. and Gupta, R.K., 2016. Preparation of kaolin-based low-cost porous ceramic supports using different amounts of carbonates. Desalin. Water Treat., 57, 15154-15163. DOI: 10.1080/19443994.2015.1068226

Karlsson, M.C., Álvarez-Asencio, R., Bordes, R., Larsson, A., Taylor, P. and Steenari, B.M., 2019. Characterization of paint formulated using secondary TiO2 pigments recovered from waste paint J. Coatings. Technol. Res. 16, 607-614. DOI: 10.1007/s11998-018-0132-x

Kazemimoghadam, M. and Mohammadi, T., 2007. Chemical cleaning of ultrafiltration membranes in the milk industry. Desalin., 204, 213-218. DOI: 10.1016/j.desal.2006.04.030

Kholssi, R., Marks, E.A., Miñón, J., Montero, O., Debdoubi, A. and Rad, C., 2019. Biofertilizing effect of Chlorella sorokiniana suspensions on wheat growth. J. Plant Growth Regul., 38, 644-649. DOI: 10.1007/s00344-018-9879-7

Khemakhem, S., Larbot, A. and Amar, R.B., 2009. New ceramic microfiltration membranes from Tunisian natural materials: application for the cuttlefish effluents treatment. Ceram. Int. 35, 55-61. DOI: 10.1016/j.ceramint.2007.09.117

Knuckey, R.M., Brown, M.R., Robert, R. and Frampton, D.M., 2006. Production of microalgal concentrates by flocculation and their assessment as aquaculture feeds. Aquacult. Eng., 35, 300-313. DOI: 10.1016/j.aquaeng.2006.04.001

Kim, D.G., La, H.J., Ahn, C.Y., Park, Y.H. and Oh, H.M., 2011. Harvest of Scenedesmus sp. with bioflocculant and reuse of culture medium for subsequent high-density cultures. Biores. Technol., 102, 3163-3168. DOI: 10.1016/j.biortech.2010.10.108

Kiser, M.A., Westerhoff, P., Benn, T., Wang, Y., Perez-Rivera, J. and Hristovski, K., 2009. Titanium nanomaterial removal and release from wastewater treatment plants. Environ. Sci. Technol. 43, 6757-6763. DOI: 10.1021/es901102n

Konstantinou, I.K. and Albanis, T.A., 2004. TiO_2-assisted photocatalytic degradation of azo dyes in aqueous solution: kinetic and mechanistic investigations: a review. Appl. Catal., B 49, 1-14. DOI: 10.1016/j.apcatb.2003.11.010

Kumar, R.V., Basumatary, A.K., Ghoshal, A.K. and Pugazhenthi, G., 2015a. Performance assessment of an analcime-C zeolite–ceramic composite membrane by removal of Cr (VI) from aqueous solution. RSC Adv., 5, 6246-6254. DOI: 10.1039/C4RA14527E

Kumar, R.V., Ghoshal, A.K. and Pugazhenthi, G., 2015b. Elaboration of novel tubular ceramic membrane from inexpensive raw materials by extrusion method and its performance in microfiltration of synthetic oily wastewater treatment. J. Membr. Sci. 490, 92-102. DOI: 10.1016/j.memsci.2015.04.066

Kumar, R.V., Goswami, L., Pakshirajan, K., and Pugazhenthi, G., 2016. Dairy wastewater treatment using a novel low cost tubular ceramic membrane and membrane fouling mechanism using pore blocking models. J. Water Process Eng., 13, 168-175. DOI: 10.1016/j.jwpe.2016.08.012

Kumar, R. V. and Pugazhenthi, G., 2017. Removal of chromium from synthetic wastewater using MFI zeolite membrane supported on inexpensive tubular ceramic substrate. J. Water Reuse Desalin., 7, 365-377. DOI: 10.2166/wrd.2016.096

Kumakiri, I., Hashimoto, K., Nakagawa, Y., Inoue, Y., Kanehiro, Y., Tanaka, K. and Kita, H., 2014. Application of FAU zeolite membranes to alcohol/acrylate mixture systems. Catal. Today, 236, 86-91. DOI: 10.1016/j.cattod.2013.11.064

Kumar, M. and Pakshirajan, K., 2021. Continuous removal and recovery of metals from wastewater using inverse fluidized bed sulfidogenic bioreactor. J. Cleaner Prod., 284, 124769. DOI: 10.1016/j.jclepro.2020.124769

Kumari, S.V.G., Manikandan, N.A., Pakshirajan, K. and Pugazhenthi, G., 2020. Sustained drug release and bactericidal activity of a novel, highly biocompatible and biodegradable polymer nanocomposite loaded with norfloxacin for potential use in antibacterial therapy. J. Drug Delivery Sci. Technol., 59, 101900. DOI: 10.1016/j.jddst.2020.101900

Kurth, C.J., Wise, B.L. and Smith, S., 2018. Design considerations for implementing ceramics in new and existing polymeric UF systems. Water Pract. Technol., 13, 725-737. DOI: 10.2166/wpt.2018.081

Kurniawati, H.A., Ismadji, S. and Liu, J.C., 2014. Microalgae harvesting by flotation using natural saponin and chitosan. Bioresour. Technol., 166, 429-434. DOI: 10.1016/j.biortech.2014.05.079

Kurniawan, S.B., Purwanti, I.F. and Titah, H.S., 2018. The effect of pH and aluminium to bacteria isolated from aluminium recycling industry. J. Ecological Eng., 19, 154-161. DOI: 10.12911/22998993/86147

Kusworo, T.D., Aryanti, N. and Utomo, D.P., 2018. Oilfield produced water treatment to clean water using integrated activated carbon-bentonite adsorbent and double stages membrane process. Chem. Eng. J., 347, 462-471. DOI: 10.1016/j.cej.2018.04.136

Kühnl, W., Piry, A., Kaufmann, V., Grein, T., Ripperger, S. and Kulozik, U., 2010. Impact of colloidal interactions on the flux in cross-flow microfiltration of milk at different pH values: A surface energy approach. J. Membr. Sci. 352, 107-115. DOI: 10.1016/j.memsci.2010.02.006.

Kruger, N.J., 2009. The Bradford method for protein quantitation. The protein protocols handbook, 17-24. DOI: 10.1007/978-1-59745-198-7_4

Issaoui, M. and Limousy, L., 2019. Low-cost ceramic membranes: Synthesis, classifications, and applications. Comptes Rendus Chimie, 22, 175-187. DOI: 10.1016/j.crci.2018.09.014

Larronde-Larretche, M. and Jin, X., 2017. Microalgal biomass dewatering using forward osmosis membrane: Influence of microalgae species and carbohydrates composition. Algal Res., 23, 12-19. DOI: 10.1016/j.algal.2016.12.020

Lau, A.K., Bilad, M.R., Nordin, N.A.H.M., Faungnawakij, K., Narkkun, T., Wang, D.K., Mahlia, T.M.I. and Jaafar, J., 2020. Effect of membrane properties on tilted panel performance of microalgae biomass filtration for biofuel feedstock. Renewable Sustainable Energy Rev., 120, 109666. DOI: 10.1016/j.rser.2019.109666.

Le, T., Wang, Q., Pan, B., Ravindra, A.V., Ju, S. and Peng, J., 2019. Process regulation of microwave intensified synthesis of Y-type zeolite. Microporous Mesoporous Mater., 284, 476-485. DOI: 10.1016/j.micromeso.2019.04.029

Le, M.H., Kim, K.J., Jeong, S. and Jang, A., 2019. Effect of charged nano-particles on ceramic microfiltration membrane fouling. J. Ind. Eng. Chem., 72, 125-132. DOI: 10.1016/j.jiec.2018.12.012.

Lee, S. and Elimelech, M., 2007. Salt cleaning of organic-fouled reverse osmosis membranes. Water Res., 41, 1134-1142. DOI: 10.1016/j.watres.2006.11.043

Lee, S.J. and Kim, J.H., 2014. Differential natural organic matter fouling of ceramic versus polymeric ultrafiltration membranes. Water Res., 48, 43-51. DOI: 10.1016/j.watres.2013.08.038

Lee, S.J., Dilaver, M., Park, P.K. and Kim, J.H., 2013. Comparative analysis of fouling characteristics of ceramic and polymeric microfiltration membranes using filtration models. J. Membr. Sci., 432, 97-105. DOI: 10.1016/j.memsci.2013.01.013

Lee, S.A., Choo, K.H., Lee, C.H., Lee, H.I., Hyeon, T., Choi, W. and Kwon, H.H., 2001. Use of ultrafiltration membranes for the separation of TiO_2 photocatalysts in drinking water treatment. Ind. Eng. Chem. Res. 40, 1712-1719. DOI: 10.1021/ie000738p

Lee, J.H., Ryu, H.S., Seo, J.H., Chang, B.S. and Lee, C.K., 2010. A 90-day intravenous administration toxicity study of CaO-SiO_2-P_2O_5-B_2O_3 glass-ceramics (BGS-7) in rat. Drug Chem. Toxicol., 33, 38-47. DOI: 10.3109/01480540903373647

Li, C., Sun, W., Lu, Z., Ao, X. and Li, S., 2020. Ceramic nanocomposite membranes and membrane fouling: A review. Water Res., 175,115674. DOI: 10.1016/j.watres.2020.115674

Li, M., Yao, Y., Zhang, W., Zheng, J., Zhang, X. and Wang, L., 2017. Fractionation and concentration of high-salinity textile wastewater using an ultra-permeable sulfonated thin-film composite. Environ. Sci. Technol., 51, 9252-9260. DOI: 10.1021/acs.est.7b01795

Li, M., Zhao, Y., Zhou, S., Xing, W. and Wong, F.S., 2007. Resistance analysis for ceramic membrane microfiltration of raw soy sauce. J. Membr. Sci., 299, 122-129. DOI: 10.1016/j.memsci.2007.04.033

Li, Q., Kang, C. and Zhang, C., 2005. Wastewater produced from an oilfield and continuous treatment with an oil-degrading bacterium. Process Biochem., 40, 873-877. DOI: 10.1016/j.procbio.2004.02.011. DOI: 10.1016/j.procbio.2004.02.011

Li, Q., Kong, H., Li, P., Shao, J. and He, Y., 2019. Photo-Fenton degradation of amoxicillin via magnetic TiO_2-graphene oxide-Fe_3O_4 composite with a submerged magnetic separation

membrane photocatalytic reactor (SMSMPR). J. Hazard. Mater., 373, 437-446. DOI: 10.1016/j.jhazmat.2019.03.066

Liao, D.L., Wu, G.S. and Liao, B.Q., 2009. Zeta potential of shape-controlled TiO2 nanoparticles with surfactants. Colloids. Surf., A, 348, 270-275. DOI: 10.1016/j.colsurfa.2009.07.036

Liu, B., Zhou, R., Yogo, K. and Kita, H., 2019. Preparation of CHA zeolite (chabazite) crystals and membranes without organic structural directing agents for CO_2 separation. J. Membr. Sci., 573, 333-343. DOI: 10.1016/j.memsci.2018.11.059

Liu, P.; Hou, J.; Zhang, Y.; Li, L.; Lu, X.; Tang, Z. Two-dimensional material membranes for critical separations. Inorg. Chem. Front. 2020, 7, 2560– 2581, DOI: 10.1039/d0qi00307g

Luque, S., Gómez, D. and Álvarez, J.R., 2008. Industrial applications of porous ceramic membranes (pressure-driven processes). Membr. Sci. Technol., 13, 177-216. DOI: 10.1016/S0927-5193(07)13006-0

Lu, M., Zhang, Z., Yu, W. and Zhu, W., 2009. Biological treatment of oilfield-produced water: A field pilot study. Int. Biodeterior. Biodegrad. 63, pp.316-321. DOI: 10.1016/j.ibiod.2008.09.009

Luo, Y., Liang, J., Zeng, G., Chen, M., Mo, D., Li, G. and Zhang, D., 2018. Seed germination test for toxicity evaluation of compost: Its roles, problems and prospects. Waste Manage. 71, 109-114. DOI: 10.1016/j.wasman.2017.09.023

Luo, H., Peng, H. and Zhao, Q., 2022. High flux Mg^{2+}/Li^{+} nanofiltration membranes prepared by surface modification of polyethylenimine thin film composite membranes. Appl. Surf. Sci., 579, 152161.DOI: 0.1016/j.apsusc.2021.152161

Majouli, A., Younssi, S.A., Tahiri, S., Albizane, A., Loukili, H. and Belhaj, M., 2011. Characterization of flat membrane support elaborated from local Moroccan Perlite. Desalin., 277, 61-66. DOI: 10.1016/j.desal.2011.04.003

Maghsoudi, H. and Soltanieh, M., 2014. Simultaneous separation of H_2S and CO_2 from CH_4 by a high silica CHA-type zeolite membrane. J. Membr. Sci., 470, 159-165. DOI: 10.1016/j.memsci.2014.07.025

Maguire-Boyle, S.J., Huseman, J.E., Ainscough, T.J., Oatley-Radcliffe, D.L., Alabdulkarem, A.A., Al-Mojil, S.F. and Barron, A.R., 2017. Superhydrophilic functionalization of microfiltration ceramic membranes enables separation of hydrocarbons from frac and produced water. Sci. Rep., 7,1-9. DOI: 10.1038/s41598-017-12499-w

Maher, A., Sadeghi, M. and Moheb, A., 2014. Heavy metal elimination from drinking water using nanofiltration membrane technology and process optimization using response surface methodology. Desalin., 352, 166-173. DOI: 10.1016/j.desal.2014.08.023

Mahajani, V. V., Mokashi, S. M., Chemical project economics, second ed., Rajiv Beri, India, 2005.

Majhi, A., Monash, P. and Pugazhenthi, G., 2009. Fabrication and characterization of γ-Al_2O_3–clay composite ultrafiltration membrane for the separation of electrolytes from its aqueous solution. J. Membr. Sci., 340, 181-191. DOI: 10.1016/j.memsci.2009.05.030

Majouli, A., Younssi, S.A., Tahiri, S., Albizane, A., Loukili, H. and Belhaj, M., 2011. Characterization of flat membrane support elaborated from local Moroccan Perlite Desalin. 277, 61-66. DOI: 10.1016/j.desal.2011.04.003

Majouli, A., Tahiri, S., Younssi, S.A., Loukili, H. and Albizane, A., 2012. Elaboration of new tubular ceramic membrane from local Moroccan Perlite for microfiltration process. Application to treatment of industrial wastewaters. Ceram. Int. 38, 4295-4303. DOI: 10.1016/j.ceramint.2012.02.010

Malik, N., Bulasara, V.K. and Basu, S., 2020. Preparation of novel porous ceramic microfiltration membranes from fly ash, kaolin and dolomite mixtures. Ceram. Int. 46, 6889-6898. DOI: 10.1016/j.ceramint.2019.11.184

Malmali, M., Askegaard, J., Sardari, K., Eswaranandam, S., Sengupta, A. and Wickramasinghe, S.R., 2018. Evaluation of ultrafiltration membranes for treating poultry processing wastewater. J. Water. Process. Eng. 22, 218-226. DOI: 10.1016/j.jwpe.2018.02.010

Manni, A., Achiou, B., Karim, A., Harrati, A., Sadik, C., Ouammou, M., Younssi, S.A. and El Bouari, A., 2020. New low-cost ceramic microfiltration membrane made from natural magnesite for industrial wastewater treatment. J. Environ. Chem. Eng. 8, 103906. DOI: 10.1016/j.jece.2020.103906

Manikandan, N.A., Pakshirajan, K. and Pugazhenthi, G., 2019. A novel ceramic membrane assembly for the separation of polyhydroxybutyrate (PHB) rich Ralstonia eutropha biomass from culture broth. Process Saf. Environ. Prot. 126, 106-118. DOI: 10.1016/j.psep.2019.04.001

Manouchehri, M. and Kargari, A., 2017. Water recovery from laundry wastewater by the cross flow microfiltration process: A strategy for water recycling in residential buildings. J. Cleaner Prod., 168, 227-238. DOI: 10.1016/j.jclepro.2017.08.211

Marbelia, L., Mulier, M., Vandamme, D., Muylaert, K., Szymczyk, A. and Vankelecom, I.F., 2016. Polyacrylonitrile membranes for microalgae filtration: Influence of porosity, surface charge and microalgae species on membrane fouling. Algal Res., 19, 128-137. DOI: 10.1016/j.algal.2016.08.004

Mendoza-Roca, J.A., Galiana-Aleixandre, M.V., Lora-García, J. and Bes-Piá, A., 2010. Purification of tannery effluents by ultrafiltration in view of permeate reuse. Sep. Purif. Technol., 70, 296-301. DOI: 10.1016/j.seppur.2009.10.010

Meng, X., Guo, X., Zhong, Y., Pei, Y., Chen, N. and Xie, Q., 2019. Synthesis of a high-quality NaP zeolite from epidesmine by a hydrothermal method. Bull. Mater. Sci., 42, 1-8. DOI: 10.1007/s12034-019-1918-x

Mestre, S., Gozalbo, A., Lorente-Ayza, M.M. and Sánchez, E., 2019. Low-cost ceramic membranes: A research opportunity for industrial application. J. Eur. Ceram. Soc., 39, 3392-3407. DOI: 10.1016/j.jeurceramsoc.2019.03.054

Min, K.J., Kim, J.H. and Park, K.Y., 2021. Characteristics of heavy metal separation and determination of limiting current density in a pilot-scale electrodialysis process for plating wastewater treatment. Sci. Total Environ., 757, 143762. DOI: 10.1016/j.scitotenv.2020.143762

Mo, W., Soh, L., Werber, J.R., Elimelech, M. and Zimmerman, J.B., 2015. Application of membrane dewatering for algal biofuel. Algal Res., 11, 1-12. DOI: 10.1016/j.algal.2015.05.018

Mondal, S., 2016. Polymeric membranes for produced water treatment: an overview of fouling behavior and its control. Rev. Chem. Eng., 32, 611-628. DOI: 10.1515/revce-2015-0027

Mouiya, M., Abourriche, A., Bouazizi, A., Benhammou, A., El Hafiane, Y., Abouliatim, Y., Nibou, L., Oumam, M., Ouammou, M., Smith, A. and Hannache, H., 2018. Flat ceramic microfiltration membrane based on natural clay and Moroccan phosphate for desalination and industrial wastewater treatment. Desalin., 427, 42-50. DOI: 10.1016/j.desal.2017.11.005

Mourouzidis-Mourouzis, S.A. and Karabelas, A.J., 2006. Whey protein fouling of microfiltration ceramic membranes—pressure effects. J. Membr. Sci., 282, 124-132. DOI: 10.1016/j.memsci.2006.05.012

Munshi, F.M., Church, J., McLean, R., Maier, N., Sadmani, A.A., Duranceau, S.J. and Lee, W.H., 2018. Dewatering algae using an aquaporin-based polyethersulfone forward osmosis membrane. Sep. Purif. Technol., 204, 154-161. DOI: 10.1016/j.seppur.2018.04.077

Murthy, Z.V.P. and Choudhary, A., 2011. Separation of cerium from feed solution by nanofiltration. Desalination, 279, 428-432. DOI: 10.1016/j.desal.2011.06.014

Muthukrishnan, M. and Guha, B.K., 2008. Effect of pH on rejection of hexavalent chromium by nanofiltration. Desalin., 219, 171-178. DOI: 10.1016/j.desal.2007.04.054

Nabavi, M.S., Mohammadi, T. and Kazemimoghadam, M., 2014. Hydrothermal synthesis of hydroxy sodalite zeolite membrane: Separation of H_2/CH_4. Ceram. Int., 40, 5889-5896. DOI: 10.1016/j.ceramint.2013.11.033

Nasef, M.M. and Güven, O., 2012. Radiation-grafted copolymers for separation and purification purposes: Status, challenges and future directions. Prog. Polym. Sci., 37, 1597-1656. DOI: 10.1016/j.progpolymsci.2012.07.004

Nassar, M.Y. and Abdelrahman, E.A., 2017. Hydrothermal tuning of the morphology and crystallite size of zeolite nanostructures for simultaneous adsorption and photocatalytic degradation of methylene blue dye. J. Mol. Liq., 242, 364-374. DOI: 10.1016/j.molliq.2017.07.033

Nalaparaju, A., Wang, J. and Jiang, J., 2019. Enhancing water permeation through alumina membranes by changing from cylindrical to conical nanopores. Nanoscale, 11,9869-9878. DOI: 10.1039/C8NR09602C

Nandi, B.K., Uppaluri, R. and Purkait, M.K., 2008. Preparation and characterization of low cost ceramic membranes for micro-filtration applications. Appl. Clay Sci., 42, 102-110. DOI: 10.1016/j.clay.2007.12.001

Nandi, B.K., Das, B., Uppaluri, R. and Purkait, M.K., 2009. Microfiltration of mosambi juice using low cost ceramic membrane. J. Food. Eng. 95, 597-605. DOI: 10.1016/j.jfoodeng.2009.06.024.

Nayak, V., Balakrishna, R.G., Padaki, M. and Soontarapa, K., 2017. Zwitterionic ultrafiltration membranes for As(V) rejection. Chem. Eng. J., 308, 347-358. DOI: 10.1016/j.cej.2016.09.096

Obotey Ezugbe, E. and Rathilal, S., 2020. Membrane technologies in wastewater treatment: a review. Membranes, 10, 89. DOI: 10.3390/membranes10050089

Olabarrieta, J., Monzón, O., Belaustegui, Y., Alvarez, J.I. and Zorita, S., 2018. Removal of TiO_2 nanoparticles from water by low pressure pilot plant filtration. Sci. Total Environ. 618, 551-560. DOI: 10.1016/j.scitotenv.2017.11.003

Olguín, E.J., 2012. Dual-purpose microalgae–bacteria-based systems that treat wastewater and produce biodiesel and chemical products within a Biorefin. Biotechnol. Adv., 30, 1031-1046. DOI: 10.1016/j.biotechadv.2012.05.001

Oun, A., Tahri, N., Mahouche-Chergui, S., Carbonnier, B., Majumdar, S., Sarkar, S., Sahoo, G.C. and Amar, R.B., 2017. Tubular ultrafiltration ceramic membrane based on titania nanoparticles immobilized on macroporous clay-alumina support: elaboration, characterization and application to dye removal. Sep. Purif. Technol., 188, 126-133. DOI: 10.1016/j.seppur.2017.07.005

Ozel, H.U., 2012. Biosorption of Cd (II) ions by nordmann fir cones. Fresenius Environ. Bull., 21, 2527-2535

Pan, J., Liu, L., Tao, Y., Zhao, L., Yu, X., Wu, B., Zhao, X. and Liu, L., 2021. Green Fabrication of Tertrabutylammonium Styrene Sulfonate Cation-Exchange Membranes via a Solvent-Free Photopolymerization Strategy. Ind. Eng. Chem. Res. DOI: 10.1021/acs.iecr.1c03274

Panagopoulos, A., 2021. Beneficiation of saline effluents from seawater desalination plants: fostering the zero liquid discharge (ZLD) approach-A techno-economic evaluation. J. Environ. Chem. Eng., 9, 105338. DOI: 10.1016/j.jece.2021.105338

Pan, M. and Lin, Y.S., 2001. Template-free secondary growth synthesis of MFI type zeolite membranes. Microporous Mesoporous Mater., 43, 319-327. DOI: 10.1016/S1387-1811(01)00212-8

Park, S.H., Park, Y.G., Lim, J.L. and Kim, S., 2014. Evaluation of ceramic membrane applications for water treatment plants with a life cycle cost analysis. Desalin. Water Treat., 54, 973-979. DOI: 10.1080/19443994.2014.912162

Paul, T., Baskaran, D., Pakshirajan, K. and Pugazhenthi, G., 2019. Continuous bioreactor with cell recycle using tubular ceramic membrane for simultaneous wastewater treatment and bio-oil production by oleaginous *Rhodococcus opacus*. Chem. Eng. J., 367, 76-85. DOI: 10.1016/j.cej.2019.02.050

Paul, T., Baskaran, D., Pakshirajan, K., Pugazhenthi, G., & Rajamanickam, R. (2021). Bio-oil production by hydrothermal liquefaction of *Rhodococcus opacus* biomass utilizing refinery wastewater: Biomass valorization and process optimization. Environ. Technol. Innovation, 21, 101326. DOI: 10.1016/j.eti.2020.101326

Peydayesh, M., Mohammadi, T. and Nikouzad, S.K., 2020. A positively charged composite loose nanofiltration membrane for water purification from heavy metals. J. Membr. Sci., 611, 118205. DOI: 10.1016/j.memsci.2020.118205

Petrusevski, B., Bolier, G., Van Breemen, A.N. and Alaerts, G.J., 1995. Tangential flow filtration: a method to concentrate freshwater algae. Water Res., 29, 1419-1424. DOI: 10.1016/0043-1354(94)00269-D

Potdar, A., Shukla, A. and Kumar, A., 2002. Effect of gas phase modification of analcime zeolite composite membrane on separation of surfactant by ultrafiltration. J. Membr. Sci., 210, 209-225. DOI: 10.1016/S0376-7388(02)00324-1

Purwanti, I.F., Kurniawan, S.B., Ismail, N.I., Imron, M.F. and Abdullah, S.R.S., 2019. Aluminium removal and recovery from wastewater and soil using isolated indigenous bacteria. J. Environ. Manage. 249, 109412. DOI: 10.1016/j.jenvman.2019.109412

Qin, G., Lü, X., Wei, W., Li, J., Cui, R. and Hu, S., 2015. Microfiltration of kiwifruit juice and fouling mechanism using fly-ash-based ceramic membranes. Food Bioprod. Process. 96278-284. DOI: 10.1016/j.fbp.2015.09. 006.

Raj, D. and Antil, R.S., 2011. Evaluation of maturity and stability parameters of composts prepared from agro-industrial wastes. Bioresour. Technol., 102, 2868-2873. DOI: 10.1016/j.biortech.2010.10.077

Rani, S.L.S. and Kumar, R.V., 2021. Insights on applications of low-cost ceramic membranes in wastewater treatment: A mini-review. Case Studies in Chemical and Environmental Engineering, 4, p.100149. DOI: 10.1016/j.cscee.2021.100149

Rashad, M., Logesh, G., Sabu, U. and Balasubramanian, M., 2021. A novel monolithic mullite microfiltration membrane for oil-in-water emulsion separation. J. Membr. Sci., 620, 118857. DOI: 10.1016/j.memsci.2020.118857

Ravanchi, M.T., Kaghazchi, T. and Kargari, A., 2009. Application of membrane separation processes in petrochemical industry: a review. Desalin., 235, 199-244. DOI: 10.1016/S0376-7388(00)85121-2

Rawat, M. and Bulasara, V.K., 2018. Synthesis and characterization of low-cost ceramic membranes from fly ash and kaolin for humic acid separation. Korean J. Chem. Eng., 35, 725-733. DOI: 10.1007/s11814-017-0316-6

Resasco, D.E., Crossley, S.P., Wang, B. and White, J.L., 2021. Interaction of water with zeolites: a review. Catalysis Rev., 63,302-362. DOI: 10.1080/01614940.2021.1948301

Riley, S.M., Oliveira, J.M., Regnery, J. and Cath, T.Y., 2016. Hybrid membrane bio-systems for sustainable treatment of oil and gas produced water and fracturing flowback water. Sep. Purif. Technol., 171, 297-311. DOI: 10.1016/j.seppur.2016.07.008

Rossi, N., Jaouen, P., Legentilhomme, P. and Petit, I., 2004. Harvesting of cyanobacterium Arthrospira platensis using organic filtration membranes. Food Bioprod. Process. 82, 244-250. DOI: 10.1205/fbio.82.3.244.44177

Sadegh, H. and Ali, G.A., 2021. Potential applications of nanomaterials in wastewater treatment: nanoadsorbents performance. In Research Anthology on Synthesis, Characterization, and Applications of Nanomaterials (pp. 1230-1240). IGI Global. DOI: 10. 4018/978-1-5225-5754-8.ch004

Saffaj, N., Persin, M., Younsi, S.A., Albizane, A., Cretin, M. and Larbot, A., 2006. Elaboration and characterization of microfiltration and ultrafiltration membranes deposited on raw support prepared from natural Moroccan clay: application to filtration of solution containing dyes and salts. Appl. Clay Sci., 31, 110-119. DOI: 10.1016/j.clay.2005.07.002

Salehi, E., Khajavian, M., Sahebjamee, N., Mahmoudi, M., Drioli, E. and Matsuura, T., 2022. Advances in nanocomposite and nanostructured chitosan membrane adsorbents for environmental remediation: a review. Desalin., 527, 115565. DOI: 10.1016/j.desal.2022.115565

Sahnoun, R.D. and Baklouti, S., 2013. Characterization of flat ceramic membrane supports prepared with kaolin-phosphoric acid-starch. Appl. Clay. Sci. 83, 399-404. DOI: 0.1016/j.clay.2013.07.015.

Salim, M.M. and Malek, N.A.N.N., 2016. Characterization and antibacterial activity of silver exchanged regenerated NaY zeolite from surfactant-modified NaY zeolite. Mater. Sci. Eng., C, 59, 70-77. DOI: 10.1016/j.msec.2015.09.099

Saikia, B.J. and Parthasarathy, G., 2010. Fourier transform infrared spectroscopic characterization of kaolinite from Assam and Meghalaya, Northeastern India. J. Mod. Phys, 1, 206-210. DOI: 10.4236/jmp.2010.14031

Sert, Ş., Kütahyali, C., İnan, S., Talip, Z., Çetinkaya, B. and Eral, M., 2008. Biosorption of lanthanum and cerium from aqueous solutions by Platanus orientalis leaf powder. Hydrometallurgy, 90, 13-18. DOI: 10.1016/j.hydromet.2007.09.006

Selatile, M.K., Ray, S.S., Ojijo, V. and Sadiku, R., 2018. Recent developments in polymeric electrospun nanofibrous membranes for seawater desalination. RSC Adv., 8, 37915-37938. DOI: 10.1039/C8RA07489E

Sebastian, V., Mallada, R., Coronas, J., Julbe, A., Terpstra, R.A. and Dirrix, R.W., 2010. Microwave-assisted hydrothermal rapid synthesis of capillary MFI-type zeolite–ceramic membranes for pervaporation application. J. Membr. Sci., 355, 28-35. DOI: 10.1016/j.memsci.2010.02.073

Sgarlata, C., Arena, G., Longo, E., Zhang, D., Yang, Y. and Bartsch, R.A., 2008. Heavy metal separation with polymer inclusion membranes. J. Membr. Sci., 323, 444-451. DOI: 10.1016/j.memsci.2008.07.004

Shahnaz, T., Priyan, V.V., Jayakumar, A. and Narayanasamy, S., 2022. Magnetic nanocellulose from Cyperus rotundas grass in the absorptive removal of rare earth element cerium (III): Toxicity studies and interpretation. Chemosphere, 287, p.131912. DOI: 10.1016/j.chemosphere.2021.131912

Shams Ashaghi, K., Ebrahimi, M. and Czermak, P.J.O.E.S., 2007. Ceramic ultra-and nanofiltration membranes for oilfield produced water treatment: a mini review. Open Environ. Sci., 1. DOI: 10.2174/1876325100701010001

Shen, Y., Yuan, W., Pei, Z.J., Wu, Q. and Mao, E., 2009. Microalgae mass production methods. Trans. Asabe., 52, 1275-1287. DOI: 10.13031/2013.27771

Shon, H.K., Phuntsho, S., Chaudhary, D.S., Vigneswaran, S., Cho, J., 2013. Nanofiltration for water and wastewater treatment–a mini review. Drink Water Eng Sci. 6, 47-53. DOI: 10.5194/dwes-6-47-2013.

Shokrkar, H., Salahi, A., Kasiri, N. and Mohammadi, T., 2012. Prediction of permeation flux decline during MF of oily wastewater using genetic programming. Chem. Eng. Res. Des., 90, 846-853. DOI: 10.1016/j.cherd.2011.10.002

Shukla, A. and Kumar, A., 2005. Characterization of chemically modified zeolite–clay composite membranes using separation of trivalent cations. Separation and purification technology, 41, 83-89. DOI: 10.1016/j.seppur.2004.05.001

Shukla, R., Tandon, R., Nguyen, M. and Cheryan, M., 2000. Microfiltration of starch suspensions using a tubular stainless steel membrane. Membr. Technol. 120, 5-8. DOI: 10.1016/S0958-2118(00)88585-7.

Siciliano, A., Guida, M., Pagano, G., Trifuoggi, M., Tommasi, F., Lofrano, G., Suarez, E.G.P., Gjata, I., Brouziotis, A.A., Liguori, R. and Libralato, G., 2021. Cerium, gadolinium, lanthanum, and neodymium effects in simplified acid mine discharges to Raphidocelis subcapitata, Lepidium sativum, and Vicia faba. Sci. Total Environ., 787, 147527. DOI: 10.1016/j.scitotenv.2021.147527

Singh, P., Manikandan, N.A., Purnima, M., Pakshirajan, K. and Pugazhenthi, G., 2020. Recovery of lignin from water and methanol using low-cost kaolin based tubular ceramic membrane. J. Water Process Eng., 38, 101615. DOI: 10.1016/j.jwpe.2020.101615

Slaninova, A., Machova, J. and Svobodova, Z., 2014. Fish kill caused by aluminium and iron contamination in a natural pond used for fish rearing: a case report. Veterinarni Medicina, 59(11).

Singh, D.N. and Kolay, P.K., 2002. Simulation of ash–water interaction and its influence on ash characteristics. Prog. Energy Combust. Sci., 28, 267-299. DOI: 10.1016/S0360-1285(01)00018-1

Singh, G. and Patidar, S.K., 2018. Microalgae harvesting techniques: A review. J. Environ. Manage., 217, 499-508. DOI: 10.1016/j.jenvman.2018.04.010

Sun, C., Srivastava, D.J., Grandinetti, P.J., and Dutta, P.K., 2016. Synthesis of chabazite/polymer composite membrane for CO_2/N_2 separation. Microporous Mesoporous Mat., 230, 20.8-216. DOI: 10.1016/j.micromeso.2016.04.042

Sunil, K., Karunakaran, G., Yadav, S., Padaki, M., Zadorozhnyy, V. and Pai, R.K., 2018. Al-Ti_2O_6 a mixed metal oxide based composite membrane: A unique membrane for removal of heavy metals. Chem. Eng. J., 348, 678-684. DOI: 10.1016/j.cej.2018.05.017

Sushma, C., Chandan, D. and Ramagopal, U., 2020. Feasibility of low-cost kaolin–based ceramic membranes for organic Lagernaria siceraria juice production. Food Bioprocess Technol. 13, 1009-1023. DOI:10.1007/s11947-020-02455-4

Suresh, K., Pugazhenthi, G. and Uppaluri, R., 2016. Fly ash based ceramic microfiltration membranes for oil-water emulsion treatment: Parametric optimization using response surface methodology. J. Water. Process. Eng. 13, 27-43. DOI: 10.1016/j.jwpe.2016.07.008

Tang, T., Zhang, Z. and Zhu, X., 2019. Toxic effects of TiO_2 NPs on zebrafish Int. J. Environ. Res. Public Health. 16, 523. DOI: 10.3390/ijerph16040523

Tanudjaja, H.J., Tarabara, V.V., Fane, A.G. and Chew, J.W., 2017. Effect of cross-flow velocity, oil concentration and salinity on the critical flux of an oil-in-water emulsion in microfiltration. J. Membr. Sci. 530, 11-19. DOI: 10.1016/j.memsci.2017.02.011

Tavolaro, A. and Tavolaro, P., 2007. LTA zeolite composite membrane preparation, characterization and application in a zeolitic membrane reactor. Catalysis Communications, 8, 789-794. DOI: 10.1016/j.catcom.2006.09.001

Taylor, A.T., Iraganje, E. and Lai, E.P., 2020. A method for the separation of TiO_2 nanoparticles from Water through encapsulation with lecithin liposomes followed by adsorption onto poly (L-lysine) coated glass surfaces. Colloids Surf., B 187, 110732. DOI: 10.1016/j.colsurfb.2019.110732

Thamaphat, K., Limsuwan, P. and Ngotawornchai, B., 2008. Phase characterization of TiO_2 powder by XRD and TEM. Agric. Nat. Sci, 42, 357-361

Thong, Z., Han, G., Cui, Y., Gao, J., Chung, T.S., Chan, S.Y. and Wei, S., 2014. Novel nanofiltration membranes consisting of a sulfonated pentablock copolymer rejection layer for heavy metal removal. Environ. Sci. Technol., 48, 13880-13887. DOI: 10.1021/es5031239

Tibi, F., Charfi, A., Cho, J. and Kim, J., 2020. Fabrication of polymeric membranes for membrane distillation process and application for wastewater treatment: Critical review. Process Saf. Environ. Prot., 141, 190-201. DOI: 10.1016/j.psep.2020.05.026

Ummalyma, S.B., Gnansounou, E., Sukumaran, R.K., Sindhu, R., Pandey, A. and Sahoo, D., 2017. Bioflocculation: an alternative strategy for harvesting of microalgae–an overview. Bioresour. Technol., 242, 227-235. DOI: 10.1016/j.biortech.2017.02.097

Ulbricht, M., 2004. Membrane separations using molecularly imprinted polymers. Journal of chromatography B, 804, 113-125. DOI: 10.1016/j.jchromb.2004.02.007

Van der Bruggen, B., Vandecasteele, C., Van Gestel, T., Doyen, W. and Leysen, R., 2003. A review of pressure-driven membrane processes in wastewater treatment and drinking water production. Environ. Prog., 22, 46-56. DOI: 10.1002/ep.670220116

Van Heyden, H., Mintova, S. and Bein, T., 2008. Nanosized SAPO-34 synthesized from colloidal solutions. Chem. Mater., 20, 2956-2963. DOI: 10.1021/cm703541w

Vijayaraghavan, K., Sathishkumar, M. and Balasubramanian, R., 2010. Biosorption of lanthanum, cerium, europium, and ytterbium by a brown marine alga, Turbinaria conoides. Ind. Eng. Chem. Res., 49, 4405-4411. DOI: 10.1021/ie1000373

Vasanth, D., Pugazhenthi, G. and Uppaluri, R., 2011. Fabrication and properties of low cost ceramic microfiltration membranes for separation of oil and bacteria from its solution. J. Membr. Sci., 379, 154-163. DOI: 10.1016/j.memsci.2011.05.050

Vasanth, D., Pugazhenthi, G. and Uppaluri, R., 2012. Biomass assisted microfiltration of chromium (VI) using Baker's yeast by ceramic membrane prepared from low cost raw materials Desalin. 285, 239-244. DOI: 10.1016/j.desal.2011.09.055.

Vela, M.C.V., Blanco, S.Á., García, J.L. and Rodríguez, E.B., 2008. Analysis of membrane pore blocking models applied to the ultrafiltration of PEG. Sep. Purif. Technol., 62, 489-498. DOI: 10.1016/j.seppur.2008.02.028

Von Clausbruch, S.C., Schweiger, M., Höland, W. and Rheinberger, V., 2000. The effect of P_2O_5 on the crystallization and microstructure of glass-ceramics in the SiO_2–Li_2O–K_2O–ZnO–P_2O_5 system. J. Non-Cryst. Solids, 263, 388-394. DOI: 10.1016/S0022-3093(99)00647-X

Vyas, H.K., Bennett, R.J. and Marshall, A.D., 2000. Influence of feed properties on membrane fouling in crossflow microfiltration of particulate suspensions. Int. Dairy J., 855-861. DOI: 10.1016/S0958-6946(01)00030-9.

Vu, D.Q., Koros, W.J. and Miller, S.J., 2002. High pressure CO_2/CH_4 separation using carbon molecular sieve hollow fiber membranes. Ind. Eng. Chem. Res., 41, 367-380. DOI: 10.1021/ie010119w

Wang, X., Meng, B., Zhang, X., Tan, X. and Liu, S., 2014. Synthesis of stable Ti-containing mesoporous tubular membrane using silicalite-1 nanoparticles as seeds. Chem. Eng. J., 255, 344-355. DOI: 10.1016/j.cej.2014.06.051

Wang, Y.H., Zhang, Y., Liu, X. and Meng, G.Y., 2006. Microstructure control of ceramic membrane support from corundum-rutile powder mixture. Powder Technol., 168, 125-133. DOI: 10.1016/j.powtec.2006.07.010

Wang, Z., Wu, Z. and Tang, S., 2009. Extracellular polymeric substances (EPS) properties and their effects on membrane fouling in a submerged membrane bioreactor. Water Res., 43, 2504-2512. DOI: 10.1016/j.watres.2009.02.026

Wang, X., Sun, K., Zhang, G., Yang, F., Lin, S. and Dong, Y., 2022. Robust zirconia ceramic membrane with exceptional performance for purifying nano-emulsion oily wastewater. Water Res., 208, 117859. DOI: 10.1016/j.watres.2021.117859

Wang, H.T., Ye, Y.Y., Qi, J., Li, F.T. and Tang, Y.L., 2013. Removal of titanium dioxide nanoparticles by coagulation: effects of coagulants, typical ions, alkalinity and natural organic matters. Water. Sci. Technol. 68, 1137-1143. DOI: 10.2166/wst.2013.356.

Wang, P., Qi, N., Ao, Y., Hou, J., Wang, C. and Qian, J., 2016. Effect of UV irradiation on the aggregation of TiO2 in an aquatic environment: Influence of humic acid and pH. Environ. Pollut. 212, 178-187. DOI: 10.1016/j.envpol.2016.01.030

Waszak, M. and Gryta, M., 2016. The ultrafiltration ceramic membrane used for broth separation in membrane bioreactor. Chem. Eng. J., 305, 129-135. DOI: 10.1016/j.cej.2015.11.058

Wei, X., Hong, J., Zhu, S., Chen, J. and Lv, B., 2017. Structure–performance study of polyamide composite nanofiltration membranes prepared with polyethyleneimine. Journal of Materials Science, 52, 11701-11714. DOI: 10.1007/s10853-017-1225-0

Wei, Z., Hu, Y., Han, H., Sun, W., Wang, R., Sun, W., Wang, J., Gao, Z., Wang, L., Zhang, C. and Sun, L., 2019. Selective separation of scheelite from calcite by self-assembly of H_2SiO_3 polymer using Al^{3+} in Pb-BHA flotation. Mineral., 9, 43. DOI: 10.3390/min9010043

Weimin, X.I. and Geissen, S.U., 2001. Separation of titanium dioxide from photocatalytically treated water by cross-flow microfiltration. Water. Res. 35, 1256-1262. https://doi.org/10.1016/S0043-1354(00)00378-X

Weir, A., Westerhoff, P., Fabricius, L., Hristovski, K. and Von Goetz, N., 2012. Titanium dioxide nanoparticles in food and personal care products. Environ. Sci. Technol. 46, 2242-2250. DOI: 10.1021/es204168d.

Weschenfelder, S.E., Borges, C.P. and Campos, J.C., 2015a. Oilfield produced water treatment by ceramic membranes: Bench and pilot scale evaluation. J. Membr. Sci., 495, 242-251. DOI: 10.1016/j.memsci.2015.08.028

Weschenfelder, S.E., Louvisse, A.M., Borges, C.P., Meabe, E., Izquierdo, J. and Campos, J.C., 2015b. Evaluation of ceramic membranes for oilfield produced water treatment aiming reinjection in offshore units. J. Pet. Sci. Eng., 131, 51-57. DOI: 10.1016/j.petrol.2015.04.019

Winter, O., 1969. Preliminary economic evaluation of chemical processes at the research level. Ind. Eng. Chem. 61, 45-52.

Workneh, S. and Shukla, A., 2008. Synthesis of sodalite octahydrate zeolite-clay composite membrane and its use in separation of SDS. J. Membr. Sci., 309, 189-195. DOI: 10.1016/j.memsci.2007.10.033

Wu, S., Yang, J., Lu, J., Zhou, Z., Kong, C. and Wang, J., 2008. Synthesis of thin and compact mesoporous MCM-48 membrane on vacuum-coated α-Al_2O_3 tube. J. Membr. Sci., 319, 231-237. DOI: 10.1016/j.memsci.2008.03.057

Wu, Z., Faiz, R., Li, T., Kingsbury, B.F. and Li, K., 2013. A controlled sintering process for more permeable ceramic hollow fibre membranes. J. Membr. Sci., 446, 286-293. DOI: 10.1016/j.memsci.2013.05.040

Wu, T., Diaz, M.C., Zheng, Y., Zhou, R., Funke, H.H., Falconer, J.L. and Noble, R.D., 2015. Influence of propane on CO_2/CH_4 and N_2/CH_4 separations in CHA zeolite membranes. J. Membr. Sci., 473, pp.201-209. DOI: 10.1016/j.memsci.2014.09.021

Xiao, R. and Zheng, Y., 2016. Overview of microalgal extracellular polymeric substances (EPS) and their applications. Biotechnol. Adv., 34, 1225-1244. DOI: 10.1016/j.biotechadv.2016.08.004

Xu, R., 2008. Progress in nanoparticles characterization: Sizing and zeta potential measurement. Particuology, 6, 112-115. DOI: 10.1016/j.partic.2007.12.002.

Xu, A., Yang, A., Young, S., demontigny, D. and Tontiwachwuthikul, P., 2008. Effect of internal coagulant on effectiveness of polyvinylidene fluoride membrane for carbon dioxide separation and absorption. J. Membr. Sci., 311, 153-158. DOI: 10.1016/j.memsci.2007.12.008

Yahaya, S., Jikan, S.S., Badarulzaman, N.A. and Adamu, A.D., 2017. Chemical composition and particle size analysis of kaolin. Path of Sci., 3, 1001-1004.

Yang, X., Zhou, S., Li, M., Wang, R. and Zhao, Y., 2017. Purification of cellulase fermentation broth via low cost ceramic microfiltration membranes with nanofibers-like attapulgite separation layers. Sep. Purif. Technol. 175, 435-442. DOI: 10.1016/j.seppur.2016.11.012.

Yang, L., Wang, L., Ren, S., Pan, B., Li, J., Zhang, X., Chen, Y. and Hu, Q., 2019. Harvesting of Scenedesmus acuminatus using ultrafiltration membranes operated in alternative feed directions. J. Biosci. Bioeng., 128, 103-109. DOI: 10.1016/j.jbiosc.2019.01.007

Zarghami, S., Mohammadi, T. and Sadrzadeh, M., 2019. Preparation, characterization and fouling analysis of in-air hydrophilic/underwater oleophobic bio-inspired polydopamine coated PES membranes for oily wastewater treatment. J. Membr. Sci., 582, 402-413. DOI: 10.1016/j.memsci.2019.04.020

Zawrah, M.F., Khattab, R.M., Girgis, L.G., El Shereefy, E.E. and Sawan, S.A., 2014. Effect of CTAB as a foaming agent on the properties of alumina ceramic membranes. Ceram. Int., 40, 5299-5305. DOI: 10.1016/j.ceramint.2013.10.106

Zhang, X., Hu, Q., Sommerfeld, M., Puruhito, E. and Chen, Y., 2010. Harvesting algal biomass for biofuels using ultrafiltration membranes. Bioresour. Technol., 101, 5297-5304. DOI: 10.1016/j.biortech.2010.02.007

Zhang, H., Quan, X., Chen, S., Zhao, H., Zhao, Y. and Li, W., 2006. Zirconia and titania composite membranes for liquid phase separation: preparation and characterization Desalin. 190, 172-180. DOI: 10.1016/j.desal.2005.08.008.

Zhang, G., Zhang, J., Wang, L., Meng, Q. and Wang, J., 2012. Fouling mechanism of low-pressure hollow fiber membranes used in separating nanosized photocatalyst. J. Membr. Sci. 389,532-543. DOI: 10.1016/j.memsci.2011.11.027

Zhang, H., Ma, Y., Song, K., Zhang, Y. and Tang, Y., 2013. Nano-crystallite oriented self-assembled ZSM-5 zeolite and its LDPE cracking properties: effects of accessibility and strength of acid sites. J. Catal., 302, 115-125. DOI: 10.1016/j.jcat.2013.03.019

Zhang, X., Fan, L. and Roddick, F.A., 2013. Understanding the fouling of a ceramic microfiltration membrane caused by algal organic matter released from Microcystis aeruginosa. J. Membr. Sci., 447, 362-368. DOI: 10.1016/j.memsci.2013.07.059

Zhang, W. and Ding, L., 2015. Investigation of membrane fouling mechanisms using blocking models in the case of shear-enhanced ultrafiltration. Separation and Purification Technology, 141, pp.160-169. DOI: 10.1016/j.seppur.2014.11.041

Zhang, S., Peh, M.H., Thong, Z. and Chung, T.S., 2015a. Thin film interfacial cross-linking approach to fabricate a chitosan rejecting layer over poly (ether sulfone) support for heavy metal removal. Ind. Eng. Chem. Res., 54, 472-479. DOI: 10.1021/ie503809c

Zhang, Y., Zhang, S. and Chung, T.S., 2015b. Nanometric graphene oxide framework membranes with enhanced heavy metal removal via nanofiltration. Environ. Sci. Technol., 49, 10235-10242. DOI: 10.1021/acs.est.5b02086

Zhang, W., Ding, L., Luo, J., Jaffrin, M.Y. and Tang, B., 2016. Membrane fouling in photocatalytic membrane reactors (PMRs) for water and wastewater treatment: A critical review. Chem. Eng. J., 302, 446-458. DOI: 10.1016/j.cej.2016.05.071

Zhang, B., Yu, S., Zhu, Y., Shen, Y., Gao, X., Shi, W. and Tay, J.H., 2019. Efficiencies and mechanisms of the chemical cleaning of fouled polytetrafluoroethylene (PTFE) membranes during the microfiltration of alkali/surfactant/polymer flooding oilfield wastewater. RSC Adv., 9, 36940-36950. DOI: 10.1039/C9RA06745K

Zhang, S., Lv, T., Feng, Z., Liu, X., Wang, Y. and Meng, C., 2020. Solid-State and Organic Template-Free Synthesis of Zeolite Omega by Conversion of Magadiite in the Presence of Seed Crystals and Investigation of Conversion Mechanism. Ind. Eng. Chem. Res., 59, 19574-19583. DOI: 10.1021/acs.iecr.0c01212

Zhao, Y., Zhong, J., Li, H., Xu, N. and Shi, J., 2002. Fouling and regeneration of ceramic microfiltration membranes in processing acid wastewater containing fine TiO_2 particles. J. Membr. Sci. 208, 331-341. DOI: 10.1016/S0376-7388(02)00314-9

Zhao, Y., Zhang, Y., Xing, W. and Xu, N., 2005. Influences of pH and ionic strength on ceramic microfiltration of TiO_2 suspensions. Desalin. 177, 59-68. DOI: 10.1016/j.desal.2004.10.032.

Zheng, Y., Hu, N., Wang, H., Bu, N., Zhang, F. and Zhou, R., 2015. Preparation of steam-stable high-silica CHA (SSZ-13) membranes for CO_2/CH_4 and C2H4/C2H6 separation. J. Membr. Sci., 475, 303-310. DOI: 10.1016/j.memsci.2014.10.048

Zhou, M.Y., Zhang, P., Fang, L.F., Zhu, B.K., Wang, J.L., Chen, J.H. and Abdallah, H., 2019. A positively charged tight UF membrane and its properties for removing trace metal cations via electrostatic repulsion mechanism. J. Hazard. Mater., 373, 168-175. DOI: 10.1016/j.jhazmat.2019.03.088

Zhu, B., Myat, D.T., Shin, J.W., Na, Y.H., Moon, I.S., Connor, G., Maeda, S., Morris, G., Gray, S. and Duke, M., 2015. Application of robust MFI-type zeolite membrane for desalination of saline wastewater. J. Membr. Sci., 475, 167-174. DOI: 10.1016/j.memsci.2014.09.058

Zhu, L., Chen, M., Dong, Y., Tang, C.Y., Huang, A. and Li, L., 2016. A low-cost mullite-titania composite ceramic hollow fiber microfiltration membrane for highly efficient separation of oil-in-water emulsion. Water Res., 90, 277-285. DOI: 10.1016/j.watres.2015.12.035

Zhu, L., Ji, J., Wang, S., Xu, C., Yang, K. and Xu, M., 2018. Removal of Pb(II) from wastewater using Al_2O_3-NaA zeolite composite hollow fiber membranes synthesized from solid waste coal fly ash. Chemosphere, 206, 278-284. DOI: 10.1016/j.chemosphere.2018.05.001

Zou, S., Gu, Y., Xiao, D. and Tang, C.Y., 2011. The role of physical and chemical parameters on forward osmosis membrane fouling during algae separation. J. Membr. Sci., 366, 356-362. DOI: 10.1016/j.memsci.2010.10.030

Zola, A.S., Barros, M.A.S.D., Sousa-Aguiar, E.F. and Arroyo, P.A., 2012. Determination of the maximum retention of cobalt by ion exchange in h-zeolites. Braz. J. Chem. Eng., 29, 385-392. DOI: 10.1590/S0104-66322012000200018

Zsirai, T., Al-Jaml, A.K., Qiblawey, H., Al-Marri, M., Ahmed, A., Bach, S., Watson, S. and Judd, S., 2016. Ceramic membrane filtration of produced water: Impact of membrane module. Sep. Purif. Technol., 165, 214-221. DOI: 10.1016/j.seppur.2016.04.001

Appendix

Detailed Cost analysis of Kaolin-HPMC membrane fabrication

The membrane cost was evaluated based on the costs for raw materials, labor, laboratory, equipment, depreciation, maintenance and electricity in USD and as detailed below.

1. Labor cost

$$C_a = \text{manpower cost per day} \times \text{total number of working days} \quad \text{(A.1)}$$

Where C_a is the total labor cost

2. Laboratory cost

$$C_b = 20\% \text{ of labor cost} \quad \text{(A.2)}$$

Where C_b laboratory cost (Winter 1969)

3. Equipment cost

$$C_c = \left(\frac{\text{Book value} \times \text{time of equipment use}}{\text{Service life} \times \text{total working hours/year}} \right) \quad \text{(A.3)}$$

Where C_c is the total equipment cost

4. Depreciation cost

Depreciation cost was calculated by using straight line method (Mahajani 2005; Winter 1969)

$$D_{SLM} = \frac{(V_0 - V_s) \times t}{n} \quad \text{(A.4)}$$

Where D_{SLM} – Depreciation cost, V_0 – original value of the equipment, V_s – salvage value of the equipment, n- life span of the equipment, t- total working hours.

5. Repair and maintenance cost

$$C_e = \frac{1\% \times \text{Fixed capital cost}}{\text{Day}} \quad \text{(A.5)}$$

Where C_e is the repair and maintenance cost (Winter 1969)

6. Electricity cost

$$C_f = \text{Power requirement} \times \text{time of equipment use} \times \text{electricity tariff} \quad \text{(A.6)}$$

where C_f is the total electricity cost

Calculations

Basis:

1. Kaolin based tubular ceramic membrane (Kaolin-HPMC) was fabricated with the following dimensions: Outer Diameter (OD): 11.5 mm; Inner Diameter (ID): 5.5 mm; Length (L): 100 mm.
2. Membrane filtration area = 17.27×10^{-4} m^2
3. For each batch, 60 membranes were fabricated according to the furnace capacity available for sintering process.
4. Total number of working days in a year = 330 (Salehi et al., 2014)

A. Raw material cost

Weight of one membrane (g) = 11.5

Weight required for preparing 60 membranes (g) = 690

Table A.1 Cost of the raw materials used in this study

Material	Weight required for preparing 60 membranes (kg)	Unit price (USD[#]/kg)	Cost of raw material for the fabrication of 60 membranes (USD)
Kaolin	0.337	0.16	0.054
Quartz	0.1687	0.27	0.0456
Calcium carbonate	0.1687	8.08	1.3635
HPMC	0.015	34.2	0.513
Total cost for preparing 60 membranes (USD)			1.9761

[#]1 USD = 74.0 INR (8th November 2021)

B. Labor cost

Basis:

Labor cost in India is 6.75 USD/day for total 8 working hours per day (Sushma et al., 2020).

Total working days to make 60 tubular membranes = 1

Labor cost for preparing 60 membranes (USD) = 6.75

C. Laboratory cost = 1.351

D. Equipment cost

The membranes were extruded by extrusion machine. The membranes were sequentially dried using hot air oven first at 100 ^{o}C for 12 h and 200 ^{o}C for 12 h to reduce crack formation. Further, in furnace, sintering was carried out by raising temperature from 200 ^{o}C to 950 ^{o}C at a heating rate of 0.5 ^{o}C/min and the membranes were sintered at 950 ^{o}C for 6 h. Finally, membranes were polished with C-220 SiC abrasive paper and sonicated to remove loosely bounded particles from the membrane. Total equipment cost was calculated based on the following:

Table A. 2 Book value of each equipment used for fabrication of tubular ceramic membrane

Equipment used	**Book value (USD)**
Extruder	4041
Hot air oven	547.9
Bath sonicator	479.5
Furnace	2054.8
Fixed capital cost	**7123.2**

Basis: Life span of equipment is 10 years

1. Extruder

$$\text{Cost for 1 h use (USD)} = \frac{4041}{10 \times 330 \times 24} = 0.051$$

Total time of use to prepare 60 membranes (h) = 3.75

Cost for preparing 60 membrane (USD) = $0.051 \times 3.75 = 0.1912$

Table A. 3 Equipment cost for fabrication of tubular ceramic membrane

Equipment used	Cost for 1 h use (USD)	Time of use (h)	Cost for preparing 60 membranes (USD)
Extruder	0.051	3.75	0.1912
Hot air oven	6.918×10^{-3}	24	0.166
Furnace	0.0259	31	0.8
Bath sonicator	6.054×10^{-3}	0.33	1.99×10^{-3}
Total cost of equipment used for preparing 60 membranes (USD)			**1.1592**

E. Depreciation cost

Basis:

1. Salvage value of equipment (Vs) = 0 (Because most of the equipment in the chemical industry is still in service after its depreciable life so the salvage value is zero (Gaeta-Bernardi et al., 2016).
2. Life span of equipment = 10 years

Depreciation cost (USD) determined based on the above expression (4) = 0.72

F. Repair and maintenance cost (USD) = 0.215

G. Electricity cost

Current tariff charge for electricity in Assam region as per the Indian standards is 0.087 USD/kWh (Education institutions tariff, Assam).

1. Extruder

0.5 HP motor was used in the extruder

Time of use (h) = 3.75

Electricity cost for preparing 60 membranes (USD) $= 3.75 \times 0.745 \times 0.5 \times 0.087 = 0.122$

Table A. 4 Electricity cost for fabrication of tubular ceramic membrane

Equipment used	**Power (kW)**	**Time of use (h)**	**Electricity cost for preparing 60 membranes (USD)**
Extruder	0.3725	3.75	0.122
Hot air oven	1.5	24	3.132
Furnace	4	31	10.788
Bath sonicator	0.12	0.33	0.00431
Total electricity cost for preparing 60 membranes (USD)			**14.046**

Total cost for preparing 60 membranes (USD) = A+B+C+D+E+F+G

= 1.9761+6.75+1.351+1.1592+0.72+0.215+14.046 **26.22**

Estimated manufacturing cost for one membrane (USD) **0.437**

Estimated manufacturing cost for unit area of membrane (USD/m^2) **253**

List of publications

Publications in international journal

1. **Madu Purnima,** N. A. Manikandan, K. Pakshirajan, and G. Pugazhenthi, Recovery of microalgae from its broth solution using kaolin based tubular ceramic membranes prepared with different binders, **Separation and Purification Technology**, 250 (2020) 117212. DOI: 10.1016/j.seppur.2020.117212

2. **Madu Purnima**, K. Pakshirajan, and G. Pugazhenthi, Separation of TiO_2 particles from suspension using indigenous low-cost ceramic microfiltration membrane. **Journal of Water Process Engineering**, 49 (2022) 103123. DOI: 10.1016/j.jwpe.2022.103 123

3. **Madu Purnima**, T. Paul, K. Pakshirajan and G. Pugazhenthi, Onshore oil field produced water treatment using a hybrid microfiltration-biological process by kaolin based ceramic membrane and oleaginous *Rhodococcus opacus*. **Chemical Engineering Journal**, 453 (2022) 139850. DOI: 10.1016/j.cej.2022.139850

4. **Madu Purnima**, K.P Goswami, M. Kumar, K. Pakshirajan and G. Pugazhenthi, Facile synthesis of organic template-free chabazite zeolite coated kaolin ceramic membrane for continuous separation of cerium from aqueous solution. **ACS Applied Engineering Materials,** (2023). DOI: 10.1021/acsaenm.3c00047

5. **Madu Purnima**, K.P Goswami, M. Kumar, K. Pakshirajan and G. Pugazhenthi, Low-cost and highly durable kaolin supported CHA zeolite composite membrane for efficient removal of heavy metals from aqueous solution. **Environmental Technology & Innovation,** 30, (2023), 103102. DOI: 10.1016/j.eti.2023.103102

6. P. Singh, N. A. Manikandan, **Madu Purnima**, K. Pakshirajan, and G. Pugazhenthi, Recovery of lignin from water and methanol using low-cost kaolin based tubular ceramic membrane. **Journal of Water Process Engineering**, 38 (2020) 101615. DOI:10.1016/j.jwpe.2020.101615

7. A. K. Basumatary, K. P. Goswami, **Madu Purnima**, B. Deka, and G. Pugazhenthi, Fabrication and characterization of low-cost tubular ceramic membrane for microfiltration of oily wastewater, **Journal of Water Chemistry and Technology**, 44 (2022) 175-181. DOI:10.3103/S1063455X2203002X

Presentation in international/national conferences

1. **Madu Purnima**, N. A. Manikandan, K. Pakshirajan and G. Pugazhenthi, Fabrication of low-cost kaolin based tubular ceramic membrane and their application for algal separation, ***International Conference on Multifunctional and Hybrid Materials for Chemical Process, Energy, Environment and Medical Applications (ICMHCEE 2019),*** 9-11 September 2019, National Institute of Technology Tiruchirappalli, India.

2. **Madu Purnima**, N. A. Manikandan, K. Pakshirajan and G. Pugazhenthi, Preparation and characterization of low-cost kaolin based tubular ceramic membrane for algal separation, ***Green Technologies for Sustainable Water*** **(GTSW 2019)**, 1- 5 December 2019, Rex Hotel - 141 Nguyen Hue Boulevard, District 1, Ho Chi Minh City, Vietnam.

3. **Madu Purnima** and G. Pugazhenthi, An efficient alternative to recover titanium dioxide particles from solution using kaolin based tubular ceramic membrane, ***Emerging Trends in Separation Science and Technology (e-SESTEC-2020)***, 22-26 March 2021, Bhabha Atomic Research Centre, Mumbai 400085, India.

4. **Madu Purnima**, K. Pakshirajan and G. Pugazhenthi, Treatment of Onshore Oil Field Produced Water using Kaolin based Tubular Ceramic Microfiltration Membrane, ***International Conference on Advances in Chemical and Environmental Engineering (ACEE-2021)***, 16-17 December 2021, National Institute of Technology Raipur, India.

5. **Madu Purnima** and G. Pugazhenthi, Facile synthesis of OSDA-free Chabazite (CHA) zeolite crystals coated kaolin ceramic support for the lab-scale continuous recovery of cerium ions from aqueous solution, ***Second International Conference on Sustainable Technologies for Water Treatment and Desalination (STWTD – 2022)***, 28-29 January 2022, National Institute of Technology Calicut, India.

6. **Madu Purnima**, K. P. Goswami, M. Kumar, K. Pakshirajan and G. Pugazhenthi, Development of kaolin supported CHA zeolite composite membrane for the removal of cadmium from aqueous solution, ***International Symposium on Water Sustainability & Green Technologies (WSGT 2022)***, 25-26 November 2022, Rex Hotel - 141 Nguyen Hue Boulevard, District 1, Ho Chi Minh City, Vietnam.